NASA Tech Briefs

National
Aeronautics and
Space
Administration

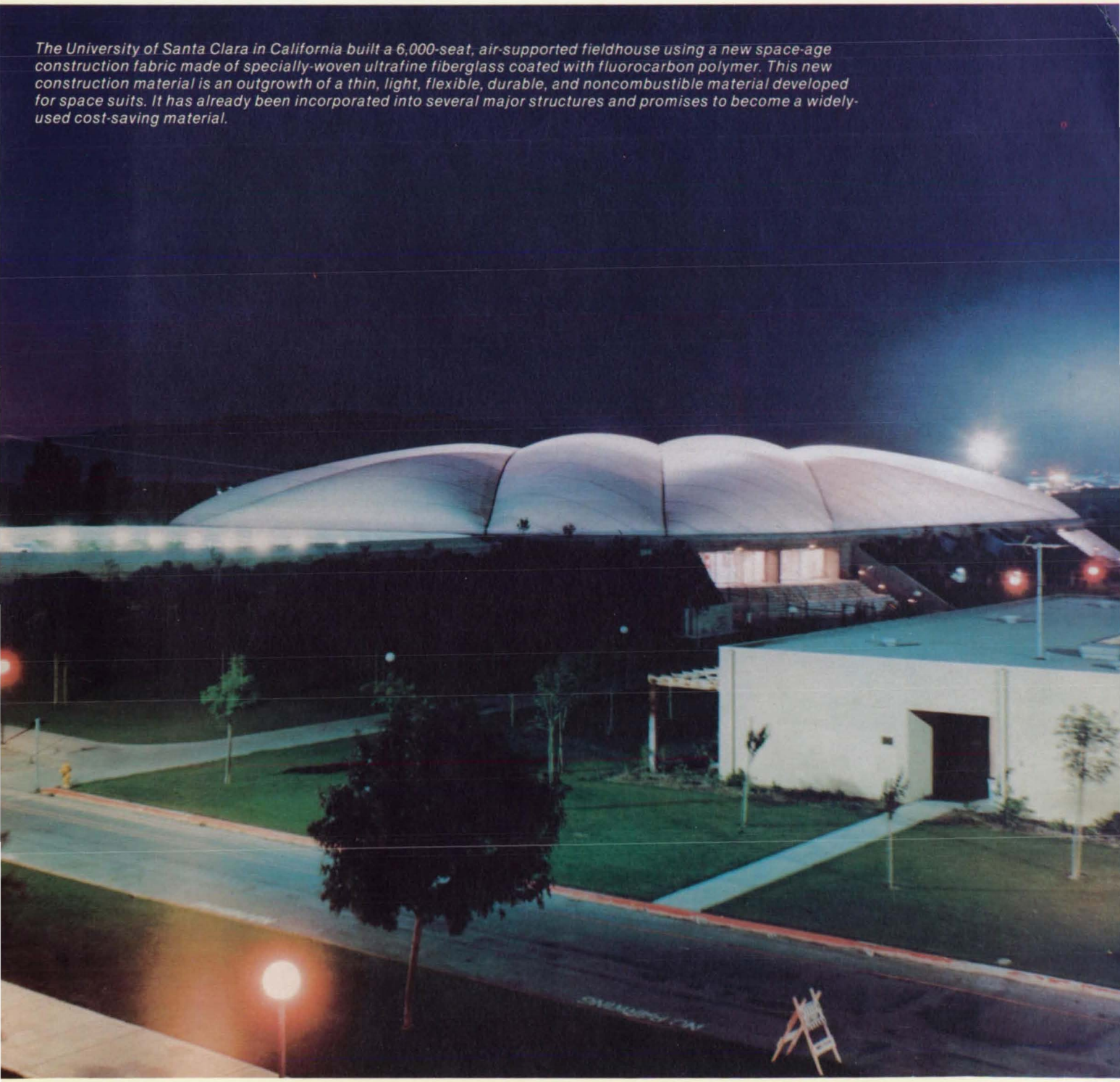

The University of Santa Clara in California built a 6,000-seat, air-supported fieldhouse using a new space-age construction fabric made of specially-woven ultrafine fiberglass coated with fluorocarbon polymer. This new construction material is an outgrowth of a thin, light, flexible, durable, and noncombustible material developed for space suits. It has already been incorporated into several major structures and promises to become a widely-used cost-saving material.

Vol. 3, No. 3

FALL 1978

About the NASA Technology Utilization Program

The National Aeronautics and Space Act of 1958, which established NASA and the United States civilian space program, requires that "The Administration shall provide for the widest practicable and appropriate dissemination of information concerning its activities and the results thereof."

To help carry out this objective the NASA Technology Utilization (TU) Program was established in 1962. It offers a variety of valuable services to facilitate the transfer of aerospace technology to nonaerospace applications, thus assuring American taxpayers maximum return on their investment in space research; thousands of spinoffs of NASA research have already occurred in virtually every area of our economy.

The TU Program has worked for engineers, scientists, technicians, and businessmen. And it can work for you.

NASA Tech Briefs

Tech Briefs is published quarterly and is free to any U.S. citizen or organization. It is both a current-awareness medium and a problem-solving tool. Potential products ... industrial processes ... basic and applied research ... shop and lab techniques ... computer software ... new sources of technical data ... concepts ... you will find them all in NASA Tech Briefs. The first section highlights a few of the potential new products contained in Tech Briefs. The remainder of the volume is organized by technical category to help you quickly review new developments in your areas of interest. Finally, a subject index makes each issue a convenient permanent reference file.

Further Information on Innovations

Although many articles are complete in themselves, others are backed up by Technical Support Packages (TSP's). TSP's are available without charge and may be ordered by simply completing the enclosed TSP Request Card. Further information on some innovations is available for a nominal fee from other sources, as indicated at the ends of the articles. In addition, Technology Utilization Officers at NASA Field Centers will assist you directly when necessary. (See page A4.)

Patent Licenses

Many of the inventions described are under consideration for patents or have been patented by NASA. Unless NASA has decided not to apply for a patent, the patent status is described at the end of each article. For further information about the Patent Program see page A8.

Other Technology Utilization Services

To assist engineers, industrial researchers, business executives, city officials, and other potential users in applying space technology to their problems, NASA sponsors six Industrial Applications Centers. Their services are described on page A6. In addition, an extensive library of computer programs is available through COSMIC, the Technology Utilization Program's outlet for NASA-developed software. (See page A5.)

Applications Program

To help solve public-sector problems in such areas as safety, health, transportation, and environmental protection, NASA TU Applications Teams, staffed by professionals from a variety of disciplines, work with Federal agencies, local governments, and health organizations to identify critical problems amenable to technical solutions. Among their many significant contributions are a rechargeable heart pacemaker, a lightweight fireman's breathing apparatus, aids for the handicapped, and safer highways.

Reader Feedback

We hope you find the information in NASA Tech Briefs useful. A reader feedback card has been included because we want your comments and suggestions on how we can further help you apply NASA innovations and technology to your needs. Please use it, or if you need more space, write us a letter.

NASA Tech Briefs

National Aeronautics and Space Administration

FALL 1978
Volume 3, Number 3

COVERS: The photographs on the front and back covers illustrate recent developments by NASA and its contractors that resulted in commercial and nonaerospace spinoffs. You can use the TSP Request Card at the end of this issue to learn more about the Fiberglass Fabric [Circle 78] and Multimode Electronic Lights [Circle 79].

About This NASA Publication

NASA Tech Briefs, a quarterly publication, is distributed free to U.S. citizens to encourage commercial application of U.S. space technology. For information on publications and services available through the NASA Technology Utilization Program, write to the Director, Technology Utilization Office, P. O. Box 8757, Baltimore/Washington International Airport, Maryland 21240.

"The Administrator of National Aeronautics and Space Administration has determined that the publication of this periodical is necessary in the transaction of the public business required by law of this Agency. Use of funds for printing this periodical has been approved by the Director of the Office of Management and Budget through December 31, 1978."

Change of Address

Change of Address: If you wish to have NASA Tech Briefs forwarded to your new address, use one of the Subscriptions cards enclosed in the back of this volume of NASA Tech Briefs. Be sure to check the appropriate box indicating change of address.

Communication Concerning Editorial Matter

For editorial comments or general communications about NASA Tech Briefs, you may use the self-addressed Feedback card in the back of NASA Tech Briefs, or write to: The Publications Manager, Technology Utilization Office (E TU-6), NASA Headquarters, Washington, DC 20546. Technical questions concerning specific articles should be directed to the Technology Utilization Officer of the sponsoring NASA Center (addresses listed on page A4).

NASA TECH BRIEFS Published Quarterly by the National Aeronautics and Space Administration, Technology Utilization Branch, Washington, DC

Administrator: **Robert A. Frosch;** Chief, Technology Utilization Branch: **Louis Mogavero;** Publications Program Manager: **Judson O. Harrison III**

Prepared for the National Aeronautics and Space Administration by **Logical Technical Corp.**: Editor-in-Chief: **Graham L. Gross;** Art Director: **Ernest Gillespie;** Managing Editor: **Jay Kirschenbaum;** Senior Editor: **Donald Blattner;** Chief Copy Editor: **Oden Browne;** Staff Editors: **Michael Binder, Michael Polchaninoff, Jonathan Rogers, Ted Selinsky, George Watson;** Graphics: **Concetto Auditore, Judy Tenenbaum;** Editorial & Production: **Richard Johnson, Rose Giglietti, Vincent Susinno, John Tucker, Madeline Tucker, Ernestine Walker, Carl Woolridge**

NASA TU SERVICES

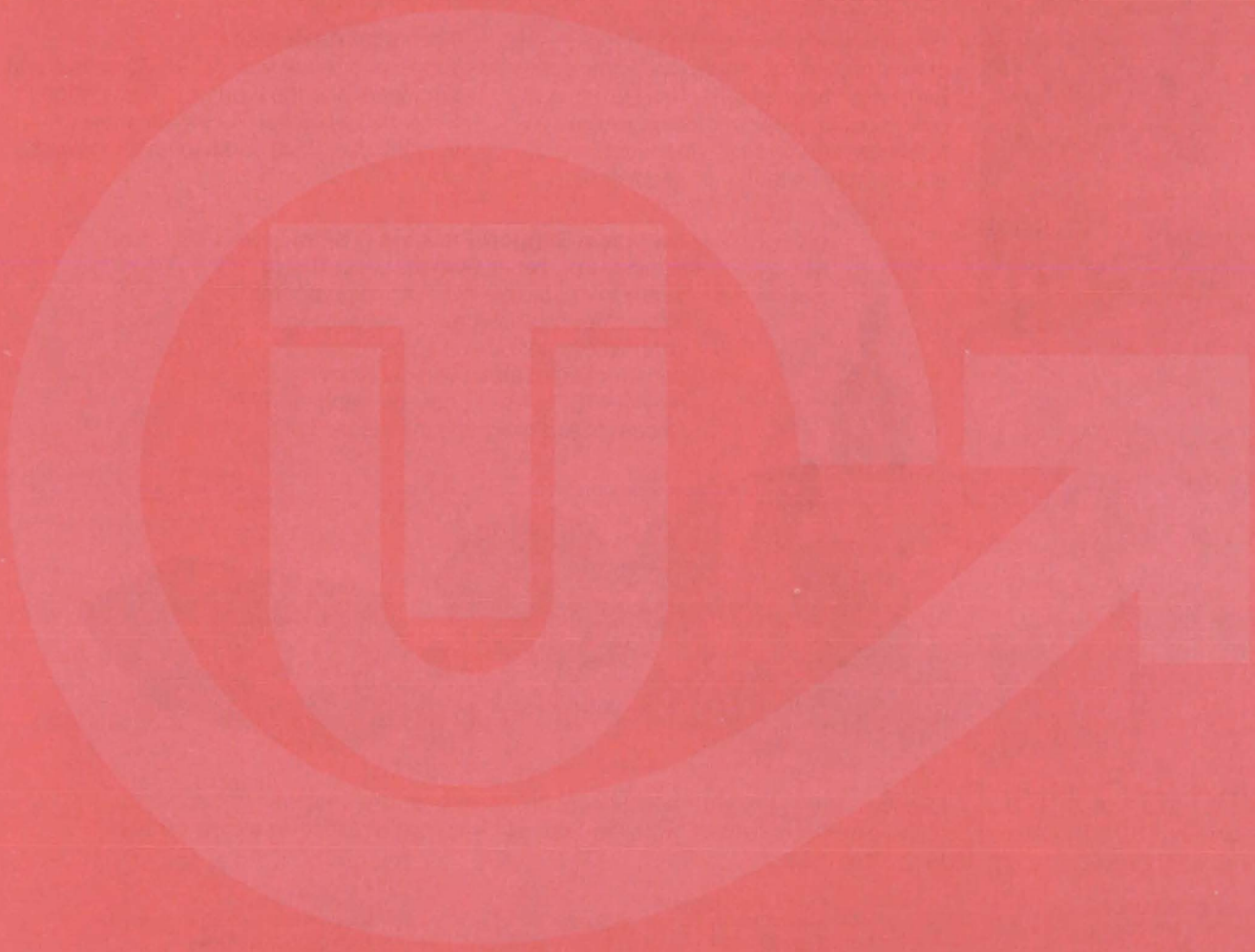

THE NASA TECHNOLOGY UTILIZATION OFFICERS

They will help you apply the innovations described in Tech Briefs.

The Technology Utilization Officer (TUO)
Each NASA Center has a Technology Utilization Officer — An applications engineer whose job is to help you make use of new technology developed at his center. He brings you the NASA Tech Briefs and other special publications, sponsors conferences, and arranges for expert assistance in solving technical problems.

Technical Assistance
Working together with NASA Scientists and Engineers and the Industrial Applications Centers, the center TUO's can answer specific questions about innovations and related NASA technology.

Technical Support Package (TSP's)
For many of the innovations described in Tech Briefs, the center TUO has prepared additional material that will help you in detailed evaluation and actual use or construction of the new technology. You may get TSP's free of cost by using the TSP Request Card or writing the center TUO.

Who to Contact. Of course, many technical questions about Tech Briefs are answered in the TSP's, but when no TSP is available, or you have further questions, write the Technology Utilization Officer at the center that sponsored the research at the address listed below.

Charles C. Kubokawa
Ames Research Center
Code AU: 240-2
Moffett Field, CA 94035
(415) 965-5554

Donald S. Friedman
Goddard Space Flight Center
Code 702.1
Greenbelt, MD 20771
(301) 982-6242

John T. Wheeler
Johnson Space Center
Code AT3
Houston, TX 77058
(713) 483-3809

Raymond J. Cerrato
John F. Kennedy Space Center
Code SA-RTP
Kennedy Space Center, FL 32899
(305) 867-2780

John Samos
Langley Research Center
Mail Stop 139A
Hampton, VA 23665
(804) 827-3281

Paul Foster
Lewis Research Center
21000 Brookpark Rd.
Cleveland, OH 44135
(216) 433-4000, Ext. 6832

Aubrey D. Smith
Marshall Space Flight Center
Code AT01
Marshall Space Flight Center, AL 35812
(205) 453-2224

John C. Drane
NASA Resident Legal Office-JPL
4800 Oak Grove Drive
Pasadena, CA 91103
(213) 354-6420

Gilmore H. Trafford
Wallops Flight Center
Wallops Island, VA 23337
(804) 824-3411, Ext 201

Louis Mogavero, Chief
Technology Utilization Branch
Code ETU-6
NASA Headquarters
Washington, DC 20546
(202) 755-2220

COSMIC

(Computer Software Management & Information Center)

AN ECONOMICAL SOURCE OF COMPUTER PROGRAMS DEVELOPED BY THE GOVERNMENT.

COSMIC is sponsored by NASA to give you access to over 1400 computer programs developed by NASA and the Department of Defense, and selected programs from other government agencies. It is one of the Nation's largest software libraries.

COSMIC charges very reasonable fees for programs to help cover part of their expenses—and NASA pays for the remainder. Programs generally cost from $500 to $1000, but a few are more expensive and many are less. Documentation is available separately and very inexpensively.

COSMIC collects and stores software packages, insures that they are complete, prepares special announcements (such as Tech Briefs), publishes an indexed software catalog, and reproduces programs for distribution. COSMIC helps customers to identify their software needs, follows up to determine the successes and problems, and provides updates and error corrections. In some cases, NASA engineers can offer guidance to users in installing or running a program.

COSMIC programs range from management (pert scheduling) to information science (retrieval systems) and computer operations (hardware and software). Hundreds of engineering programs perform such tasks as structural analysis, electronic circuit design, chemical analysis, and design of fluid systems. Others determine building energy requirements, optimize mineral exploration, and draw maps of water-covered areas using NASA satellite data. In fact, the chances are, if you use a computer, you can use COSMIC.

COSMIC is eager to help you get the programs you need. For more information about services or software available from COSMIC, fill out and mail the COSMIC Request Card in this issue.

COSMIC: Computer Software Management and Information Center

Suite 112, Barrow Hall, University of Georgia, Athens, Georgia 30602 Phone: (404) 542-3265

WHERE IS THE WORLD'S LARGEST BANK OF TECHNICAL DATA

?

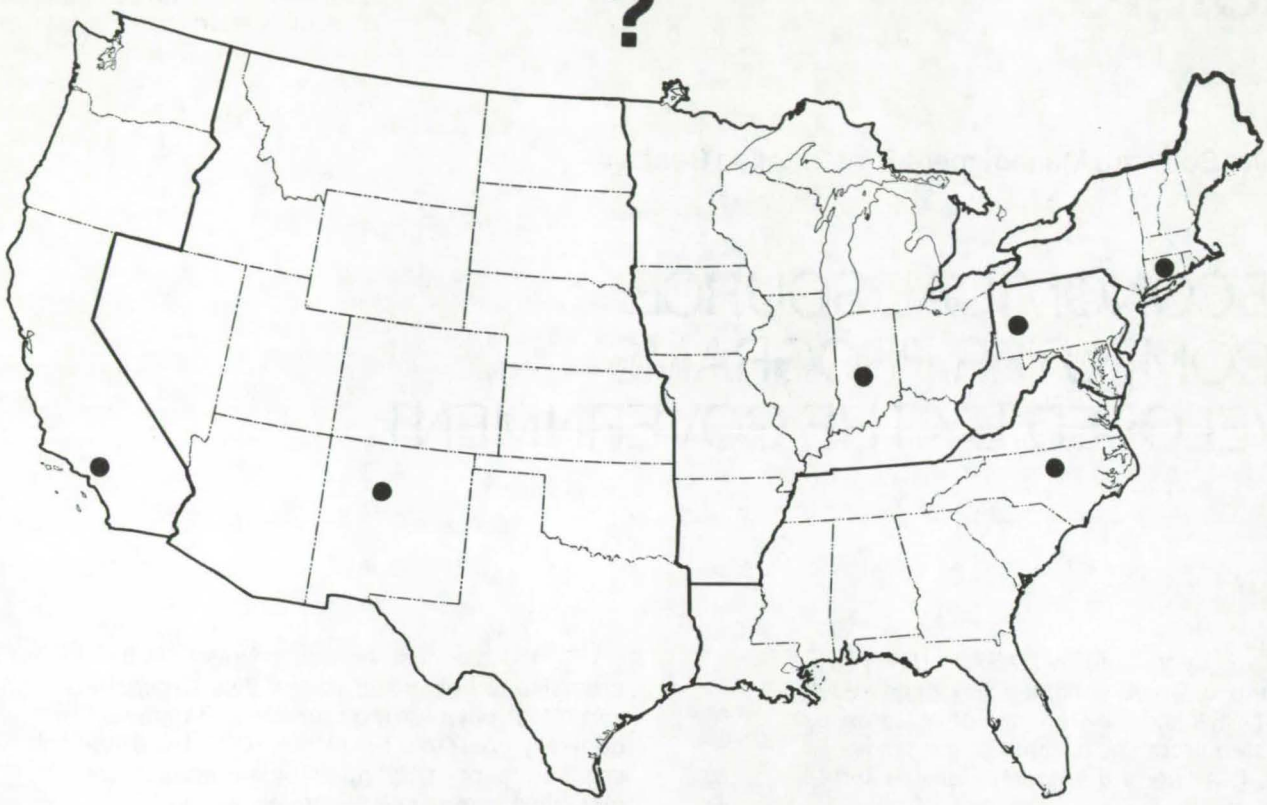

It's in Indianapolis and Pittsburgh, it's in Storrs, Connecticut and Research Triangle Park, North Carolina; and it's in Albuquerque and Los Angeles.

NASA IAC's — INDUSTRIAL

You can get more information and more data on more technical subjects through NASA's network of IAC's than anywhere else in the world. About 8,000,000 documents and growing at the rate of 50,000 more each month!

Major sources include:

- 750,000 NASA Technical Reports
- Selected Water Resources Abstracts
- NASA Scientific and Technical Aerospace Reports
- Air Pollution Technical Information Center
- NASA International Aerospace Abstracts
- Chem Abstracts Condensates
- Engineering Index
- Energy Research Abstracts
- NASA Tech Briefs
- Government Reports Announcements

and many other specialized files on food technology, textile technology, metallurgy, medicine, business, economics, social sciences, and physical science.

The IAC's are one of the most economical ways of staying competitive in today's world of exploding technology. The help available from the network ranges from literature searches through expert technical assistance.

Literature Searches
Help in designing your search, typically from 30 to 300 abstracts in as narrow or broad an area as you need, and complete reports when you need them. The most complete "search before research" available!

Current Awareness
Consult with our applications engineers to design your personal program — selected monthly or quarterly abstracts on new developments in your speciality. It's like having your own journal!

Technical Assistance
Our applications engineers will help you evaluate and apply your literature-search results. They can help find answers to your technical problems and put you in touch with scientists and engineers at NASA Field Centers.

To obtain more information about how NASA's IAC's can help you —
Check the IAC box on the TSP Request Card in this issue,
Or write or call the IAC nearest you.

APPLICATIONS CENTERS

How to get reports and other documents discussed in this issue of Tech Briefs

Many of the innovations in Tech Briefs are described in detail in reports available at a reasonable cost through one or more of the IAC's. To order a report, call or write the IAC referenced at the end of the Tech Brief article at the address below. Be sure to list the titles and accession numbers (N76-..., N75-..., etc.) of those you wish to purchase.

Aerospace Research Application Center (ARAC)
Indiana University-Purdue University at Indianapolis
1201 E. 38th St.
Indianapolis, IN 46205
E. Guy Buck, Director
(317) 264-4644

Knowledge Availability Systems Center (KASC)
University of Pittsburgh
Pittsburgh, PA 15260
Dr. Edmond Howle, Director
(412) 624-5211

New England Research Application Center (NERAC)
Mansfield Professional Park
Storrs, CT 06268
Dr. Daniel U. Wilde, Director
(203) 486-4533

North Carolina Science & Technology
Research Center (NC/STRC)
P. O. Box 12235
Research Triangle Park, NC 27709
Peter J. Chenery, Director
(919) 549-0671

Technology Application Center (TAC)
University of New Mexico
Albuquerque, NM 87131
Stanley A. Morain, Director
(505) 277-4000

Western Research Application Center (WESRAC)
901 Exposition Boulevard, Room 205
University of Southern California
University Park
Los Angeles, CA 90007
Radford King, Director
(213) 741-6132

NASA INVENTIONS AVAILABLE FOR LICENSING

Over 3,500 NASA inventions are available for licensing in the United States - both exclusive and nonexclusive.

Nonexclusive Licenses

Nonexclusive licenses for commercial use are encouraged to promote competition and to achieve the widest use of inventions. They must be used by a negotiated target date but are usually royalty free.

Exclusive Licenses

An exclusive license may be granted to encourage early commercial development of NASA inventions, especially when considerable private investment is required. These are generally for 5 to 10 years and usually require royalties based on sales or use.

The NASA patent licensing program also provides for licensing of NASA-owned foreign patents. In addition to inventions described in Tech Briefs, "NASA Patent Abstract Bibliography," containing abstracts of all NASA inventions, can be purchased from: National Technical Information Service, Springfield, Va., 22161. This document is updated semi-annually.

Patent Licenses and the NASA Tech Brief

Many of the inventions reported in Tech Briefs are patented or are under consideration for a patent at the time they are published. When this is the case, the current patent status is described at the end of the article; otherwise, there is no statement about patents. **If you want to know more about the patent program or are interested in license for a particular invention, write the Patent Counsel at the NASA Field Center** that sponsored the research. Be sure to refer to the NASA reference number in parenthesis at the end of the Tech Brief.

Robert F. Kempf
NASA Headquarters, Code GP-4
400 Maryland Ave., S.W.
Washington, DC 20546
(202) 755-3932

Darrell G. Brekke
Ames Research Center
Mail Code: 200-11A
Moffett Field, CA 94035
(415) 965-5104

John O. Tresansky
Goddard Space Flight Center
Mail Code: 204
Greenbelt, MD 20771
(301) 982-2351

Marvin F. Matthews
Lyndon B. Johnson Space Center
Mail Code: AM
Houston, TX 77058
(713) 483-4871

James O. Harrell
John F. Kennedy Space Center
Mail Code: SA-PAT
Kennedy Space Center, FL 32899
(305) 867-2544

Howard J. Osborn
Langley Research Center
Mail Code: 279
Hampton, VA 23665
(804) 827-3725

Norman T. Musial
Lewis Research Center
Mail Code: 500-311
21000 Brookpark Road
Cleveland, OH 44135
(216) 433-4000

Leon D. Wofford, Jr.
Marshall Space Flight Center
Mail Code: CC01
Marshall Space Flight Center, AL 35812
(205) 453-0020

Monte F. Mott
NASA Resident Legal Office
4800 Oak Grove Drive
Pasadena, CA 91103
(213) 354-2700

NEW PRODUCT IDEAS

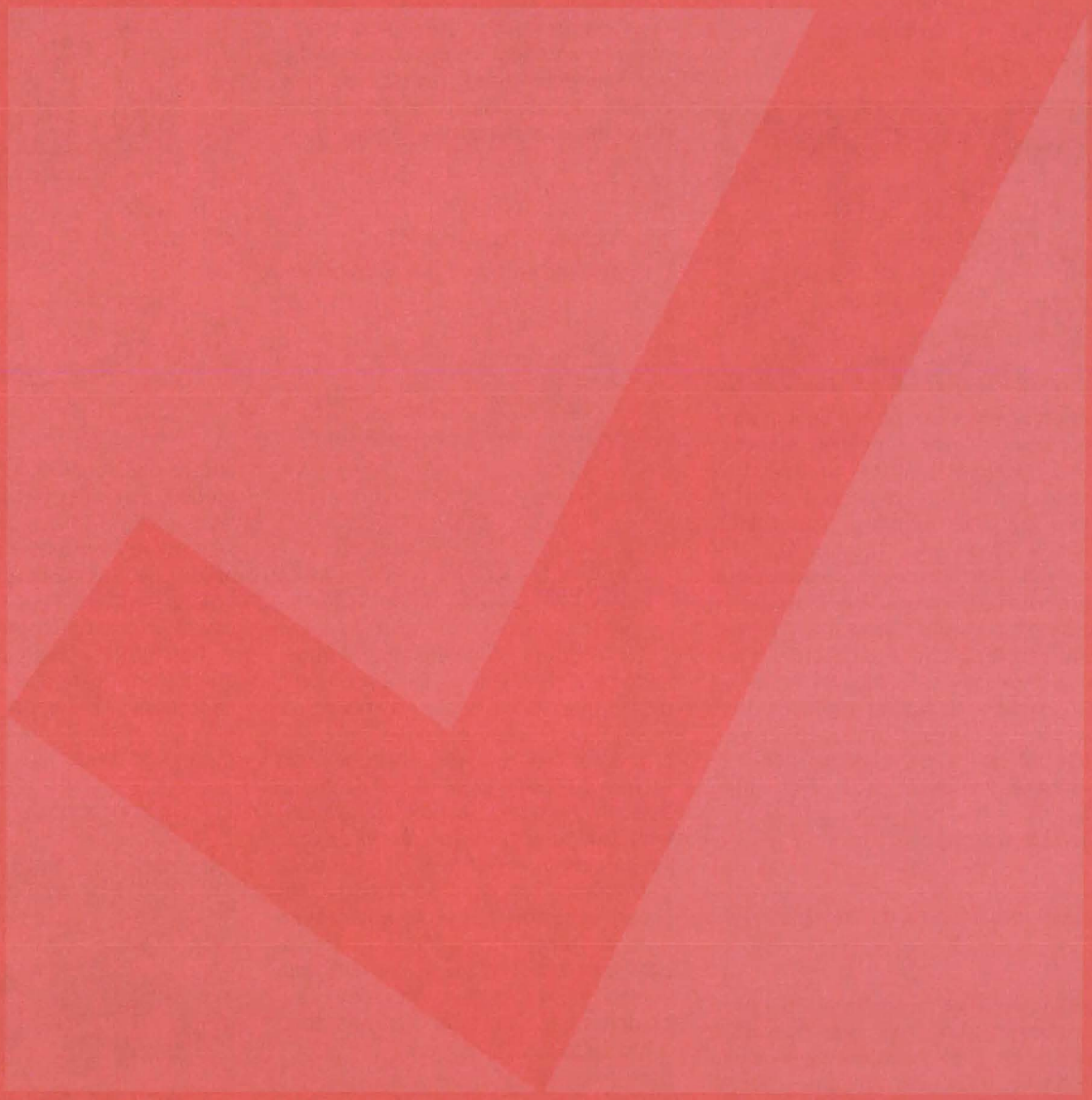

NEW PRODUCT IDEAS are just a few of the many innovations described in this issue of NASA Tech Briefs and having promising commercial applications. Each is discussed further on the referenced page in the appropriate section in this issue. If you are interested in developing a product from these or other NASA innovations, you can receive further technical information by requesting the TSP referenced at the end of the full-length article or by writing the Technology Utilization Office of the sponsoring NASA center (see page A4). NASA's patent-licensing program to encourage commercial development is described on page A8.

Precision Cleaver for "Soft" Crystals

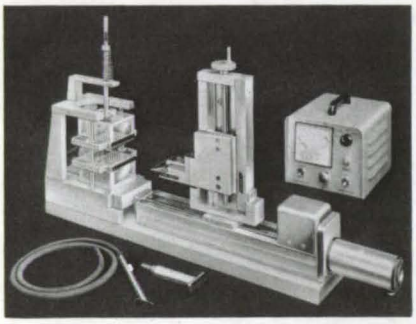

Soft crystals can be cut as thin as 5 mils using a new precision cleaver. Slice thickness may be controlled to within 1 mil. The crystal is held in place by two neoprene-rubber-lined platens that grip the crystal by vacuum. The cleaver incorporates a horizontally-driven cutting blade. The blade is adjusted along the vertical axis by a lead screw to determine the slice thickness. The cleaver replaces earlier manual cutting methods that were inaccurate and produced uneven cuts. It can slice various medium-hardness materials with high precision.

(See page 366.)

Heat-Resistant Nontoxic Structural Laminate

Laminated panels made from a new nonepoxy resin have superior heat resistance and release fewer toxic products than conventional epoxy laminates when exposed to heat or flame. Among possible applications for the lightweight panels are the interiors of automobiles and other vehicles and structural parts on aircraft. Various bismaleimides, with or without diamine compounds, are polymerized to produce the new resin. In one laminate, the resin is mixed with carbon microballoons to form a composite that fills a honeycomb core. Outer layers of glass cloth preimpregnated with polybismaleimide resin complete the laminated structure. In addition to their nontoxicity and superior heat resistance, the panels are also easier to shape and finish than conventional epoxy laminates.

(See page 374.)

Remotely-Powered Intracranial Pressure Monitor

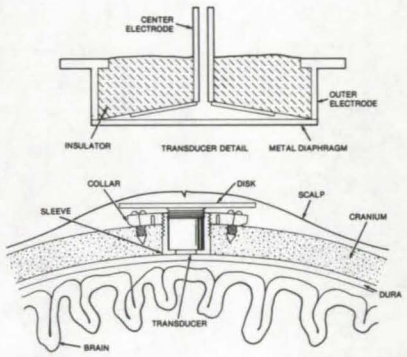

An electronic oscillator that can be implanted in the skull of a cerebral dysfunction victim is stable enough to monitor very slow changes in intracranial pressure, and it does not require batteries or wire connections through the scalp. A new transducer with a stiff diaphragm produces up to a 10-percent change in the tuning capacitance of the oscillator. The sensor is powered by radio waves sent from a remote transmitter. In tests over a period of 50 days, the unit was stable to within 0.1 torr/day, as compared to previous systems that drifted about 0.7 torr/day.

(See page 381.)

Cosine-Corrected Optical Diffuser

A new "cosine diffuser" collimates and transmits light such that its output is proportional to the cosine of the angle of incidence. When placed at the entrance aperture of a spectroradiometer or other light-measuring instrument, it improves the accuracy of radiation-flux measurements for off-axis angles of incidence. A fused-

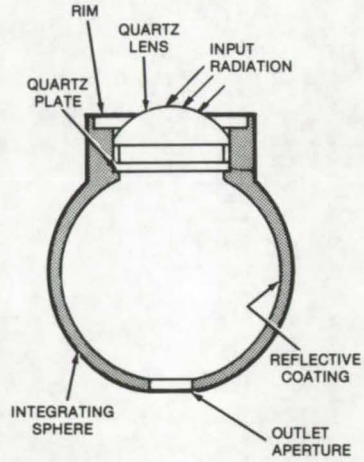

quartz planoconvex lens and several ground planar surfaces transmit the incident light into a spherical cavity with reflective walls. This combination efficiently scatters light through an aperture at the outlet side of the cavity. In addition to its potential uses in laboratory optical measurements, the diffuser can also be a valuable accessory for solar- and sky-flux measurements in the field.

(See page 347.)

Automated Syringe Sampler

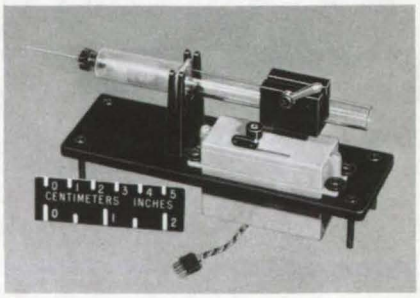

A remote-controlled syringe sampler collects air or water samples on location for pollution studies. The device can also be deposited in hazardous areas and later removed to test for the presence of dangerous chemicals. The sampler includes an evacuated, glass sampling tube. This tube, sealed by a rubber septum, is driven by a servo against a hypodermic needle. After the needle

punctures the septum and the sample rushes into the tube, the servo is activated again to withdraw the tube from the needle.
(See page 393.)

High-Speed, High-Power, Switching Transistor

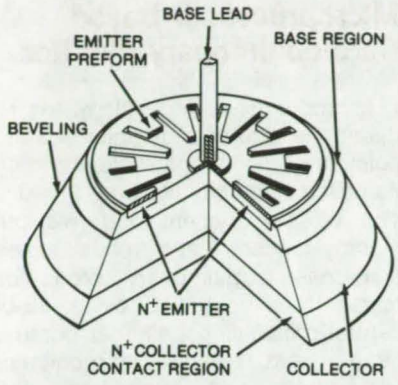

A silicon npn switching transistor combines the speed and positive control of a transistor with the power-handling capacity of a thyristor. Rated at 200 amperes with a switching speed of 0.5 microsecond, the new semiconductor device has possible applications in power converters, motor drives, RF induction heaters, and medical electronics. Its power-handling efficiency and speed are made possible by a novel blend of triple-diffused silicon technology and an interdigitated emitter/base structure. Besides competing directly with the thyristor in high-power circuits, the transistor should also stimulate new power-switching applications for which transistors have not previously been considered.
(See page 320.)

Sweat Collection Capsule

Perspiration samples at specific locations on the body can be collected with a simple capsule that holds a disk of filter paper against the skin.

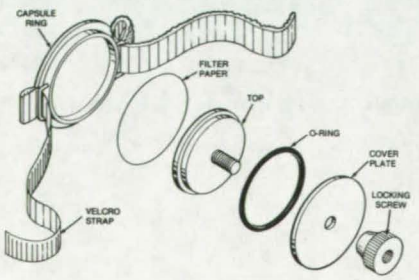

The paper can be weighed before and after installation in the capsule to determine the amount of sweat collected, and it can be analyzed chromatographically to determine the sweat constituents. Designed for long- and short-term perspiration monitoring, the capsule can also be used to measure the number of sweat glands under the collecting surface. This is done by placing a high-starch-content paper in the capsule and painting the skin surface with tincture of iodine. The starch/iodine reaction produces dots on the paper opposite the active sweat glands.
(See page 387.)

Penetrating Fire Extinguisher

A new extinguisher with a penetrating tip can dispense fire-extinguishing chemicals in hard-to-reach areas.

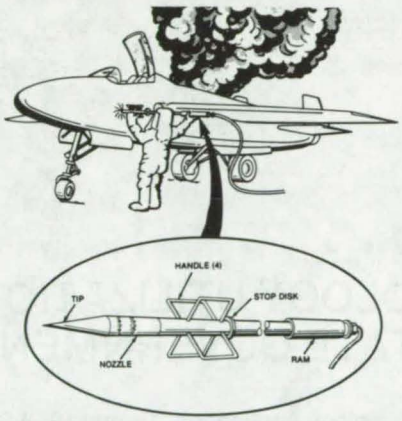

Originally developed for use aboard the Space Shuttle, the extinguisher can also penetrate the metal skins of aircraft and other vehicles, and it can pierce wood, plasterboard, metal, and plastic panels in buildings. To use the extinguisher, an operator places the tip against a wall or other surface and slides an integral ram along the body until it strikes a stop disk. The impact drives the tip through the surface so that the chemical agent can be injected. Overlapping discharge streams from the nozzle spray the chemical over a wide area.
(See page 416.)

Shaft Speed Control

A simple mechanism controls the rotation of a heavy-duty shaft by mechanical comparison with the rotation of a small, precise, stepper

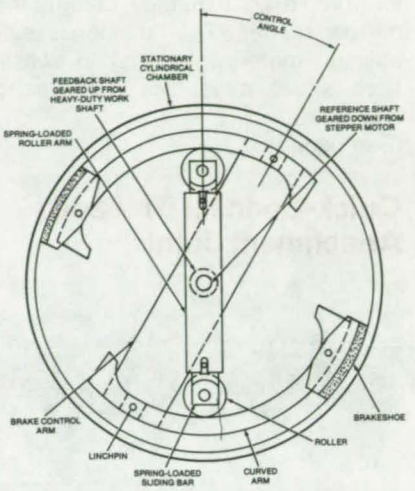

motor. The mechanism can be used to limit winding and unwinding speeds of large spools and reels and to control the speed of other rotating shafts. The setup incorporates a reference shaft geared down from the stepper motor and a feedback shaft geared up from the shaft to be controlled. The feedback and the reference shafts are coupled with a brake assembly inside a stationary cylinder. When the work shaft speeds up, the brakes are activated automatically to slow it down.
(See page 432.)

Fastener for Thin Fragile Materials

A new two-piece fastener is ideal for securing thin delicate parts that might be damaged by conventional fasteners, such as rivets or upset collars. Nevertheless, the strength of the new fastener approaches that of a riveted connection. Easily fabricated, the fastener consists of a plastic button and a spring-steel collar. These parts have a large contact area, to distribute loads on delicate assemblies, and a

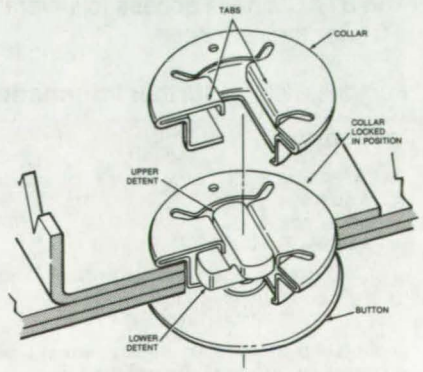

(continued on next page)

low profile so that they can fit into narrow spaces. The fastener is suitable for materials ranging in density from sheet metal to fabric sandwiches.
(See page 451.)

Quick-Connect Threaded Attachment Joint

A threaded tapered joint is self-alining and tightens with only 65° of rotation for quick connects and disconnects. Made of injection-molded plastics or cast or machined aluminum, the joint can carry wires, tubes, liquids, or gases. When the two parts of the joint are brought together, their shapes aline them. Small projections on the male section and slots on the female section further aid alinement; slight rotation of the male form engages the projections in the slots. At this point, the threads engage, and the male section is rotated until the joint is fully engaged.
(See page 430.)

Corona-Discharge Air-Purification System

A system uses electrical discharge to remove trace contaminants from air in closed environments. Typical contaminants that can be handled by the system range from metabolic products, such as alcohols, esters, hydrogen sulfide, and ammonia, to lubricant solvents, such as Freons, aromatics, alcohols, and ketones. The air is purified in a plasma glow-discharge chamber powered by a variable radio-frequency source. The contaminants are oxidized into water, carbon dioxide, and carbon monoxide, which are removed by a scrubber. Purified air is returned to the environment.
(See page 368.)

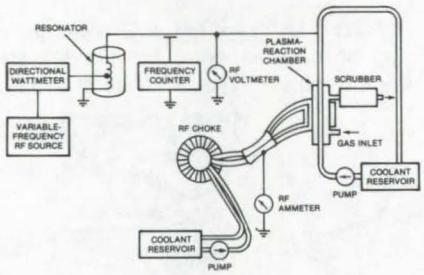

Microprocessor-Based Cardiopulmonary Monitor

Microprocessor technology has reduced the size of a complete cardiopulmonary-monitoring system and cut its power requirements from 1,000 to 100 W. The system performs pulmonary-function and physiological time-constant/pulmonary blood-flow tests. It is controlled by a 16-bit central-processing unit that controls heart- and respiratory-monitoring transducers and supervises data acquisition and analysis. The firmware to control and monitor the tests is contained in 5K of programable read-only memory. Real-time data are displayed on a printer and a video monitor.
(See page 388.)

Electronic Components and Circuits

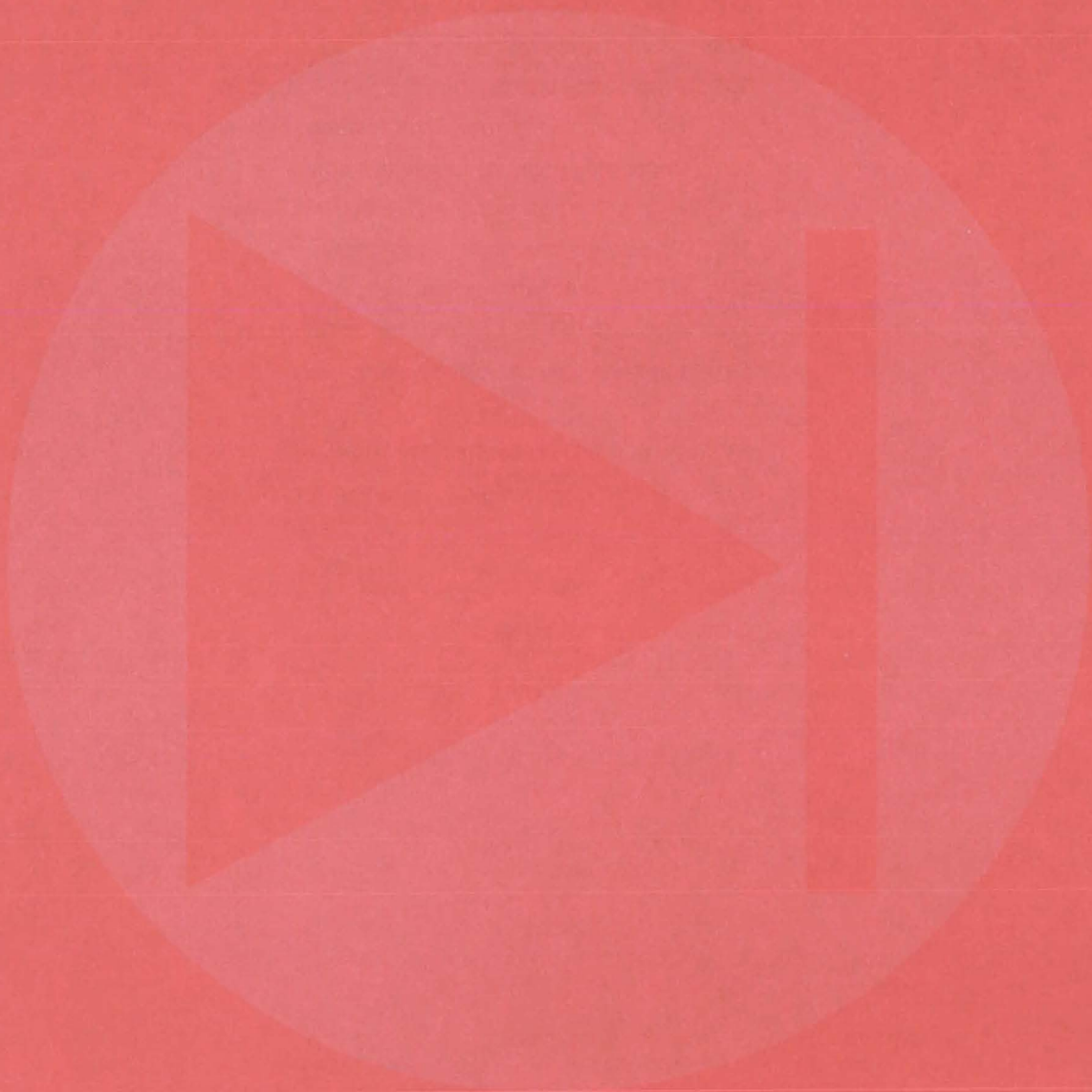

Hardware, Techniques, and Processes

Books and Reports

Automatic Gain-Balancing Circuit

Gains through multiple signal paths are automatically balanced to 1 part in 10,000.

Langley Research Center, Hampton, Virginia

Automatic gain-balancing circuitry designed for the MAPS (Monitoring Air Pollution from Satellites) Gas Filter Correlation Spectrometer allows precision differencing of two or more output signals so that comparative determinations may be made of extremely small differences in signal amplitudes.

Infrared energy emitted from the Earth's surface passes through the atmosphere to the spectrometer. Gases in the atmosphere produce narrow absorption lines in the transmitted energy at wavelengths corresponding to gas-molecule resonances. Each gas species has a unique signature of absorption lines. Energy reaching a sensor is collected by a telescope, modulated by a chopper, spectrally filtered, and simultaneously directed onto two detectors, as shown in Figure 1.

To permit precision differencing of the optical signals at the two detector branches, the optical and electrical responsivities must be balanced. With the new circuitry, the gains through two or more signal paths can be automatically balanced to approximately 1 part in 10,000. The circuit compensates for slow changes in both the optical and electrical gains common to gas-filter correlation spectrometers.

A stable reference signal, R (see Figure 2), is chopped at frequency f_1 and fed into the inputs, optical or electrical, of the amplification channels. These signals are designated R_1, R_2, . . . R_n. The signals to be amplified and balanced are chopped at frequency $f_{1/2}$, which is phase-synchronized with the reference chopping f_1. These are signals $S_1, S_2, \ldots S_n$.

The summed signals, $(S_1 + R_1)$ to $(S_n + R_n)$, are amplified and fed into the gain balancing circuit. The two signals are then subtracted and demodulated with respect to the reference modulation-timing signal. Any differences in the amplitudes of R_1 and R_2, for example, are fed as an error signal

(continued on next page)

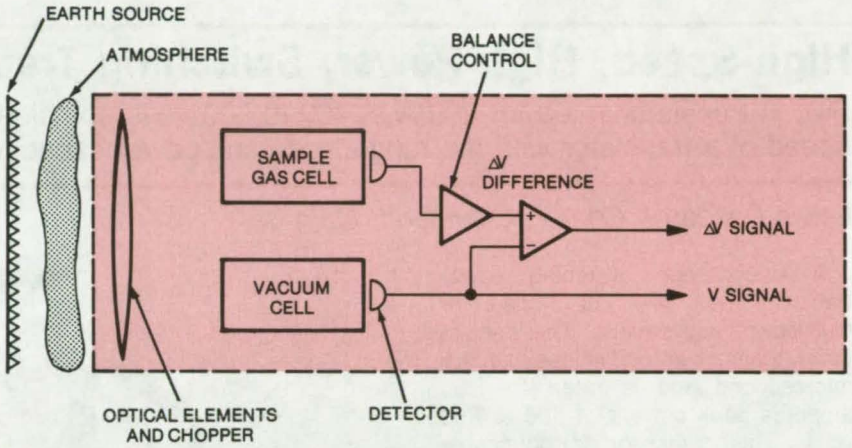

Figure 1. In the **IR Atmospheric Analyzer,** a gas cell containing a sample of the gas to be sensed is used as a spectral filter. The output signals from the detectors are differenced and demodulated to determine the correlation between the spectral content of collected energy and the spectral absorption lines of the gas cell. The difference signal can be related to the amount of gas of interest present in the atmosphere.

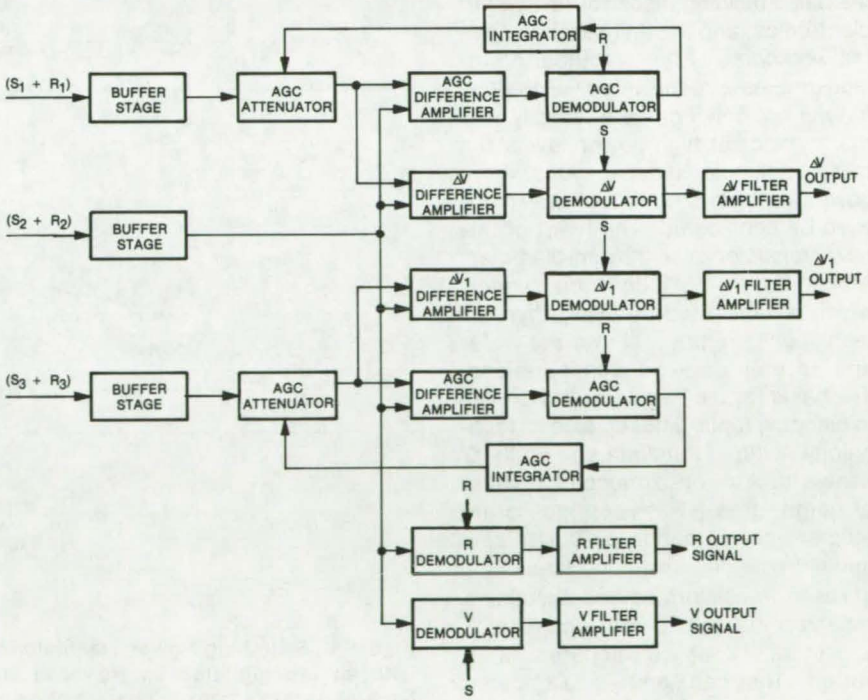

Figure 2. **Signal-Processing Electronics** for the spectrometer in Figure 1 balance gains through the V and ΔV signal paths.

to an automatic-gain control-loop integrator, the output of which adjusts the gain of the (S_1 + R_1) channel. Therefore, the gain is always adjusted to make R_1 and R_2 equal. A second difference amplifier and a demodulator operating with respect to the signal modulation timing then provide the desired output signal (S_1 – S_2). The circuit operation is essentially the same for a two-, three-, or n-channel gas correlator.

This work was done by Dennis F. Eisenhut of TRW, Inc., for **Langley Research Center.** *Further information may be found in NASA CR-145137, "Monitoring Air Pollution From Satellites [MAPS]," [N77-19560] Vol. 1, Technical Report [$11.75] and [N77-19561] Vol. 2, Appendices [$13.25]. A copy may be purchased [prepayment required] from the National Technical Information Service, Springfield, Virginia 22151. LAR-12074*

High-Speed, High-Power, Switching Transistor

Silicon transistor rated for 200 A at 400 to 600 volts combines the switching speed of a transistor with the ruggedness and power capacity of a thyristor.

Lewis Research Center, Cleveland, Ohio

A silicon npn switching power transistor has been developed for high-power applications. The transistor switches on and off in less than 0.5 microsecond and is rated for 200 amperes peak current at 400 to 600 volts. This transistor introduces a unique combination of increased power-handling capability, unusually-low saturation and switching losses, and submicrosecond switching speeds.

For years the transistor has been the basic building block for low-power electronics, and the thyristor has been the workhorse of the electrical power industry. As a result this new transistor will not only compete directly with the thyristor at high-power levels but has also stimulated applications where power transistors could not previously even be considered. The heart of this new transistor is a 23-mm-diameter, triple-diffused, silicon npn wafer, which is fabricated by using thyristor techniques. Figure 1 shows the wafer and several package configurations. The basis for the transistor design lies in blending triple-diffused silicon technology with interdigitated emitter/base structure on a monolithic wafer of large area. This permits large, efficient power handling, but retains submicrosecond switching speeds.

These transistors have a sustaining voltage of 400 to 600 volts and feature a gain of 12 at 50 amperes rated current. They can handle 100 amperes continuously and 200 amperes of peak current at reduced, but useful, gains. The high-voltage capability and large power-handling capacity, combined with the largest forward and reserve safe-operating-area (SOA) of any transistor on the market, give extremely rugged performance in high-energy circuits. Although large in size, the extremely fast switching speeds of the transistor (less than 0.5 microsecond) and low saturation voltage (less than 1.0 volt at rated current) allow reductions in the size and weight of associated circuit components and promote more efficient use of energy.

Figure 1. **Switching Power Transistor** combines triple-diffused silicon technology with an interdigitated emitter-base structure on a large-area monolithic wafer. Several possible packagings are shown above.

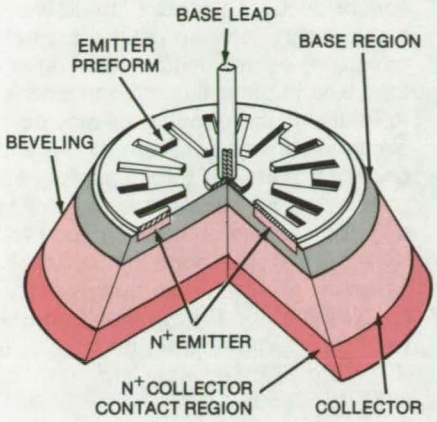

Figure 2. The **Elements of a High-Power Transistor** are shown in cross section (vertical scale expanded for clarity). The wafer thickness is typically 0.15 mm, the collector diameter of 23 mm, and the beveling angle 5° to 6° above the horizontal.

Figure 2 shows a schematic diagram of the transistor wafer. The basic diffusion and masking steps, alloying, and bevel-etch procedures are conveniently done on a thyristor-type assembly line. The compression-bonded encapsulation (CBE) developed for thyristors eliminates the usual problems of solder voids and emitter lead attachments that have plagued large-area transistors in the past.

By utilizing the processing and packaging techniques of the thyristor, the new transistor combines the high-power, ruggedness, and reliability advantages of the thyristor with the switching-speed and positive circuit-control advantages of the transistor. Thus all of the advantages are combined in the one device.

Using the thyristor-type processing and packaging techniques produces other desirable results, such as high yields, low production costs, and extremely reproducible characteristics. It also points the way to even larger area transistors with up to four times the effective emitter area that will handle four times as much power. This technology should lead to a family of power transistors that will find applications in increasingly higher power systems.

These transistors have already been successfully evaluated in power conversion circuits up to 10 kW in 20- to 50-kHz dc-dc inverters, control and drive systems for 17-hp dc motors, and 300-Vdc solid-state remote power controllers. Other potential applications include high-power switching regulators, linear amplifiers, chopper controls for high-frequency electric vehicle drives, VLF transmitters, RF induction heaters, kitchen cooking ranges, and electronic scalpels for medical surgery.

This work was done by D. Carnahan, C. K. Chu, and P. L. Hower of Westinghouse Electric Corp. for **Lewis Research Center.** *Further information may be found in NASA CR-135013 [N76-28470], "Development and Fabrication of Improved Power Transistor Switches," a copy of which may be obtained at cost from the New England Research Application Center* *[see page A7]*.

Inquiries concerning rights for the commercial use of this invention should be addressed to the Patent Counsel, Lewis Research Center *[see page A8]*. *Refer to LEW-13021.*

Simple Digital Pulse-Programing Circuit

A pulse-sequencing circuit uses only a shift register and Exclusive-OR gates.

NASA's Jet Propulsion Laboratory, Pasadena, California

It is sometimes necessary to generate a sequence of pulses having precise variable widths and delays. Multivibrators can be used in these applications, but have the drawback that they require precision outboard capacitors and resistors to maintain accurate time periods. They are also sensitive to temperature fluctuations. Certain all-digital circuits, such as recirculating shift registers and Johnson counters, can produce variable-delay pulses; however, these either do not give variable widths or require an initialization sequence.

The all-digital circuit shown in the figure, used extensively in the Viking Orbiter (1975) data-storage system, produces pulses of variable delays and widths, using only standard integrated-circuit Exclusive-OR gates and a serial-input/parallel-output shift register. The circuit also serves as a data-transition edge detector (for either rising or falling edges).

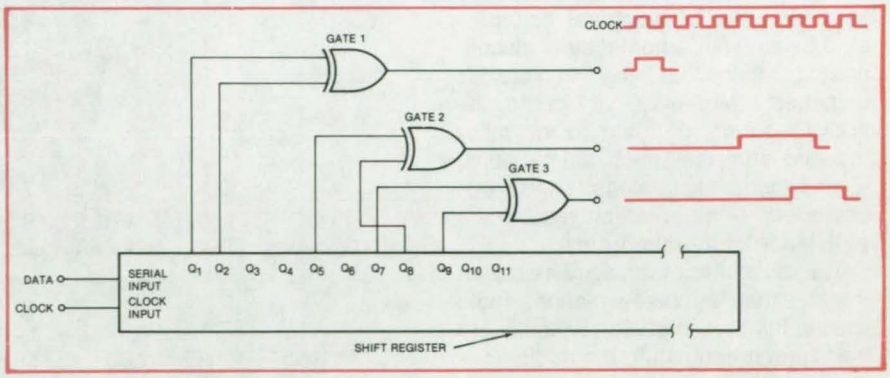

This **Pulse-Programing Circuit** uses only a shift register and Exclusive-OR gates. The pulse widths are determined by the propagation times of the data edge from the first tap location to the second tap location of each gate. The delays are determined by the propagation times from tap Q_1 to the first tap on each gate.

In this circuit, a transition at the data input triggers the sequence of pulses. The next transition is negative, but is not allowed to occur until N clock periods later, where N is the number of stages in the shift register. The shift register propagates the data edge at the clock rate.

The Exclusive-OR gates compare the states of different sections of the

(continued on next page)

shift register. When the two outputs monitored by a gate are different, the gate produces an output as long as the states are different. Hence, each gate produces a pulse delayed by the time corresponding to the propagation time of the data from the input to the first tap connection of the gate. The pulse width is determined by the propagation time of the edge from the first tap location to the second tap location of the gate.

As shown, gate 1 is connected between the first two taps Q_1 and Q_2 of the shift register. Therefore, the output of gate 1 produces a pulse beginning with the first positive clock transition following the data edge; its width is exactly one clock period, T.

The output from gate 2 is delayed with respect to the leading edge of output 1 by precisely four clock periods, and its duration is 3T. The third output is delayed two additional clock periods, and it has a duration 2T. The pulses can overlap partially or completely, depending on the relative positions of the gate connections along the shift register.

This circuit can be used in sample-and-hold and analog-to-digital conversion sequence control, multiphase-clock logic, precise delay control, computer control logic, edge detectors, and in other timing applications. In addition, the circuit can provide a simple means to generate timing and control signals for data transfer, for addressing, and for mode control in microprocessors and minicomputers.

This work was done by James L. Langston of Texas Instruments, Inc., for **NASA's Jet Propulsion Laboratory.** *For further information, Circle 1 on the TSP Request Card.*
NPO-13747

Automatic Circuit Interrupter

Audio circuits between space vehicle and ground are turned off automatically as vehicle is launched.

Lyndon B. Johnson Space Center, Houston, Texas

In a technique developed for the Space Shuttle Orbiter, the voice circuits connecting the crew's cabin to the launch station through the umbilical connector are used to disconnect automatically the unused, or dead-end, portion of the circuits immediately after the vehicle is launched. This eliminates the possibility that the unused wiring might interfere with voice communications within the vehicle and eliminates the need for a manual cutoff switch and its associated wiring.

The technique could also be applied to other types of electrical actuation circuits as well, automatically disconnecting them as the vehicle is launched. Moreover, it could be applied during the launch of other manned vehicles, such as balloons, submarines, test sleds, and test chambers — all of which require the assistance of a ground crew.

The disconnect technique relies on the fact that for noise isolation, audio lines in the launch station typically are transformer coupled to the audio lines in the space vehicle. The lines are terminated at each end in a center-tapped transformer. The null points provided by these center taps are used to complete through the audio lines themselves an independent circuit that operates a turnoff relay. This relay opens automatically and disconnects the audio lines leading to the launch station when the umbilical connector is disengaged at launch.

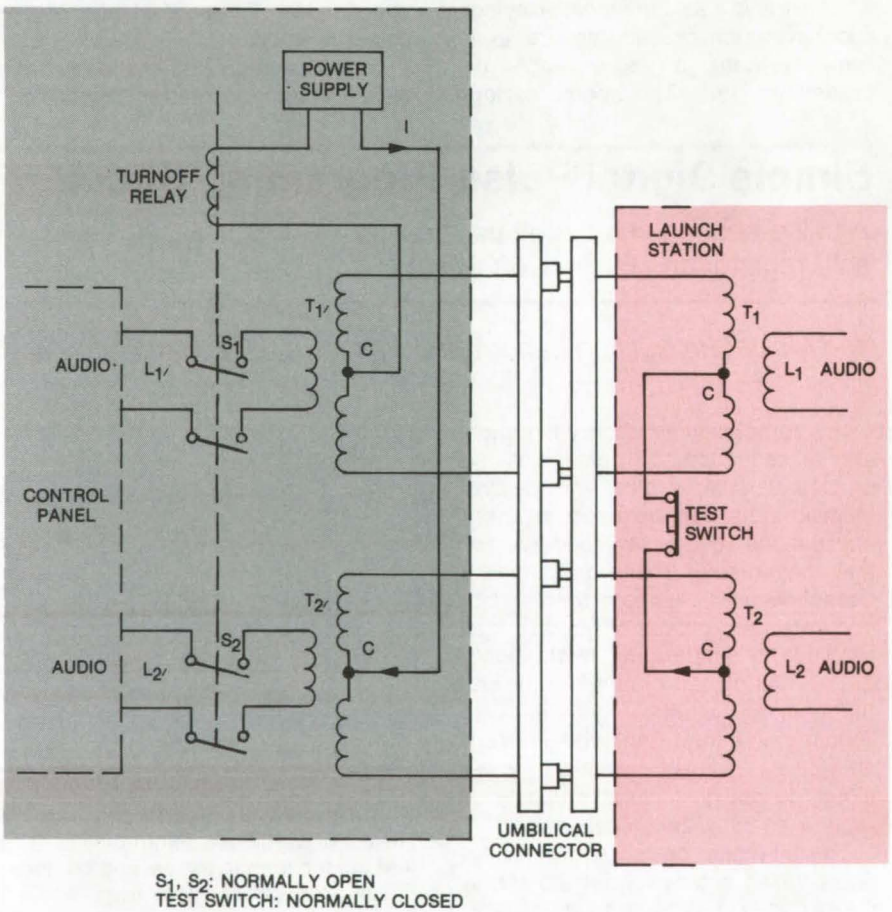

Switching Circuit for Audio Lines L_1' and L_2' passes through center-tapped secondaries of isolation transformers T_1, T_2 and T_1', T_2'. When the umbilical connector opens at launch, the turnoff relay is deenergized, opening switches S_1 and S_2 and disconnecting the audio lines automatically.

As shown in the schematic, audio lines L_1-L_2 and L_1'-L_2' are coupled through two pairs of center-tapped transformers. Normally-open switches S_1 and S_2 in the vehicle disconnect the lines from the transformers after the umbilical connector separates. These switches are closed before launch, their coil powered by an ac or a dc power supply. (A 6-V dc solid-state relay is being used on the Shuttle program.)

In the launch station on the ground, the center taps, C, of the transformers are interconnected by a low-impedance circuit that includes a manually-operated, and normally-closed, test switch. This launch-station circuit provides a continuous path for the switching circuit in the vehicle when the connectors in the umbilical connector are mated. Supply current, I, flows into the center tap of transformer T_2' and out the center tap of transformer T_2, through the closed test switch, and into the center tap of transformer T_1. The current then flows back to the vehicle, out the center tap of transformer T_1', and through the turnoff relay to the power supply.

With null points at the center taps, current I divides equally and flows in opposite directions through the secondary windings of the transformers. Thus, the current will not interfere with communications carried by the audio lines. At launch, the umbilical connector separates, opening the ground-station half of the switching circuit. This deenergizes the turnoff relay, opening switches S_1 and S_2. The result is to disconnect audio lines L_1' and L_2' from the then unused transformers T_1' and T_2' and from the associated wiring that could be the source of interference.

The manual test switch also makes it possible to test the switching system from the launch station before launch. Opening this switch simulates launch; the switching circuit opens, the turnoff relay is deenergized, and switches S_1 and S_2 open.

This work was done by William S. Dwinell of Rockwell International Corp. for **Johnson Space Center.** *For further information, Circle 2 on the TSP Request Card.*

This invention is owned by NASA, and a patent application has been filed. Inquiries concerning nonexclusive or exclusive license for its commercial development should be addressed to the Patent Counsel, Johnson Space Center [see page A8]. Refer to MSC-16697.

Easily-Wired Toggle Switch

Crimp-type connectors would reduce assembly (and disassembly) time.

Lyndon B. Johnson Space Center, Houston, Texas

A conceptual design for hermetically-sealed toggle switches makes the attachment of leads faster and simpler. The concept calls for crimp-type connectors instead of soldered connections.

The usual procedure for attaching and sealing the leads to a toggle switch is to clean the switch terminals, strip the insulation from the wires and clean and tin it, insert the wires into the terminal eyelets, bend the wires to hold them in place, solder the wires to the terminals, and finally, apply a primer and a conformal coating to protect against corrosion.

With the new design, no switch preparation is necessary. Socket contacts are merely crimped to the wires and inserted in a module attached to the back of the toggle switch. The sockets engage pins within the module to make the electrical connections. The wires are easily removed with a standard detachment tool.

A basic version of the concept (see figure) replaces the conventional terminal lugs on a toggle switch with the module having receptacles in which the socket contacts can be inserted.

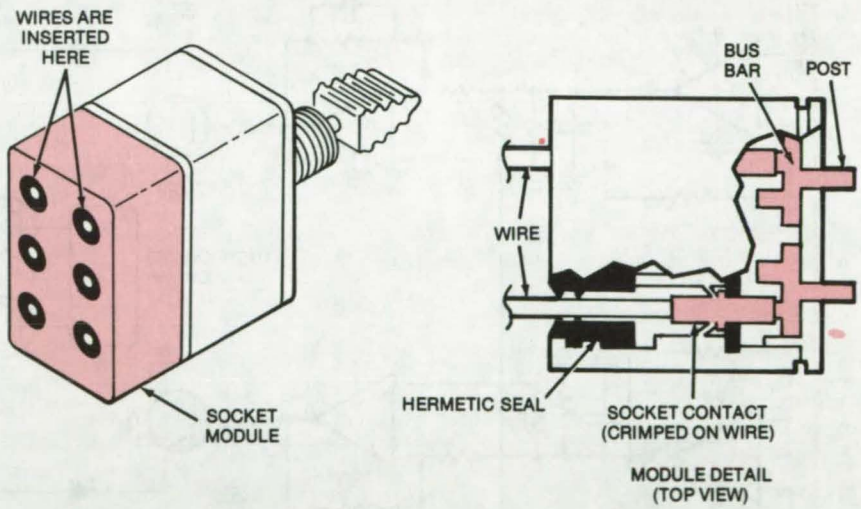

Hermetically-Sealed Modular Toggle Switch uses crimp connectors instead of the usual soldered terminals. The posts on the rear face of the module are used to make the electrical connections within the switch.

The outside dimensions of the modular switch could be the same as those of a conventional switch. Wire of virtually any gage can be accommodated in the new design, and as many terminals can be placed on the switch as the wire gage and switch dimensions will allow.

This work was done by William T. Dean and Eugene J. Stringer of Rockwell International Corp. for **Johnson Space Center.** *For further information, Circle 3 on the TSP Request Card.*

MSC-18102

Automatic Load Sharing in Inverter Modules

Active feedback loads transistors equally with little power loss.

NASA's Jet Propulsion Laboratory, Pasadena, California

An active feedback circuit balances the currents delivered by parallel inverters to a common load. The circuit compensates for differences in open-circuit voltage and internal impedance among the modules and ensures that individual modules and components are not overstressed.

The feedback circuit is suitable for balancing modular inverters in such applications as spacecraft, computer power supplies, solar electric-power generators, and electric vehicles. Modular inverters are becoming increasingly popular in such equipment because systems can be tailored to new requirements simply by the addition or removal of modules and because the current levels in the modules are within the capability of readily-available semiconductor devices.

Previous methods of balancing parallel inverters used a resistor as the output impedance for each module so that a short circuit on one module would not affect the others. These resistors greatly reduce the efficiency of the inverters. Another technique, employed in modular ac-to-dc converters, adjusts the duty cycle of each module according to differences in output current. But this method is not appropriate for inverters, which must operate at a fixed duty cycle of 50 percent. Until now, the only alternatives to series resistors were precise matching of saturation characteristics of the module power transistors or precise adjustment of the winding ratios of the output transformers to compensate for the differences in saturation characteristics.

The new current-balancing circuit senses the difference between the peak value of the collector current for each power transistor and the average value of the load currents for all

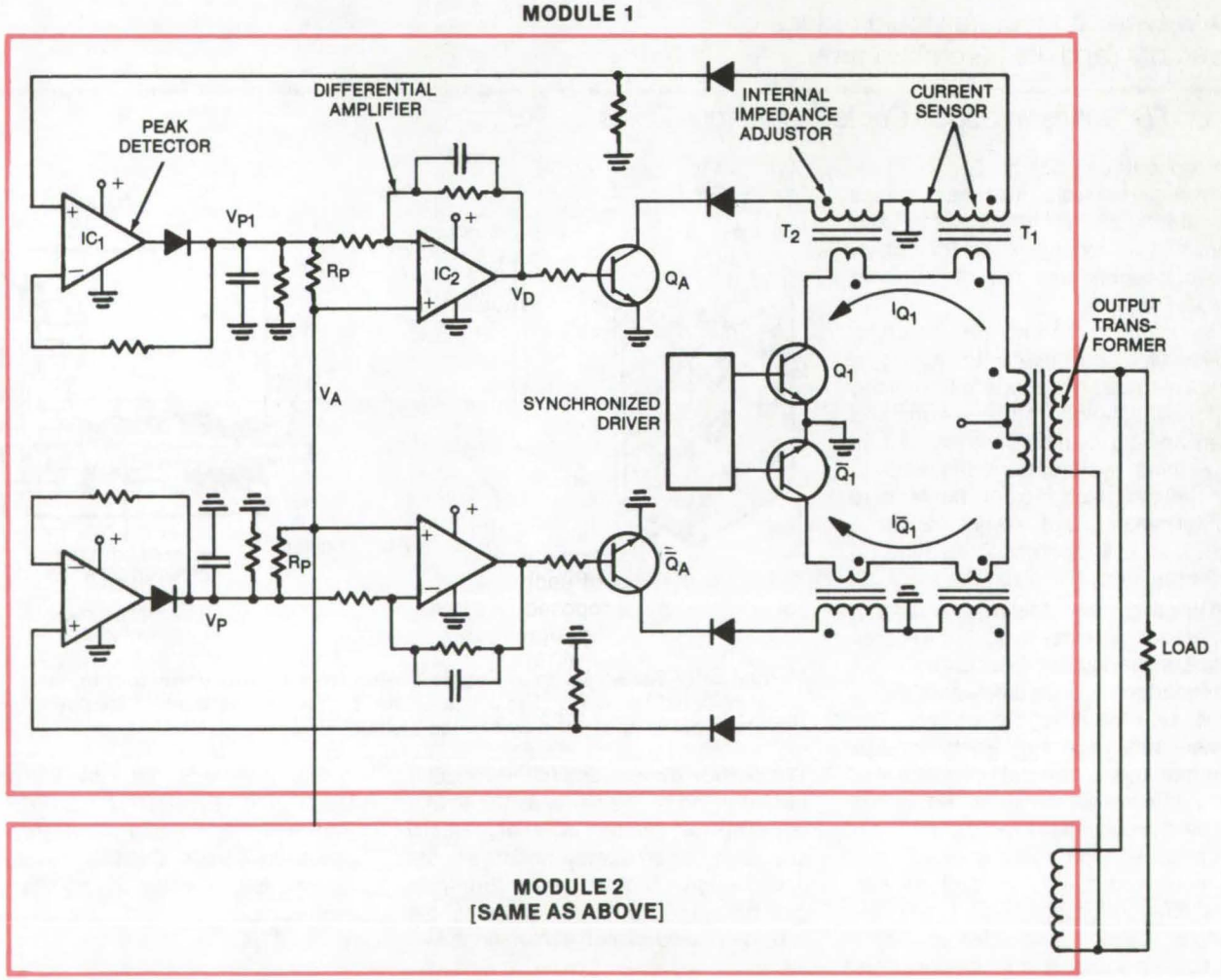

This **Two-Module Inverter** with active feedback shares current load equally between its modules. A four-module inverter, each module operating at 100 watts, has been built. The technique can be used for any number of modules at any power level.

the power transistors. The circuit then changes an impedance in the collector circuit to any transistor that carries too much or too little current; the impedance change adjusts the current to the average.

The figure shows the balancing arrangement for a two-module inverter (the principle is the same for any number of modules in parallel). The collector circuit of each power transistor contains two current transformers in series. One transformer (T_1) is the current-sensing transducer; the other (T_2) is the impedance adjuster.

Each current-sensing circuit (including T_1, a current-sensing resistor, and a diode) connects to a separate peak-detector circuit that consists of an operational amplifier (IC_1), a second diode detector, and a capacitor/resistor network with a peak-sensing resistor (R_P). This last resistor is connected across a differential amplifier (IC_2). The noninverting inputs of the differential amplifiers are connected together to produce the average value of the load currents, represented by the voltage V_A. This voltage serves as a reference at each of the differential amplifiers for comparison with the individual peak currents, represented by V_P.

If V_A is larger than V_{P1} — that is, if the collector current of transistor Q_1 is less than the average for all transistors — then the output of Q_1's differential amplifier goes positive, turning on transistor Q_A and making its emitter/collector impedance go low. This impedance reduction is reflected to the secondary winding of current transformer T_2; the collector circuit of Q_1 therefore has a lower impedance, so its collector current increases. Conversely, if V_A is lower than V_{P1}, the collector impedance of Q_1 goes higher, decreasing Q_1's current.

Because the collector currents of all the power transistors are controlled with reference to the average peak collector current, all are automatically set at the same peak level; therefore the total load is shared equally, each module operating with its output transistors balanced on each half cycle.

The additional impedance in each collector circuit is proportional only to the difference between the individual peak collector current and the average of all peak collector currents. This impedance becomes very small when all the collector currents are balanced, so additional power dissipation is also very low. This method also automatically balances the operation of the push-pull inverter within a module.

The principle is effective not only in fixed duty-cycle inverters but also in converters, which operate at variable duty cycles.

This work was done by Satoshi Nagano of Caltech for **NASA's Jet Propulsion Laboratory.** *For further information, Circle 4 on the TSP Request Card.*

This invention is owned by NASA, and a patent application has been filed. Inquiries concerning nonexclusive or exclusive license for its commercial development should be addressed to the Patent Counsel, NASA Resident Legal Office-JPL [see page A8]. *Refer to NPO-14056.*

Hall Devices Improve Electric Motor Efficiency

Asymmetric radial forces can be sensed and counteracted by Hall devices on the excitation or control windings.

Marshall Space Flight Center, Alabama

The efficiency of electric motors and generators can be reduced by radial magnetic forces created by asymmetric fields within the device. The major causes of this effect are gap or bearing asymmetries, poor electromechanical tolerances, and temperature and voltage variations.

A proposed method of compensating for these forces would employ Hall-effect devices on the surface of the excitation or control windings to sense the magnetic field that causes the asymmetry. The Hall outputs would drive a feedback circuit that controls current to the windings to counteract the unwanted magnetic forces.

In one suggested implementation, the Hall devices are connected in a bridge circuit, and pairs of sensors are used to obtain differential signals proportional to the radial flux distribution. The elements of each pair would be diametrically opposed for maximum sensitivity. The signals can be either quasi-steady, as in dc motors and torquers, or oscillatory, as in ac motors. Since the forces in the radial and tangential directions are a direct function of the flux density in the gap, the Hall generators would directly measure the forces and would provide compensating control of any asymmetry. No additional measurements would be needed for calibrating the feedback control loop.

This work was done by Walter Haeussermann of **Marshall Space Flight Center.** *For further information, Circle 5 on the TSP Request Card.*

Inquiries concerning rights for the commercial use of this invention should be addressed to the Patent Counsel, Marshall Space Flight Center [see page A8]. *Refer to MFS-23828.*

Improved Driver for Capacitive Loads

The standby power is reduced by using transistorized current sources instead of bias resistors.

Langley Research Center, Hampton, Virginia

In order to reduce the standby power consumed by a transistorized switch, bias resistors with large voltage swings can be replaced by transistorized current sources, and the bias currents can be reduced to a level where the beta of the devices is acceptable. This circuit innovation, which was originally designed for low-power row-and-column drivers in ferroelectric-addressed liquid-crystal matrix displays, should have other applications in circuits that drive pulsed capacitive loads.

The modified column driver is shown in the figure. Transistors Q_1, Q_2, Q_3, Q_4, and Q_5 are connected as a constant-current differential amplifier that is controlled by the input signal. If the input voltage is below the voltage at the base of Q_1, the current through resistor R_2 passes through Q_1 and drives transistors Q_6, Q_8, and Q_9 into full conduction.

Alternatively, if the input voltage is above the voltage at the base of Q_1, the current through R_2 passes through Q_5 and drives transistors Q_7 and Q_{10} into full conduction. Resistors R_7, R_8, and R_9 are used to limit the surge current below the maximum rating of transistors Q_8, Q_9, and Q_{10}. The blocks labeled N(OC) act as inverter switches that sweep out the minority carriers and also sink the leakage current of the transistors. The delay and storage times of the transistors are minimized by sweeping out the minority carriers, and the sinking of the leakage current allows a higher operating temperature for the devices without substantially increasing the power consumption.

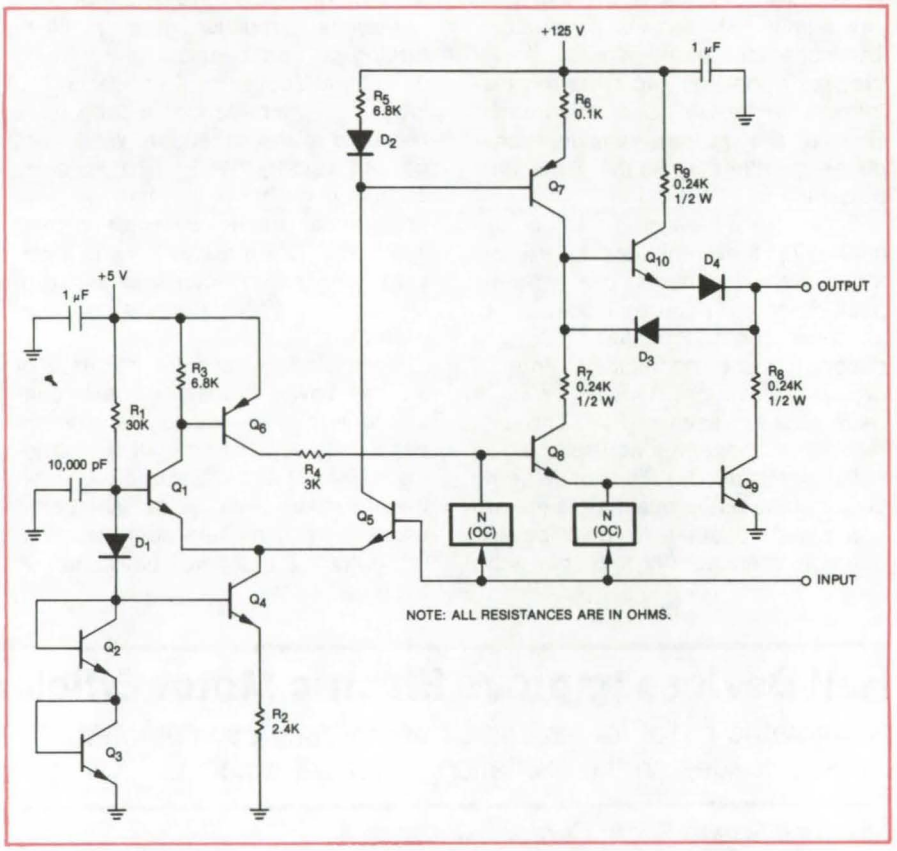

This Driver Circuit for Capacitive Loads utilizes transistorized current sources rather than bias resistors to reduce standby power.

A variation of the circuit, in which two inputs control a three-level voltage output, was developed as a row driver for the ferroelectric-addressed display. In another version, an additional transistor stage was added at the output to drive a higher capacitance load.

This work was done by Raymond T. Matsumoto of Rockwell International Corp. for **Langley Research Center.** *For further information, Circle 6 on the TSP Request Card.*
LAR-11609

Z-Axis Control Loop for Cathode-Ray Tubes

A PIN diode samples the brightness
to provide a z-axis error-control signal.

NASA's Jet Propulsion Laboratory, Pasadena, California

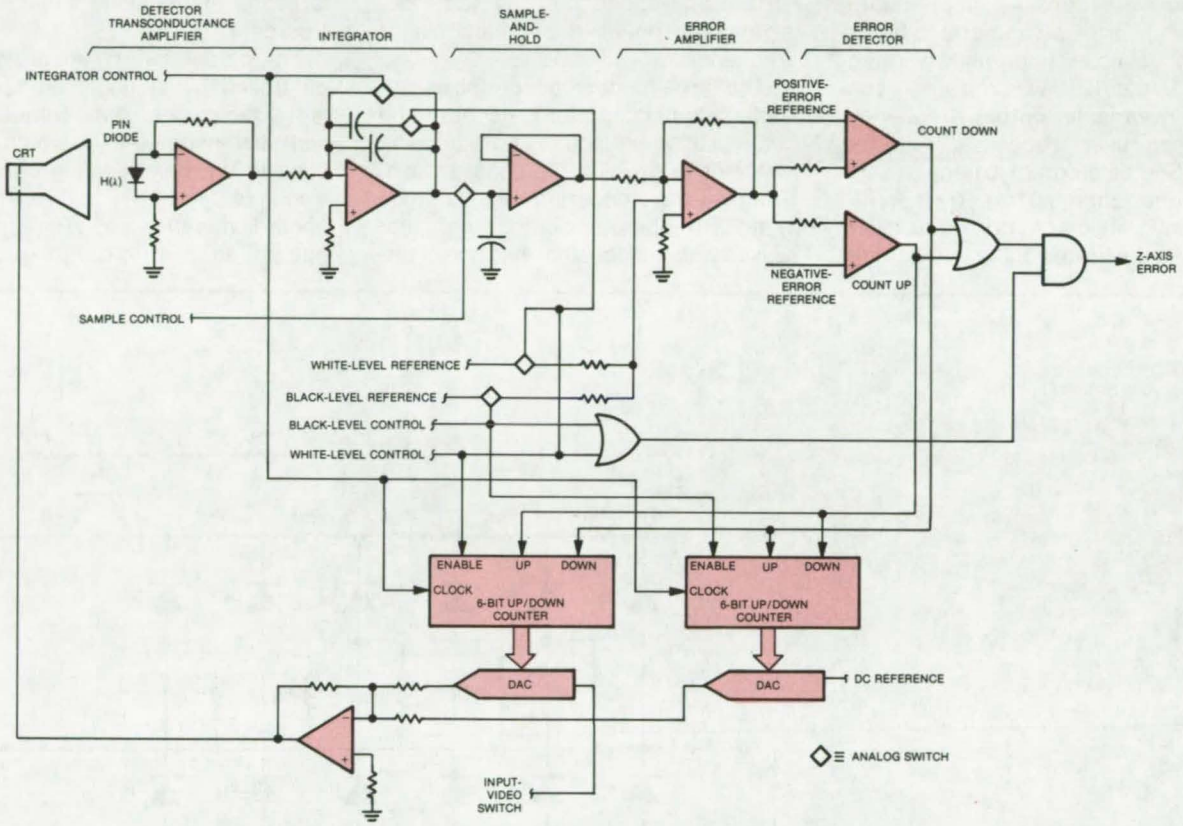

Z-Axis Control-Loop Circuit for a CRT is enabled between frames during the film-advance period. The white- and black-level controls determine whether a black-level or white-level scan is being done and place the appropriate reference voltage at the error-amplifier input. These two switches also enable white- and black-level up/down counters that control the digital-to-analog converters. The input video switch blanks the white-level DAC during the black-level scans.

The long-term light-output stability of a cathode-ray tube is affected by aging, electrical parameter changes, and its environment. If the CRT is the image source for a photograph, these factors can cause nonuniform film exposure and a loss of the recorded data. The CRT brightness and contrast can be adjusted manually, but this is time consuming and can lower the fidelity of the exposure densities. Closed-loop control methods that use a sensitive photodetector to monitor the light intensity are expensive and require additional optics to focus the CRT image onto the detector.

A new film recorder system overcomes these obstacles. An inexpensive PIN diode detector samples the screen brightness between each frame, to generate an error signal for feedback control of the intensity.

The system is diagramed in the figure. The CRT is raster-driven synchronously with the camera. During the film-advance period (when the video is normally blanked), the raster sequence is controlled to execute several black-level scans and then several white-level scans. The detector output is amplified and integrated during each complete scan. At the end of a scan, the integrator output is transferred to a hold circuit, and the integrator is reset. The hold-circuit output is summed with the appropriate level reference to generate an error input to a magnitude comparator. If the absolute value of the error is greater than the error limits, a countup or countdown signal is generated. The counter output is converted by a digital-to-analog converter into the z-axis control signal. If an error is detected in the black or white level, the control signal adjusts the dc offset or gain of the CRT video buffer driver to reduce the error.

The system has been tested by taking flat-field exposures at several density levels over a 4-hour test period. The processed-film density levels, as measured by a densitometer, were determined to vary by less than ±10 percent. Usually the variations were close to ±8 percent.

This work was done by Arthur J. Ray, Jr., of Ball Brothers Research Corp. for **NASA's Jet Propulsion Laboratory.** *For further information, Circle 7 on the TSP Request Card.*
NPO-13775

Three-Function Signal Generator

Variable-frequency circuit develops
sine, square, and triangular waveforms.

Lyndon B. Johnson Space Center, Houston, Texas

Three waveforms — sine, square, and triangular — are generated by the relatively simple circuit shown in Figure 1. This circuit, which gives a continuously-variable output frequency, has been used successfully in the Space Shuttle program to generate signals in the range 0.01 to 10 Hz for an electrohydraulic-actuator tester. By changing the values of the outboard resistors and capacitors, the same design could be used at much higher frequencies.

The three-function generator uses a variable-rate integrator to generate the triangular wave and a zero-crossing detector to develop the square wave. The sine-wave generator uses a diode matrix to operate on the triangular wave; with this design, harmonic distortion of the resulting output is below 1 percent.

The output rate of integrator U_1 is controlled by setting the "range select" switch and the "frequency adjust" potentiometer. This output is applied to the commutating circuit consisting of U_2, R_2, R_3, and R_4 and reference diodes VR_1 and VR_2. U_2 is configured as a zero-crossing detector

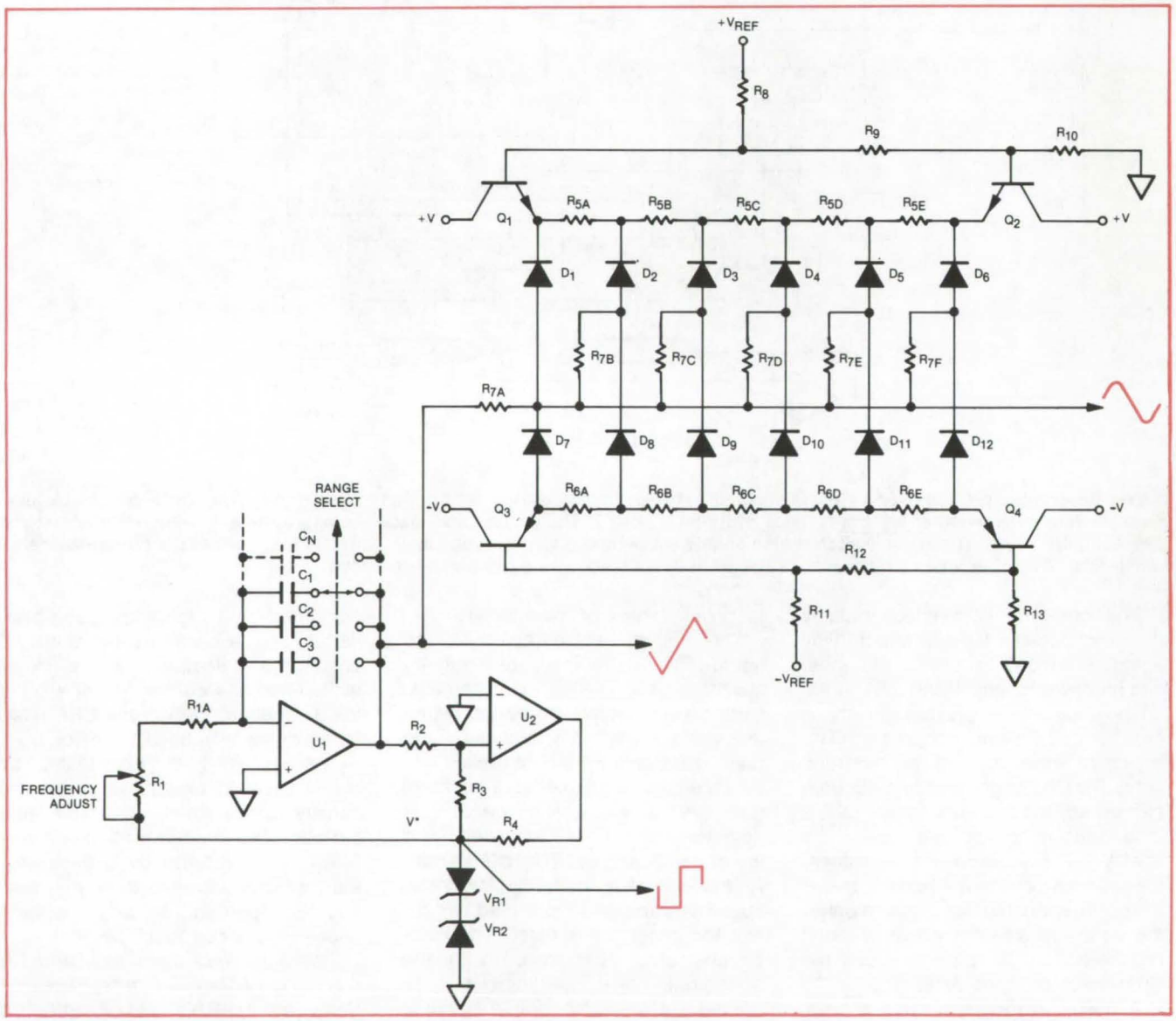

Figure 1. **Three-Function Generator** can be used for low or high frequencies.

$$F = \frac{1}{2R_1C_N(R_2/R_3)}$$

$$A_{square} = 2V^{*}(\text{PEAK TO PEAK})$$

$$A_{triangle} = 2(R_2/R_3)V^{*}(\text{PEAK TO PEAK})$$

$$\text{for } R_2 = R_3,\ A_{square} = A_{triangle}$$

Figure 2. Expressions for the **Frequency (F) and Amplitude (A)** of the square and triangular waveforms

with positive feedback. The output of U_2 is a square wave with its amplitude determined by the supply voltage and with its rise and fall times determined primarily by the slew rate of U_2. R_4 is a current-limiting resistor. Expressions for the output frequency and amplitudes are given in Figure 2.

The sine-wave generator operates piecewise linearly on the triangular wave. The diode network is symmetric about its centerline. Emitter/followers Q_1 through Q_4 establish the operating points. The voltage taps along the divider chain determine the breakpoints of the linear segments. The slopes of the segments are determined by resistors R_7. Since the synthesis of the sine wave is only a function of the input amplitude, the operating frequency can extend into the megahertz range.

This work was done by Gerald F. Kopp of Honeywell Inc. for **Johnson Space Center.** *No further documentation is available.*
MSC-16672

Power-Switch dV/dt Sensing

A simple means for controlling voltage risetime and powerline noise uses three transistors and capacitive feedback.

Lyndon B. Johnson Space Center, Houston, Texas

The rate of change (dV/dt) of the voltage across a load is reduced and controlled by the relatively simple circuit shown in the figure. In this circuit, Q_1 is a power-switching transistor, and Q_2, Q_3, and capacitor C form the control circuit. The controller limits the voltage risetime across the load and can also attenuate powerline noise at the load. This can reduce crosstalk and noise in tightly bundled wires.

Application of a turn-on command at the circuit input causes Q_3 to saturate and draw current I_3, determined by the emitter voltage of Q_2 and the value of R. When I_3 flows, a nearly equal current (I_2) flows in the collector of Q_2, which is connected in a common-base configuration. Current I_2 begins to turn on switch Q_1, but the change in load voltage appears across C and causes a current flow that supplies part of I_3 and reduces I_2. This limits the change in load current through Q_1. In addition, noise generated on the powerline will be attenuated at the load because it is dropped across Q_1 and Q_2.

The circuit should be useful where large wire bundles are subject to noise and crosstalk due to rapid current switching. It is presently included in hybrid power switches used extensively aboard the Space Shuttle.

This work was done by Robert L. Jones of Rockwell International Corp. for **Johnson Space Center.** *No further documentation is available.*
MSC-16707

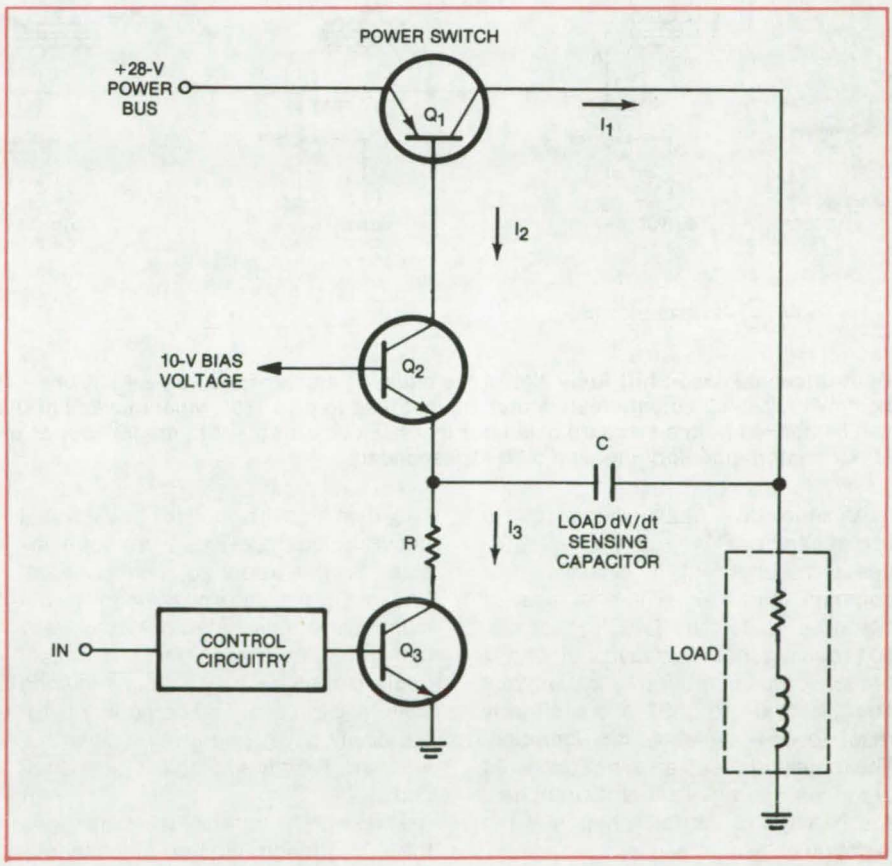

This **Power-Switch Controller** limits the voltage risetime across the load by generating a feedback signal through capacitor C. This controls current I_2 and the load current (I_1) through Q_1.

Phase-Shift Array, Arbitrary and Continuous Through 360°

New design simplifies multiple phase control.

Langley Research Center, Hampton, Virginia

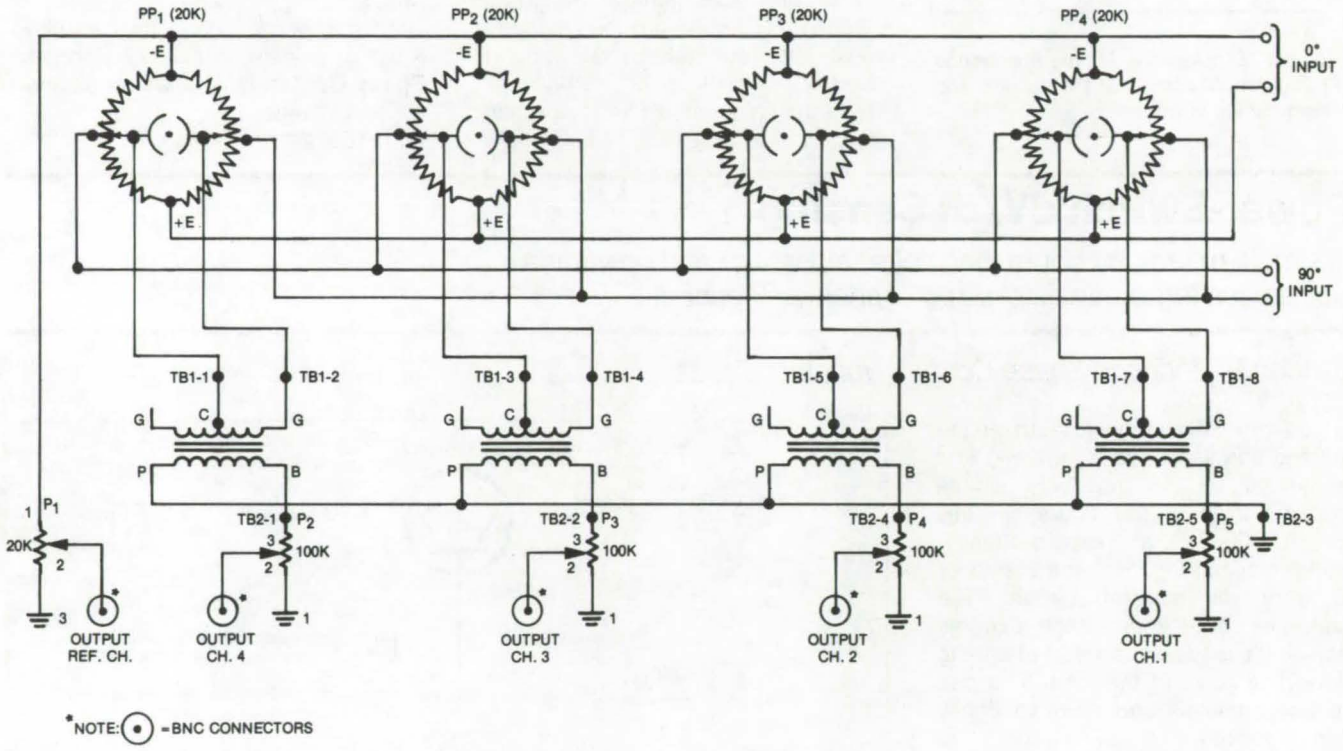

Four-Channel Phase-Shift Array allows the phase of any branch to be set anywhere between 0° and 360°. PP1 through PP4 are commercial 20-kΩ potentiometers that are modified to give 180° wiper movement (instead of 90°). The 0° and 90° signal inputs can be derived from a standard oscillator that has two outputs that are 90° out of phase. The output fransformers each have a 40-kΩ centertapped primary and a 10-kΩ secondary.

An innovative phase-shift array, in use at Langley Research Center, satisfies a requirement to phase-shift a common source signal into an array of branch circuits. The Langley application requires that the phase shift of any branch can be arbitrarily set at any angle from 0° to 360° and arbitrarily reset to any angle during operation. The largest of these arrays in use is 24 branches, the smallest is 4 branches. A schematic of the four-channel array is shown in the figure.

Although the design of the newly-developed phase-shift arrays was based on known principles of electrical networks, such devices were not available in the required configuration. Previously-available phase-control designs were unsatisfactory, generally being frequency-sensitive and phase-angle limited (±180°), thus requiring switching circuits. The components for the newly developed arrays, nevertheless, are readily-available off-the-shelf items.

Phase-shift control is continuous from 0° through 360° on all channels, with a precision-controlled operating range of 0 to 10 volts at frequencies covering the entire audio spectrum. The system wiring and assembly are uncomplicated, no switching networks are required, and the system can be operated at any desired frequency, being insensitive to frequency variations. This design appears to provide a simple and effective solution to the problem of multiple phase-shift control.

This work was done by Andrew C. Dibble, Jr., and Robert E. Grandle of **Langley Research Center.** *No further documentation is available.*
LAR-12272

Implementing OQASK by Using MSK

New concept would simplify the implementation of an offset quadrature amplitude-shift-keyed signal.

NASA's Jet Propulsion Laboratory, Pasadena, California

A new concept would simplify the hardware needed to implement offset quadrature amplitude-shift-keyed (OQASK) modulation when encoding digital information for transmission. Unlike other approaches, the new scheme combines minimum-shift-keyed (MSK) signals to shape the spectrum of the transmitted signal, instead of using analog modulators or band-pass filters. Although it was originally developed for deep-space radio transmission, this concept should find applications in other bandwidth-constrained systems and in digital radio communications in general. It should be particularly useful in high-volume data transmission as a means of encoding and decoding; for example, it could be used in modems similar to those that now prepare data signals for transmission.

Offset quadrature phase-shift-keyed (OQPSK) systems permit the bandwidth of the carrier synchronization loop to be doubled without increasing the signal-to-noise ratio or probability of error. In addition, the spectrum of a filtered OQPSK signal retains its band-limiting characteristics after the signal has been passed through a nonlinear (hard-limiting) channel. Similar qualitative results apply to OQASK.

Ordinarily, OQASK modulation is done with rectangularly-shaped symbol pulses. Therefore the resulting spectra have poor rolloff characteristics because of the sharp discontinuities in the modulated carrier waveform at points where data transitions occur. It is conceivable that baseband pulse shaping could be used to prevent such discontinuities, but in that case, an analog modulator would be needed instead of a simple digital modulator. The new system would avoid these difficulties by using half-cycle sinusoids instead of conventional rectangular symbol pulses.

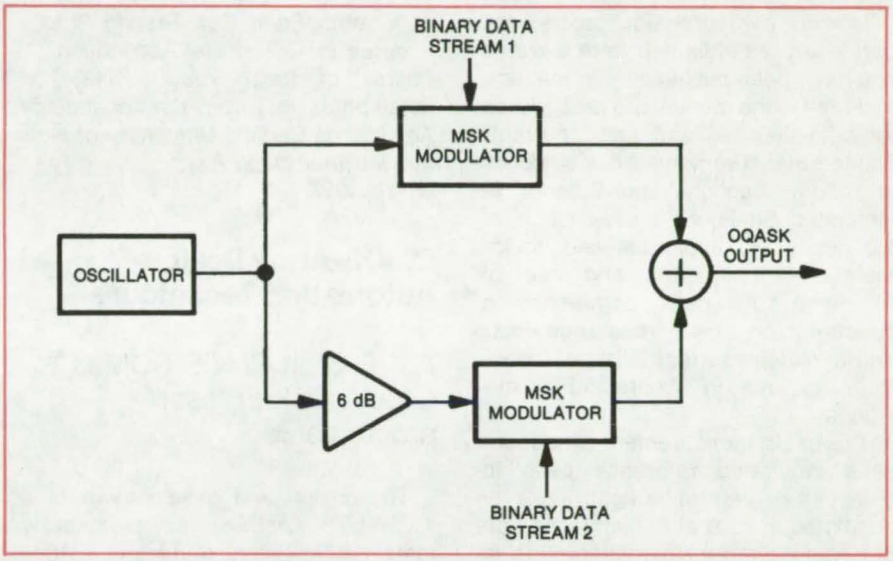

Two Minimum-Shift-Keyed Signals can be combined to create the equivalent of an offset quadrature amplitude-shift-keyed waveform except that half-cycle sinusoids are used instead of rectangular symbol pulses.

In particular it is possible to show that an OQASK waveform with half-cycle sinusoidal pulse-shaping is mathematically equivalent to the sum of two MSK signals that differ in power by 6 dB. These two signals can be generated by frequency-modulating the same oscillator with two independent binary data streams. A transmitter of the form shown in the figure could be used to generate the OQASK signal. A conventional MSK receiver could be modified to decode the received signal.

The two-component MSK signal can be generalized to n components for comparison with an equivalent OQASK signal. In this case the kth component k = 2, 3, . . . n would have an amplitude that is 2^{k-1} times that of the first component.

This work was done by Marvin K. Simon of Caltech for **NASA's Jet Propulsion Laboratory.** *For further information, Circle 8 on the TSP Request Card.*
NPO-13896

Books and Reports

These reports, studies, and handbooks are available from NASA as Technical Support Packages (TSP's) when a Request Card number is cited; otherwise they are available from one of NASA's Industrial Application Centers or the National Technical Information Service.

Terrestrial Photovoltaic Measurements

Revised measurement and calibration procedures

Proceedings and measurement procedures are now available from the second Terrestrial Photovoltaic Measurements Workshop jointly sponsored by the former Energy Research and Devlopment Administration (ERDA), now the Department of Energy, and the National Aeronautics and Space Administration (NASA). Building upon the results of the first such conference, the second workshop utilized further experience gained in solar-cell

(continued on next page)

research to define and to explore the additional measurement needs of the photovoltaic community. This second workshop was structured around three topics that were considered to be of major import: (1) terrestrial solar irradiance, (2) solar simulation and reference cell calibration, and (3) cell and array measurement procedures.

Interim measurement procedures previously established were revised and have been published in a manual. Included in the manual are procedures for obtaining cell and array current-voltage measurements both outdoors in natural Sunlight and indoors in simulated Sunlight, a description of the necessary apparatus and equipment, the calibration and use of reference solar cells, comments on concentration cell measurements, and a revised terrestrial solar spectrum for use in theoretical calculations.

The basic measurement procedure uses calibrated reference cells to establish or determine light levels of simulated or natural Sunlight; the use of pyranometers or pyrheliometers is discouraged. The absolute irradiance scale, to be adopted as soon as possible, will be the scale defined by the PACRAD III type of radiometer. Standard atmospheric conditions have been defined as: irradiance 1,000 W/m^2, temperature 28 ° C, air mass 1.5, water content 2 cm, and turbidity 0.5. Acceptable light sources for solar simulation are short-arc xenon lamps, pulsed xenon lamps, and dichroic-modified 3,400 K tungsten lamps.

This work was done by Henry W. Brandhorst, Jr., and Henry B. Curtis of **Lewis Research Center.** *Further information may be found in:*

NASA CP-2010 [N77-30521], "Terrestrial Photovoltaic Measurements II" [workshop proceedings],

NASA TM 73788 [N78-14629], "U.S. Terrestrial Solar Cell Calibration and Measurement Procedures," and

NASA TM 73702 [N77-29603], "Terrestrial Photovoltaic Measurement Procedures."

Information on the first "Terrestrial Photovoltaic Measurements Workshop," announced in NASA Tech Briefs, Fall 1976, Vol. 1, No. 3, p. 375 [LEW-12643], may be found in:

NASA TM-X-71802 [N76-71615], "Terrestrial Photovoltaic Measurements — Workshop Proceedings," and

NASA TM-X-71771 [N75-30650], "Interim Solar Cell Testing Procedures for Terrestrial Applications."

Copies of these reports may be obtained at cost from the Technology Application Center, University of New Mexico [see page A7].

LEW-13057

CMOS-Array Design-Automation Techniques

A 4,096-bit CMOS ROM is either mask or laser programable.

The design and development of a 4,096-bit CMOS (complementary metal-oxide semiconductor) ROM (read-only memory) are detailed in a report that is now available. The chip, which uses silicon-on-sapphire (SOS) technology, is organized into 512 words by 8 bits and is programable either at the metal-mask level during fabrication or by a directed laser beam after processing. The chip operates with a single supply voltage of from 3 to 15 V. At 10 V, its worst-case address time is 126 ns; chip-select access takes 44 ns. The average static power dissipation is 3 μW per bit at 10 V.

The chip is housed in a 24-pin package. In addition to address lines, there are four chip-select lines (for compatibility with existing bipolar ROM's) that control the eight output drivers.

Each of the eight outputs is a tristate configuration. The tristates are preferred to open-collector outputs since they can be designed in CMOS without appreciably increasing the chip area; they also reduce power consumption by eliminating the need for pull-up resistors. Current spiking, which can occur when two or more tristates turn on simultaneously is reduced by the higher "on" resistance of the CMOS devices. The CMOS tristate outputs can drive capacitive loads of from 40 to 80 pF and still maintain the target speed.

The chip is programed by altering the next-to-last (sixth) mask in the fabrication process. This is followed only by a mask that opens holes in the passivation layer. Thus, most of the processing is complete before the metal programing mask is used to define a unique chip. Consequently, many wafers could be partially processed before specific ROM patterns are defined, reducing the turnaround time.

An alternative to metal-mask programing is a directed laser beam. SOS technology is ideally suited to this approach because the epitaxial silicon islands that form transistors in the memory array are normally separated from one another by the sapphire substrate. Sapphire acts as a fine surface on which to cut metal lines with a laser without damaging the active transistor semiconductor. Numerous cuts through the metal interconnects, using a 1,200-nm-wavelength laser beam, have not affected transistor performance.

The 34-page report is divided into six sections plus an appendix. Section 1 deals briefly with background and a discussion of ROM chips. Section 2 describes design goals for this chip; its implementation is detailed in section 3. Chip statistics, conclusions, and recommendations are presented in section 4 through 6; and detailed information for locating the programing links is provided in the appendix.

This work was done by A. Feller and T. Lombardi of RCA Corp. for **Marshall Space Flight Center.** *Further information may be found in NASA CR-150221 [N77-78784], "CMOS Array Design Automation Techniques," a copy of which may be obtained at cost from the New England Research Application Center [see page A7].*

MFS-23762

Electronic Systems

Hardware, Techniques, and Processes

Automatic Acquisition and Ranging System

Digital circuitry automatically demodulates received radio-frequency ranging signals for phase comparison with the transmitted signal.

NASA's Jet Propulsion Laboratory, Pasadena, California

A new all-digital system automatically demodulates and correlates square-wave-modulated ranging signals. The received IF carrier is digitized in an analog-to-digital (A/D) converter and is fed into an accumulator. There, with the aid of a computer, weighting coefficients and the phase of the range code (with respect to the transmitted reference) can be computed. The computer controls the system integration times, so that its bandwidth can be adjusted for each application. In addition, the system continuously monitors the phase and adjusts itself for optimal demodulation. All-digital circuitry makes the system more stable than its analog predecessor and makes automatic operation easier and simpler.

In the NASA Deep Space Network, for which the system was originally developed, a 10-MHz IF signal is digitized at 40 MHz by the 4-bit A/D converter (see figure). Sampling is precisely controlled by a coherent 40-MHz pulse so that four equally spaced samples are taken at the same phases on sequential cycles of the 10-MHz signal. The samples, representing the amplitude of the IF carrier, are added or subtracted in the accumulator. The choice of addition or subtraction is determined by a control function **A** composed of the receiver coder output **R,** a coherent 10-MHz square-wave **Y,** and a chopper signal **C** according to the relationship

$$\mathbf{A} = \mathbf{R} + \mathbf{Y} + \mathbf{C}$$

When **A** is a zero, the new sample is subtracted in the accumulator; and when it is a one, the sample is added.

The accumulator hardware is duplicated in a second channel, except that the receiver coder output is shifted with respect to the output in the other channel by 90°. Thus, the two accumulators provide the in-phase and quadrature signals needed to determine the delay of the range code.

Since there are four samples during each 10-MHz cycle, the phase of the 10-MHz reference with respect to the 10-MHz IF signal can be determined. Weighting coefficients for each of the four samples can be computed and used to adjust the samples according to the particular phase relationship.

The computer receives the accumulated data from each of the four phases and first computes the weighting coefficients. Then the computer uses data representing in-phase and quadrature correlation voltages to compute the phase of the range code.

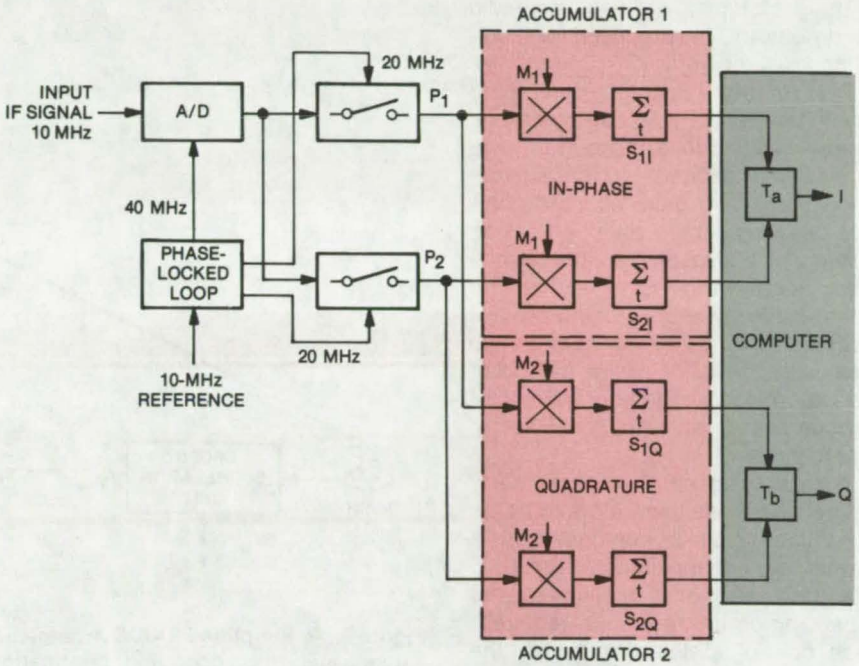

The **Returned Code is Compared to the Transmitted Code** in this all-digital demodulator/correlator. The A/D converter output is coherently sampled with the 10-MHz reference. The samples are routed to the paths P_1 and P_2 (two samples to each path) and are multiplied by signals M_1 and M_2 derived from the 10-MHz reference. The multiplier outputs are integrated to yield the signal correlation functions I and Q.

This work was done by Richard M. Goldstein, William P. Hubbard, James W. Layland, Warren L. Martin, and Arthur I. Zygielbaum of Caltech for **NASA's Jet Propulsion Laboratory.** *For further information, Circle 9 on the TSP Request Card.*

This invention is owned by NASA, and a patent application has been filed. Inquiries concerning nonexclusive or exclusive license for its commercial development should be addressed to the Patent Counsel, NASA Resident Legal Office-JPL [see page A8]. Refer to NPO-13982.

Air-Traffic Surveillance Systems

Passive ground-based radio-interferometry systems monitor local air traffic.

NASA's Jet Propulsion Laboratory, Pasadena, California

Three systems, all based on radio interferometry, are proposed for monitoring local air traffic.

The simplest radio-interferometric locating system (RILS) can determine aircraft position in a plane (i.e., two dimensions) defined by the surveillance area. Two pairs of interferometer stations are positioned along orthogonal edges of the surveillance area, as shown in Figure 1. The first pair scans hyperbolic surfaces of revolution overlaying the map of the area, with the stations being the foci of the hyperboloids. The second pair of stations covers an orthogonal set of hyperboloids.

Aircraft flying within the area carry inexpensive noise generators to transmit unique signals comprised of a normal voice channel approximately 5 kHz wide and one or two spurts, depending on the resolution required. Each pair of stations time-tags the received signals and directs them to a central location for cross-correlation. Information from one station determines a series of possible aircraft positions on a hyperbolic arc; similar information from the second pair defines a second hyperbolic arc that intersects the first arc to yield the aircraft position within approximately 20 ft (6 m) in a horizontal plane.

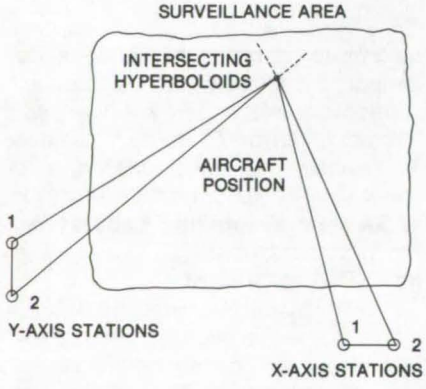

Figure 1. A **Two-Dimensional RILS** covers a plane surveillance area. The system incorporates two pairs of orthogonally-positioned interferometer stations that receive signals from the aircraft. The stations time-tag the incoming signals and direct them to a central processing facility that determines the position of the aircraft at the intersection of two hyperboloids.

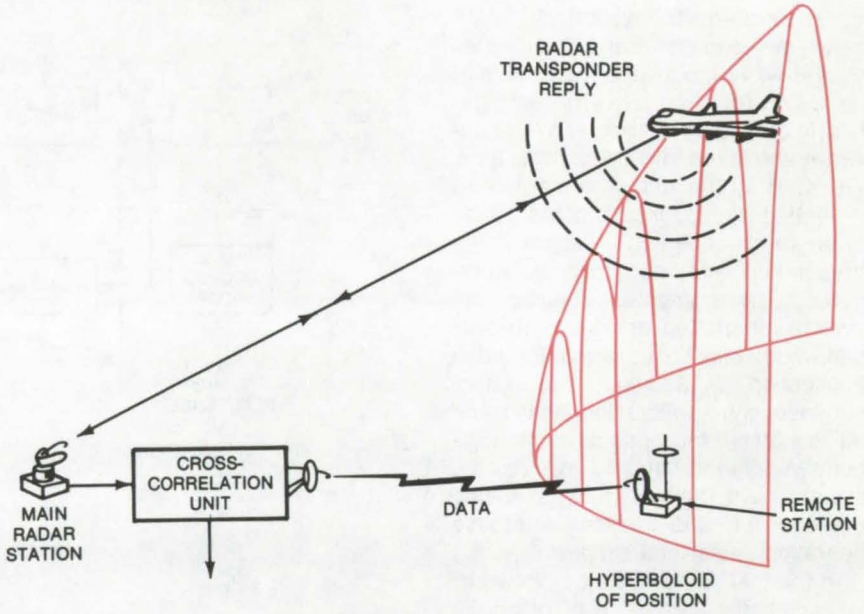

Figure 2. A **Simplified RAIDS Arrangement** is shown with one of a series of remote antenna stations in operation. Information from the cross-correlation unit is fed to a computer to determine the three-dimensional position of the aircraft.

A similar RILS arrangement may be used to determine aircraft positions in three dimensions. This more elaborate version includes a third pair of stations located at an altitude approximately 2,000 ft (610 m) above the other two. The intersection of three hyperbolic arcs identifies the three-dimensional aircraft position.

Finally, a third variant on RILS is RAIDS or Radar Altitude Information and Detection System that is more suitable for commercial aviation (see Figure 2). The technique utilizes the transponder beacon existing in most aircraft, but the signal is received in a slightly different way.

The RAIDS includes a conventional surveillance radar that functions in the usual way for determining the azimuth and range of aircraft. In addition, a series of small narrow-acceptance-beam omnidirectional antenna stations is spread in azimuth pattern around the central surveillance facility. These stations determine the difference in arrival times of the radar transponder signals. The hyperbolic surface that the aircraft must lie on is obtained from these differences. This information, when combined with azimuth and range information obtained by radar, helps to determine the three-dimensional aircraft position without expensive encoding altimeters.

This work was done by Peter F. MacDoran of Caltech for **NASA's Jet Propulsion Laboratory.** *For further information, Circle 10 on the TSP Request Card.*

This invention is owned by NASA, and a patent application has been filed. Inquiries concerning nonexclusive or exclusive license for its commercial development should be addressed to the Patent Counsel, NASA Resident Legal Office-JPL [see page A8]. Refer to NPO-14173.

Optimizing Multislot Feeds for Reflecting Antennas

The number of variables can be reduced by considering symmetry and the corrective effect of each phase mode.

NASA's Jet Propulsion Laboratory, Pasadena, California

A multislot feed can be used to correct for phase errors in reflecting antennas. Such errors, which can arise because of departures from true curvature in the reflecting dish, can be cancelled by adjusting the phases of the signals from the individual slots. The problem of calculating the correct phase angles while optimizing main-beam efficiency is a complex task that requires the computation and integration of the antenna pattern, for different phases and amplitudes of the elements.

The computation can be simplified by an analysis that has been used in designing a 19-slot feed for a (2.695-GHz) parabolic torus reflector (parabolic in one plane and circular in the orthogonal plane) used aboard the Space Shuttle. If this array had to be optimized directly, it would have required solving for 36 degrees of freedom (38 phases and amplitudes, minus 2 references).

To make the problem tractable, the array was visualized as producing seven beams, each illuminating a portion of the reflector (see figure).

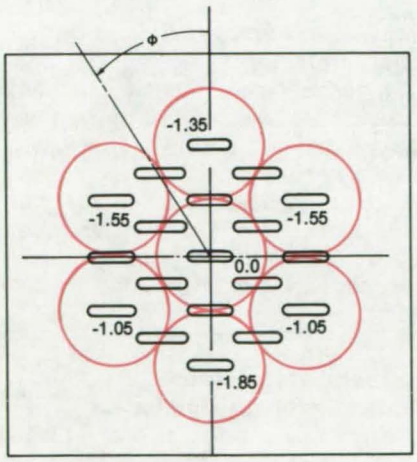

Radiation From a 19-Slot Array is visualized as seven beams illuminating the parabolic torus reflector. The optimized phase of each beam relative to the center beam is shown. (Phase angles are given in radians.)

Order	Type	Expression	Dominant Effect
0	Even	$\Phi = \Phi_0$	Focus Correction
1	Even	$\Phi = \Phi_1 \cos \varnothing$	Elevation Scan
1	Odd	$\Phi = \Phi_2 \sin \varnothing$	Azimuth Scan
2	Even	$\Phi = \Phi_3 \cos 2 \varnothing$	Principal-Plane Astigmatism
2	Odd	$\Phi = \Phi_4 \sin 2 \varnothing$	Diagonal-Plane Astigmatism
3	Even	$\Phi = \Phi_5 \cos 3 \varnothing$	Third-Order Phase

Phase Modes and Their Effect in the seven-beam antenna

The amplitude of each outside beam was set at -8 dB relative to the center to give an aperture illumination of the required shape. The scan angle of each outer beam was 21° from broadside. An amplitude distribution that gave a side-lobe level of -25 dB for the individual beams was used.

If the phase of the center beam was arbitrarily set at 0°, the phases of the remaining beams would leave six degrees of freedom to be optimized. Even if symmetry is considered to reduce the number of variables, there would still be four degrees of freedom left, too many to be easily solved.

The six degrees of freedom can be identified with the phase modes of the six outer beams, as shown in the accompanying table.

The odd modes can be eliminated by considering the symmetry of the reflector. The order 1 even mode can be eliminated because it primarily corrects for the scan angle of the beam. (In the Space Shuttle antenna the beam did not have to be at a particular angle above the horizon.) The order 2 even mode can be eliminated from preliminary calculations, since little astigmatism was found in phase plots for a simple feed. Therefore, only focus and third-order phase errors — two degrees of freedom — had to be considered.

The optimum third-order correction was only 0.25 radian. The focus correction was a tradeoff between main-beam efficiency and beamwidth. With 1.4 radians of focus correction, the effective aperture size is slightly over 1.6 meters, and the efficiency of the main beam is 91.64 percent. A final correction for astigmatism was made; 0.2 radian of astigmatism correction gave a slight decrease in beamwidth at the expense of 0.11 percent in efficiency.

The optimized 19-slot array had an efficiency of 93.18 percent, as compared to only 84.81 percent for a simple four-dipole feed. Gain was 31.61 dB, as compared to 30.84 dB for the simple feed.

This work was done by Douglas K. Waineo of Rockwell International Corp. for **NASA's Jet Propulsion Laboratory.** *For further information, Circle 11 on the TSP Request Card.*
NPO-14064

28-Bit Serial Word Simulator/Monitor

Modular interface expedites variable-word-length communication between computers.

Lyndon B. Johnson Space Center, Houston, Texas

A modular interface unit, developed for serial communication between 28-bit Manchester-coded computers aboard the Space Shuttle and a remote 16-bit minicomputer, transfers data at high speed along four channels. The compact unit occupies only 5 vertical inches of rack space, and features variable word and message lengths and has flexible formatting and control functions. Its operation, under software control by the minicomputer, eases the exchange of bit information by automatically reformatting coded input data and status information to match the requirements of the output. The unit can operate concurrently with other programs running on the minicomputer.

Specific features of the interface include:

- variable word length from 1 to 32 bits,
- variable message length from 0 to 65,535 words,
- relocatable addressing,
- direct memory access (DMA) transfer of data,
- detecting of parity and transmission errors,
- "suction pump" capability, and
- variable read/write-mode control-field decode.

The Serial Word Simulator/Serial Word Monitor (SWS/SWM) is controlled in three basic sequences of commands. Each sequence is initiated by loading an accumulator with a sequence-select code and issuing a "data-out" command. Sequence 1 is used to set up the command word. Sequence 2 is used to set up the starting address of the minicomputer and/or the word count (the number of words to be transferred). Data transfer is initiated in sequence 3, along with other optional modes, such as a "status-inhibit" mode.

Normal operation of the interface in an input/output mode to transfer data from a buffer location in the memory of the minicomputer would begin with the setup of the data words in the buffer. The interface would then proceed through sequence 1 and set up the command-word register. Next, in sequence 2, the starting address and word length would be loaded into the interface. Data transfer (sequence 3) would follow. When the interface completes the data transfer, it generates an interrupt. The programer can then interrogate the interface for transmission errors, word count, and other information.

In the Shuttle system, each 28-bit word on the Manchester bus is loaded during two memory accesses. In the first access, 16 bits of data are retrieved from the data section of memory and are loaded into bits 9 to 24 of a register in the interface. In the second access, bits 4 to 8 (the interface-unit address) and bits 25 to 27 (error-check bits) are retrieved from a status memory block displaced by 1,024 words from the data block. Bits 1 to 3 are a synchronization code, and bit 28 is a parity bit.

This work was done by James W. Durbin of Rockwell International Corp. for **Johnson Space Center.** *For further information, Circle 12 on the TSP Request Card.*
MSC-16418

Signal-Interleaving Device

A new cubic interleaving device combines and duplicates optical, electronic, and other energy-carrying signals. The interleaver consists of many flat, square, energy-carrying layers. When combined with optical AND or OR gates, it can form multiple-input gates, logic arrays, flip-flops, and memory cells.
(See page 344.)

Wideband EMG Telemetry System

A wideband electromyographic telemetry system monitors the gaits of people suffering from cerebral palsy. The system consists of miniature, crystal-controlled RF transmitters located at each electrode site of the patient's body. The transmitters have a linear response of from 20 to 20,000 Hz and an operating range of 15 m.
(See page 394.)

Automated Chromosome Analysis

A minicomputer-controlled system analyzes blood samples automatically and displays the characteristics of a cell nucleus. It includes a specimen preparation unit and an automated microscope. Blood samples are placed on slides, stained, and fed into the microscope. The results are digitized and displayed.
(See page 383.)

Processing Multispectral Signals From a Discrete-Sensor Array

A technique for encoding and decoding color-image signals from an array of discrete sensors can simplify the fabrication of a remote-sensing imaging system. The imaging system projects the output on a charge-coupled-device array. A computerized matrix decoding scheme decodes the image.
(See page 457.)

Modulation Improves Electro-optic Object Detector

An optical detector that senses the presence or absence of silicon wafers on an integrated circuit is insensitive to interference from ambient light. The wafers are detected by reflected light, using a modulated light-emitting diode and logic circuit. The sensing circuit responds only to the modulated signal.
(See page 402.)

Microprocessor-Based Cardiopulmonary Monitor

A modified cardiopulmonary diagnostic system has been reduced in size, and its power requirements have been cut from 1,000 to 100 W. The system utilizes a microprocessor to control pulmonary tests and physiological time-constant/pulmonary blood-flow tests. Recorded data are displayed on a printer and a video monitor.
(See page 388.)

Portable Data System

A compact system for data recording, manipulation, and transmission uses readily available components.

Ames Research Center, Moffett Field, California

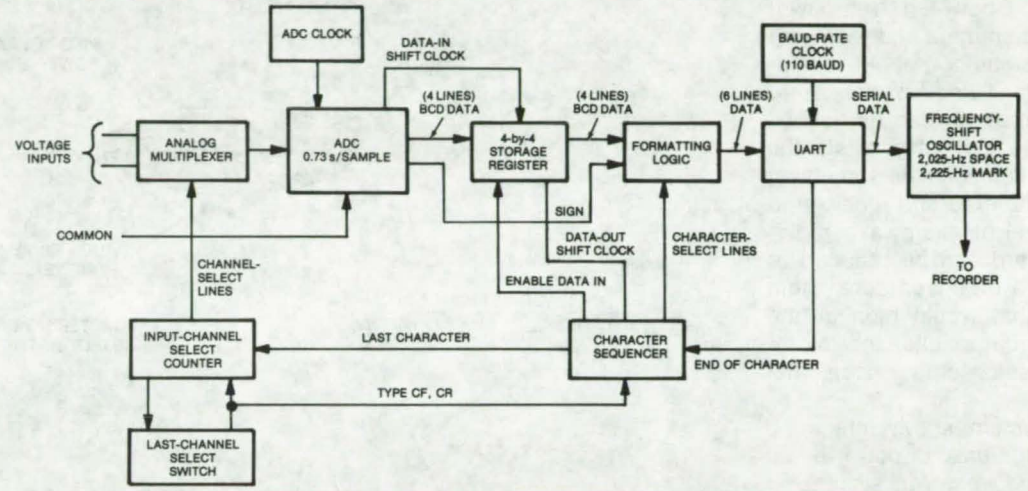

Figure 1. The **Portable Data System** has eight channels with an input range from ±1.999 to ±10.00 volts. The data output rate is 110 baud, and the reading rate is 1.4 channels/second.

A portable data system originally designed for high-altitude research could be used with the appropriate sensors for monitoring transportation systems, biomedical data, weather stations, mineral exploration equipment, and numerous other tasks. Data are formatted as audio tones and are stored on a small tape-recorder cassette. The tape can then be played back through a MODEM-equipped teleprinter to print formatted data.

The system accepts up to eight channels of bipolar analog voltages and records them in real time on the recorder. Low-power logic elements are used to keep power consumption below 1.5 watts. The tape recorder can be connected to a telephone for long-distance transmission, and a message-answering unit could be used to interrogate by phone in real time. The teleprinter compatibility also allows the data to be entered into a time-sharing computer for further processing.

The system as shown in Figure 1 presents a serial stream of frequency-shifted audio tones that cause a MODEM-equipped teleprinter to perform the operations shown in Figure 2. Timing is controlled by the baud-rate clock and the universal asynchronous receiver/transmitter (UART). At the end of each character transmitted, a pulse from the UART causes the character sequencer to advance.

Up to eight analog voltages are sequentially presented by an analog multiplexer to a dual-slope analog-to-digital converter. The specific analog channel presented is determined by the channel select. The ADC operates asynchronously and continually at 8 readings per second.

The UART serial output is used to control a variable-frequency oscillator. A logic-zero output results in a 2,025-Hz output corresponding to a SPACE tone. A logic-one output generates a 2,225-Hz frequency, corresponding to a MARK tone. The oscillator output is filtered by a 3-kHz low-pass filter and is buffered to present a low output impedance. This output can drive a small speaker that could be placed over the MODEM input of a teleprinter; or the data could be stored on a cassette recorder.

STATE	OPERATION
0	No Operation
1	Print Space
2	Print Space, Store ADC Data
3	Print Data Sign
4	Print Thousands Digit
5	Print Hundreds Digit
6	Print Tens Digit
7	Print Units Digit, Advance Channel Select, Reset Character Sequencer If Not Last Channel, Otherwise Go to State 8
8	Print Line Feed
9	Print Carriage Return, Go to State 0

Figure 2. These **Character-Sequencer Functions** are formatted for printing on a conventional teleprinter.

This work was done by Michael Dix of **Ames Research Center.** *For further information, Circle 13 on the TSP Request Card.*
ARC-11136

Microwave-Beam Safety Subsystem

A system for monitoring the airspace covered by high-power microwave transmissions

NASA's Jet Propulsion Laboratory, Pasadena, California

The airspace between high-power microwave transmitters and receivers may be dangerous to people, equipment or birds flying in the area. Although these areas can be defined on maps, there inevitably exists the possibility of someone or something straying into the area and receiving a dangerous level of microwave radiation. This hazard can be reduced or eliminated by a proposed subsystem (see figure) that would monitor the area and interrupt or alter the microwave transmission during accidental intrusions.

In the subsystem, shown integrated into a satellite-based power-beam transmitter and receiver system, a pilot-beam transmitter sends an uplink beam of energy to a pilot-beam receiver array on the satellite. The pilot-beam receiver array is diplexed such that beam time-of-arrival phase information at each antenna element can be used to set the phase of the satellite power transmitters and shape the power beam transmitted to ground. A computer on the spacecraft would look at the received power distribution to detect the direction and scattering characteristics of an intruding object.

On the ground, another computer (or a data link to the satellite computer) would monitor the power distribution in the power-beam receiving-antenna elements to determine additional scattering characteristics. This information would augment the pilot-beam receiver distribution. Other inputs to the control-computer could be derived from additional receiving antennas at the power-beam transmitter and surrounding the receiver area. Although there may be some redundancy in the received information, it may help to accurately determine the position and shape of a small object.

If an object intrudes into the microwave beam, it will alter the computer input by either scattering or absorbing microwave energy. This will be detected by continuous computer sampling. The computer then provides phase data to an interrupter that controls power input to the transmitter to dim or douse the microwave beam.

The computer could also be used to send phase information to divert, shape or dim the beam in accordance with stored programs. For example, a low-level power-beam signal could be sent when the system is first turned on to detect abnormalities or interfering objects before full power is applied. Also, objects of known size and scattering characteristics could be flown into the radiation area to test and calibrate the subsystem.

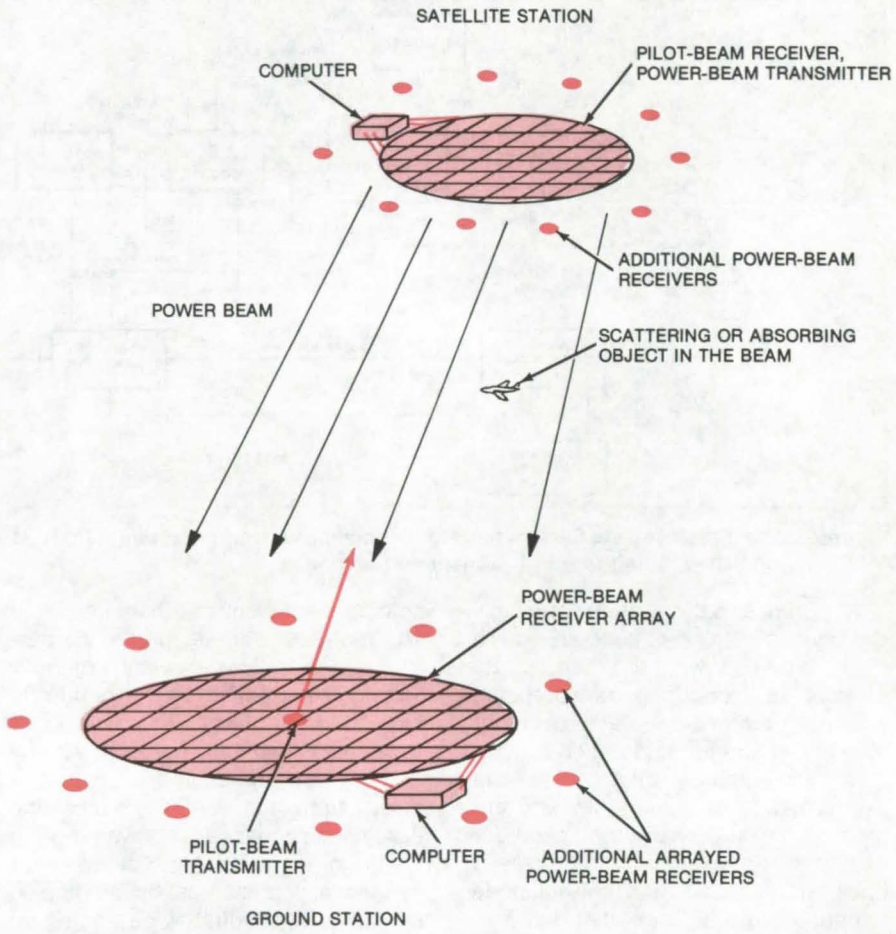

Microwave-Power-Transmission Safety Subsystem is shown as it would be implemented in a satellite-based microwave system. Any intrusion is detected by analyzing changes in the power distribution at the pilot-beam receiver. This information is processed to dim or douse the power beam.

This work was done by Richard M. Dickinson of Caltech for **NASA's Jet Propulsion Laboratory.** *For further information, Circle 14 on the TSP Request Card.*

This invention is owned by NASA, and a patent application has been filed. Inquiries concerning nonexclusive or exclusive license for its commercial development should be addressed to the Patent Counsel, NASA Resident Legal Office-JPL [see page A8]. Refer to NPO-14224.

Physical Sciences

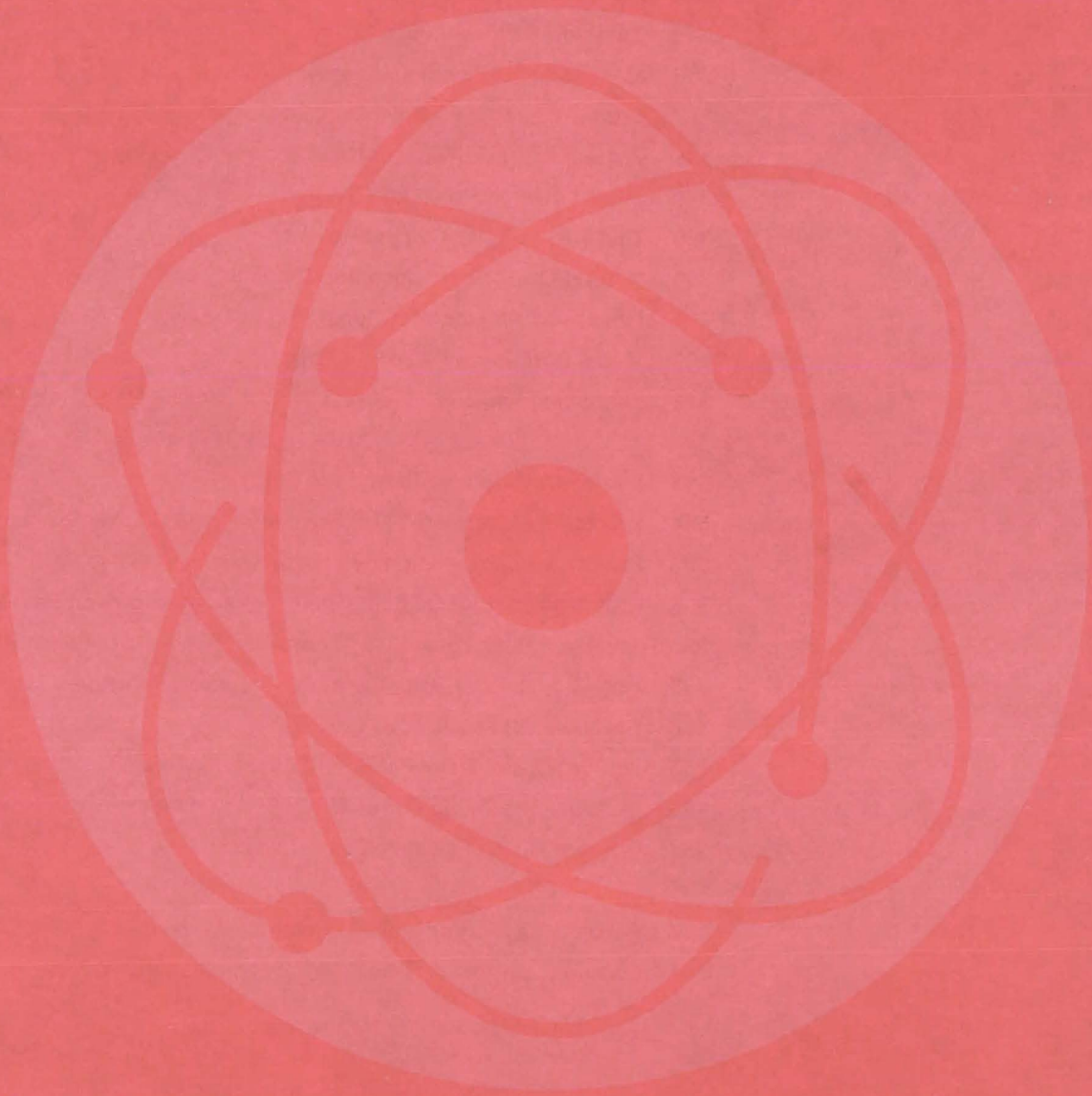

Hardware, Techniques, and Processes

Books and Reports

Computer Programs

"Pseudobackscatter" Laser Velocimeter

Laser instrument measures the speed of fluid flow with the sensitivity of a forward-scatter velocimeter and the convenience of a backscatter device.

Ames Research Center, Moffett Field, California

A "pseudobackscatter" laser velocimeter combines the best features of forward-scatter and backscatter velocimeters. The new velocimeter has sensitivity and accuracy comparable to forward-scatter instruments; but, like the backscatter version, it does not require precise alinement of transmitting and receiving elements on opposite sides of the scatterer. The new instrument is intended for measuring airflow around aircraft and in wind tunnels and for other fluid-flow measurement applications.

The unique feature of the new velocimeter is that it uses a corner-cube reflector to return the scattered laser beam to its source, where it is diverted to a collector and processed to determine the velocity of the gas medium through which it has traveled. Conventional forward-scatter laser velocimeters require a collector on the opposite side of the medium. In these devices, the collector must be carefully alined and must move with the source. This is difficult to arrange in a wind tunnel and virtually impossible between two airplanes (when measuring airflow velocities).

The true backscatter velocimeter depends on light scattered backward by particles in the medium. To obtain sufficient backscattered intensity, particles such as smoke must sometimes be deliberately introduced into the gas flow. This is an inconvenience that may require that an aircraft first lay a smokescreen, then fly back through the smokescreen while backscatter velocity measurements are made. Aside from being awkward, this procedure creates turbulence that is dangerous to the aircraft and perturbs the airflow to be measured.

In the new instrument (see figure), an argon laser or similar device generates a coherent, monochromatic light output. A beam splitter separates the output into two beams. These beams pass through a lens that focuses them so that they intersect at a point in the medium where the velocity measurement is to be made.

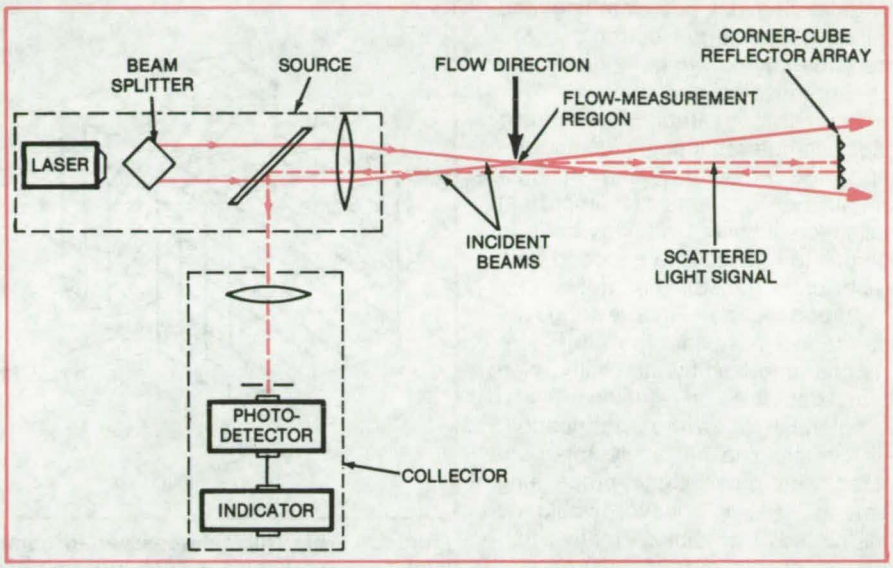

Two Beams Derived From a Laser intersect at a point in a flowing gas. The light is scattered and frequency-shifted by the gas and is allowed to fall on an array of corner cubes that reflect it back to the collector. The Doppler shifts of the light scattered from the two laser beams produce a difference frequency that measures the speed of the flowing gas.

A fringe pattern is formed at the intersection of the beams. As particles in the flowing medium move through the fringe pattern, they scatter the light in all directions; however, the scattering is strongest in the forward direction. The moving particles Doppler shift the frequency of the light by an amount that is proportional to their velocity.

The Doppler-shifted forward-scattered light continues to a bank of corner cubes arranged in a mosaic pattern, which reflects the light back to the lens in the source. A mirror in the source directs the reflected forward-scattered light into the collector. The difference between the Doppler shifts of the two scattered light beams is proportional to the velocity. The photodetector responds to this difference frequency to give an electrical output that is proportional to the velocity of the scattering particles in the flow. An indicator displays the magnitude of the electrical signal.

Since the forward-scattered radiation is much stronger than the backscattered component and the corner cubes can reflect radiation incident at angles between +60° and -60° of the optical axis, alinement between the cubes and the source is not too critical. They could, for example, be mounted on two aircraft that follow the same flight pattern.

This work was done by William D. Gunter of **Ames Research Center.** *For further information, Circle 15 on the TSP Request Card.*

This invention is owned by NASA, and a patent application has been filed. Inquiries concerning nonexclusive or exclusive license for its commercial development should be addressed to the Patent Counsel, Ames Research Center [see page A8]. *Refer to ARC-10970.*

Signal-Interleaving Device

Simple cubic interleaver would give high transmission efficiency for optical image processing and other applications.

Goddard Space Flight Center, Greenbelt, Maryland

Interleaving devices combine and duplicate optical, electronic, and other energy-carrying signals in signal-processing applications. They are needed, for example, in recording heads, in interconnecting logic elements in computers, and in data transmission systems. An important application of optical interleavers is to manipulate images and encoded data in fiber-optic transmission networks.

A proposed new interleaving device, shown in a basic form in Figure 1, is characterized by simplicity, high energy-transmission efficiency, and the potential for low-cost fabrication. It is designed to be easily interconnected with other signal-processing elements. The interleaver would be constructed by joining many flat, square, energy-carrying layers to form a laminated cube. Each layer is composed of parallel energy-carrying

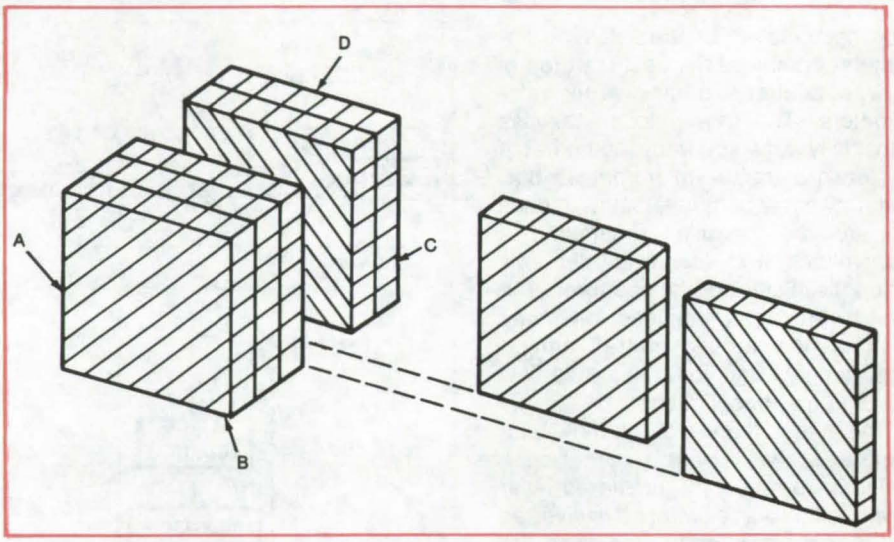

Figure 1. This **Cubic Interleaver** is composed of many energy-carrying square laminae. Each lamina is formed from parallel conduits (light pipes, for example) alined parallel to a diagonal axis of the square. The axes are displaced by 90° in adjacent layers. Energy into any of the active faces (A, B, C, or D) will be duplicated at the two adjacent active faces.

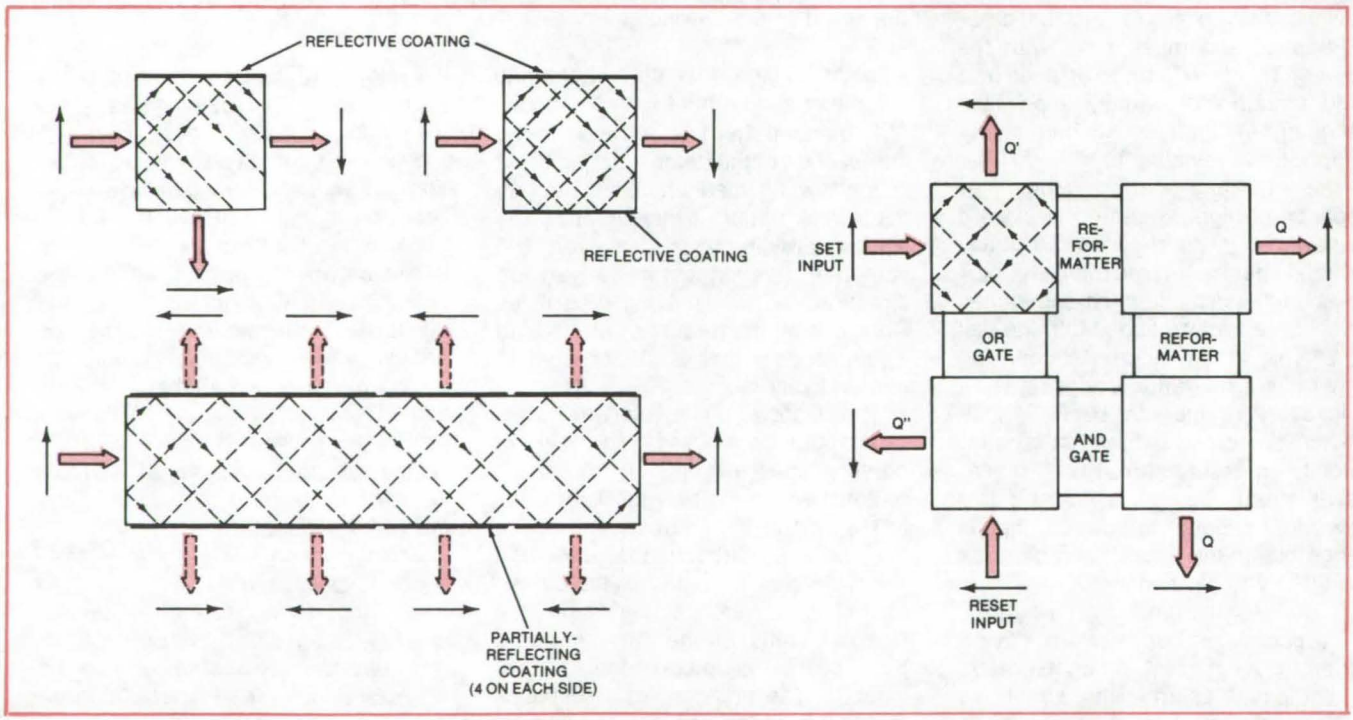

Figure 2. **Reflective Coatings** on the cubic interleaver are added to form image inverters (top, left) and a multiple-output generator (bottom, left). A set/reset flip-flop is shown at the right.

conduits, which might be square optical fibers or conducting wires, alined so that they point along a diagonal of the layer. When the layers are joined, they are oriented so that the transmission axes of alternating layers are displaced by 90°.

This simple element can serve as an image duplicator. If optical fibers are used as the energy carriers, an optical image projected on surface C will be duplicated at surfaces B and D, with each image having one-half of the original intensity. Similarly, the device functions as an image combiner if input images are projected on surfaces B and D. The resulting output, at surface C or A, will be the combination of the two images. Any of the active faces A, B, C, or D can be used as the input face for combining or duplicating.

Image inverters could be constructed by including a reflective coating on one or more of the active faces. For example, if one output face is coated, the cubic interleaver would produce two images at one-half the intensity, one inverted and one noninverted, as shown in Figure 2 (top left). If two parallel active surfaces are coated, as in Figure 2, top right, a single inverted output would result, with no loss of intensity through the sides.

An extension of this concept, shown in Figure 2, center, is a multiple-image generator. This device, which is equivalent to four cubic interleavers placed side by side, could be extended to any length, provided transmission losses are not too severe. The output images, through the partially-silvered upper and lower faces, alternate between inverted and noninverted.

The same effect, without transmission losses, can be obtained by using adjacent cubic interleavers separated by amplifying elements called reformatters. The reformatters perform no logical or processing function other than to furnish gain. They do, however, introduce small propagation delays that can accumulate to unacceptable levels for long strings. For these applications the element shown in Figure 2, center, which introduces no delay, may be preferred.

Combinations of the basic cubic interleaver with other elements are possible. For example, the optical interleaver can be combined with optical two-input AND gates and OR gates to form multiple-input gates and logic arrays. Flip-flops and memory cells can also be constructed. In the implementation of an optical set/reset flip-flop (Figure 2, bottom), with the set input low and the reset input high, the Q output retains its previous state. The truth table for this device is:

S	R	Q	Q'	Q''
0	0	0	0	0
0	1	Q_{N-1}	Q_{N-1}	1
1	0	0	1	1
1	1	1	1	1

Q_{N-1} = Previous Output State

This work was done by James R. Fischer of **Goddard Space Flight Center.** *For further information, Circle 16 on the TSP Request Card.*

This invention is owned by NASA, and a patent application has been filed. Inquiries concerning nonexclusive or exclusive license for its commercial development should be addressed to the Patent Counsel, Goddard Space Flight Center *[see page A8]**. Refer to GSC-12111.*

Common-Cavity Pumped Laser

Two lasers linked by a dichroic coupler are packaged in a single cavity.

Goddard Space Flight Center, Greenbelt, Maryland

In conventional optically pumped lasers, in which a source laser is excited by radiation from another laser (the pump), the pump and source lasers are usually separate elements, each with its own resonant optical cavity.

Probably the most serious deficiency of these two laser systems is that with two separate resonators, considerable pump energy is lost in the optics and in the window of the source laser cavity. Consequently only 50 percent of the pump radiation, or less, may be available for excitation of the source. The lasers are also sensitive to reflection of the pump radiation off the source and back to the pump, an effect that can cause frequency pulling and amplitude instabilities in the pump.

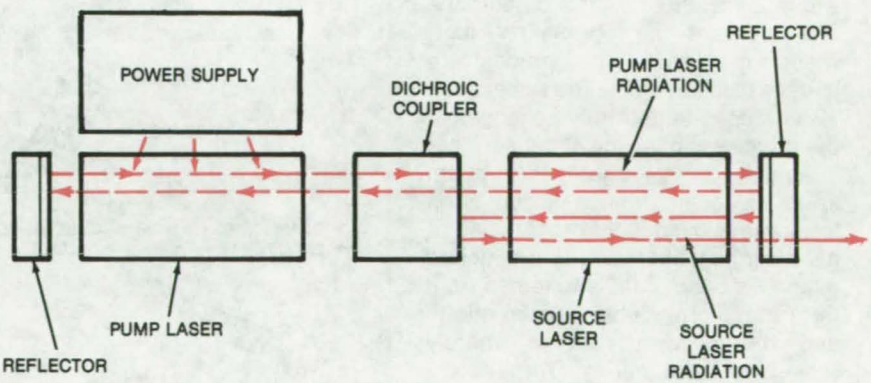

In this **Common-Cavity Laser,** the pump energy resonates between the left- and right-hand reflectors; the source resonates in the smaller cavity between the dichroic coupler and the right-hand mirror. Depending on the type of pump laser used, the power supply could excite the pump with an electric discharge or with optical energy from a flash tube.

These problems are reduced or eliminated by a new design in which the source is located within the pump resonant cavity. The resulting system is more compact, efficient, and durable than conventional two-cavity lasers. One such system, using a carbon dioxide laser pump and a methylcyanide source laser, has been built and tested.

In the new design (see figure), a dichroic coupler placed between the pump and the source transmits light at the pump wavelength, but reflects light at the source wavelength. In this arrangement, the pump radiation oscillates between the reflectors at the ends of the cavity and passes through the dichroic coupler and the source laser. No pump radiation leaves the cavity.

The radiation from the source is confined to the region between the dichroic coupler and the reflector at the right. That reflector is opaque to the pump radiation, but is partially transparent to the source radiation and thus permits the laser beam to exit from the cavity.

Since the only significant losses of pump radiation (other than those in the source material) are in the dichroic coupler, it is possible to get very high efficiency when using a low-loss coupler. Also, since the pump radiation is built up to a high-amplitude standing wave within the source material, coupling between the pump and the source is considerably better than in the two-resonator systems.

For the dichroic coupler, a reflector with a hole in the center can be used. Since the pump beam is small and can be sharply focused by a lens, it can pass through the hole. Only an insignificant part of the larger-diameter source beam is lost in the opposite direction through the hole.

Other types of dichroic couplers can be used. For example, if the pump radiation is polarized perpendicularly to the source radiation, a Brewster plate with a coating can reflect pump light and transmit source light to a mirror. In another arrangement, a pair of prisms can be used in combination with a coating that reflects the pump beam into the source laser but allows part of the source radiation to exit.

Portable pumped lasers emitting in the submillimeter wavelength region may be possible with the common-cavity design. Such instruments are needed for spectroscopy for plasma diagnostics, in atmospheric research (e.g., to measure pollutants and the effects of fluorocarbons), and in radarlike devices for "seeing" through dense fog or smoke.

This work was done by Gerhard A. Koepf of the National Academy of Sciences for **Goddard Space Flight Center.** *For further information, Circle 17 on the TSP Request Card.*

This invention is owned by NASA, and a patent application has been filed. Inquiries concerning nonexclusive or exclusive license for its commercial development should be addressed to the Patent Counsel, Goddard Space Flight Center [see page A8]. *Refer to GSC-12237.*

Measuring Surface Displacements Optically

Laser system measures changes in the position or roughness of a surface without physical contact.

Marshall Space Flight Center, Alabama

Using an optical correlation technique, the displacement of a surface can be measured by the reflection of a laser beam and a holographic correlation filtering system. A photomultiplier with a translatable pinhole detects the movement of the correlation spot, which is directly proportional to surface displacement. The system can also be used to determine changes in the roughness or shape of the surface.

As shown in the figure, the system splits the beam from a helium-neon laser into two paths that recombine at a Vander Lugt filter used as a matched filter. One beam path is reflected from the surface of the object under study, and the second path is merely redirected by a mirror. The recombined beams are focused on a pinhole in the plate in front of a photomultiplier. The pinhole is moved to obtain a maximum intensity reading, which occurs when the hole is at the correlation spot. The motion of this spot corresponds to the motion of the

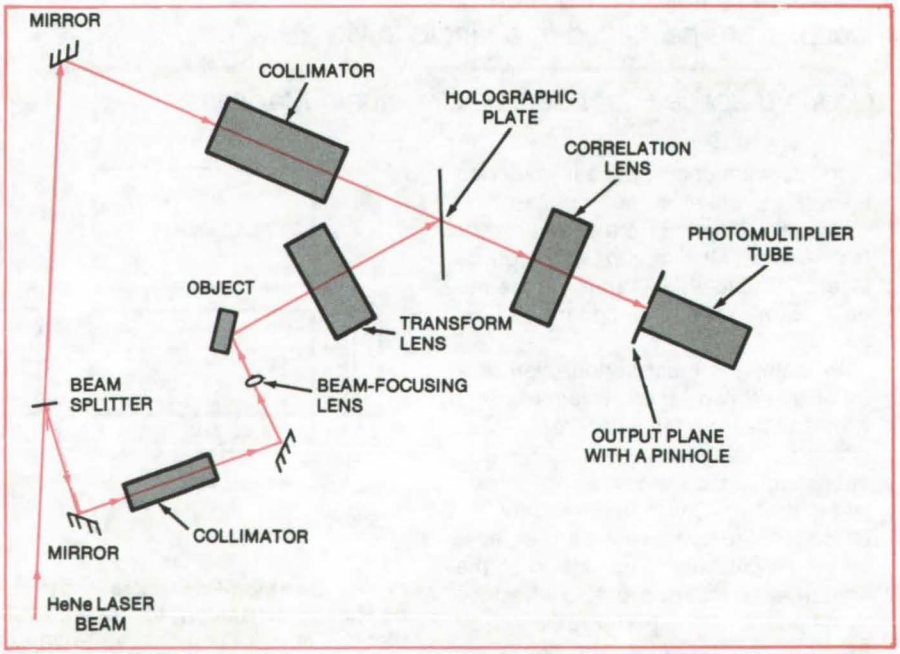

A **Laser Holographic Correlation** filtering system is used to measure displacements of surfaces or changes in surface condition, such as changes in roughness. Measurements are performed on a translated output plane with a pinhole located at the photomultiplier input.

surface: When the displacement of the object surface is perpendicular to the optical axis of the system, the correlation spot also moves the same distance perpendicular to the axis, but in the opposite direction; surface displacements parallel to the optical axis cause the correlation spot to move along the axis. If translators are arranged for movement of the output pinhole in three dimensions, an object surface displacement in three dimensions can be measured. The surface condition of the object can be determined by measuring the intensity of the output.

This work was done by Robert B. Owen of **Marshall Space Flight Center.** *For further information, Circle 18 on the TSP Request Card.*

Inquiries concerning rights for the commercial use of this invention should be addressed to the Patent Counsel, Marshall Space Flight Center [see page A8]. Refer to MFS-23861

Cosine-Corrected Optical Diffuser

Window optics for spectroradiometer make flux in collimator proportional to cosine of incidence angle.

NASA's Jet Propulsion Laboratory, Pasadena, California

In solar-energy utilization studies, it is important to measure accurately the combined solar and sky flux incident on an area. Optical radiometers and spectroradiometers measure the incident radiation centered on the optical axis of the instrument, but for correct evaluation, it is also necessary to measure the flux arriving at other angles to the optical axis. This is accomplished by using a "cosine diffuser" that delivers to the collimator an amount of radiation proportional to the cosine of the angle of incidence of the incoming rays. However, most conventional cosine diffusers have limited accuracy and spectral range.

A newly-developed cosine diffuser significantly reduces measurement errors. The device, shown in the illustration, is a combination of radiation transmitter and diffuser that cooperates with a collimated optical instrument in such a way that the relative aperture of the instrument is filled.

The radiation transmitter/diffuser uses an integrating sphere and includes a planoconvex lens of fused quartz, with the convex upper surface polished and the lower surface ground. A quartz plate ground on both surfaces is mounted a short distance below the lens, flush with the inner wall of the sphere. An aperture at the bottom of the sphere passes the beam into the cone of incidence of the optical instrument. The inside surface of the sphere is coated with high-reflectance paint.

Radiation from any given direction is refracted in the lens to irradiate its ground surface, producing partial diffusion. The flux is further diffused by the two ground surfaces of the plate. In addition to these diffusions, the flux that is in the sphere but does not enter the cone of incidence impinges on the inner sphere surface and is reflected onto the ground undersurface of the plate. This flux is then diffusely reflected into the cone of incidence, augmenting the total flux input. The efficiency of this arrangement significantly enhances the cosine proportionality.

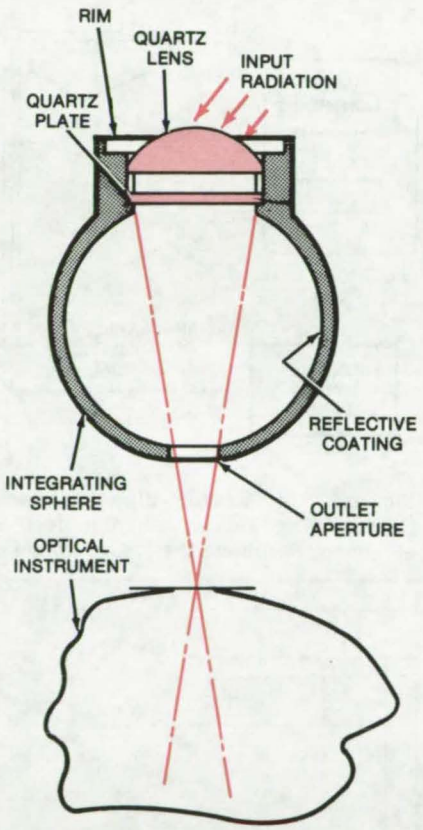

The Cosine-Corrected Diffusing Element uses an integrating sphere coated inside with highly reflective paint. Diffusion is provided by the flat ground lens surface and by two ground surfaces on the quartz plate. The total flux output measured at the outlet aperture is proportional to the cosine at the angle of incidence.

The magnitude of the flux redirected downward by the ground plate undersurface is dependent on the reflectance of the paint on the inner sphere surface and is reduced by the areas of the inlet and outlet apertures. In this configuration the gain in the sphere wall radiance by multiple reflectance is about 6.

In cosine diffusers, the error at 90° is usually severe because scattered flux enters the system to produce spurious values as the 90° cutoff is approached. The rim used on this device can be adjusted with respect to the vertex of the lens to provide an accurate empirical control of the residual cosine error in the 80° to 90° region. Refraction at the convex surface of the lens turns the obliquely incident rays toward the axis. The choice of the lens curvature influences the effectiveness of the rim and the cosine correction in the region near 45°.

This work was done by Roger S. Estey of Caltech for **NASA's Jet Propulsion Laboratory.** *For further information, Circle 19 on the TSP Request Card.*

NPO-14288

Vacuum-Ultraviolet Laser Uses Superfluid Helium

Optical pumping would increase the lifetime of the metastable state.

NASA's Jet Propulsion Laboratory, Pasadena, California

High-power coherent ultraviolet radiation has potential applications in molecular reaction studies, power transmission in space, and biomedical research. In a new proposal, a vacuum ultraviolet laser in the wavelength range around 0.800 micron would be produced by using optical pumping to increase the lifetimes of excited metastable molecules in superfluid helium.

In the proposed method, superfluid helium would be pumped electronically to produce excited He_2 and then pumped by circularly-polarized 0.9096-micron radiation to aline the excited He_2 molecular spins. Experiments with gaseous helium discharges indicate that spin is conserved in two-molecular collisions. If so, molecules with alined spins would be prevented from deexciting to a state of spin zero or 1.

There is considerable experimental evidence that high-energy (>100-keV) electron bombardment produces excited helium atoms and molecules in superfluid helium. Most of these decay rapidly, but some survive to give metastable populations on the order of 10^{12} to 10^{13} cm^{-3}. By alining the spins of the excited molecules in the superfluid through optical pumping, their deexcitation in bimolecular collisions could be suppressed, and concentrations on the order of 10^{18} cm^{-3} may be possible. Saturation populations are expected to have lifetimes of a few seconds.

A possible experimental system for a double-pumped superfluid helium laser is shown in Figure 1. The superfluid is excited by a 100- to 200-keV (10-μA or less) electron beam to produce the metastable population (transition A, Figure 2). This population is spin-alined by optically pumping it with a 100-μW circularly-polarized CW laser at 0.9096 μm (transistions B and B′). When a high concentration of spin-alined molecules has been generated, a strong microwave pulse initiates transition C from which lasing action (transition D) is triggered. The microwave pulses are timed to allow high concentrations of the metastable population to build up. Transition E is the lower-state depopulating transition.

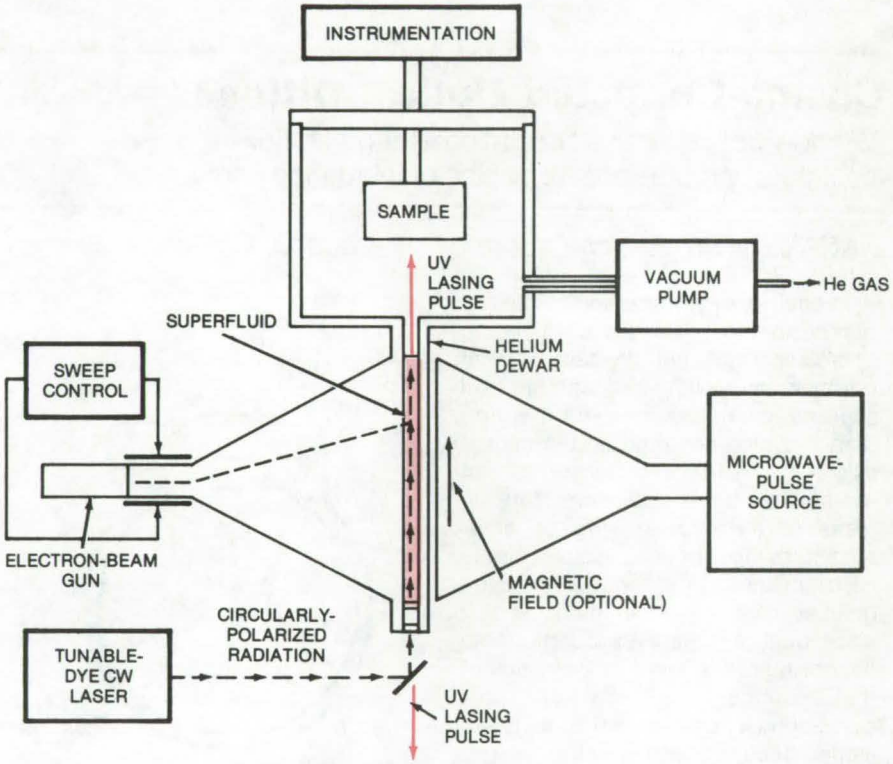

Figure 1. This **Vacuum-Ultraviolet Laser** would use electronic and optical pumping to produce spin-alined helium molecules. Microwave pulses would destroy the spin alinement to initiate the lasing transition.

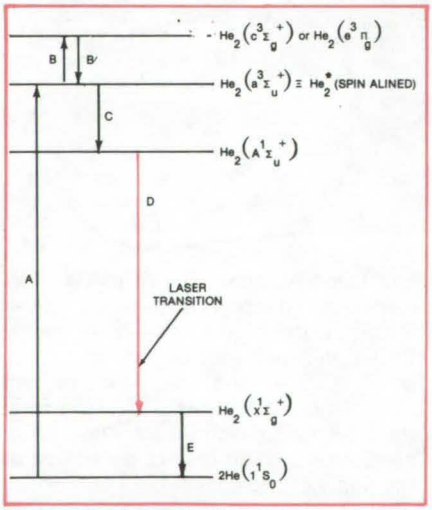

Figure 2. These **Helium Energy Levels** are involved in the lasing action. An alternate optical pumping scheme ($e^3\Pi g \leftarrow a^3\Sigma_u$) would use laser wavelengths at about 0.4650 μm.

This work was done by Jonas S. Zmuidzinas of Caltech for **NASA's Jet Propulsion Laboratory.** *For further information, Circle 20 on the TSP Request Card.*

This invention is owned by NASA, and a patent application has been filed. Inquiries concerning nonexclusive or exclusive license for its commercial development should be addressed to the Patent Counsel, NASA Resident Legal Office-JPL [see page A8]. Refer to NPO-13993.

Solar-Powered Hot-Water System

A proposed hot-water system would require no external power except solar energy.

NASA's Jet Propulsion Laboratory, Pasadena, California

A proposed solar-powered hot-water system (see Figure 1) includes a solar-powered pump, solar-thermally and hydrothermally operated valves, and a large storage tank filled with open-celled foam to maintain thermal stratification in the stored water. The system is self-controlling and would require no external energy sources, other than solar energy. It is installed in series with the standard domestic water supply.

The solar-powered pump could be a steam engine or other heat engine driving a conventional rotary pump. Another possible approach would use a series of bimetallic elements that are alternately exposed to and shielded from Sunlight. The elements would change shape when heated by the Sun and then would return to their original shape when cooled. This would create a reciprocating motion that could power a pump.

One such pump, which is being developed, uses a series of bimetallic disks (see Figure 2) mounted on a spindle. The perimeters of adjacent disks are welded together to form unitary elements. The left end of the assembly is anchored to a fixed surface, and the right end is connected to the spindle. When heat is applied, the spindle translates to the right; and when the assembly is cooled, the spindle shifts back to its original position.

It has been calculated that for a stack of 132 disks with outside diameters of 1.5 in. (3.8 cm) and thicknesses of 0.031 in. (0.079 cm), a temperature difference of 50° F (10° C) would give a movement of about 0.03 in. (0.76 mm) and produce a force of about 72 oz (20 N).

In the typical installation shown in Figure 1, the solar collectors are mounted above the storage tank. During daylight hours, the solar-energy-operated mechanical pump delivers cold water from the bottom of the tank into the collectors. The less-dense hot water from the collectors flows through a hydrothermally operated valve. The purpose of this valve, which may be either a bimetallic system or a small bellows filled with paraffin, is to separate hot and cold water in the water tank. The valve directs hot water to the top of the tank. If it senses cold water, at night, or in inclement weather, it directs it to the bottom of the tank.

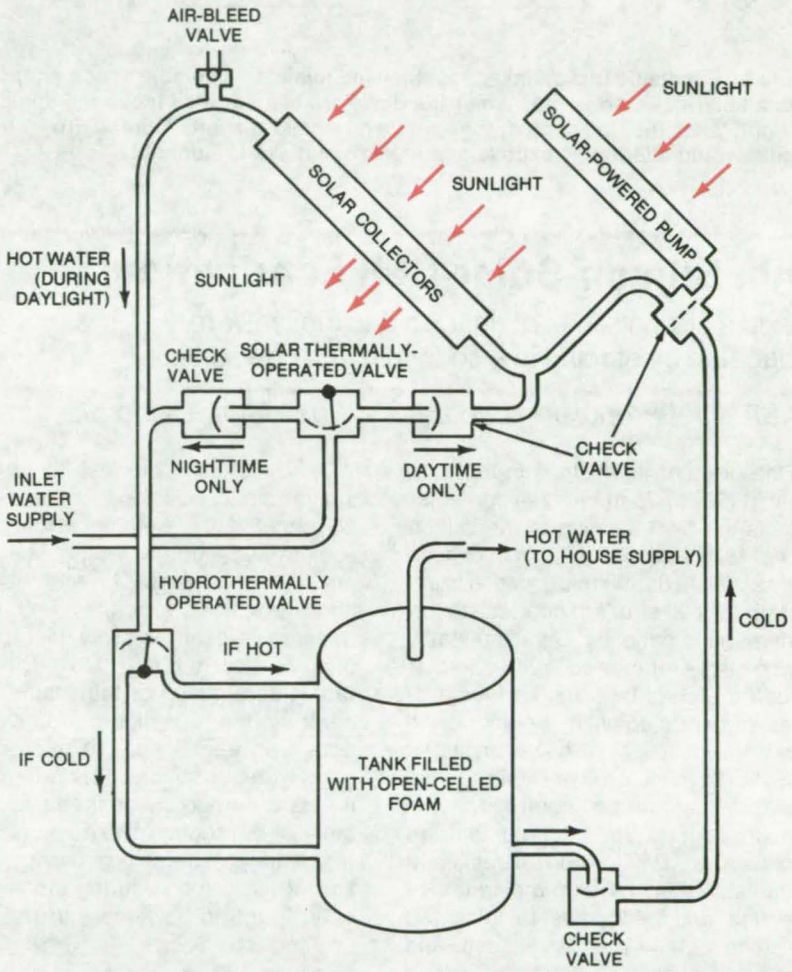

Figure 1. This proposed **Solar-Powered Hot-Water System** would operate on solar energy only. In daylight, a solar-powered pump delivers cold water from the tank into the solar heater. The hot water from the solar heater is directed into the upper portion of the storage tank. A layer of open-celled foam inside the tank maintains thermal stratification between the hot- and cold-water levels. Predicted hot-water temperatures would vary between 100° and 120° F (38° and 49° C).

The tank is filled with open-celled foam that reduces turbulence and helps to keep the hot and cold water in separate layers. Typically, the tank would be larger than in conventionally-operated hot-water systems to store enough hot water to last for an entire night. At night, as the hot water is used, the cold-water level would rise automatically.

The external water supply is directed by the solar-thermally operated valve. This valve is similar in principle to the hydrothermally operated valve except that it is activated by solar

(continued on next page)

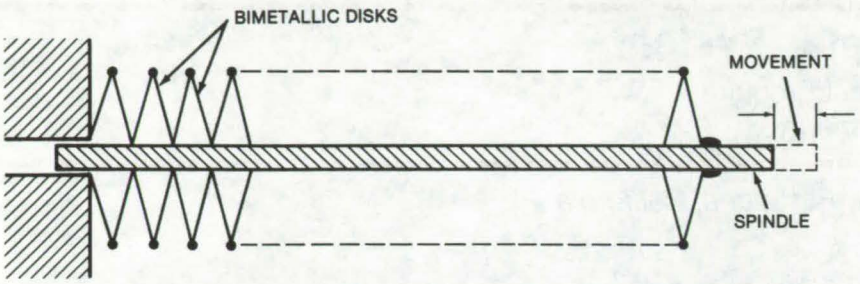

Figure 2. **Bimetallic Disks,** linked together and joined to a spindle at one end, could drive a solar-powered pump. When the disks are heated, they move the spindle to the right, when they are cooled, the spindle returns to the left. A baffle driven by the spindle would alternately expose and shield the disks in Sunlight.

heat. In daylight, it routes the inlet water through a check valve into the solar heater; at night, it routes the water into the lower part of the tank to prevent the cold water from being cooled even further in the inactive solar heater.

This work was done by Earl R. Collins of Caltech for **NASA's Jet Propulsion Laboratory.** *For further information, Circle 21 on the TSP Request Card.*
NPO-14270

Thin Silicon-Solar-Cell Fabrication

Flexible silicon slices of uniform thicknesses are fabricated by etching in a sodium hydroxide solution.

NASA's Jet Propulsion Laboratory, Pasadena, California

One of the critical steps in fabricating thin (50- to 75-micron) silicon solar cells is the final thinning of the silicon slices. Maintaining a uniform thickness across a slice during this process is important for cell strength and resistance to damage in handling. Conventionally, silicon slices for microcircuitry or solar cells are etched by using various mixtures of hydrofluoric, hydrochloric, nitric, and acetic acids; however, when the slices must be very thin, these etchants cannot be controlled well enough to give the required uniform thicknesses. Thin silicon slices have been fabricated by a combination of chemical and mechanical thinning and polishing, but this process is costly and time consuming.

A new etching process for producing flexible, thin silicon slices uses 5- to 25-percent (by weight) solutions of sodium hydroxide in water. The etchant is heated to approximately 100° C, and the starting slices are immersed, oriented vertically to allow the etch solution to flow around them. The etch rate is determined by the solution concentration and temperature; it averages between 5 and 10 microns for each side per minute. This rate makes it easy to trim to the desired thickness, but it is not so slow as to be production-rate limiting in batch processing. Agitation of the solution during etching has been found to be necessary to maintain a uniform thickness, especially for batches of slices.

Slices formed by this method have a very reproducible surface that has a fine "orange peel" texture. The mechanical survival of slices prepared with this technique is far superior to that of slices prepared by other methods. Phosphorous diffusion has been carried out successfully on cells prepared by this technique.

This work was done by Joseph Lindmayer of Solarex Corp. for **NASA's Jet Propulsion Laboratory.** *For further information, Circle 22 on the TSP Request Card.*
NPO-14047

Natural-Oxide Solar-Collector Coatings

Optically selective coatings for solar collectors are produced by thermally treating stainless steel.

Marshall Space Flight Center, Alabama

Natural-oxide coatings, suitable for use on solar-collector surfaces, are produced by oxidizing stainless steel in a furnace after a series of cleaning and soaking operations. The coatings are inexpensive to produce, highly production oriented, and environmentally stable.

The coating method was developed during experiments on stainless-steel tubes, using 302, 304, and 316 alloys. Stainless-steel tubes electroplated with sulfamate nickel or bright nickel 0.25 mil (0.006 mm) in thickness were also tested as substrates. The most promising results were obtained with 304-alloy stainless, for which natural-oxide coatings with absorptances of 0.89 and emittances of 0.07 were produced.

The major items of equipment necessary for the coating process are a chemical cleaning tank, a pickle tank, and a 1,650° F (900° C) furnace. Several cleaning and degreasing stages, an alkaline soaking, and acid pickling are part of the process.

To prepare a naturally-oxidized 304-steel matt surface, the tube is

hand-wiped with xylene, and the surface is buffed with a wire wheel to obtain a uniform texture. It is then wiped and degreased with perchlorethylene at 250° F (120° C), alkaline-soaked at 170° F (77° C) for 20 minutes, and hand-wiped. After another alkaline soaking for 5 minutes, the tube is rinsed in distilled water. It is then pickled at ambient temperature for 1 hour in an HNO_3/HF solution, rinsed, and blow-dried.

The dried tube is placed in a nylon tube and then into a tube furnace at 1,650° F. Oxidation of a 2-ft (0.6-m) working length is carried out at 4.5 in./min (11.5 cm/min).

Similar processes are used to obtain coatings on mill-finished 304 stainless steel, on bright-annealed surfaces, and on vacuum-brazed surfaces. Experiments with the sulfamate nickel-plated samples have produced stable coatings with good optical properties. This coating is superior to the steel-oxide surface in its resistance to saltwater spray.

Both the steel-oxide and sulfamate nickel oxide coatings have withstood 18-month exposure tests at 100 percent relative humidity and temperatures of 95° F (35° C). The same durability was exhibited during 250 equivalent Sun-hours of ultraviolet exposure. The steel oxide also withstood 25 days of thermal cycling between 1,000° F (540° C) and room temperature.

This work was done by Albert C. Krupnick, Marion L. Roberts, and Max H. Sharpe of **Marshall Space Flight Center.** *For further information, Circle 23 on the TSP Request Card.*

This invention has been patented by NASA [U.S. Patent No. 4,104,134]. Inquiries concerning nonexclusive or exclusive license for its commercial development should be addressed to the Patent Counsel, Marshall Space Flight Center [see page A8]. Refer to MFS-23518

Mounting Procedure for Geological Samples

A mounting procedure originally developed for lunar samples preserves geological specimens.

Lyndon B. Johnson Space Center, Houston, Texas

A specimen-mounting procedure, originally developed for lunar samples, displays tiny chips and grains for microscopy and other applications. The sequence of potting and grinding operations produces thin sections through the grains that are easy to handle and are well protected for storage.

In the method (see figure), a small polyethylene cylinder is epoxied to a glass or silica substrate, (Step 1) and a thin film of epoxy with an area slightly larger than the area of the grains to be mounted is spread on the surface of the substrate (Step 2). The grains are carefully arranged, using a binocular microscope, so as to be at or near the center of the cylinder.

Next the cylinder is nearly filled with epoxy, the air is evacuated, and the epoxy is cured (Step 3). Following this, the polyethylene cylinder is pulled away, leaving the epoxy cylinder with the grains attached to the substrate, and the cylinder is ground down to the grains by using a grinding machine (Steps 4 and 5). The cylinder is further carefully ground by hand to the major horizontal dimensions of the grains. For a range of grain sizes, an average of the largest horizontal dimensions can be used.

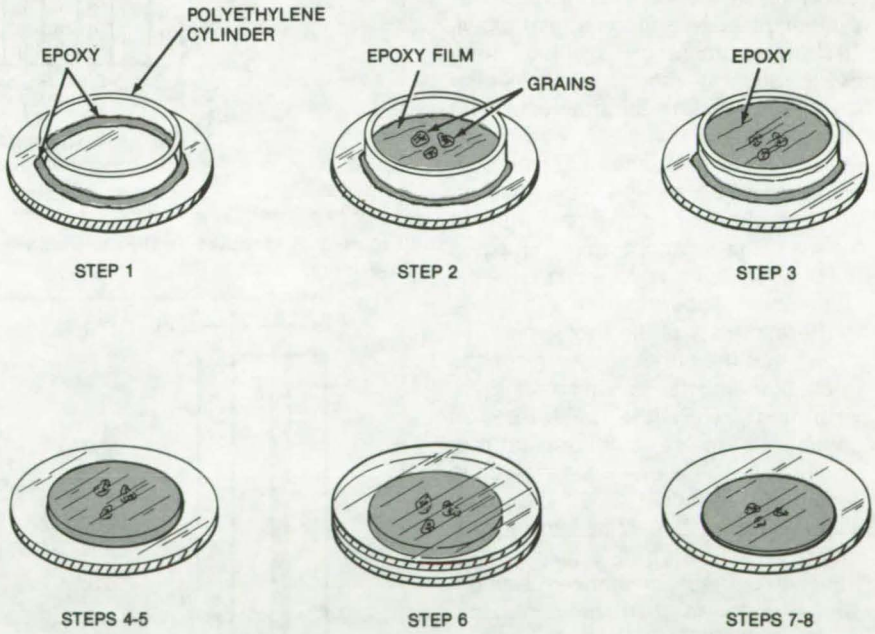

The **Steps for Mounting Fine-Grain Geological Samples** are: (1) mounting of a polyethylene cylinder on a substrate; (2) placing the samples on an epoxy film; (3) filling the cylinder with epoxy; (4-5) removing the polyethylene cylinder, followed by grinding and polishing; (6) applying new substrate; and (7-8) inverting the assembly, grinding off the original substrate, and grinding and polishing the sample to its final dimension.

The surface is then hand ground and polished (Step 6). After polishing, it is covered with a thin film of epoxy, a new substrate is applied to the surface, and the epoxy is cured.

Finally, the first substrate is ground away, and the sample is reduced to approximately 35 to 40 microns for a section that is to have a final thickness of 30 microns. It is hand

(continued on next page)

ground and polished to the final dimension (Steps 7 and 8).

When compared with previous methods that did not use the polyethylene cylinder, the new method was found to result in more representative sections of a mixture of grains of different sizes. In the earlier approaches, either the smallest grains were completely ground away or sections of large grains represented only a portion of the edges of the grains. The new method was also more effective in distributing the grains uniformly over the slide.

This work was done by Daniel I. Jezek of Northrop Services, Inc., for **Johnson Space Center.** *For further information, Circle 24 on the TSP Request Card.*
MSC-18206

Modular Heat-Pipe-Radiator Panel

Modular construction improves reliability and thermal performance.

Lyndon B. Johnson Space Center, Houston, Texas

A new heat-pipe panel (see figures) is assembled by joining a series of heat-pipe modules. Each module is identical and includes its own radiator fins and fluid-header section. Thus, a panel of any area can be formed by welding the required number of heat-pipe submodules together.

A prototype of the new design includes one low-freezing-point propane heat pipe at the inlet, all of the other submodules use ammonia heat pipes. This arrangement gives a high turndown ratio (maximum load/minimum load) by permitting the ammonia heat pipes to freeze under low-load conditions while the propane heat pipe continues to operate. When the load increases due to rising temperature at the inlet, the adjacent ammonia pipes thaw by cross-fin conduction until the entire panel is operative.

Thermal tests of the prototype have shown that the panel quickly responds to changes in inlet conditions and environment, with the performance coming very close to theoretical predictions. The maximum heat rejection recorded was about 2,800 W, which exceeded the 2,200-W design requirement. Performance during the freeze/thaw test sequences demonstrated a low-load (frozen-panel) capacity of 76 W, which yields a turndown ratio of 36/1.

In a test of a propane/ammonia heat-pipe system a panel with all ammonia pipes frozen was thawed within 3 hours in a −300° F (−184° C) environment by simply increasing the fluid inlet temperature. After thawing, several steady-state test points were rerun, and no performance degradation due to the freeze/thaw cycle was found.

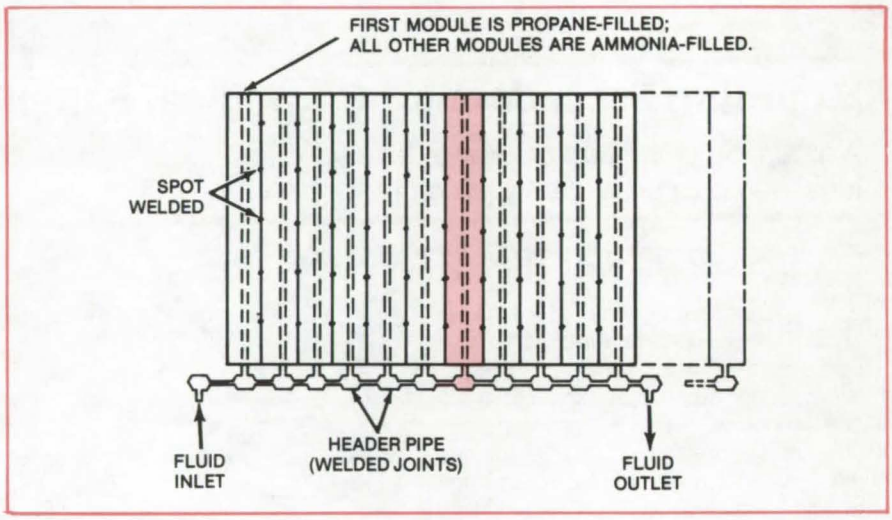

Figure 1. A **Modular Heat-Pipe-Radiator Panel** can be expanded or reduced to match the user's needs.

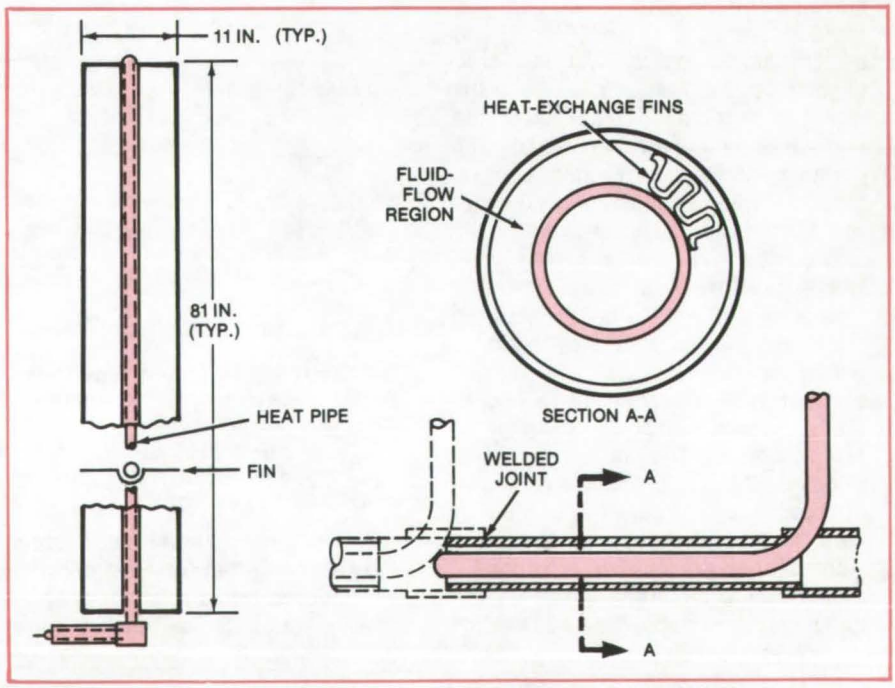

Figure 2. **Heat-Pipe Submodule (Left) and Fluid-Header Joint (Right)** are shown in detail.

The thermal response of the panel to programed oscillations in the inlet temperature was also good, with fluid heat rejection closely following the changes in inlet conditions.

The new heat-pipe-radiator panel should be competitive in thermal performance with fluid-loop systems used in waste-heat rejection applications. The advantage of heat pipes is that they are not subject to single-point failures, as are fluid loops that can fail due to tube-wall puncture.

This work was done by Joseph Alario of Grumman Aerospace Corp. for **Johnson Space Center.** *No further documentation is available.*
MSC-16625

Estimating Regional Heat Flux From Scanning Radiometer Data

A statistical method is useful in meteorological studies.

Langley Research Center, Hampton, Virginia

By accurately measuring the radiation flux of the Earth, scanning radiometers on satellites contribute significantly to our understanding of climatic changes and oceanic and atmospheric circulation. In these experiments, accurate radiation-flux information is needed for regions with boundaries that are typically 10° by 10° to 20° by 20° on great-circle arcs. Since the scanning radiometer produces high-resolution data over a much smaller area (typically 100 km across), the researcher must combine the scanning data to determine the average heat flux over the entire region.

The data can be averaged by a statistical method for extracting regional heat-flux information from the scanning data. In this approach, the radiative-flux distribution is represented by an unbiased, truncated double Fourier series with coefficients to be determined from measurements. The method uses a matrix approach to determine the best linear estimate of the total flux consistent with the condition of minimum variance. With it, researchers can study various options in scanner design, such as varying the scan pattern, the scan rate, and the radiometer field-of-view.

In an application of the method, a scanning radiometer is assumed to operate at an altitude of 833 km. The sensor has a circular field-of-view of 6°, and the size of the region to be scanned is approximately 310 by 750 km. The scanning mode is a cross-track scan in which the scanner sweeps out a path nearly perpendicular to the satellite velocity vector at a rate of 27° per second. It is assumed that measurements over the regions being scanned do not overlap.

In the example, six measurement patterns, ranging from a single measurement to 21 measurements, were considered. The standard deviations of the average regional radiation-flux estimates were calculated for each case. The example also investigated the effect of moving the measurement field over the region. The results show that the standard deviation of the average-flux estimate decreases as the number of measurements increases, from about 19 W/m^2 for a single measurement to about 3 W/m^2 for 21 measurements, which fill the region. Moving the measurement field within the region also had a slight effect.

This work was done by T. Dale Bess and G. Louis Smith of **Langley Research Center.** *For further information, Circle 25 on the TSP Request Card.*
LAR-12158

Books and Reports

These reports, studies, and handbooks are available from NASA as Technical Support Packages (TSP's) when a Request Card number is cited; otherwise they are available from one of NASA's Industrial Application Centers or the National Technical Information Service.

Energy Conversion Alternatives Study

Comparison of advanced coal-based energy systems

A summary report describing the Energy Conversion Alternatives Study (ECAS) is now available. This study was undertaken to identify and compare various advanced energy conversions systems that can use coal or coal-derived fuels for baseload electric power generation. The study was an integrated government/industry effort sponsored by the National Science Foundation, the Energy Research and Development Administration (now the Department of Energy), and NASA.

The objectives of ECAS were (1) to provide information, at a comparable level of detail for each system, that would enable impartial evaluation of a variety of advanced concepts for

(continued on next page)

electric-utility baseload powerplants using coal or coal-derived fuels and (2) to define the relative potential of these concepts for meeting the Nation's future electrical-generating needs and environmental constraints. For each powerplant concept, the study provides estimates of the overall efficiency (coal pile to bus bar) in converting coal to electricity, powerplant capital costs, the cost of electricity, environmental intrusion, and the resources and time required to bring the powerplant to a state of readiness for commercial service.

ECAS was conducted in two phases. Phase 1 consisted of a parametric analysis; phase 2 treated conceptual design of certain selected powerplants together with development plans and an implementation assessment. In phase 1, emphasis was placed on broad coverage of the energy conversion systems over a wide range of variable conditions. Approximately 900 parametric points were calculated, and the results were compared and evaluated.

Based on the results of the phase 1 parametric analysis, an Interagency Steering Committee selected 11 concepts for more detailed evaluation in phase 2. Focus on a relatively small number of advanced energy conversion concepts in phase 2 permitted technical and economic evaluation to be made in much greater depth than that in the phase 1 parametric analysis. The systems studied in phase 2 included steam systems with both atmospheric- and pressurized-fluidized-bed boilers; combined-cycle gas-turbine/steam systems with integrated gasifiers or fired by a semi-clean coal-derived fuel; a potassium/steam system with a pressurized-fluidized-bed boiler; a closed-cycle gas-turbine/organic system with a high-temperature, atmospheric-fluidized-bed furnace; a direct-coal-fired, open-cycle magnetohydrodynamic/steam system; and a molten-carbonate fuel cell/steam system with an integrated gasifier.

Based on the phase 2 results using the ECAS ground rules, three systems showed substantial potential for higher overall efficiency together with lower cost of electricity: (1) the low-Btu gasifier/molten-carbonate fuel cell/steam system, (2) the coal/open-cycle MHD/steam system, and (3) the low-Btu gasifier/gas-turbine/steam combined-cycle system.

The ECAS reports provide government, industry, and the general public with a technically consistent basis for comparing a number of advanced-technology power system options of interest for fossil-fired electric-utility application.

This work was done by Lloyd I. Shure of **Lewis Research Center.** *Further information may be found in NASA TM-73871 [N78-24659], "Energy Conversion Alternatives Study [ECAS] Summary Report, September 1977," a copy of which may be obtained at cost from the New England Research Application Center* *[see page A7]*.
LEW-13096

Problems Encountered in Solar Heating and Cooling Systems

A compilation of problems and their resolutions can assist designers of solar-energy systems and prevent a repetition of errors.

Some of the experiences of workers at Marshall Space Flight Center in developing solar heating and cooling systems are compiled in a new report. Hardware problems that were encountered (and resolved) during design, production, installation, and operation phases are organized in a 29-page tabular format that can help others to reduce the development time of solar-energy systems. A six-page summary of work at Marshall and by contractors in support of Department of Energy (DOE) solar-energy programs is also included in the report.

The hardware problems are compiled in five tables. These give the problems encountered and one resolution for each. The resolution can vary with hardware, locality, and other factors peculiar to each system. Table 1 lists general problems that could be found in most collectors; tables 2 and 3 are restricted to problems of liquid and air collectors; respectively; table 4 describes problems with storage subsystems; and table 5 describes system problems.

Some of the problems became obvious during design, production, installation, and checkout. Others, particularly those associated with deterioration under long-term usage and at stagnation temperatures, did not become apparent until the system was in operation. Some problems were caused by poor workmanship, resulting from not recognizing the more stringent requirements of solar installations as compared to normal plumbing and heating systems.

Many of the problems were quite subtle. For example, in certain systems, sheet-metal panels that had been sheared and bent to form collector housings had not been treated with a corrosion inhibitor along the sheared edges and began to deteriorate along the edges.

Other problems encountered were the contamination of heat exchangers by machine oil and metal filings and the loosening of fluid seals during shipping. In some systems, algae were found in tanks and transport lines after long periods of operation. In all, over 150 separate problems are addressed, covering virtually all aspects of system operation.

The solar-energy systems installed for the Marshall program have monitoring sensors (e.g., temperature, flow, power, insolation, and wind velocity and direction) to determine the performance of the system. The outputs of the sensors are fed to a site data-acquisition subsystem (SDAS) that scans all the sensors at 5-minute intervals (some can be scanned more rapidly if necessary) and records the data on tape. A central computer calls the SDAS through a telephone line and reads the data on the tape. Then, the tape is erased and is ready to continue recording data. The central computer calculates and prints the performance of the system in a predetermined format.

This work was done by Mitchell Cash of **Marshall Space Flight Center.** *Further information may be found in DOE/NASA TM-78172, "Hardware Problems Encountered in Solar Heating and Cooling Systems," a copy of which may be obtained at cost from the New England Research Application Center* *[see page A7]*.

Inquiries concerning rights for the commercial use of this invention should be addressed to the Patent Counsel, Marshall Space Flight Center *[see page A8]*. *Refer to MFS-23974.*

Prototype Solar-Heating System — Design Package

Package contains documents and drawings sufficient to assemble a working system.

A 171-page design package for a complete residential solar-heating system has been published. The system is described in "Prototype Solar-Heating System" (MFS-23916) on page 201 of *NASA Tech Briefs*, Vol. 3, No. 2.

The first prototype of this system, which includes air flat-plate collectors and pebble-bed heat storage, was installed in Huntsville, Alabama. A second prototype is being installed at Carlsbad Caverns, New Mexico. The prototypes were designed for buildings in the size range from 1,500 to 2,500 ft^2 (139 to 232 m^2); however, they can be scaled up or down to accommodate heating and hot-water requirements for other single-family or multifamily dwellings or for commercial buildings.

The package includes documents and drawings that describe the performance, design, verification standards, and hazard analysis of the system with sufficient information to assemble a working system.

[Also see related articles: "Prototype Solar-Heating System — Engineering Analysis" (MFS-23910) and "Prototype Solar-Heating System — Installation Manual" (MFS-23907) on page 213 of *NASA Tech Briefs*, Vol. 3, No. 2.

This work was done by IBM Corp. for **Marshall Space Flight Center.** *Further information may be found in NASA CR-150614 [N78-21589], "System Design Package for IBM System One Solar Heating And Domestic Hot Water," a copy of which may be obtained at cost from the New England Research Application Center [see page A7].*
MFS-23945

Prototype Residential Solar-Energy System — Design Package

A compilation of documents and drawings for a complete solar-heating system

A complete solar-heating system, described in "Prototype Residential Solar-Energy System" (MFS-23932) on page 211 of *NASA Tech Briefs*, Vol. 3, No. 2, can be assembled with the help of a design package that has recently been made available. The 108-page package includes documents and drawings for the design, performance verification, and hazard analysis of the prototype.

The system, which includes a silicone-fluid collector subsystem and hot-water storage, has been installed in a residential building on the grounds of the Veterans' Administration Hospital, Togus, Maine. It can be adapted to other buildings without changing the basic design.

[Also see related article: "Prototype Residential Solar Energy System — Engineering Analysis" (MFS-23929) on page 212 of *NASA Tech Briefs*, also Vol. 3, No. 2.]

This work was done by IBM Corp. for **Marshall Space Flight Center.** *Further information may be found in NASA CR-15021, "System Design Package for SIMS Prototype System 2, Solar Hot Water," a copy of which may be obtained at cost from the New England Research Application Center [see page A7].*
MFS-23953

Prototype Residential Solar-Energy System — Installation Package

Installation guidelines for the architect and engineer

The installation package for the prototype residential solar-heating system described in the preceding article can be obtained by requesting the reported cited below.

Included in the package are a brief functional description of the system and a summary of its operation. General guidelines for installation of the separate components, including the collectors, the heat exchanger, the tanks, and the insulation, assist the architect or builder in developing a detailed installation plan. A section on operation, maintenance, and repair is partly devoted to a discussion of preventive maintenance. Drawings complement the text material.

This work was done by IBM Corp. for **Marshall Space Flight Center.** *Further information may be found in NASA CR-150639, "Installation Package for SIMS Prototype System 2, Solar Hot Water," a copy of which may be obtained at cost from the New England Research Application Center [see page A7].*
MFS-23956

Hot-Air Flat-Plate Solar Collector — Design Package

Includes design data, drawings, and performance specifications

A 35-page report contains design data, performance specifications, and detailed drawings for an hot-air flat-plate solar-energy collector. [See "Prototype Air Flat-Plate Solar Collector" (MFS-23893) and "Flat-Plate Solar Collector — Installation Package (MFS-23921) on page 214 of *NASA Tech Briefs*, Vol. 3, No. 2.] The report should be useful to engineers and architects who might want to include this unit in a solar-energy System.

The collector, a 4- by 8-ft (1.2- by 2.4-m) panel, is supported on a lower frame made of aluminum angle extrusion. An inner aluminum frame supports tempered glass covering a "floating" absorber panel that allows for expansion and contraction. The absorber panel is coated with high-absorptivity black paint. The primary method of heat transfer is by forced air convection through a plenum below the absorber.

Insulation is placed on the outside of the collector to minimize heat

(continued on next page)

losses and to avoid contamination of the glazings by outgassing of the insulation. The insulation is installed between the back of the collector and the roof, between adjacent collectors, and around the perimeter of the collector.

The performance specifications contained in the report include a plot of minimum collector efficiency versus the inlet/ambient temperature differential. Over 16 pages of design drawings are supplied.

This work was done by Life Sciences Engineering for **Marshall Space Flight Center.** *Further information may be found in NASA CR-150611, "Subsystem Design Package for Solar II Collector," a copy of which may be obtained at cost from the New England Research Application Center* [see page A7].
MFS-23941

Evaluation of an Air Solar Collector

A performance verification under simulated conditions

The performance of an air solar collector [see "Prototype Air Flat-Plate Solar Collector" (MFS-23893) and "Flat-Plate Solar Collector — Installation Package (MFS-23921) on page 214 of *NASA Tech Briefs,* Vol. 3, No. 2] was tested by using the Marshall Space Flight Center solar simulator. The evaluation included thermal performance tests, time-constant tests, and incident-angle-modifier tests. The results are presented as tables and graphs and are analyzed in detail.

The collector is a double-glazed flat plate with air as the heat-transfer medium. Its gross area is 32 square feet (2.9 m^2). The absorber plate is black-coated.

Thermal performance data are presented for flow rates of 66 and 120 $stdft^3/min$ (1.9 and 3.4 m^3/min) and inlet temperatures between 67.8° and 166° F (19.8° and 74.4° C). Stagnation tests were run with the flow inlet and flow outlet capped and the collector exposed to a simulated solar flux of about 1,500 Btu/ft^2-d (407 cal/cm^2-d).

In the incident-angle-modifier tests, the radiation was allowed to strike the collector at angles (Θ) of 30°, 40°, 50°, and 60° with respect to the normal to the collector surface. The results are presented as a plot of incident-angle modifier versus $(\cos \Theta)^{-1} - 1$.

This work was done by the Solar Energy Systems Division of Wyle Laboratories for **Marshall Space Flight Center.** *Further information may be found in DOE/NASA CR-150665, "Indoor Test for Thermal Performance Evaluation on Life Sciences Engineering [Air] Solar Collector," a copy of which may be obtained at cost from the New England Research Application Center* [see page A7].
MFS-23978

Indoor Tests of a Hot-Air Solar Collector

Data taken by using a solar simulator can be compared with outdoor test data.

The hot-air solar collector referenced in "Thermal Performance of a Hot-Air Solar Collector" (MFS-23891) on page 215 of *NASA Tech Briefs,* Vol. 3, No. 2, has been tested indoors, using the Marshall Space Flight Center solar simulator. The test data may be compared with data taken during outdoor tests in previous studies.

The test article is a single-glazed collector with a nonselective absorber plate, an aluminum box frame, and isocyanurate foam insulation 1 inch (2.54 cm) in thickness. The 65-pound (29.4-kg) collector has a surface area of 25.6 ft^2 (2.38 m^2).

The indoor test data, including thermal-performance tests, time-constant tests, and incident-angle modifier tests, are presented in a series of tables and graphs. Each of the data sets is discussed and analyzed.

This work was done by Wyle Laboratories for **Marshall Space Flight Center.** *Further information may be found in NASA CR-150631, "Indoor Thermal Performance Evaluation of The SEPCO Air Collector," a copy of which may be obtained at cost from the New England Research Application Center* [see page A7].
MFS-23954

Performance Evaluation of an Air Solar Collector

Indoor tests on a single-glazed flat-plate collector

The procedures and results of evaluation tests on a flat-plate air solar collector are described in a new report, referenced at the end of this article. The tests were made by using the Marshall Space Flight Center solar simulator. They included stagnation tests and an evaluation of the collector thermal performance under various combinations of flow rate, incident flux, inlet temperature, and wind speed. Time-constant tests and incident-angle-modifier tests were also carried out to determine the transient effect and the incident-angle effect. The results are presented in graphs and tables and are discussed.

The single-glazed collector uses air as the heat-transfer medium. The glazing is 3/16 in. (0.48 cm) in thickness, with 92 percent transmittance; the absorber is copper sheet with a selective black coating. It has 0.90 absorptivity and 0.12 emissivity. Outside dimensions are 36 by 84 by 4 in. (91.4 by 213.4 by 10.2 cm). The gross area is 21.0 ft^2 (1.95 m^2).

The thermal-performance tests were done at inlet temperatures of from 0° to 100° F (0° to 55.5° C) above ambient in steps of 25° F (13.8° C). Airflow rates were 42 and 105 $stdft^3/min$ (1.2 and 3.0 m^3/min); insolation rates were 250 and 300 $Btu/h\text{-}ft^2$ (0.019 and 0.022 $cal/s\text{-}cm^2$); and wind speed was 7.5 mi/h (3.3 m/s). The measured efficiencies approached 60 percent under the most favorable conditions.

This work was done by the Solar Energy Systems Division of Wyle Laboratories for **Marshall Space Flight Center.** *Further information may be found in DOE/NASA CR-150666, "Indoor Test for Thermal Performance Evaluation of the Sunworks [Air] Solar Collector," a copy of which may be obtained at cost from the New England Research Application Center* [see page A7].
MFS-23968

Outdoor Tests of a Liquid Solar Collector

Thermal efficiency was tested under varied conditions.

The results of an outdoor test program to evaluate the thermal performance of a liquid solar collector are presented in a new report. The test article is a flat-plate collector with an antifreeze solution as the working fluid. Its absorber plate is aluminum. The stainless-steel tubing through which the fluid flows is 1/2 inch (1.27 cm) in diameter. Tables and graphs show the variation of the collector efficiency with inlet temperature, flow rate, and windspeed.

Twenty tests were conducted at flow rates of 380 and 680 lb/h (172 and 308 kg/h) and inlet temperatures from 24.5° to 157.6° F (14° to 87° C) above ambient. Windspeed varied between 2 and 9 mi/h (0.9 and 4 m/s). The thermal efficiency of the collector was determined in each test; it ranged between 18.1 and 54.2 percent.

This work was done by the Solar Energy Systems Division of Wyle Laboratories for **Marshall Space Flight Center.** *Further information may be found in DOE/NASA CR-150675, "Outdoor Thermal Efficiency Evaluation of the Ying Solar Collector," a copy of which may be obtained at cost from the New England Research Application Center* *[see page A7]*.
MFS-23969

Computer Programs

These programs may be obtained at very reasonable cost from COSMIC, a facility sponsored by NASA to make new programs available to the public. For information on program price, size, and availability, circle the reference letter on the COSMIC Request Card in this issue.

Power Loss for High-Voltage Solar-Cell Arrays

Electric field, particle collection, and power loss are all calculated.

The power loss for high-voltage solar-cell arrays is computed by calculating the three-dimensional electric field surrounding an arbitrary two-dimensional rectangular grid of potentials. These are arbitrarily assigned to represent an uninsulated solar array.

The program calculates particle fluxes or densities, that is, moment integrals of the velocity distribution at arbitrary points in space, when the electric field is given. (A moment integral is expressed as an integral of the phase space density over the three-dimensional velocity space.) Replacement of the triple integral by an approximating Gaussian quadrature sum is equivalent to representation of the contributions of a continuum of trajectories by those of a finite number.

On each trajectory the phase space density is constant. The trajectories are dynamically reversible in the time-independent field, and by following each trajectory backward in time to its origin (meaning "infinity" in the plasma or a nearly emitting surface) where the phase space density is considered known, one may evaluate the terms in the quadrature sum. The power loss to the array surface is then given by an integration of power fluxes, which are products of local voltage and current density over the surface. Space charge effects are not considered in this program.

The inputs to the program are:

- The two-dimensional array configuration.
- The particle population and particle energy in space.
- The number and space of array and three-dimensional grid points to be used in the computation.

The outputs of the program are:

- The three-dimensional electric field around the array.
- The rate of charged-particle collection at each grid point on the two-dimensional array.
- The total charged-particle collection on the array and the resultant total power loss.

The computer program can incorporate positive and negative charge flows, and the balance between positive and negative flows can be performed by iteration.

The program is written in FORTRAN IV for use on a UNIVAC 1100/40 computer.

This program was written by Lee W. Parker of Lee W. Parker, Inc., for **Lewis Research Center.** *For further information, Circle A on the COSMIC Request Card.*
LEW-12865

Ocean-Wave Ray or Crest Diagrams in Shoaling Waters

Automatic generation of diagrams requires minimal computer resources.

A program developed to aid studies of linear ocean-wave refraction features random-access modular storage of bathymetry data to minimize computer resource requirements. Any of three bottom-topography approximation techniques are available for varying degrees of bathymetry data smoothing. This allows the user to assess the sensitivity of computed results to the degree of smoothing chosen. Wave ray patterns can be generated and plotted automatically with either a specified, uniform, deep-water ray spacing or a constrained, nearshore ray spacing. As an option, wave crest patterns can be constructed and plotted by using a cubic polynomial to approximate individual crest segments between adjacent rays. This

(continued on next page)

program is a study tool that could be used to forecast ocean conditions for ship routing and offshore activities.

Wave refraction diagrams can be interpreted as either a group of wave crests at a particular time or as the successive positions of a particular wave crest as it moves shoreward. The model used is based on one developed by Dobson that couples wave ray construction by using a grid of water depths and a finite-difference solution to the wave intensity equation developed by Munk and Arthur. Bathymetry data are stored and used in modular form by using random-access techniques. This approach allows very large geographical regions to be studied with fewer computer resources but does not restrict the applicability of the model to smaller areas.

Ocean bottom topography can be approximated by quadratic least squares, cubic least squares, or constrained bicubic interpolation techniques. In the normal mode, the spatial position of the initial point on each wave ray in a particular set is computed automatically to achieve a uniform deepwater ray density. In this mode the user can readily identify areas of relatively high or low energy on the resultant refraction diagram as areas of convergent and divergent ray groups.

As an alternative, one can request automatic computation of deepwater ray spacing required to satisfy specified constraints on nearshore ray density. This option provides increased directional information in the nearshore zone while sacrificing the easy identification of high- or low-energy regions. Wave crests can be constructed by using a cubic polynomial to approximate the crest segment between corresponding points on adjacent rays. A request for crest output requires selection of the controlled nearshore ray-density option.

This program is written in FORTRAN IV for batch execution and has been implemented on a CDC Cyber 173 with a central memory of approximately 75K octal of 60-bit words. For plotted output a CALCOMP or similar plotting system is required.

This program was written by W. Douglas Morris and Lamont R. Poole of **Langley Research Center** *and Stuart R. LeCroy of Vought Corp. For further information, Circle B on the COSMIC Request Card.*
LAR-12380

Materials

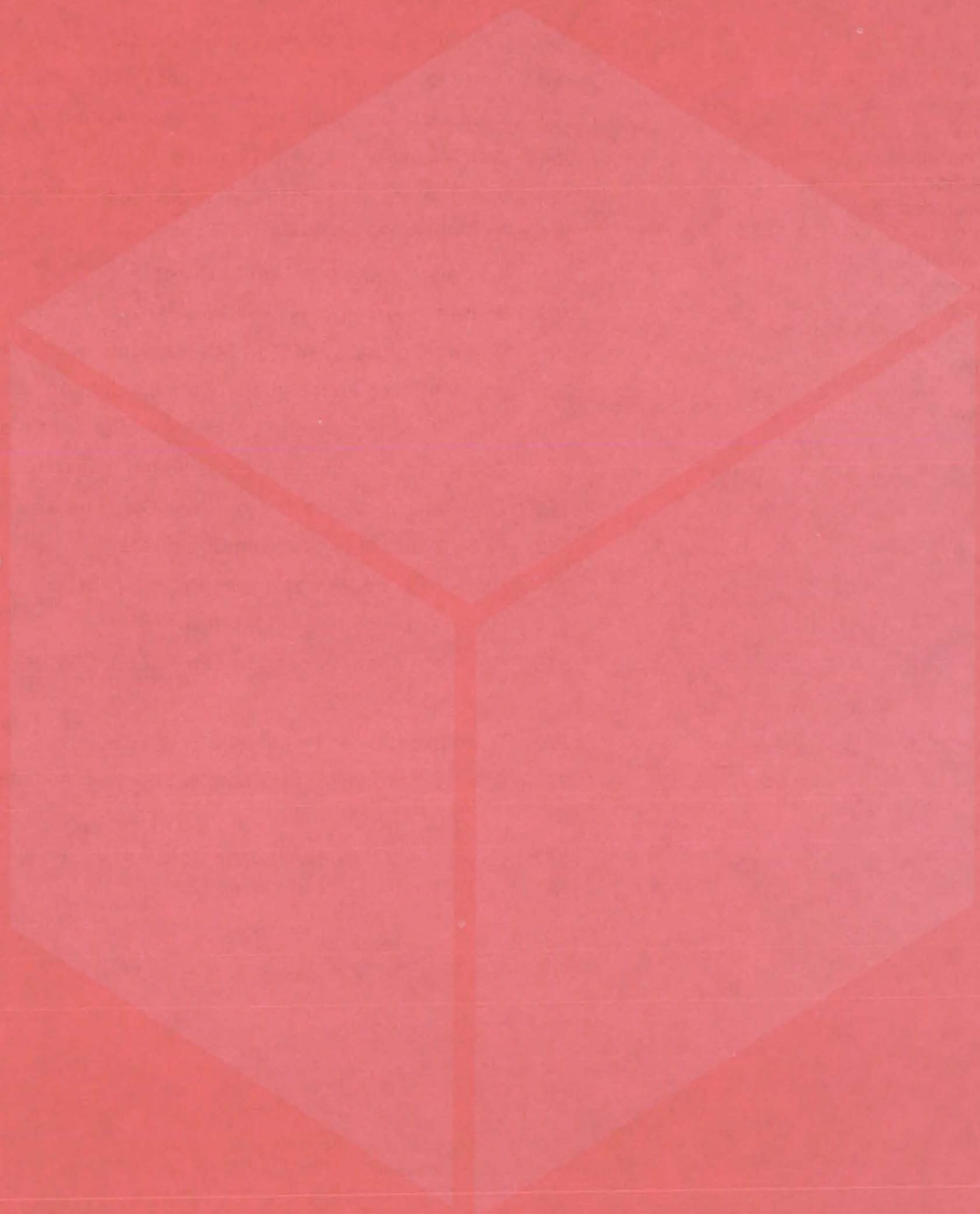

Hardware, Techniques, and Processes

Books and Reports

Computer Programs

Coal Desulfurization With Iron Pentacarbonyl

Treatment under mild conditions removes up to 80 percent of organic sulfur.

NASA's Jet Propulsion Laboratory, Pasadena, California

Most present-day coal desulfurization processes are quite expensive. They require large amounts of hydrogen or petroleum derivatives, expensive equipment, and high temperatures and pressures. Furthermore, the extreme conditions are hard on equipment, causing major maintenance expenses.

Preliminary tests on an iron pentacarbonyl desulfurization process suggest it may be economical enough to encourage more extensive investigation of its use for coal desulfurization. Iron pentacarbonyl in low-cost aromatic solvents has removed up to 80 percent of the organic sulfur present in high-sulfur bituminous coal at low temperatures and atmospheric pressure.

The method is based on the reactions shown in Figure 1. A slurry of powdered coal (200 mesh) and iron pentacarbonyl in benzene or toluene is heated in a stirred glass reactor at 70° to 100° C and a pressure of 1 atmosphere for less than 6 hours. This treated slurry is heated in a stainless-steel cylinder at 160° C for 15 minutes to 4 hours to decompose any unreacted iron pentacarbonyl. Then it is filtered, and the coal is dried.

The pyritic sulfur and ash can be removed by froth floatation. Another possible method of removing these impurities from the coal is outlined in Figure 2. In this process, a slight excess of iron pentacarbonyl is used; following desulfurization, the slurry and gas are heated to decompose the iron pentacarbonyl. According to the literature, the decomposition results in a thin skin of magnetic material on ash and the pyritic sulfur but not on the coal. Magnetic separation can remove the ash and pyrites.

The sulfur-containing acid gas, COS, in the product gas stream can be economically recovered as a byproduct of the sulfinol process. The iron pentacarbonyl can be regenerated by passing CO gas through a hot (200° C) bed of iron filings. If the cost of safety measures in handling the toxic $Fe(CO_5)$ gas can be solved economically, this process with its mild operating conditions could produce environmentally-acceptable clean coal at a reasonable cost.

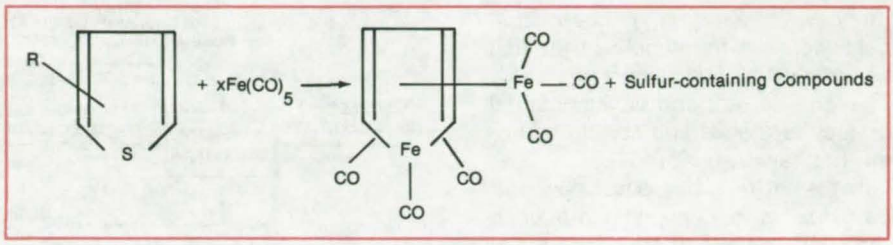

Figure 1. The **Iron Pentacarbonyl Desulfurization Process** is based on the reaction of thiophene compounds and $Fe(CO)_5$. The sulfur-containing compounds resulting from iron pentacarbonyl treatment may include COS and compounds containing iron and sulfur.

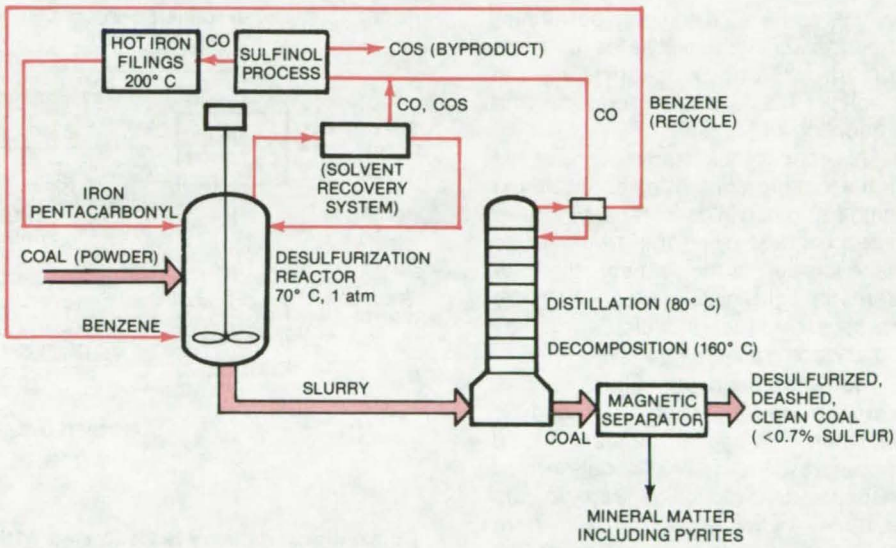

Figure 2. The **Desulfurization Reactor** is equipped with a solvent recovery system for reflux of benzene. The reacted slurry is distilled to recover benzene for recycle in the system. The desulfurized coal is further treated either by magnetic separation or froth floatation to remove minerals including pyritic and sulfate sulfur. The final product is a desulfurized and deashed clean coal.

This work was done by George C. Hsu of Caltech for **NASA's Jet Propulsion Laboratory.** *For further information, Circle 26 on the TSP Request Card.*

Inquiries concerning rights for the commercial use of this invention should be addressed to the Patent Counsel, NASA Resident Legal Office-JPL [see page A8]. Refer to NPO-14272.

Coal Liquefaction To Increase Jet Fuel Production

Coal liquefaction, in conjunction with a modified petroleum refinery, could increase jet fuel supply.

Langley Research Center, Hampton, Virginia

A new processing concept that could increase the supply of jet fuel has been developed as part of a study of several current and developmental methods for converting coal to hydrogen, methane, and jet fuel.

In the new processing concept, heavy fuel oil and naphtha produced from coal liquefaction are converted to a high-aromatic-content gasoline that is sent to petroleum-refinery octane pools. By introducing the coal-derived gasoline into the refinery product supply, some of the highly-paraffinic, low-aromatic light distillates that are normally reformed catalytically to gasoline stock are freed for the production of jet fuel.

This concept takes advantage of the high aromatic content of coal-derived liquids to make high-octane gasoline, instead of destroying the aromatics to make jet fuel. In the refinery, the low-aromatic light distillate can then be directed to jet fuel, in which aromatics are undesirable.

The accompanying figure shows how the operation of the catalytic reformer in a typical refinery would change by the use of coal-derived gasoline. By reducing feed to the refinery catalytic reformer from 42,000 to 33,000 barrels/day, 9,000 barrels/day of light distillate material (kerosene) would be released for use as jet fuel. The loss of 7,530 barrels/day of reformate is made up with coal-derived high-octane gasoline. The refinery energy balance is slightly improved, and there are savings in capital and operating costs because less reforming is required. The coal liquefaction plant studies in the report could make 45,805 barrels/day of gasoline. This could be divided among six refineries.

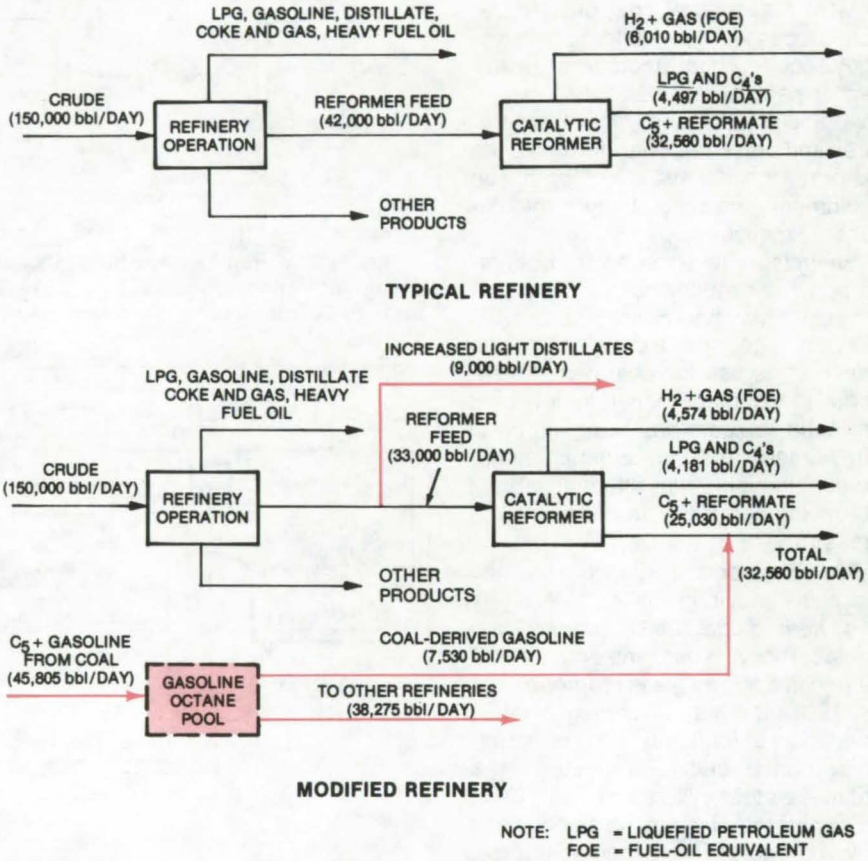

A **Conventional Refinery Is Compared With a Modified Refinery.** The top part of the illustration shows a typical refinery process. The bottom part shows the modified refinery using the coal-derived gasoline to free light distillates for the production of jet fuel.

This work was done by the Institute of Gas Technology for **Langley Research Center.** *Further information may be found in NASA CR-145028 [N78-75465], "Study of Conversion of Coal to Hydrogen, Methane, and Liquid Fuels for Aircraft," a copy of which may be obtained at cost from the National Technical Information Service, Springfield, Virginia 22151.*
LAR-12038

Improved Nucleonic Coal-Thickness Monitor

New design features independent hydropneumatic suspension of the radiation source and the detector.

Marshall Space Flight Center, Alabama

An improved design for a coal-thickness-sensing instrument may help to bring fully-automated coal mining closer to reality. The instrument, intended for mounting on a coal-cutting machine, emits gamma rays into the coal vein and measures the intensity of gamma rays scattered from the coal/rock interface on the back face of the vein. Unlike previous nucleonic thickness monitors, the new instrument uses a source and a detector that are independently mounted, to follow the contour of the coal surface more closely and to eliminate errors caused by variations in the airgap along the radiation path.

The thickness monitor would allow a uniform layer to be left on the mine surfaces after the coal-cutting operation. This layer is needed to prevent a cave-in of loose material, to avoid cutting noncommercial-quality coal, and to prevent contact between the shearing picks of the cutter and the rock formations around the vein.

In the new design, the gamma-ray source and a scintillation detector are mounted side by side in separate housings on the mining machine (see figure). These two components are independently suspended with hydropneumatic springs so that each can track the coal surface.

The steel housing for the gamma-ray source contains cesium 137 in a lead shield. When the cutting machine starts, the source is automatically moved into position against the coal surface, and the cesium is simultaneously positioned in front of a hole in the shield that directs gamma rays into the coal. (The hole is sealed with a polyurethane diaphragm to prevent coal and rock particles from entering the detector.)

The steel housing for the detector contains a commercially-manufactured scintillation detector, mounted inside a lead cylinder to block spurious radiation. Backscattered rays enter the detector through a hole in the cylinder. The hole is held against the coal by the suspension system. (This hole is also sealed by a polyurethane diaphragm.) Electronic circuitry for processing the detector signal is contained in a steel box adjacent to the detector.

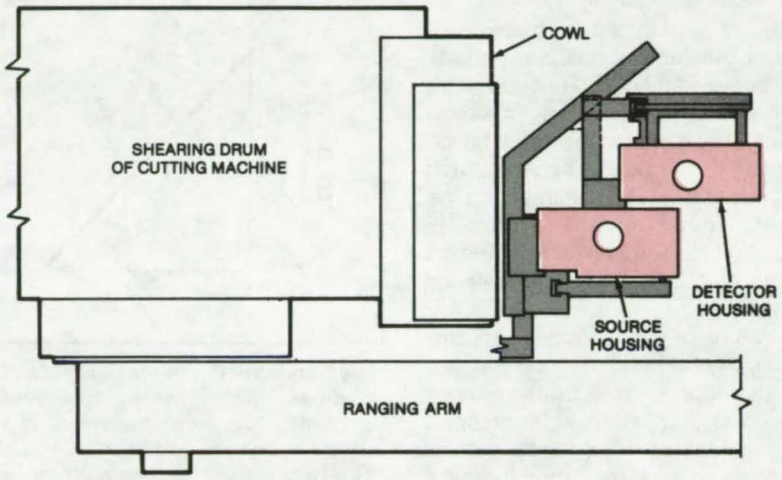

TOP VIEW

A Coal-Thickness Monitor is mounted on a coal-cutting machine. The independently suspended source and detector, shown in this top view, are held gently but firmly against the roof of a coal deposit by hydropneumatic suspension, to follow the contours of the surface.

In one proposed design, the distance between the source and the detector is adjustable from 10.5 to 22.5 inches (26.7 to 57.2 cm) in 2-inch (5.1-cm) increments.

The hydropneumatic-spring suspension system consists of an accumulator in series with two hydraulic cylinders that force the housings against the coal surface. The volume of air in the accumulator is several times as large as the oil volume to prevent large changes in oil pressure during operation. Control valves direct oil flow to opposite ends of the double-acting hydraulic cylinders to extend or retract the housings.

A pressure-reducing valve allows the accumulator to be filled to a predetermined pressure, selected to give adequate dynamic response over the total range of vertical movement of the housings [±4.75 inches (±12.1 cm) for the source, ±5 inches (±12.7 cm) for the detector].

This work was done by Charles E. Crouch and Stephen D. Rose of **Marshall Space Flight Center** *and Elborn W. Jones of Mississippi State University. Further information may be found in NASA CR-150465 [N78-11454], "Nucleonic Coal Detector With Hydropneumatic Suspension," a copy of which may be obtained at cost from the New England Research Application Center [see page A7].*

Inquiries concerning rights for the commercial use of this invention should be addressed to the Patent Counsel, Marshall Space Flight Center [see page A8]. Refer to MFS-23725.

Coal Mining With a Liquid Solvent

Study suggests that carbonated water can dissolve or suspend coal and carry it to the surface.

NASA's Jet Propulsion Laboratory, Pasadena, California

Although a number of schemes for the unmanned mining of coal by solvent extraction have been proposed, a satisfactory coal solvent has yet to be developed. Compounds and mixtures such as pyridine, phenanthrene, tetralin, quinoline, and tar-oil fractions have been experimented with; but yields have been low, and the required temperatures have run as high as 600 K. The solvents tested so far have also been too expensive for commercial use.

A mixture of two abundant and inexpensive materials — carbon dioxide and water — may be the elusive coal solvent that will make unmanned mining a reality. When used with a proposed process that monitors the coal solubility with a conventional strain gage, the solvent could be the basis for rapid, cost-effective extraction of coal from underground seams.

Preliminary experiments have shown that high-strength coal is converted to an easily pulverized mass when treated with a water/carbon dioxide mixture that has approximately the same solubility parameter as the coal itself. It may even be possible to reduce the coal to a powder if the solubility parameters are precisely matched. Furthermore, recovery of the solvent would be relatively simple, and pollution would be minimal. In addition to transporting the coal slurry to the surface, the mixture could also be used as a hydraulic fluid for transporting power to the coal face.

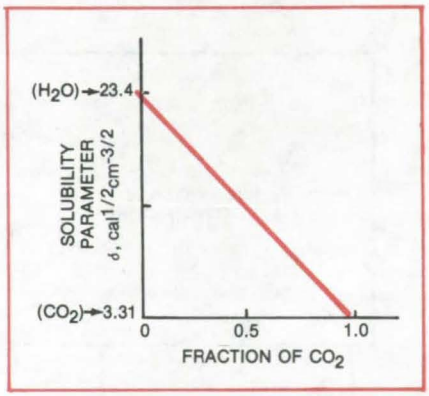

The Solubility Parameter of Water/CO_2 Mixtures varies with the relative amounts of each component. This variation can be used to control the solubility effectiveness of the mixture when used as a solvent for extracting coal from underground seams. The temperature of the mixture can also be adjusted to change the solubility parameter.

Since the matching of solubility parameters is important for obtaining the mutual solubility of two substances, a multicomponent solvent that allows its solubility parameter to be adjusted (see figure) is especially suitable for mining coal. By changing the amount of each component, the solubility can be matched to that of the coal as it changes with temperature, pressure, and depth. Even the component of the underground coal that is cross-linked to form an intrinsically insoluble gel will absorb a portion of the liquid, resulting in swelling and the rupture of cohesive bonds. The fraction that is not cross-linked (the sol) would be precipitated as a loose powder.

In the proposed method, the coal would be cut (remotely) through a small-diameter hole that is filled with solvent. The percentage of CO_2 and the temperature of the mixture would be varied as mining proceeds to adjust the solubility parameter.

For the process to be practical, it will be necessary to derive real-time measurements of the coal solubility-parameter and to adjust the solvent immediately. Solubility measurements that depend on recording the volume change of the solute over several days are clearly not applicable. However, by attaching a strain gage to a coal sample and measuring the small volume change that occurs when a test solvent is introduced, an immediate indication of the solubility could be obtained. The strain-gage signal could be fed to a controller that adjusts the CO_2 level in the mixture, for a completely-automated unmanned mining process.

This work was done by Daniel D. Lawson and Charles G. Miller of **NASA's Jet Propulsion Laboratory.** *For further information, Circle 28 on the TSP Request Card.*

Inquiries concerning rights for the commercial use of this invention should be addressed to the Patent Counsel, NASA Resident Legal Office-JPL [see page A8]. Refer to NPO-14028.

Low-Temperature Elastomer Production and Curing

Polymerization without condensation products is possible under low heat.

NASA's Jet Propulsion Laboratory, Pasadena, California

Thermally and chemically stable polymers are needed for materials applications, particularly highly-stable elastomers for solid propellant binders in which the initial high temperature required for dissolving the anhydride in the polymer would be detrimental. Polyurethane elastomers, while having the advantage of producing no by-products in the alcohol-isocyanate reaction, are unstable at elevated temperatures.

The ester linkage is believed to have considerably better thermal stability than the urethane linkage. However, polyesters are generally prepared by the alcohol-carboxylic acid reaction, which proceeds at about 200° C and liberates water as a byproduct. If a byproduct-free polyester is produced without a solvent system, using

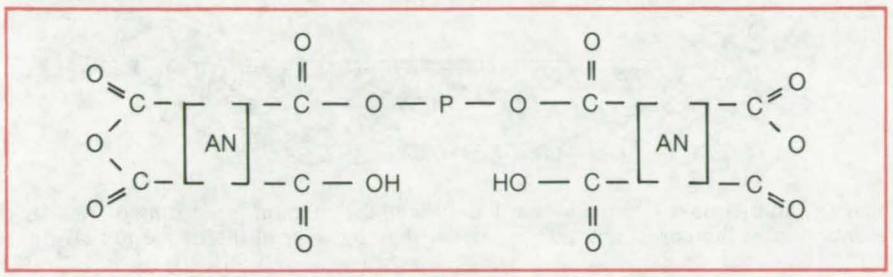

Prepolymer Dianhydride is prepared by the reaction of a prepolymer diol with an excess of a dianhydride (tetrahydrofuran-tetracarboxylic dianhydride) in a solvent such as dimethylformamide. Ferric acetylacetonate is added as a catalyst.

dianhydrides and a prepolymer diol, the mixture must still be heated to 200° C to form a proper solution before curing can proceed.

A solvent-reactant system has been developed that combines the following features: The process can be initiated at a lower temperature, about 100° C; curing can proceed at about 100° C; there are no condensation products; and the final polyester product is heat-stable.

The prepolymer dianhydrides (see figure) are prepared by the solution reaction of prepolymer diols with a great excess of dianhydride. After the reaction, unreacted dianhydride is removed. The solvents used are dimethylacetamide (DMAC), dimethylformamide (DMF), and the like. Metal acetyl acetonates are used as catalysts. Polyester linkages are formed by reacting the prepolymer dianhydride with prepolymer diols at low temperature.

This work was done by John D. Ingham and Robert A. Rhein of Caltech for **NASA's Jet Propulsion Laboratory.** *For further information, Circle 29 on the TSP Request Card.*

Inquiries concerning rights for the commercial use of this invention should be addressed to the Patent Counsel, NASA Resident Legal Office-JPL [see page A8]. Refer to NPO-13899.

Gas-Path Seal Material

Composite sealant reduces frictional heating, wear, and leakage.

Lewis Research Center, Cleveland, Ohio

In order to reduce wear of rotating compressor-blade tips in the event that they rub against the stationary engine casing, easily-abradable seal materials are commonly applied to the casing. Typically, these abradable seal materials are sintered or thermally sprayed structures having a low effective density (high porosity) so that they may be easily worn. Unfortunately, materials that are easily worn are also susceptible to erosion damage and often allow leakage through interconnected pores. Furthermore, porous materials are poor dissipators of heat; during rubbing contact with blade tips, they often smear, forming a nonporous surface and even greater frictional-heat generation. A new abradable seal material was desired that could resist erosion damage and at the same time not cause wear to the blade tips or promote severe frictional heating.

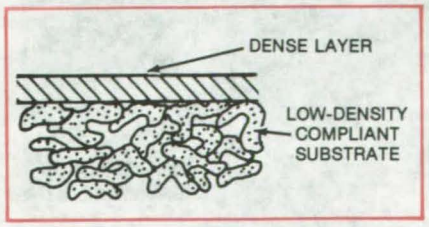

Figure 1. **Compliant-Backed Gas-Path Seal** consists of a low-density nickel substrate with a plasma-sprayed dense top layer.

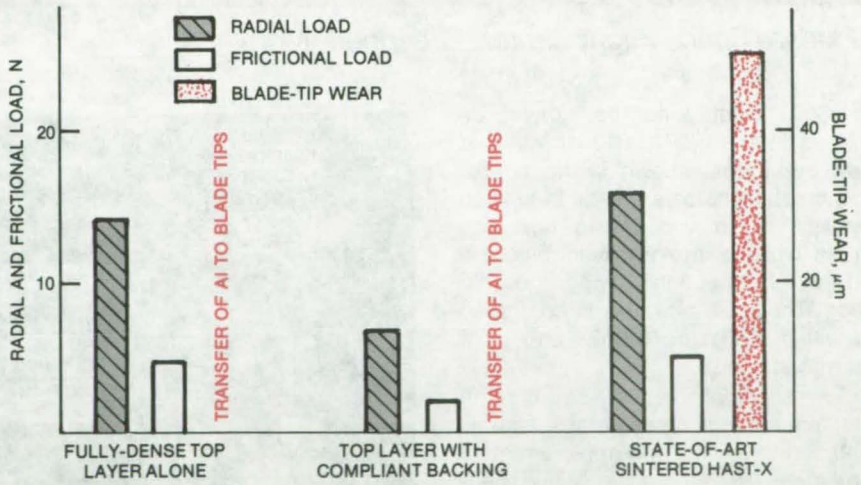

Figure 2. **Test Results** of a preliminary evaluation show that the compliant backing significantly reduces loads and blade-tip wear.

An approach having the potential of combining all of the characteristics desired in an abradable seal material is shown in Figure 1. Briefly, the concept consists of a low-density, compliant substrate supporting a thin, dense top layer adjacent to the gas path. For demonstration purposes, a 15-percent-dense nickel substrate with a 95- to 98-percent-dense plasma-sprayed aluminum top layer 15 to 20 mils thick was evaluated. When a rub occurs, the thin top layer and the low-density substrate are

(continued on next page)

easily deformed without developing high contact loads with consequent frictional heating and wear of the blade tips.

Preliminary evaluation of the concept was conducted on a test rig simulating a rub between rotating blade tips and the seal material. Measured radial and frictional loads are summarized in Figure 2. The compliant-backed seal evaluated in these tests was not optimized with respect to the thickness of the dense layer. Nevertheless, the presence of the low-density compliant backing reduced the contact and frictional loads to about one-half the value measured for the dense top-layer material alone. Furthermore, loads and blade-tip wear are significantly less than for the case of rubbing against a commonly-used low-density, sintered, abradable seal material.

Metallographic sectioning of the compliant-backed seal indicates that the rubbing was accommodated by the easily-deformable low-density substrate (Figure 3). Little wear to the dense top layer took place; the layer itself remained intact and provided a heat conduction path away from the rub surface.

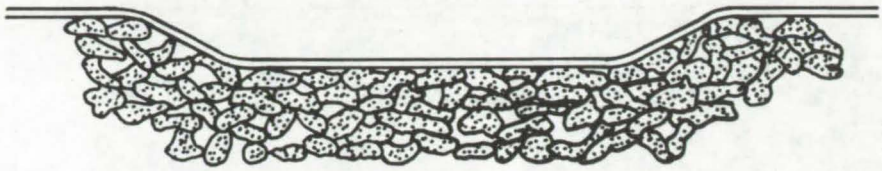

Figure 3. **Rub-Groove Cross Section** illustrates how rubbing is accommodated by deformation of the compliant backing rather than by wear of the dense top layer.

This work was done by Robert L. Johnson and Lawrence P. Ludwig of **Lewis Research Center** *and Robert C. Bill of the U.S. Army Research & Technology Labs. Further information may be found in:*

NASA TP-1128 [N78-15229], "Friction and Wear of Several Compressor Gas-Path Seal Materials," and

NASA TM-X-73650 [N77-23489], "Friction and Wear of Sintered Fiber-Metal Abradable Seal Materials."

Copies of these reports may be obtained at cost from the New England Research Application Center [see page A7].

This invention is owned by NASA, and a patent application has been filed. Inquiries concerning nonexclusive or exclusive license for its commercial development should be addressed to the Patent Counsel, Lewis Research Center [see page A8]. Refer to LEW-12623.

Precision Cleaver for "Soft" Crystals

Adjustable cutter can cleave uniform 5-mil slices.

Goddard Space Flight Center, Greenbelt, Maryland

"Soft" crystals can be cleaved as thin as 0.005 inch (0.013 cm) with a new apparatus, shown in the figure. The machine holds a crystal in tension by applying a vacuum to opposing faces while a motor-driven blade is advanced, "peeling" away the thin slice. The slice thickness is controlled to within 0.001 in. (0.0025 cm) by a micrometer adjust.

Thin slices of relatively-soft crystalline materials, such as potassium acid phthalate (KAP), and rubidium acid phthalate (RAP), used in X-ray spectrometers are usually cut by hand with a wire or blade. Neither method is entirely satisfactory. The wire tends to scratch the crystal surface and to produce slices of nonuniform thicknesses. With the blade, it is difficult to cut very thin slices. The new machine, however, can rapidly cut soft crystals in smooth, thin, uniform slices.

The cutter blade is secured in a holder that is positioned vertically by a hand-operated lead screw and is moved horizontally by a drive motor.

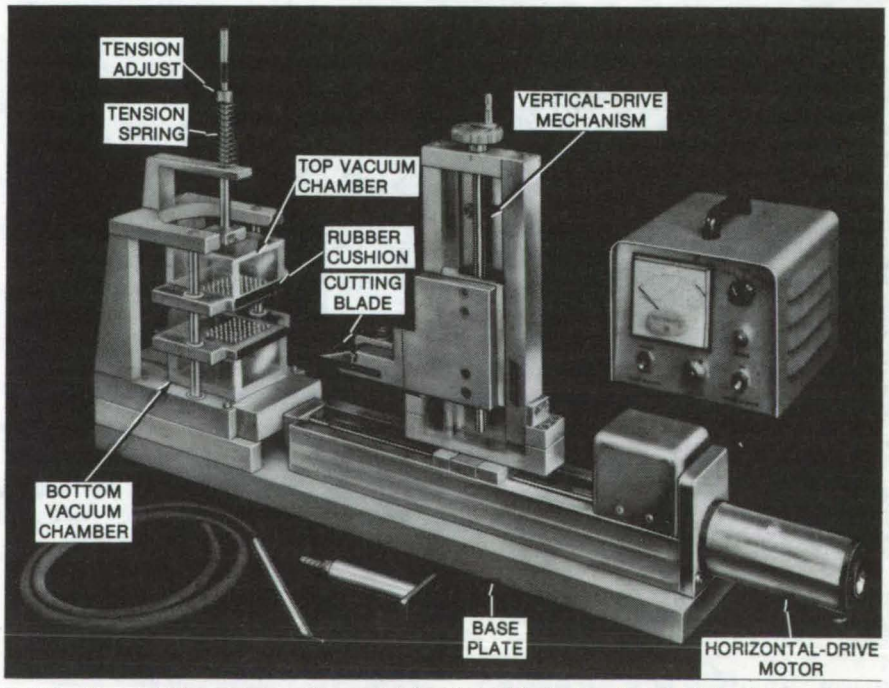

In this **Crystal Cleaver,** a soft crystal is placed between top and bottom vacuum chambers that hold the crystal under tension. The motor-driven blade advances through the crystal, cleaving slices as thin as 0.005 in.

An operator adjusts the vertical position to the desired depth of cut, and the motor advances the blade into the crystal at that level.

The crystal is held in a gripping station by upper and lower vacuum chambers. Perforated platens on the chambers grip the upper and lower faces of the crystal block by suction. The lower chamber is fixed, but the height of the upper chamber is adjustable. The upper chamber is pulled upward by a spring, putting the crystal block in tension. As the blade moves forward, the upper chamber pulls the slice away from the rest of the crystal.

The upper platen is faced with resilient, perforated neoprene rubber. The facing prevents the platen from directly contacting the upper face of the crystal and accommodates any nonuniformity in the top face of the crystal slice. The facing protects the crystal against scratches, cracks, and chips.

The motor slowly advances the cutting blade through the crystal at a speed controlled by a velocity feedback mechanism. When the cut is complete, the upper chamber holds the freshly cleaved segment until the vacuum is released. To make another slice, the operator reengages the upper vacuum chamber on the crystal block, adjusts the cutter to a lower position, and restarts the motor.

This work was done by John S. J. Benedicto, Frederick Hallberg, and Bruce E. Woodgate of **Goddard Space Flight Center.** *For further information, Circle 30 on the TSP Request Card.*

This invention is owned by NASA, and a patent application has been filed. Inquiries concerning nonexclusive or exclusive license for its commercial development should be addressed to the Patent Counsel, Goddard Space Flight Center [see page A8]. *Refer to GSC-12291.*

Embrittlementproof Nickel-Alloy Bellows

Thin interior layer of corrosion-resistant steel acts as a barrier against hydrogen.

Marshall Space Flight Center, Alabama

A thin cover of corrosion-resistant steel (CRES) can protect metal bellows and ducts against hydrogen embrittlement. Such a bellows has been developed for the Space Shuttle main engine, for example. The bellows carries hydrogen at high pressure [5,000 psi (34.5×10^6 N/m^2)] and must swing over wide arcs as the gimbaled engine moves.

To provide the necessary strength and flexibility, and to keep down size and weight, Inco 718 alloy was selected as the bellows material. However, like other nickel alloys, Inco 718 is highly susceptible to hydrogen embrittlement. The hydrogen in the bellows would soon reduce the alloy ductility so that the bellows would fail from fatigue after a relatively low number of flexures.

To keep hydrogen from directly contacting the Inco alloy, a thin [0.005-in. (0.13-mm)] ply of 316 CRES was added to the inside of the bellows (see figure). The CRES ply is welded to the Inco alloy at the ends of the bellows, but is free for most of its length. It does not matter that CRES is much lower in strength than the Inco 718, because it does not function as a load carrier but solely as a protective barrier. It is thin enough that bending does not introduce significant stresses, so fatigue life is not a problem. The CRES ply, moreover, is compatible with the heat treatment that the Inco bellows is subjected to after the two materials are welded together.

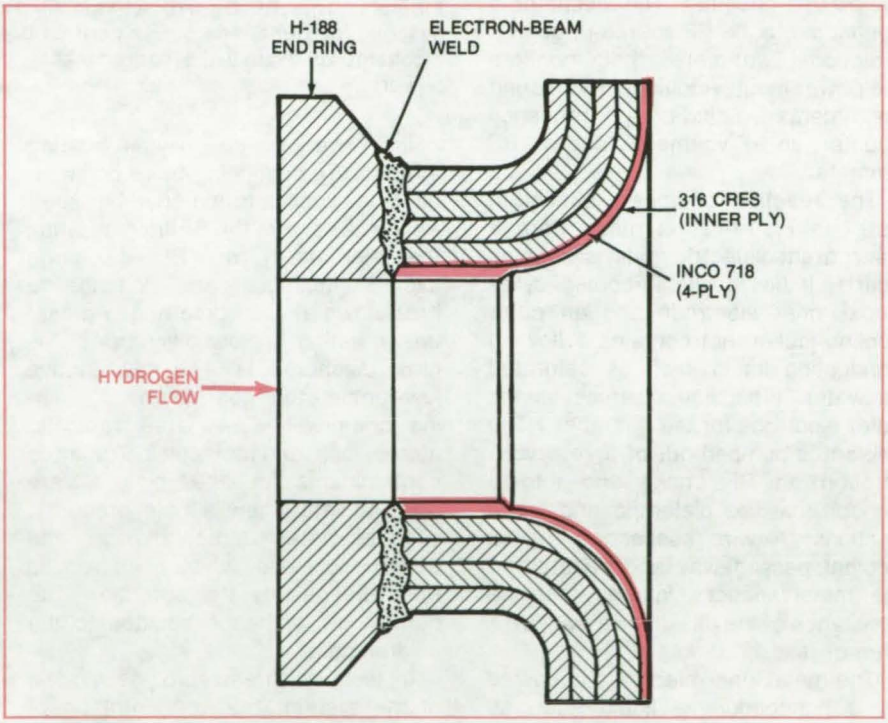

A free-moving layer of Corrosion-Resistant Steel, 0.005 in. thick, protects four plies of nickel alloy, 0.024 in. thick (0.6 mm), in this rocket-engine bellows.

This work was done by Charles M. Daniels, Jr., of Rockwell International Corp. for **Marshall Space Flight Center.** *No further documentation is available.*
MFS-19331

Corona-Discharge Air-Purification System

An electric discharge oxidizes trace contaminants to products that are removed by a scrubber.

Ames Research Center, Moffett Field, California

A plasma-reaction chamber removes trace contaminants from spacecraft, submarines, and other closed environments by oxidizing the contaminants to produce carbon dioxide and water. The contaminants range from metabolic products, such as alcohols, esters, hydrogen sulfide, and ammonia, to lubricant solvents, such as Freons, aromatics, alcohols, and ketones. The oxidized contaminants are removed from the chamber by a scrubber.

The system, as illustrated in Figure 1, includes a plasma glow-discharge chamber powered by a variable radio-frequency (RF) source. A helical resonator, or similar low-loss high-Q resonant element, generates a high voltage, sufficient to produce a glow discharge, between the electrodes in the plasma chamber. The resonator is connected to the RF source through a directional wattmeter that monitors the power input. Additional monitoring instruments include a frequency counter, an RF voltmeter, and an RF ammeter.

The reaction chamber, shown in detail in Figure 2, is made from a transparent dielectric material such as quartz. It has a liquid-cooled cylindrical inner electrode and an outer cooling jacket that contains a flowing conducting liquid such as saturated saltwater. (This liquid serves as the outer electrode for the chamber.) The coolant is pumped out of a reservoir, through an RF choke and into a conduit that has dielectric and metal sections. A wire suspended in the coolant passageway and secured to the metal sections insures that the resistance of the passageway will be 1 ohm or less.

The metal inner-electrode is cooled by a nonconductive liquid such as distilled water. The coolant reservoir is connected to the electrode through dielectric conduits attached to both electrode ends.

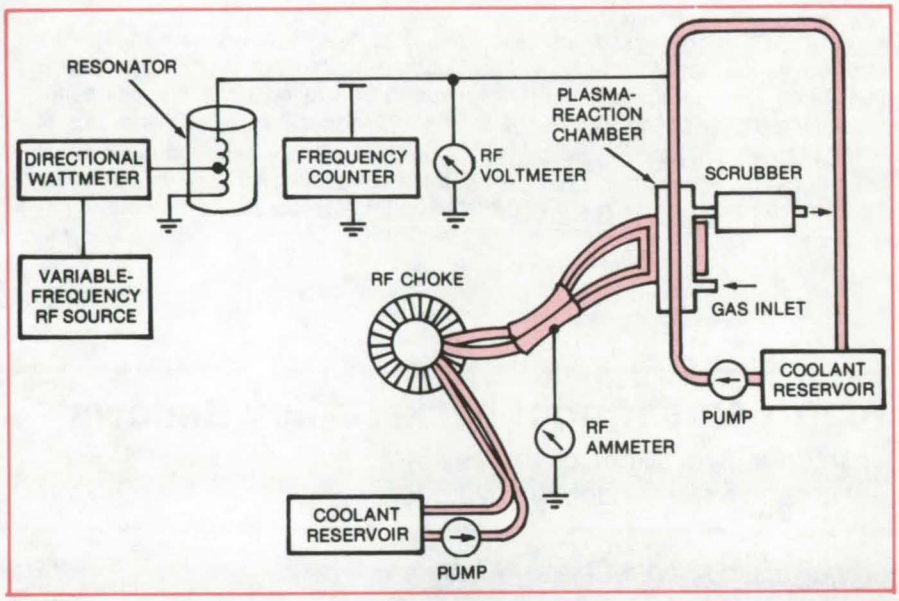

Figure 1. This **RF Glow-Discharge Air Purifier** removes trace contaminants from gaseous mixtures. The gas is purified in the chamber, which generates an electric discharge to remove the contaminants. A variable-frequency RF source supplies power.

In operation, the oxygen-bearing atmosphere containing trace contaminants is supplied to the chamber inlet. As the gas enters the RF field between the electrodes, an RF discharge excites the gas and initiates a breakdown at a predetermined pressure, creating a glow discharge. This glow discharge is a highly-reactive low-temperature gas plasma containing chemically-active free radicals, atoms, ions, and molecules. The trace contaminants in the plasma are oxidized into a few simple products, such as water, carbon dioxide, and carbon monoxide, which are removed from the gas by the scrubber. The purified air is then exhausted to the environment.

In tests on three prototype models of the system, the concentration of methane was reduced by three orders of magnitude, with the discharge operating at pressures of from 50 to 300 torr (6.7×10^3 to 39.9×10^3 N/m^2). The removal rate is independent of the concentration of the contaminant, an important advantage over other air-purification systems.

The outside diameters of the inner electrode in the prototypes were 0.079, 0.159, and 0.318 cm, respectively. The inside diameter of the quartz gas chamber was 0.5 cm, and the length of the discharge zone was 9.1 cm. The RF source operated at a frequency of 11.8 MHz. Power consumption was 240 W [at 60 torr (8.04×10^3 N/m^2)] and 350 W (at 300 torr).

In addition to the model shown, three alternative chambers have also been developed. One version uses a conductive coating to form the outer electrode. The second utilizes no liquid coolants and instead incorporates metal cooling fins encircling its middle section. The inner electrode in this case is a heat pipe that conducts the heat to the metal fins. The third

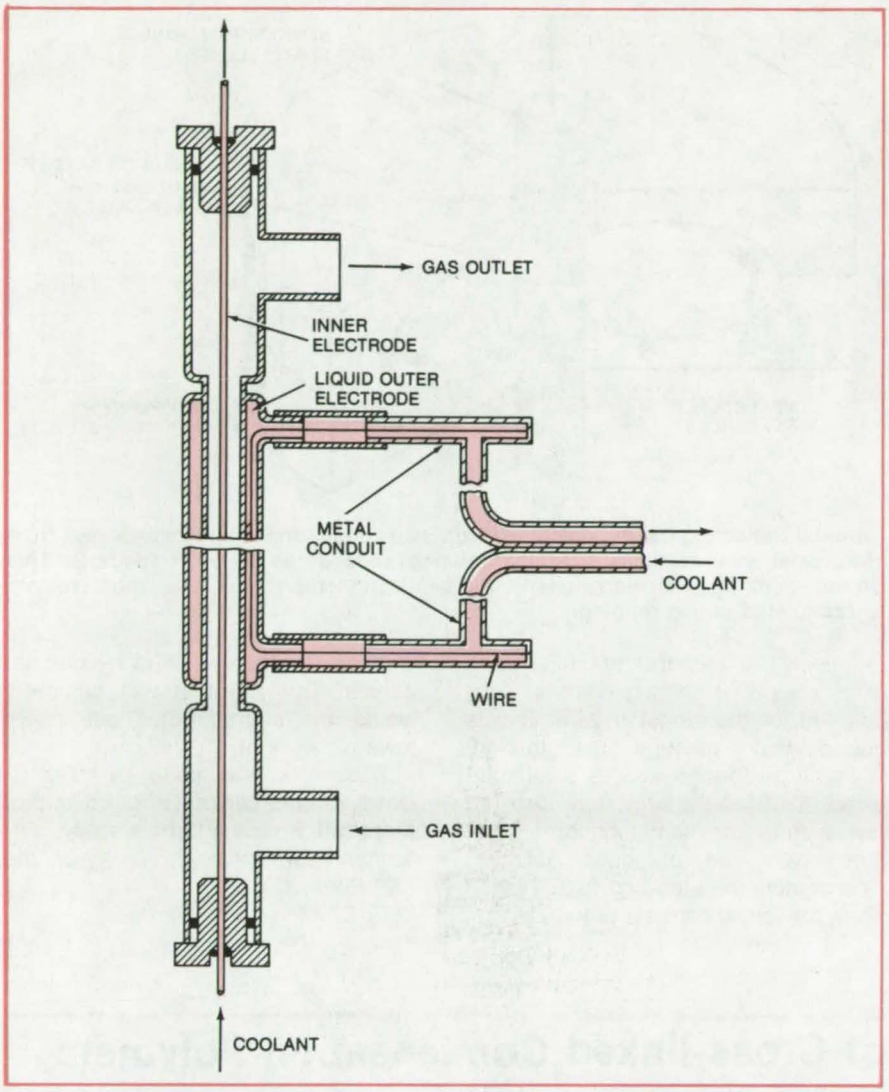

Figure 2. A **Detailed View** of the plasma-reaction chamber illustrates the cooling system and electrode arrangement. The coolant for the outer jacket is a conducting liquid and serves as the outer electrode for the glow discharge.

version uses a serpentine-shaped metal cooling coil. The operating principle is the same for all models.

This work was done by Theodore J. Wydeven, Jr., of Stanford University and Daniel L. Flamm of **Ames Research Center.** *For further information, Circle 32 on the TSP Request Card.*

This invention is owned by NASA, and a patent application has been filed. Inquiries concerning nonexclusive or exclusive license for its commercial development should be addressed to the Patent Counsel, Ames Research Center [see page A8]. Refer to ARC-10975.

Zone-Refining Encapsulated Semiconductors

Toroidal reflector focuses heat energy into narrow band around ingot.

Marshall Space Flight Center, Alabama

A newly designed reflector directs intense, sharply focused heat precisely where it is needed for zone-refining semiconductor materials. The reflector is especially suited for compound semiconductors, such as mercury-cadmium telluride, which must be sealed inside a capsule to prevent them from vaporizing during zone refining.

The reflector is a flattened toroid with an elliptical-cross-section, much like a horizontal partly-inflated inner tube. The toroid focuses are two concentric rings (see figure). A heater wire is placed at the outer focus, and the inner focus falls on the encapsulated semiconductor material.

More conventional heating methods are not adequate for zone-refining encapsulated materials. A simple ring heater cannot concentrate heat sufficiently, and electron bombardment does not penetrate the quartz capsule. An earlier reflector furnace employs a prolate ellipsoidal (football-shaped) reflector with the capsule at one focus and a heat source — an electric arc or a quartz iodide incandescent lamp — at the other focus. With this furnace, although both focuses are supposed to be points for maximum heating efficiency, the capsule is not a point, and the heat source only roughly approximates a point.

(continued on next page)

In the toroidal-reflector furnace, however, the heater wire closely approximates the ideal, lying as it does along an extended line focus. Moreover, the semiconductor material is heated uniformly around its circumference.

The reflector is machined from solid copper in two halves, the upper half being split along a diameter. In a prototype, the inside of the reflector cavity is gold-plated for high infrared reflectivity. The copper shell has an outside diameter of 243 millimeters and a center bore of 23 millimeters for pulling the semiconductor ingot through the hot zone.

Tungsten is used for the heater wire because it can operate at high temperature and because its relatively low thermal expansion stabilizes the heater radius — a critical dimension. The tungsten heater is supported by six ceramic standoffs clamped between the upper and lower halves of the cavity. To prevent the tungsten from burning up, the entire furnace is enclosed in a vacuum tank.

Experiments on the toroidal reflector have pointed the way to a more sophisticated version. The experiments were conducted to analyze the heat-ray paths inside the cavity. For simplicity, they were performed at relatively low temperatures, in air, and with a Kanthal heating element substituted for the tungsten wire. It was found that although the toroidal furnace performed well, a significant amount of heat energy was directed away from the semiconductor ingot and lost. The proposed solution: redesigning the toroid so that, viewed from the top, it consists of two distinct elliptical segments joined by circular curves. The effect of this geometry would be to redirect "lost" rays toward the ingot.

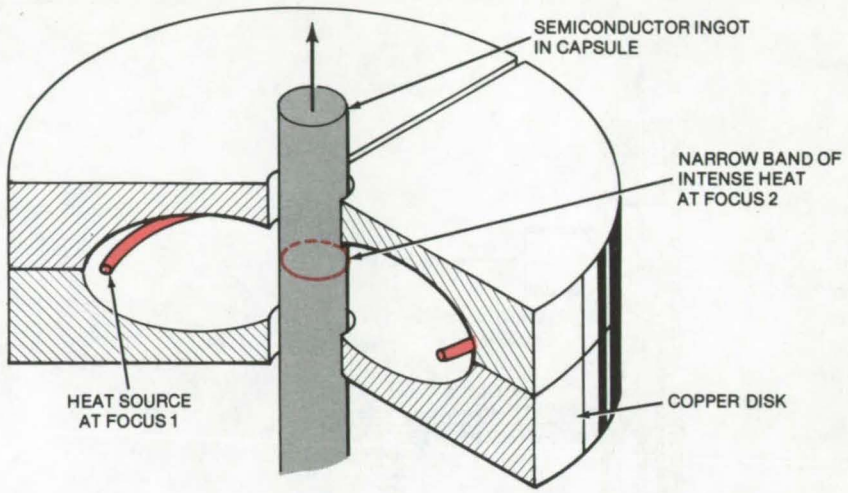

Toroidal Reflecting Cavity, machined from two copper disks, directs heat rays from the heater wire at focus 1 to the refining zone of an ingot at focus 2. This arrangement is particularly useful for semiconductor ingots that must remain encapsulated during refining.

This work was done by Mirt C. Davidson and Lawrence R. Holland of **Marshall Space Flight Center.** *For further information, Circle 33 on the TSP Request Card.*
MFS-23902

Predicting Structures of Cross-linked Condensation Polymers

Cross-link density, sol and gel fractions, chain lengths, and other parameters can be calculated.

NASA's Jet Propulsion Laboratory, Pasadena, California

A mathematical procedure can be used to predict the structure of a cross-linked condensation polymer (as differentiated from an addition polymer) resulting from a specific reaction. Cross-linked condensation polymers are found in many products, including thermosetting plastics, elastomers, plastic and rubberlike foams, solid-propellant rocket binders, coatings, and encapsulants. Until now it has not been possible to predict rigorously the structure of the end result when manufacturing this type of material, but the new procedure will greatly reduce the amount of empirical formulation and testing required to produce a desired product.

To predict the structural characteristics of a cross-linked condensation polymer resulting from a specific manufacturing process, it is necessary to know its composition, the distribution of molecules according to how many reactive groups there are on the molecules, and the extent of reaction. From this information the new mathematical procedure predicts the sol and gel fractions, concentrations of effective chains, average effective chain lengths, and distribution of a hierarchy of pendent chains (varying in size and complexity).

Flory's branching coefficient, defined as the probability that a given functional group of a branch unit leads via a chain of bifunctional units to another branch unit, is used as the basis for describing the structure of the cross-linked condensation polymers. It uses a set of relationships that deal with distributions of branch units (1) between sol and gel and (2) according to function (i.e., whether branch points, chain extenders, or chain terminators).

The branching coefficient, a, is given by

$$a = \frac{p_A p_B \sigma_B \varrho_A}{1 - p_A p_B \sigma_A \sigma_B} = \frac{p_A^2 \sigma_B \varrho_A}{r - p_A^2 \sigma_A \sigma_B}$$

Here r is the stoichiometric ratio of B to A groups, ϱ_A and σ_A are the mole fractions of A's respectively on trifunctional and bifunctional A-molecules, σ_B is the mole fraction of B's on bifunctional B-molecules (the remainder in both A and B sets consists of monofunctional components), and p_A and

p_B are the fractions of A and B groups that have reacted.

Knowing the value of a for a polymer system in some given state of cure, one can calculate the distribution of four states of trifunctional branch units. The four states are distinguished by whether none, only one, two, or all three of the branches are connected to other branch units. The relative probabilities of 0-, 1- 2-, and 3-connected branch units, respectively, are $(1-a)^3$, $3a(1-a)^2$, $3a^2(1-a)$, and a^3.

To get at the structure of the network, the only part of the polymer capable of truly elastic deformation, it is necessary to find the distribution of these four states of branch units in the gel fraction. Two key observations are used here. First, it is impossible for 0-connected branch units to be part of the network or gel. Second, Flory provides a branching coefficient for those branch units that are in the sol fraction: $a' = 1 - a$. This allows one to calculate the distribution of the four states in the sol. Distributions of the three states of branch units in the gel are calculated by difference.

Two of the four structural characteristics can be calculated from simple expressions in a:

sol fraction $= [(1 - a)/a]^3$

in mass units, and

crosslink density $=$

$10^6 d\, A_3\, [(2a - 1)/a]^3$

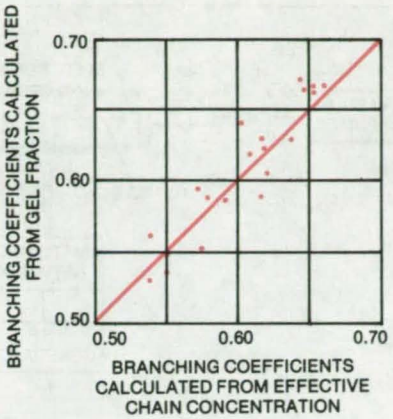

Figure 1. The **Branching Coefficients** calculated from measurements of sol/gel fractionation are correlated with those determined from equilibrium modulus. The solid line represents 100-percent correlation.

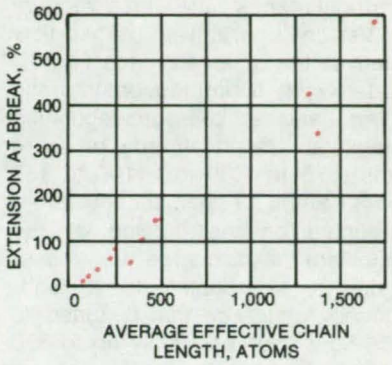

Figure 2. The **Extensibilities** at 170° F of polyester polymers are plotted against the calculated lengths of effective chains.

in moles of crosslinks per cubic meter. In this expression, d is the polymer density in gcm^{-3}, and A_3 is the concentration of trifunctional A molecules in mole g^{-1}. The other two characteristics, average effective chain length and pendent chain distributions, require complex series of calculations.

For experimental verification of the prediction procedure, ester-cured polymers of model compounds were prepared. Sol and gel fractions were measured, and effective chain concentration was determined via equilibrium modulus measurement. Correlation of branching coefficient values calculated from these data is shown in Figure 1. Samples, heated to 170° F (77° C) to avoid a crystalline phase, were pulled slowly in tension to determine extension at break. Correlation of this property with calculated effective chain length is shown in Figure 2.

This work was done by Harold E. Marsh of Caltech for **NASA's Jet Propulsion Laboratory.** *For further information, Circle 34 on the TSP Request Card.*

NPO-14007

Economical Synthesis of Potassium Superoxide

A high-frequency discharge in oxygen can be used to prepare superoxides of alkali and alkaline-earth metals.

Ames Research Center, Moffett Field, California

Superoxide compounds can be used to supply oxygen for breathing and to destroy airborne bacteria and toxic or noxious materials present in the atmosphere. However, for the past 30 years the processes used to synthesize alkali-metal superoxides were complicated and expensive. Molten potassium had been used in one process where the metal was atomized into a chamber filled with oxygen at 1.2 atmospheres and 300° C, with the superoxide product being collected at the bottom of the chamber. The raw materials for this process were expensive, however, and the accidental presence of water in the reacting vessel could cause an explosion.

A more recent process synthesized potassium superoxide by subjecting solid potassium hydroxide to an electric discharge of direct current at 1,100 volts (500 watts) sustained in an oxygen environment at 0.5 torr (67 N/m^2). The process yielded an 80.5-percent conversion of the potassium hydroxide. However, the high voltage and power required, and occasional contamination of the product due to electrode sputtering, made this process less than optimal.

An improved version of the electric discharge process uses potassium hydroxide as a starting material and a high-frequency discharge in oxygen to produce the superoxide. Since there is no direct-current discharge at the electrodes, there is no sputtering to contaminate the product, hence, a high conversion efficiency.

(continued on next page)

The reaction takes place in a cylindrical reactor tube with a vacuum pump at one end and an oxygen-flow system at the other end (see figure). Dried oxygen is introduced into the system, and a pressure-regulating system stabilizes the internal pressure to the 0.75 to 1.00 torr (100 to 133 N/m^2) needed for optimal conversion.

Mounted on the outside of the reactor are the discharge electrodes, usually three, coupled to a high-frequency generator that is tuned to 13.56 MHz and can supply up to 350 watts. A glass boat inside the reactor contains the alkaline-earth metal compound to be converted. The reaction proceeds when the electrodes are energized, and the flow rate and pressure of oxygen are adjusted. The thinly-spread potassium hydroxide melts as it reacts and recrystallizes after the reaction is complete. The induction electrodes can be moved from one end of the boat to the other so that product purity is uniform.

Typical results show a potassium conversion efficiency of 60 percent to the superoxide. Lithium and calcium, while not readily convertible to superoxides, do yield 90 percent product as peroxides.

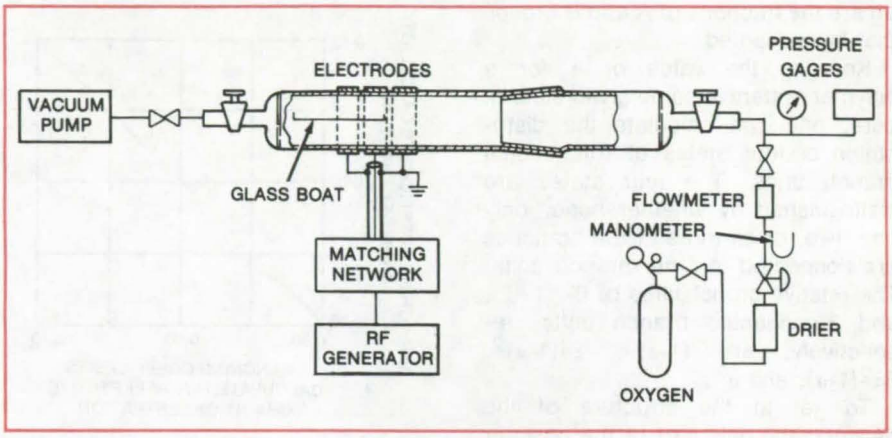

In a One-Step Operation, potassium hydroxide (KOH) in a low-pressure oxygen environment is converted to potassium superoxide (KO_2) by a radio-frequency discharge. The powdered KOH is spread thinly in the glass boat, which is positioned to be inside the glow of the discharge zone. This simple process produces high-purity superoxide from inexpensive raw material.

This work was done by Alexis T. Bell and Pasupati Sadhukhan of the University of California, Berkeley, for **Ames Research Center.** *For further information, Circle 35 on the TSP Request Card.*

This invention is owned by NASA, and a patent application has been filed. Inquiries concerning nonexclusive or exclusive license for its commercial development should be addressed to the Patent Counsel, Ames Research Center [see page A8]. Refer to ARC-10992.

Fire-Retardant Covering for Small Containers

An intumescent sheet of uniform thickness can be tightly wrapped around small objects to provide extra safety during fires.

Ames Research Center, Moffett Field, California

A new flexible intumescent coating of exceptionally uniform thickness is prepared from polymeric compositions containing microfibers of quartz. The coating is fabricated in sheets by a continuous process that involves vacuum mixing, calendering, and curing. The resulting product is easily wrapped around containers and other objects having small diameters [less than 10 in. (25.4 cm)] or convoluted surfaces to protect them from fires. Objects in this size range are usually protected by applying a spray coating; however, the thickness of the sprayed coating is difficult to control. To compensate for the uncertainty, a relatively thick coating must be applied, adding unnecessarily to the size and weight of the object.

The first step in the new process involves mixing an intumescent polymeric composition under vacuum. The intumescent agent, the ammonium salt of 1,4-nitroaniline-2-sulfonic acid, has a particle size less than 0.01 mm. In addition, the composition includes silica microfibers about 0.2 to 0.4 mm in length and about 0.003 to 0.005 mm in diameter. The polymeric component consists of a mixture of an epoxy resin with a polysulfide in a proportion such that the glass transition temperature is at or below room temperature.

The uncured paste, containing a catalyst, is calendered into a thin sheet, preferably between 0.025 and 0.25 cm in thickness, and is rapidly cured within 5 minutes under precisely controlled conditions that depend on the thickness. The cured sheet, which may also be covered by a protective polymer skin such as polyvinyl fluoride film, is bonded to a surface with a flexible adhesive by vacuum bagging.

A finished 60-mil (1.52-mm) sheet has been tested by wrapping it around a small missile (diameter less than 10 in.) and exposing it to fire along with several unprotected missiles. Results show that the protected missile ignited in a period of 409 seconds as compared to less than 60-second ignition times for the unprotected missiles.

This work was done by Salvatore R. Riccitiello and Paul M. Sawko of **Ames Research Center.** *For further information, Circle 36 on the TSP Request Card.*

This invention is owned by NASA, and a patent application has been filed. Inquiries concerning nonexclusive or exclusive license for its commercial development should be addressed to the Patent Counsel, Ames Research Center [see page A8]. Refer to ARC-11104.

Fire-Retardant Lightweight Composite

A new honeycomb structure has low density and improved fire-safety characteristics.

Ames Research Center, Moffett Field, California

Honeycomb-core laminated composite structures are frequently used as lightweight panels or structural members in aircraft and vessels and in housing applications. A major objective in fabricating these composites is to improve their fire safety while retaining their low density. To date, several fire-retardant materials have been incorporated into the fabrication of honeycomb-core composites. However, most either have not been sufficiently fire resistant or have tended to generate noxious fumes during fires.

A new low-density honeycomb-core composite has been developed to minimize these fire-safety-related problems. The core material is made from polyamide and a combination of polyimide and glass with an approximate density of 1.5 lb/ft^3 (24 kg/m^3). This structure, which is commercially available, serves as a base. Next, a compound that forms a polyquinoxaline foam on heating is introduced into the honeycomb cells. This foam has a high thermal-protection efficiency and high char yield with significantly-reduced smoke density when exposed to fire. Finally, a layer of noncombustible fibrous material impregnated with polyimide resin is laminated on the surfaces of the honeycomb base.

Examples of materials that will form the polyquinoxaline foam in the cells of the honeycomb structure include ammonium 4-nitroaniline-2-sulfonate, p-nitroaniline bisulfate, and the reaction product of p-benzoquinone dioxime and phosphoric acid. All of these are commercially available products.

The best method of introducing the compound into the cells is to dip the honeycomb core into a dispersion of the compound in a liquid medium and then to remove the core, allowing any excess dispersion to run off. Once the cells are filled, the compound is thermally polymerized to form the polyquinoxaline foam. The filled honeycomb structure can then be machined to remove surface irregularities and can be cut to approximate size.

Property	Composite Structure	
	Conventional	New
Density (ASTM D-71, kg/m^3)	96	96-113
Tensile Strength, Flatwise (ASTM C307, 24° C, kN/m^2)	610	517-690
Fire Endurance (Time to Reach Back Face Temperature of 204° C with Front Face Heat Flux of 11x10^4 W/m^2, min)	2	10
Smoke Density (NBS, Ds 4 min)	58.7	45
Specific Optical Density Component Smoke Density (Maximum Specific Optical Density, NBS Smoke Chamber)		
Polyvinyl Fluoride	7	Phenol Poly-carbonate 5
Polyamide Core	2	Polyamide Core 2
Epoxy Resin	90	Bismaleimide Resin 9
Glass	—	Glass —

New **Honeycomb-Core Laminated Composite** is compared with conventional (unfilled) composite. Fire endurance and smoke density characteristics are substantially improved with the new material.

The noncombustible fibrous material that is laminated to the foam-filled honeycomb base can be a woven (e.g., satin cloth) or nonwoven (e.g., glass mat) material. Normally, woven material is preferred because of its easier processing. This material is impregnated with a polyimide resin (e.g., bismaleimide resin). The impregnation is generally conducted in a solution of the resin in a solvent. The impregnated material then is dried to remove the solvent and is held for an additional 20 minutes at an elevated temperature to advance the resin cure. The finished prepreg is laminated to the foam-filled honeycomb structure. Lamination is accomplished by placing the prepreg containing partially cured resin on top of the honeycomb, and applying pressure.

The new structure has been tested for fire endurance and compared to conventional unfilled honeycomb structures. Results (see table) show that the fire endurance has been improved by a factor of 5 by the thermal-protection efficiency of the high-char-yield polyquinoxaline foam. Likewise, smoke tests show significant reductions in smoke density, primarily because of the use of bismaleimide resin instead of epoxy-laminating resins.

This work was done by William J. Gilwee, Jr., and John A. Parker of **Ames Research Center.** *For further information, Circle 37 on the TSP Request Card.*

This invention is owned by NASA, and a patent application has been filed. Inquiries concerning nonexclusive or exclusive license for its commercial development should be addressed to the Patent Counsel, Ames Research Center *[see page A8].* *Refer to ARC-10913.*

Heat-Resistant Nontoxic Composite Laminate

Lightweight, low-cost material is suited for auto panels, railcars, and aircraft parts.

Ames Research Center, Moffett Field, California

The interiors of most modern aircraft are a blend of glass-epoxy resins bonded to a polyamide core finished with a polyvinyl chloride outer decorative coat. The epoxy bonding material may be a hazard when exposed to heat or flames, liberating smoke and toxic gases. Moreover, the state-of-the-art panel is not a particularly good heat insulator.

By abandoning the epoxy compound and substituting new materials and processes, a new product has been created with an impressive list of advantages. The epoxy resin is replaced by a resin made by polymerizing various bismaleimides with or without diamine compounds.

The laminate is prepared from glass cloth preimpregnated with polybismaleimide resin, which is adhered to a polybismaleimide glass or aromatic polyamide paper honeycomb cell structure filled with a syntactic foam. The foam is a mixture of bismaleimide resin and carbon microballoons.

The carbon microballoons are prepared by pyrolyzing phenolic microballoons that are subsequently bonded, using a 2-percent bismaleimide solution. The laminate is cured for 2 hours at about 200° C and is bonded to the honeycomb bismaleimide adhesive at a pressure of 700×10^3 N/m^2 and a temperature of 177° C. The laminated composite is then postcured for 2 hours at 255° C to produce a composite with a density between 95 and 130 kg/m^3.

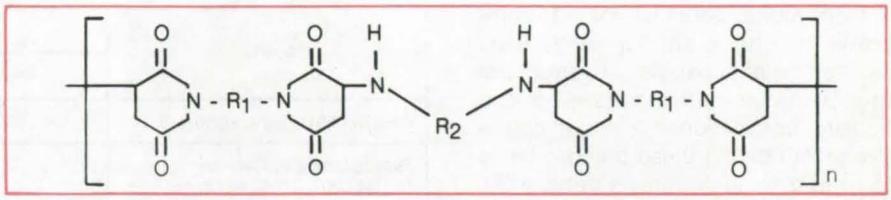

Bismaleimide Polymer used in the construction of a microballoon composite is produced by the polymerization of bismaleimides in the presence of diamines. R_1 and R_2 may be alkylene, heterocyclic, or aromatic radicals; the latter are preferred.

Physical and thermal tests show that panels made from this new formulation have several advantages over conventional laminates: Heat refraction is better — the time to reach 100° C in combustion-chamber tests is 300 s compared to 80 s; a cleaner smoke is produced having an optical density parameter of 1.0 compared to 53 for conventional formulations; and fumes of the new laminate are less detrimental to laboratory animals.

In addition to these advantages, the new laminate is easier to finish and more easily shaped, making it a significantly more attractive material than the current epoxy laminates for many applications.

This work was done by Demetrius A. Kourtides and John A. Parker of **Ames Research Center.** *For further information, Circle 38 on the TSP Request Card.*

This invention is owned by NASA, and a patent application has been filed. Inquiries concerning nonexclusive or exclusive license for its commercial development should be addressed to the Patent Counsel, Ames Research Center [see page A8]. *Refer to ARC-11040.*

Ion-Beam Texturing of Materials

Microscopic surface roughing by sputter etching and deposition.

Lewis Research Center, Cleveland, Ohio

A xenon ion-beam source has been used to create a microscopically-rough surface texture by sputter-etching a surface while simultaneously sputter-depositing a lower yield material onto the surface. The low-sputtering-yield atoms (called the seed material) agglomerate into microscopic regions that protect the higher-sputtering-yield atoms beneath. The xenon ion-beam source evolved from an auxiliary propulsion thruster that is intended for positioning spacecraft in orbit or on a planned route in space.

Ion-beam texturing using tantalum as the seed material was attempted on 30 different elements. The 26 elements that were successfully textured are tinted in Figure 1. The texturing process was unsuccessful for the four gray-tinted elements in the periodic chart. All of the elements that could not be textured are in columns VB and VIB of the periodic chart.

The elements (Nb, Mo, Ta, W) that showed no signs of texture are all relatively low-sputter-yield materials. However, several elements (C, Si, Ti, and Zr) have lower sputter yields than tantalum, but nevertheless, were still textured. Conversely, tungsten, which has a higher sputter yield than tantalum, did not texture. The elements in column IVB of the periodic chart all could be textured; however, zirconium textured at a faster rate than either hafnium or titanium.

Group	IA	IIA									IIIA	IVA	VA	VIA	VIIA	VIIIA
1							1 H									2 He
2	3 Li	4 Be									5 B	6 C	7 N	8 O	9 F	10 Ne
3	11 Na	12 Mg	IIIB	IVB	VB	VIB	VIIB	VIIIB		IB	IIB	13 Al	14 Si	15 P	16 S	17 Cl	18 Ar
4	19 K	20 Ca	21 Sc	22 Ti	23 V	24 Cr	25 Mn	26 Fe	27 Co	28 Ni	29 Cu	30 Zn	31 Ga	32 Ge	33 As	34 Se	35 Br	36 Kr
5	37 Rb	38 Sr	39 Y	40 Zr	41 Nb	42 Mo	43 Tc	44 Ru	45 Rh	46 Pd	47 Ag	48 Cd	49 In	50 Sn	51 Sb	52 Te	53 I	54 Xe
6	55 Cs	56 Ba	57′ La	72 Hf	73 Ta	74 W	75 Re	76 Os	77 Ir	78 Pt	79 Au	80 Hg	81 Tl	82 Pb	83 Bi	84 Po	85 At	86 Rn
7	87 Fr	88 Ra	89″ Ac															
′LANTHANUM SERIES			58 Ce	59 Pr	60 Nd	61 Pm	62 Sm	63 Eu	64 Gd	65 Tb	66 Dy	67 Ho	68 Er	69 Tm	70 Yb	71 Lu		
″ACTINIUM SERIES			90 Th	91 Pa	92 U	93 Np	94 Pu	95 Am	96 Cm	97 Bk	98 Cf	99 Es	100 Fm	101 Md	102 No			

Figure 1. **Ion-Beam Texturing Results** are shown on a periodic chart of the elements. The color-tinted elements were successfully textured using tantalum as the seed material. The texturing process was unsuccessful for the gray-tinted materials.

A large number of elements had textures that can be classified as either a ridge structure or a cone structure. Figure 2(a) is a photomicrograph of the convoluted ridge morphology that occurred on nickel and many of the other low-sputtering-yield materials (Ti, Fe, Co, Zr, Hf, Gd). Many of the higher-sputter-yield materials had morphologies that looked like densely packed cones or needles. The scanning-electron photomicrograph of copper shown in Figure 2(b) is an example of this second kind of morphology. The other elements that exhibit this type of structure include Mg, Cr, Ag, Au, Hg, Al, C, Si, Se, Pb, and Bi. The remaining materials that textured, but are neither ridge structure nor cone structure, are Cd, Be, Zn, In, Sn, and Sb. Their surface textures were all unique.

There are several variables in the texturing process, such as the kind of seed material, its arrival rate at the target, the net accelerating voltage, the beam current, and the target temperature.

The surface morphology created by ion-beam texturing has several potential commercial applications. This type of surface treatment can be used to modify reflectance and emissivity, to decrease secondary electron emission, to promote thin-film adhesion, to increase catalytic reactions, and to improve plastic bonding strength of adhesive bonds. The reflectance of silicon single crystals has been reduced to a few percent over the solar spectrum by ion-beam texturing the surface. Preliminary results have also shown that the secondary electron-emission yield is reduced by ion-beam texturing. Ion-beam textured graphite has demonstrated the lowest secondary electron emission of any known material.

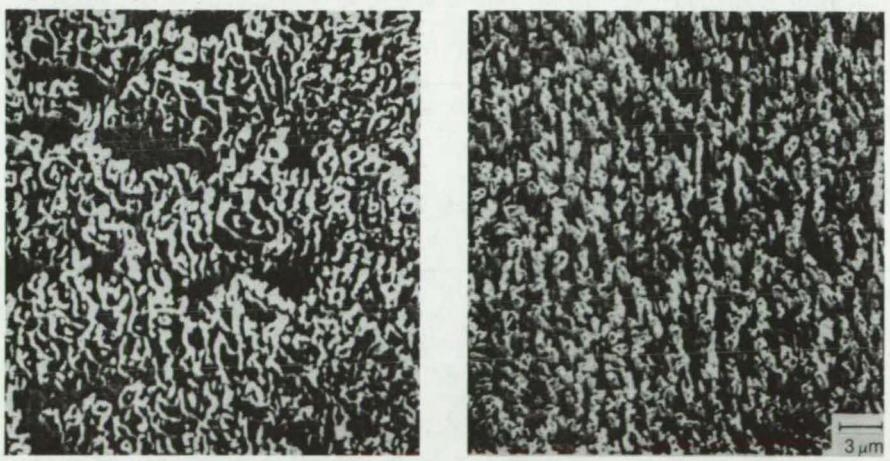

[a] [b]

Figure 2. **Ion-Beam Textured Nickel [a] and Copper [b]** are shown in scanning-electron photomicrographs. Tantalum was the seed material. The net ion energy was 1,000 volts.

This work was done by Wayne R. Hudson of **Lewis Research Center.** *Further information may be found in NASA TM-X-73470 [N76-30957], "Ion Beam Texturing," a copy of which may be obtained at cost from the New England Research Application Center [see page A7].*
LEW-12996

Chemical Agent Boosts Natural-Rubber Output

Treated guayule plants can yield up to 400 percent more rubber.

NASA's Jet Propulsion Laboratory, Pasadena, California

The guayule rubber plant, a desert shrub, is at present only a minor contributor to the U.S. natural-rubber supply. Its crop yield, 1,000 lb/acre (0.01 kg/m^2) per 2-year harvest season, is only about one-half that of the predominant Hevea brasiliensis plant. While the latex products of both plants are almost identical, the product syntheses are different, and until now has been optimized only for the Hevea plant.

Recently, however, increased latex yield of the guayule has been demonstrated by treating the plants topically with substituted triethylamines. This class of compounds has previously been found to alter the synthesis of lycopenes in fruits, causing a color change. When the triethylamines are applied to the chemically-similar polyisoprene synthesis of the guayule rubber, an increase of up to 150 percent in rubber output results. Based on these results, an increase of 400 to 500 percent appears to be possible.

The specific substitutions made in the triethylamine skeleton determine the rubber output increase. A possible mechanism for this process involves a biochemical modification of the membrane system that produces the polyisoprene latex.

The chemical inducers found to increase yield in guayule plants have the following general structure:

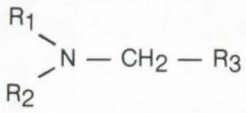

where R_1 and R_2 are alkyl groups, preferably ethyl, and where R_3 is any alkyl group or any substituted aryl group with electron withdrawing substituents, such as methoxy or halogens.

A representative compound is 2-(4-chlorophenylthio) triethylene hydrochloride (CTPA). It can be sprayed on the plants or fed to the roots as a dilute aqueous medium. The composition typically contains from 0.05 to 5 percent by weight of the agent and from 0.1 to 5.0 percent of an organic solvent such as ethanol or isopropanol. In addition, a nonionic alkylene oxide surfactant can be added to assist in penetrating the waxy surface of the plant.

Improvements in guayule rubber harvesting may help to meet the increasing demand for natural rubber, which is occurring partly in response to the rising costs of petroleum-derived synthetic rubber. The guayule has advantages over other plants in its resistance to certain diseases and in its affinity for the sandy soil of the Southwestern United States and Mexico.

This work was done by A. J. Bauman of Caltech for **NASA's Jet Propulsion Laboratory.** *For further information, Circle 39 on the TSP Request Card.*

This invention is owned by NASA, and a patent application has been filed. Inquiries concerning nonexclusive or exclusive license for its commercial development should be addressed to the Patent Counsel, NASA Resident Legal Office-JPL [see page A8]. Refer to NPO-14185.

Books and Reports

These reports, studies, and handbooks are available from NASA as Technical Support Packages (TSP's) when a Request Card number is cited; otherwise they are available from one of NASA's Industrial Application Centers or the National Technical Information Service.

Toxic Substances Handbook

Properties, safety practices, and treatments covering 187 toxic substances

A toxic substances handbook has been published in conjunction with the Toxic Substances Alert Program at the NASA Lewis Research Center. The handbook contains a toxicity profile of 187 toxic substances procured during a recent 3-1/2-year period, including 27 known or suspected carcinogens. The goal of the Toxic Substances Alert Program is to ensure that Center health and safety personnel are aware of the procurement and use of toxic substances, and to alert and inform the users of these materials as to the toxic characteristics and the control measures needed to ensure their safe use.

The handbook contains the following kinds of information:

- Chemical Formulas
- Synonyms
- Descriptions
- Fire Hazards
- Toxicity
- Treatment for Overexposure
- Personal Protection
- Spill or Leak Control
- Storage
- Disposal
- Chemical Incompatibility

Only toxic chemicals in their relatively pure state are included. Not included are trade name products representing compounds or formulated proprietary mixtures available as commercial products. It is very difficult to assess the toxicity of trade name products since the components are often unknown. In addition, the formulation may change from time to

time with substitution of different chemicals with differing toxicities, and contribution to the total toxic effect by each component is difficult to evaluate.

The handbook sets forth acceptable standards and practices for minimum safety requirements at the NASA Lewis Research Center; the information may be useful as a reference for other users of toxic materials. The handbook may also be helpful as a base against which less toxic substances might be compared.

This work was done by Thomas L. Junod of **Lewis Research Center.** *Further information may be found in NASA TM-73866 [N78-20755], "Toxic Substances Alert Program," a copy of which may be obtained at cost from the New England Research Application Center [see page A7].*
LEW-13124

Effects of Moisture on Graphite/Epoxy Composites

The effects of water absorption and temperature spiking on strength and stiffness

A recently issued report analyzes the effects of moisture on graphite/epoxy composite materials. The report describes tests made on a commercially available graphite/epoxy, used for doors on the Space Shuttle; however, it has relevance to similar materials used in other applications. For example, it relates to the behavior of automobile engine parts, since the periodic temperature rise of the engine compartment is analogous to the repetitive heating of the Shuttle doors over many reentries into the Earth's atmosphere.

The study was motivated by the problem that in a humid environment graphite/epoxy composites absorb water molecules that soften the epoxy resin. The extent of the deterioration depends on the amount of moisture absorbed.

Since the problem is too complex to analyze theoretically, tests were carried out to determine the design allowances necessary to account for the moisture effects. In the tests, the effects of moisture on the compression and shear strengths and stiffnesses of graphite/epoxy laminated sheets were determined. The objectives were to define allowance factors for laminates containing various amounts of moisture at room temperature and at 350° F (177° C) and to resolve the question of whether the compression and shear properties of moist laminates are affected by repeated exposures to 350° F.

The results, in brief, are:

1. At room temperature, the compressive and in-plane shear strengths are not adversely affected by moisture.
2. The compressive and in-plane shear strengths at 350° F are reduced substantially in proportion to the moisture content.
3. Repeated exposure to high temperature at constant moisture levels does not change the measured properties.
4. Stiffness, unlike strength, is not affected by absorbed moisture.

Specimens with moisture contents of 0, 0.6, 0.8, and 1.0 percent relative to the specimen dry weight were tested under static loads at room temperature and at 350° F. Another group of specimens was moisturized to 0.6, 0.8, and 1.0 percent of the laminate dry weight and was subjected to up to 100 short-duration exposures to 350° F. After each thermal cycle, the original moisture content was restored, and the strength of the moist specimens was measured.

This work was done by Clarence W. Dill of Rockwell International Corp. for **Johnson Space Center.** *To obtain a copy of the report, Circle 40 on the TSP Request Card.*
MSC-18045

Computer Programs

These programs may be obtained at very reasonable cost from COSMIC, a facility sponsored by NASA to make new programs available to the public. For information on program price, size, and availability, circle the reference letter on the COSMIC Request Card in this issue.

Oxygen and Nitrogen Raman Spectra

Calculating pressure-broadened spectra for molecular nitrogen and oxygen

A new engineering-design computer program calculates the rotational Raman spectrum of either nitrogen or oxygen. The program can be used to increase the performance of gas-turbine engines by predicting the extent of pressure broadening associated with temperature measurements at elevated pressures.

In the development of gas-turbine engines, there has been a continuing goal to increase turbine inlet temperature further and thereby to increase engine performance. The measurement of gas temperatures in the region of the turbine inlet and combustor exit is required for the combustor to generate the correct temperature profile as well as temperature level. These temperature measurements have traditionally been made with thermocouples; however, no thermocouple is available that will withstand the high temperatures and pressures [up to 2,400 K and 40 atm (41×10^5 N/m^2)] predicted for future turbine and combustor development.

One method for making high gas-temperature measurements is a remote-sensing, light-scattering technique utilizing Raman scattering. The Raman scattering technique can be used to focus remotely on a small volume of gas in a gas stream and to extract information associated with local gas density, composition, and temperature. Some of the problems associated with Raman scattering in measuring temperature in jet-engine exhaust gases are fluorescence, ambient light background, interference of various species of gas, and pressure broadening. The broadening has a variety of causes, among which are the fact that neither the light source

(continued on next page)

nor the detector is perfectly monochromatic and the fact that the molecules are in motion rather than being at rest. Since the broadening depends on both the temperature and pressure of the gas, it must be taken into account if Raman scattering is to be used as a tool for measuring the temperature of high-pressure gases.

In this program, all the necessary constants are read into the program, and all the various parameters are calculated, as are the number and location of the rotational lines for either oxygen or nitrogen. Then the program calculates the intensity at each wave number. The numerical integration of these functions is performed using the method of Gaussian quadrature. The resulting output is then plotted in terms of intensity as a function of wavelength. Although the best method of using these calculations to determine the temperature of a high-pressure gas has not yet been determined, it has been shown that the effects of pressure broadening are not negligible for pressures up to 70 atmospheres (7.1×10^6 N/m^2).

This program is written in FORTRAN IV for use on an IBM 360-series computer and requires a minimum of 46K bytes of memory. A plotting device and supporting graphics software are also required.

This program was written by Gustave C. Fralick of **Lewis Research Center.** *For further information, Circle C on the COSMIC Request Card.*

LEW-12849

Life Sciences

Hardware, Techniques, and Processes

Computer Programs

Remotely-Powered Intracranial Pressure Monitor

Stability of 0.1 torr/day is obtained by an implantable RF-powered cell.

Ames Research Center, Moffett Field, California

Long-term monitoring of intracranial pressure is an important diagnostic tool when treating patients suffering from brain tumors, stroke, or other cerebral dysfunctions. The treatment of sustained elevated pressures, by drugs or surgery, often depends on being able to make repeated and accurate pressure measurements.

Intracranial pressures can now be monitored by implanting a variable-frequency L/C oscillator in direct contact with the dura, the tough fibrous membrane that covers the brain. The pressure is converted to a frequency change by moving a plunger or a compliant diaphragm that forms part of a variable inductor or capacitor circuit.

Although these monitors have been used for some time, their accuracy has been limited by frequency instability and baseline drift due to stray capacitances and the "mechanical creep" of the transducer plunger or diaphragm. For many applications, very slow pressure changes that can be smaller than the inherent baseline drift of conventional transducers must be monitored. Also, the need to make wired connections through the scalp (in some models) or to install and replace batteries for power makes patient acceptance difficult.

A new implantable pressure monitor uses a capacitive transducer with a stiff metal diaphragm that gives high stability for long-term usage. Radio-frequency energy, converted to dc by a rectifier within the monitor, powers the electronics. It thus can be permanently implanted (Figure 1) and requires no batteries or wired connections through the scalp. The monitor is housed in a cylindrical package 1 cm in diameter by 1 cm in length (Figure 2).

The new monitor consists of an energy-receiving coil, the rectifier/regulator, a Hartley L/C oscillator, an output buffer, and a transmitting coil.

(continued on next page)

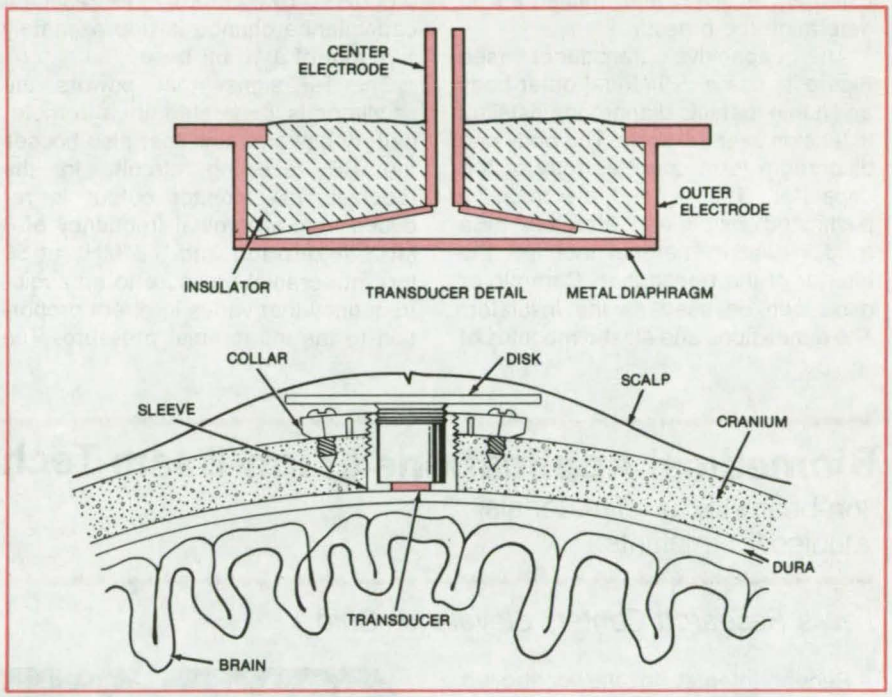

Figure 1. An **Intracranial Pressure Monitor** is implanted in the skull so that its capacitive transducer rests against the dura. The monitor is powered by RF energy from an external source. It therefore requires no batteries or wired connections through the scalp.

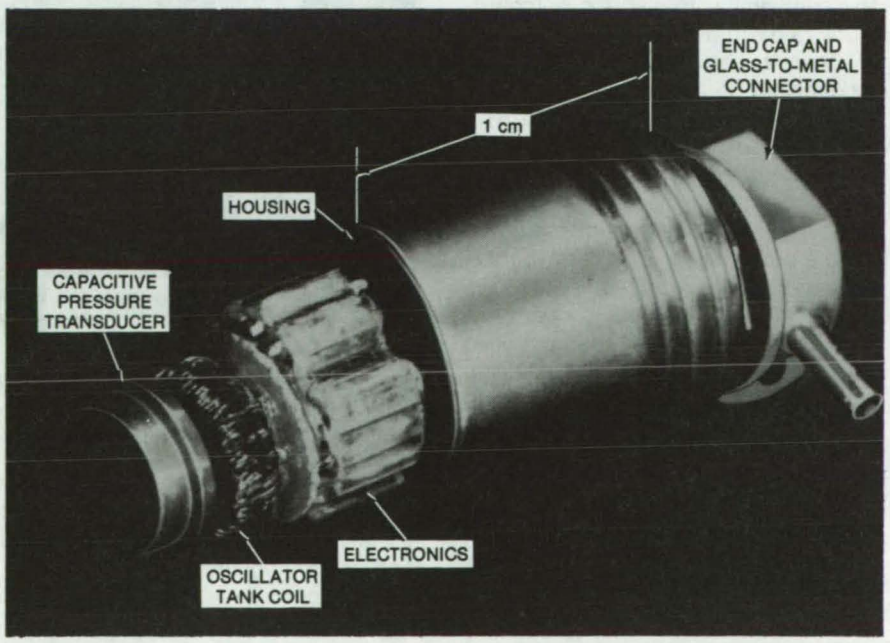

Figure 2. This **Compact Package** houses the electronics for the monitor. The transducer extends through a hole in the end of the housing. RF receiving and transmitting coils are located on a disk that rests against the end cap and are wired to the electronics through the seal on the end cap.

The capacitive transducer, in the tank circuit of the oscillator, rests against the dura and responds to pressure changes by shifting the oscillator frequency. A buffer circuit isolates the oscillator to prevent frequency pulling caused by loading of the coil. The output frequency is picked up by an external receiver and measured to determine the pressure.

The capacitive transducer (see Figure 1) has a cylindrical outer body and a thin metallic diaphragm installed in tension over the body. The body and diaphragm form one electrode of the capacitor. The second electrode is positioned inside and attached to a solid insulating material that fills the interior of the transducer. Ceramic or glass can be used as the insulator. The dimensions and elastic modulus of the end cap are chosen so that it responds as a stiff diaphragm to pressure changes. In previous monitors, large and compliant diaphragms were used, which caused the dura to distend appreciably and gave inaccurate pressure readings. In the new design, full-scale deflection is only 0.0002 in. (0.005 mm). The resultant capacitance change is approximately 1 pF out of a 10 pF base.

The RF signal that powers the oscillator is generated in a remote, battery-powered unit that also houses the RF receiving circuit. In the receiver, the monitor output is reduced from a nominal frequency of 8 MHz at zero torr and 8.3 MHz at 50 torr intracranial pressure to an audio-frequency that varies in direct proportion to the intracranial pressure. The audio signal modulates an FM transmitter to send the data to a remote recording station.

In tests at the Stanford University School of Medicine over a period of 50 days, the unit was stable to within 0.1 torr/day, as compared to previous systems that drifted about 0.7 torr/day.

This work was done by Thomas B. Fryer of **Ames Research Center.** *For further information, Circle 41 on the TSP Request Card.*

This invention is owned by NASA, and a patent application has been filed. Inquiries concerning nonexclusive or exclusive license for its commercial development should be addressed to the Patent Counsel, Ames Research Center [see page A8]. *Refer to ARC-11120.*

Biomedical Applications of Ion-Beam Technology

Ion-beam-textured materials studied for implants

Lewis Research Center, Cleveland, Ohio

Recent interest in the controlled microscopic surface texture of implants has led to the evaluation of ion-beam sputtering as a potentially-useful surface-roughening technique. Ion sources, similar to electron-bombardment ion thrusters developed for spacecraft, have been utilized to roughen the surfaces of various biocompatible alloys and polymers typically used for dental implants, orthopedic prostheses, vascular prostheses, and artificial heart components. The microscopically-rough surface texture produced by ion-beam sputtering may result in improvements in the biological response and/or performance of implanted devices. Controlled surface roughness may result in improved attachment of surgical implant materials to soft tissue, hard tissue, or components deposited from blood.

Ion-beam-textured soft and hard tissue implants were investigated during this study. Soft tissue implants are normally placed adjacent to or in connective tissue or in the blood; e.g., artificial blood vessels, artificial heart pump diaphragms, pacemakers, and percutaneous (through-the-skin) connectors.

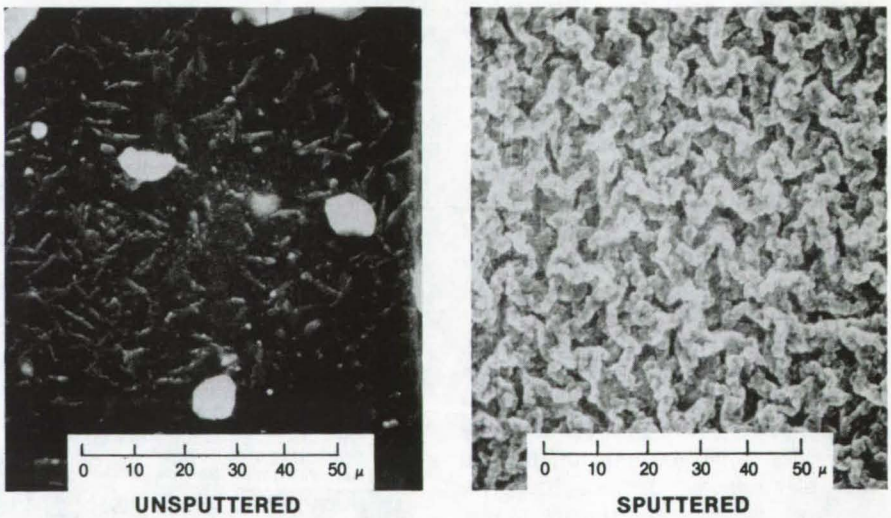

Figure 1. **Polyolefin** (carbon impregnated) is shown before ion-beam sputtering and after 4 hours of ion-beam sputtering followed by 4 hours of ion-beam sputtering while covered with nickel mask.

Hard tissue implants are normally implanted adjacent to or in bone tissue; e.g., orthopedic prostheses and dental implants.

Both polymers and metals have been ion-beam-sputtered. The polymers consisted of segmented polyurethane, copolymer silicone-polyurethane, Teflon, and polyolefin, while the metals consisted of titanium, cobalt-chromium, and stainless steel. The ion-beam sources were a 5-cm- and an 8-cm-diameter electron-bombardment ion thruster operated with inert gas.

Figure 1 shows scanning electron photomicrographs of carbon-impregnated polyolefin before and after ion-beam sputtering. Samples of various polymers and metal alloys masked

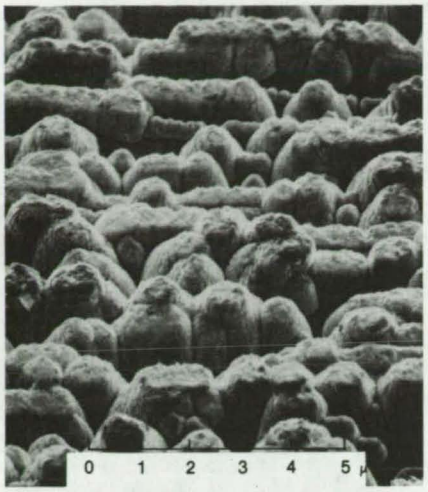

Figure 2. **Scanning Electron Photomicrograph** of 46 percent chromium and 20 percent cobalt is shown after ion-beam sputtering with a tantalum seed. Sputtering durations were 4 hours.

with a fine nickel-mesh screen were also sputtered. This masking technique resulted in an array of uniform depressions etched into the polyolefin, the depth of which can be controlled by the sputtering duration. Screens with various grid sizes and thicknesses can be used to produce surface roughness with varying pore size, depth, and spacing.

Figure 2 shows a scanning electron photomicrograph of an alloy used for orthopedic prostheses that has been textured by ion-beam sputtering.

Analysis of the results has shown that ion-beam texturing is potentially useful in determining the effect of surface morphology on the biological response to implants because surface roughness can be accurately controlled within microscopic limits.

Ion-beam-textured implants have been placed in various types of animals for variable durations up to 11 months. A variety of ion-beam-textured polymers and metals have been evaluated as vascular, dental, subcutaneous, and percutaneous implants. Analysis of the results indicates that the ion-beam texturing does not produce any change in the inflammatory tissue response, and it also showed that a significant improvement was produced in soft tissue adhesion over that of untreated polymers and metals.

This work was done by Bruce A. Banks and Albert J. Weigand of **Lewis Research Center** *and Donald F. Gibbons of Case Western Reserve University, Craig L. VanKampen of St. Luke's Hospital, and Charles A. Babbush. Further information may be found in:*

NASA TM-X-73512 [N77-11655], "Potential Biomedical Applications of Ion Beam Technology,"

NASA TM-X-73468 [N76-30797], "Ion Beam Sputter Modification of the Surface Morphology of Biological Implants," and

NASA CR-135311 [N78-18672], "Effect of Surface Texture by Ion Beam Sputtering on Implant Biocompatability and Soft Tissue Attachment."

Copies of these reports may be obtained at cost from the New England Research Application Center *[see page A7]*.

Inquiries concerning rights for the commercial use of this invention should be addressed to the Patent Counsel, Lewis Research Center *[see page A8]*. *Refer to LEW-12807.*

Automated Chromosome Analysis

Computerized chromosome analyzer displays pictures of karyotypes.

NASA's Jet Propulsion Laboratory, Pasadena, California

A minicomputer-controlled system analyzes blood samples automatically and displays a karyotype (i.e., the specific characteristics of a cell nucleus) in pictorial form on a display screen. The samples are prepared, analyzed, and displayed, by the programed machine.

The major components of the system, shown in Figure 1, are the specimen preparation unit, the automated microscope, and the computer system. Blood samples are placed on microscope slides, stained, and fed into the automated microscope. Metaphase spreads are found automatically, and the best ones are selected by the operator. The images are then digitized and fed into the computer system, which locates and measures the chromosomes, classifies them by group or by type, and prepares a digital karyotype image. This image is converted to pictorial form and constitutes the primary output of the system.

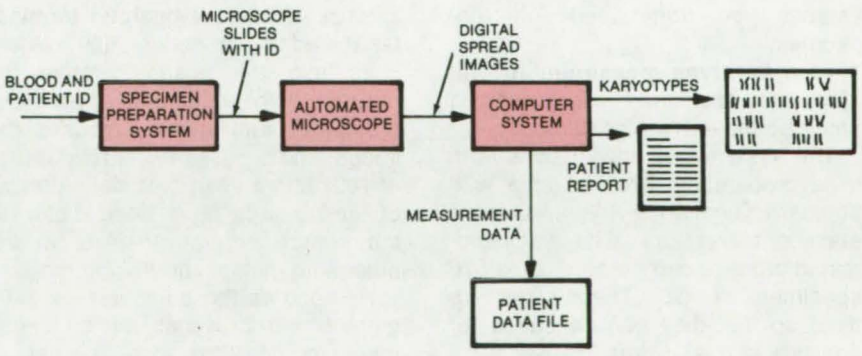

Figure 1. The **Major Components** of the automatic chromosome analyzer are all coordinated by the computer system. Operator interaction is used to assure proper system operation.

Chromosome measurement data are filed in an interactive data base for subsequent statistical analysis. After the processing of the last cell for each

(continued on next page)

patient is complete, the system prepares a patient report summarizing the result of the analysis and listing suspected abnormalities. In addition, the system includes options to produce additional data outputs as desired for specific applications. Figure 2 illustrates a typical pictorial output of the system.

The automated light microscope, the computer, and some of the video monitors are standard devices. Other portions of the system are:

- The **automatic** focus and **spread detector unit** focuses the microscope and detects the presence or absence of cells in metaphase.
- The **stage control interface,** a computer link to the microscope stage, scans the sample slide in 10-micron steps in the x and y directions.
- The **hard-copy pictorial output device** generates a picture of the chromosome spread and the computer-generated karyotype output with patient-identification information.
- Finally, computer programs have been developed to classify banded and homogeneously stained chromosomes.

Operator interaction is an important element in assuring the accuracy of the analysis and is provided at the following key points:

- In the **slide search,** the operator can reject any nonchromosome material or metaphase spreads of inadequate quality.
- In the **cell analysis stage,** the operator checks for missed chromosomes or fragmented chromosomes.
- In the **karotype measurement,** improperly positioned chromosomes may be moved into position.

The system operation begins with slide preparation. This is done with standard Giemsa or trypsin-Giemsa staining techniques. The semiautomated process can prepare up to 576 specimens per day. These slides are fixed so that they can be saved for analysis at a later date.

Once the slide is mounted on the microscope stage, the initial slide search is done at 40X or 63X, and is fully automatic. Without operator intervention the computer exercises the microscope stage in a rectangular search pattern while the automatic metaphase detector monitors the video signal for the presence of metaphase spreads. When such a spread is encountered, the x and y coordinates of the stage are logged automatically.

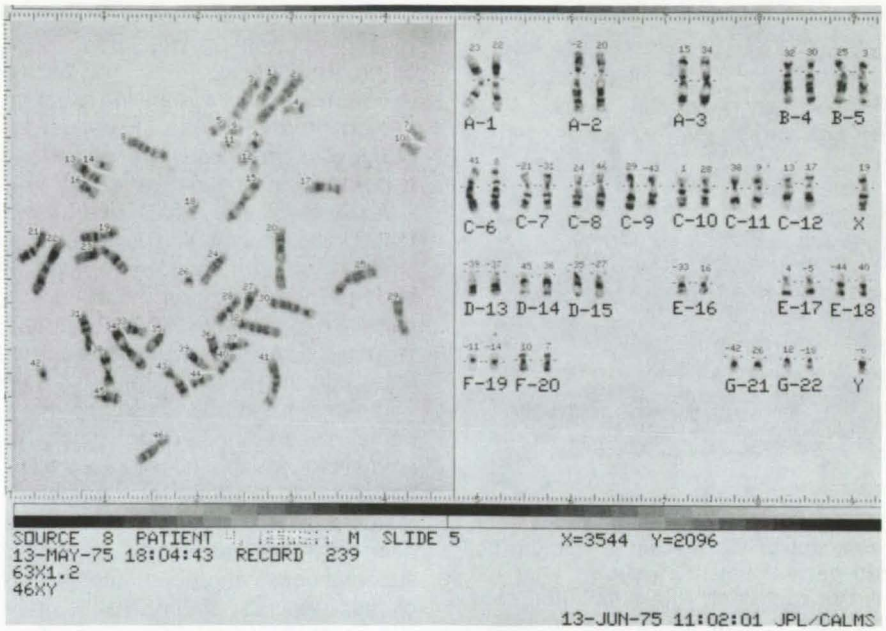

Figure 2. The **Output of the Automated System** shows the scanned and processed chromosome display. To the left is the original spread of chromosomes. To the right is the computer generator karotype.

In the editing phase of slide search, the computer automatically returns the stage to each of the previously logged positions to allow the operator to view the detected cells. The operator may either reject or accept the spread. Accepted spreads are manually centered beneath the objective by the use of a stage-control joystick. When the operator terminates the editing procedure, the system goes into the scanning mode. It returns to the accepted spread coordinates, automatically focuses the image, and digitizes the spread image at 100x into a scan data set. After all of the spreads have been digitized, the search program reverts to the automatic metaphase-finding mode.

As soon as the computer program detects the presence of a spread image in one of the scan data sets, it begins the analysis. If the cell is not to be karyotyped, the chromosomes are located, counted, and displayed to the operator for verification. However, if the cell is to be karyotyped, 16 programs are loaded in sequence and executed to effect the karyotype analysis of the cell. These programs locate the chromosomes, orient them, extract measurements, classify the chromosomes, and compose the digital karyotype.

When a properly formatted image is available in one of the output data sets, the hard-copy output program begins the transfer, line by line, to the pictorial output device. This unit requires 1-1/4 minutes for complete output of the 660- by 1,000-point picture. After one picture is complete, it begins output of the image in the next output data set.

The slide search, analysis, and output operation all run simultaneously, but on separate cells. From 4 to 20 cells per hour can be processed by this technique.

This work was done by Kenneth R. Castleman, Howard J. Frieden, Elbert T. Johnson, Paul A. Rennie, and Raymond J. Wall of Caltech for **NASA's Jet Propulsion Laboratory.** *For further information, Circle 42 on the TSP Request Card.*

This invention is owned by NASA, and a patent application has been filed. Inquiries concerning nonexclusive or exclusive license for its commercial development should be addressed to the Patent Counsel, NASA Resident Legal Office-JPL [see page A8]. Refer to NPO-13913.

Automated Controller for Liquid-Cooled Garments

Temperature controller requires no physiological sensors attached directly to the body.

Lyndon B. Johnson Space Center, Houston, Texas

Liquid-cooled garments have many potential medical and industrial applications, but their widespread use has been hampered by temperature control problems. Either the wearer must manually adjust the temperature of the coolant, or physiological sensors must be attached directly to the body for automatic control. Such sensors make the garments cumbersome and very restrictive of body movements for many applications.

The feasibility of a fully automated controller that would require no body-measurement sensors has been demonstrated during a recent study at Johnson Space Center. The automated controller, which was simulated by a computer model and tested on live subjects, would be governed only by the inlet temperature of the coolant and the temperature differential across the garment. Although it was originally intended for use by astronauts in the Space Shuttle program, the controller has other potential applications in industry, medicine, and research.

In designing the automatic controller, a computer model of human thermoregulation was used and correlated with data taken on three test subjects, two male and one female. The subjects' metabolic rates were controlled by adjusting the speed of a motor-driven treadmill. During the tests, the garment inlet and outlet temperatures were recorded, and each subject was asked to evaluate his or her thermal sensations on a scale of from 1 to 7 (ranging from cold to hot). From these data, transfer functions were developed to relate the temperature and changes in the temperature at the garment inlet to the temperature differential and changes in the temperature differential across the garment, as required for maximum comfort (see figure).

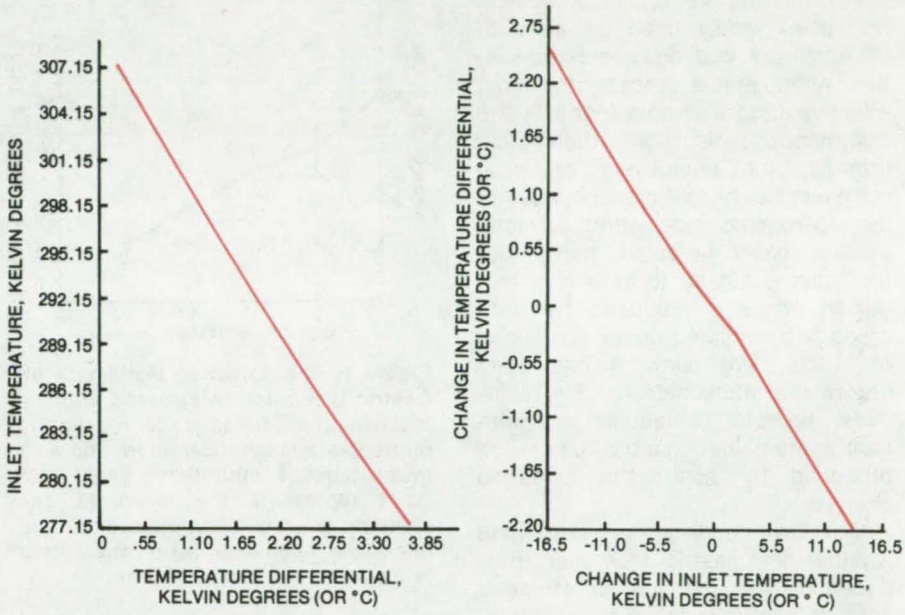

These **Transfer Functions** relate the inlet temperature of the coolant in a liquid-cooled garment to the temperature differential across the garment for maximum comfort of the wearer. They were developed during tests on three human subjects. Some refinements to these functions were made in the model of the controller that was actually used.

With the controller logic governed by these transfer functions, the inlet temperature and temperature differential were measured and used to calculate the correct inlet temperature for maximum comfort. The temperature was then set to that value, and the response of the subject was recorded. These results were compared with the inlet temperature settings determined by the subject according to his own body sensations and personal preferences.

The tests showed that the automated controller could give the same level of comfort as manual control. In fact, in the case of manual control, it was noted that the subjects tended to overcool themselves, whereas no such effect was noted with the automated controller.

The actual controller hardware would consist of a water-mixing valve coupled to a servomotor and a microcomputer that incorporates the controller logic. The microcomputer would sample the inlet temperature and temperature differential continuously and would compute the required inlet temperature. The resulting signal would operate the servomotor to change the setting of the valve to get the desired inlet temperature.

This work was done by Lawrence H. Kuznetz of **Johnson Space Center.** *Further information may be found in NASA TM-58205 [N78-11704], "Automatic Control of Human Thermal Comfort With a liquid-Cooled Garment" [$4.50]. A copy may be purchased [prepayment required] from the National Technical Information Service, Springfield, Virginia 22151.*

MSC-18055

Antihistamines Reduce Ulceration Produced by Indomethacin

Metiamide, pyrilamine, and promethazine reduce gastric damage in stressed animals that receive indomethacin. .

Ames Research Center, Moffett Field, California

For several years, indomethacin has been widely used as an anti-inflammatory and analgesic medication. Although it is probably the most effective drug available today in the treatment of patients with rheumatoid arthritis, the usefulness of indomethacin has been limited because of its ulcerogenic side effect. Animal studies have revealed that indomethacin is similar to aspirin in that gastric damage produced by both drugs is potentiated under conditions of stress. Previously it has been shown that metiamide, an H_2 histamine receptor antagonist, significantly attenuates gastric ulceration produced by aspirin in stressed animals.

In new studies to determine whether the gastric ulceration produced by indomethacin in stressed animals can be reduced by antihistamines specific for either the H_1 or H_2 histamine receptor, laboratory animals received indomethacin (6 mg/kg) and one of several doses (0 to 32 mg/kg) of antihistamine. The animals were then subjected to cold-restraint stress for a 2-hour period. Following the 2-hour stress period, the animals were sacrificed, the stomachs were removed, and an ulcer score was determined.

The studies indicate that gastric ulceration produced by indomethacin in stressed animals is reduced by metiamide (Figure 1). Additionally, pyrilamine (Figure 2), and promethazine, two H_1 receptor antagonists, successfully reduced the gastric damage. The results for metiamide and promethazine are summarized in the table. This is in contrast to the results obtained with aspirin, which indicate that only H_2 antagonist, metiamide, attenuated gastric ulceration. These studies are potentially important in the therapeutic application of antihistamines to the prevention of undesired side effect of indomethacin.

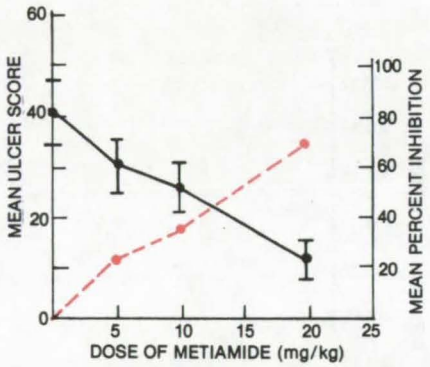

Figure 1. The **Effect of Metiamide on Gastric Ulceration** in stressed animals receiving indomethacin (6 mg/kg) is plotted as a mean ulcer score and as a mean percent inhibition. Each data point represents the mean (± the standard error) of 14 animals. The solid line is the mean ulcer score; the dotted is the mean percent inhibition.

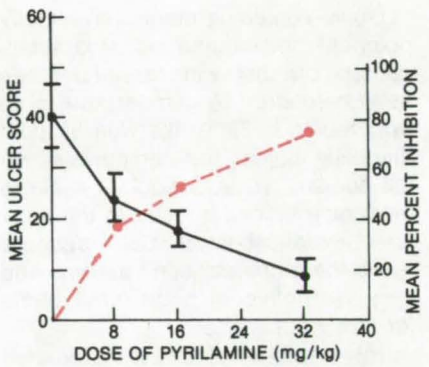

Figure 2. The **Effect of Pyrilamine on Gastric Ulceration** in stressed animals receiving indomethacin (6 mg/kg) is shown here. Each data point represents the mean (± the standard error) of 14 animals. The solid line is the mean ulcer score; the dotted line is the mean percent inhibition.

Condition	Mean (± standard error) Ulcer Score	Percent Reduction
Indomethacin[a]	46.2±6.8	0.0
Indomethacin and Metiamide[b]	14.3±2.5[d]	69.0
Indomethacin and Promethazine[c]	19.6±4.9[d]	57.0

[a] 6 mg/kg
[b] 20 mg/kg
[c] 24 mg/kg
[d] $p < 0.05$, t test

The **Antiulcer Effects** of metiamide and promethazine on indomethacin-produced ulcers in stressed rats

This work was done by Joan Vernikos-Danellis of **Ames Research Center** *and Patricia A. Brown of San Jose State University. For further information, Circle 43 on the TSP Request Card.*

This invention is owned by NASA, and a patent application has been filed. Inquiries concerning nonexclusive or exclusive license for its commercial development should be addressed to the Patent Counsel, Ames Research Center [see page A8]. *Refer to ARC-11118.*

Sweat Collection Capsule

Filter-paper insert that absorbs perspiration can be replaced while holder stays in place.

Ames Research Center, Moffett Field, California

Perspiration rate at a specific location on the body can be measured accurately with a sweat collection capsule that holds a disk of filter paper against the skin. The disk is easily inserted and removed while the capsule remains strapped in place. Weighing the paper before and after use gives the perspiration rate in $g/min/cm^2$.

In this technique for long-term perspiration monitoring, a steel ring-shaped capsule is strapped to the particular part of the body to be sampled (see figure). The back of the capsule is removable to allow insertion of a filter-paper disk that is typically 4.25 cm in diameter. The cover assembly is secured by a locking screw and an O-ring seal that provides a moisture seal.

The paper is weighed before use; and after a predetermined period of time on the subject, it is removed and weighed in an airtight container to determine the amount of sweat collected. The sample in the filter paper can also be chromatographically analyzed to determine the sweat constituents.

Another possible use for this device is the determination of the number of active sweat glands under the capsule. The skin under the capsule is painted with tincture of iodine, and a high-starch-content paper is used in the capsule. The starch/iodine reaction produces dots on the paper opposite the active sweat glands.

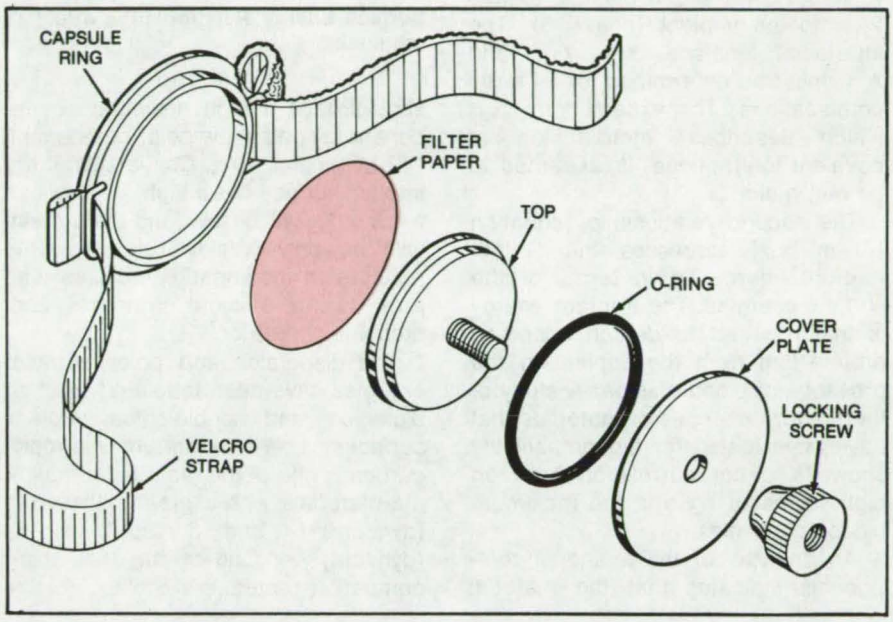

This **Sweat Collection Capsule** has a quickly-removable cover-plate assembly to simplify replacement of the filter-paper inserts. The size of the capsule ring depends on the extent of the surface to be measured.

This work was done by Robert W. Delaplaine and John E. Greenleaf of **Ames Research Center.** *No further documentation is available.*

This invention is owned by NASA, and a patent application has been filed. Inquiries concerning nonexclusive or exclusive license for its commercial development should be addressed to the Patent Counsel, Ames Research Center [see page A8]. *Refer to ARC-11031*

Biocompatibility of Surgical Implants

A consideration of surface energies can reduce trial-and-error experimentation when selecting biocompatible materials.

NASA's Jet Propulsion Laboratory, Pasadena, California

A new approach to selecting biocompatible materials for surgical implants uses fracture mechanics relationships and the surface energies of the materials in the presence of blood plasma. Using the method, 190 materials have been characterized by parameters that reflect their potential biocompatibility. Thus, the amount of actual testing required can be reduced by selecting only those materials that are the most promising candidates.

Fracture mechanics enters the biocompatibility problem because it helps to determine the adsorption and retention of a plasma-borne protein film on the implanted surfaces. If the film is strongly retained, it mediates the formation and release of thrombus at the implant and thus reduces the possibility of embolism, a major problem with implants. The surface energies determine the extent to which the film is easily "fractured" from the implanted surfaces.

One of two key relationships in the method is the expression for inter-

(continued on next page)

facial tension (γ_{ij}) between two surfaces in contact [see equation (1) in box] where α and β are the dispersion and polar components of surface tension, respectively, and the subscripts i and j refer to the phases in contact. For an implant, three phases are involved: the plasma protein film (phase 1), the blood plasma (phase 2), and the implant (phase 3). The interfacial tensions, γ_{12}, γ_{13}, and γ_{23}, must be determined for all three combinations. The excess term Δ_{ij}, which describes interdiffusion of covalent interactions, is assumed to be negligible.

The second relationship [equation (2) in box] expresses the Griffith fracture energy γ_G in terms of the surface energies. The fracture energy is that required to detach adsorbed protein film from the implant in the presence of blood plasma. A study of the fracture energies of materials that have been tested for biocompatibility shows a direct correlation between high values of γ_G and the maximum biocompatibilities.

An analysis of the α and β components indicates that the material should have a high dispersion component (α) and a low polar component (β) to maximize γ_G. Conversely, if an implant surface has a high β value and a low α, γ_G will be low, and the protein willl be only weakly retained. The result is an incompatible surface that acts as an efficient thrombus and embolus generator.

$$\gamma_{ij} = (\alpha_i - \alpha_j)^2 + (\beta_i - \beta_j)^2 + \Delta_{ij} \quad (1)$$

$$\gamma_G = (\alpha_2 - 0.5\,\alpha_1 - 0.5\,\alpha_3)^2 + (\beta_1 - 0.5\,\beta_1 - 0.5\,\beta_3)^2 - 0.25\,[(\alpha_1 - \alpha_3)^2 + (\beta_1 - \beta_3)^2] \quad (2)$$

Surface Energy Relationships affect the biocompatibility of surgically-implanted materials.

The dispersion and polar surface energies have been tabulated for 190 biological and nonbiological implant surfaces. Low-temperature isotropic carbon is one of the most biocompatible materials with α greater than 6.0 $(dyn/cm)^{1/2}$ and β less than 2.0 $(dyn/cm)^{1/2}$. One of the least biocompatible materials is Stellite 21 with a relatively low α of about 5.0 $(dyn/cm)^{1/2}$ and β above 5.0 $(dyn/cm)^{1/2}$.

The analysis can be extended to describe the effects of interface roughness and interdiffusion, which are important in microfiber scaffold surfaces, hydrogel coatings, and biological intimal surfaces of the cardiovascular system.

This work was done by David H. Kaelble of Rockwell International Corp. for **NASA's Jet Propulsion Laboratory.** *For further information, Circle 44 on the TSP Request Card.*
NPO-14291

Microprocessor-Based Cardiopulmonary Monitor

Complete, automated system performs cardiopulmonary diagnostics.

Lyndon B. Johnson Space Center, Houston, Texas

Microprocessor technology has reduced the size of a complete cardiopulmonary-monitoring system and cut its power requirements by 90 percent. The new system (see figure), originally designed to test the effects of weightlessness on astronauts, has a dedicated 16-bit central-processing unit (CPU) that controls heart- and respiratory-monitoring transducers and supervises data acquisition and analysis. The CPU controls lights and lighted pushbuttons on the control panel to guide the operator through the various experimental maneuvers.

The system performs pulmonary-function tests (PFT) and physiological time-constant/pulmonary blood-flow tests (PTC/PBF). Each of these test sequences actually consists of several submeasurements. For example, the PFT includes measurements of residual volume (the volume of air remaining in the lungs after a complete exhalation) by the nitrogen-washout method and forced-vital-capacity measurements (the maximum volume of air that can be forcefully exhaled, starting from full inspiration). The PTC/PBF series includes measurements of oxygen consumption, carbon dioxide production, minute ventilation, heart rate, and cardiac output, all of which reflect the dynamic response to stress.

The system hardware occupies only 36 vertical inches (91.4 cm) of standard rack space. In addition to the microprocessor and the control panel, the electronics include an automated blood-pressure-measuring system, an exhalation spirometer for measuring respiratory volume, an oxygen-demand regulator, and a video monitor. Also contained in the system are an analog-to-digital converter, electrocardiograph, and mass-spectrometer transducers, and a digital tape printer mounted on the control panel. A separate bicycle ergometer can be included for exercise stress.

The firmware to control and monitor the experiments is contained in 5K of programable read-only memory. An additional 8K of random-access memory are included as a data buffer and "scratch pad" memory. No data are stored in the system. Instead, real-time data are displayed on the printer and the video monitor. The data can also be transmitted to a remote data system for long-term storage.

The experimental control panel is separated into four modules, including an initialization module, a pulmonary-

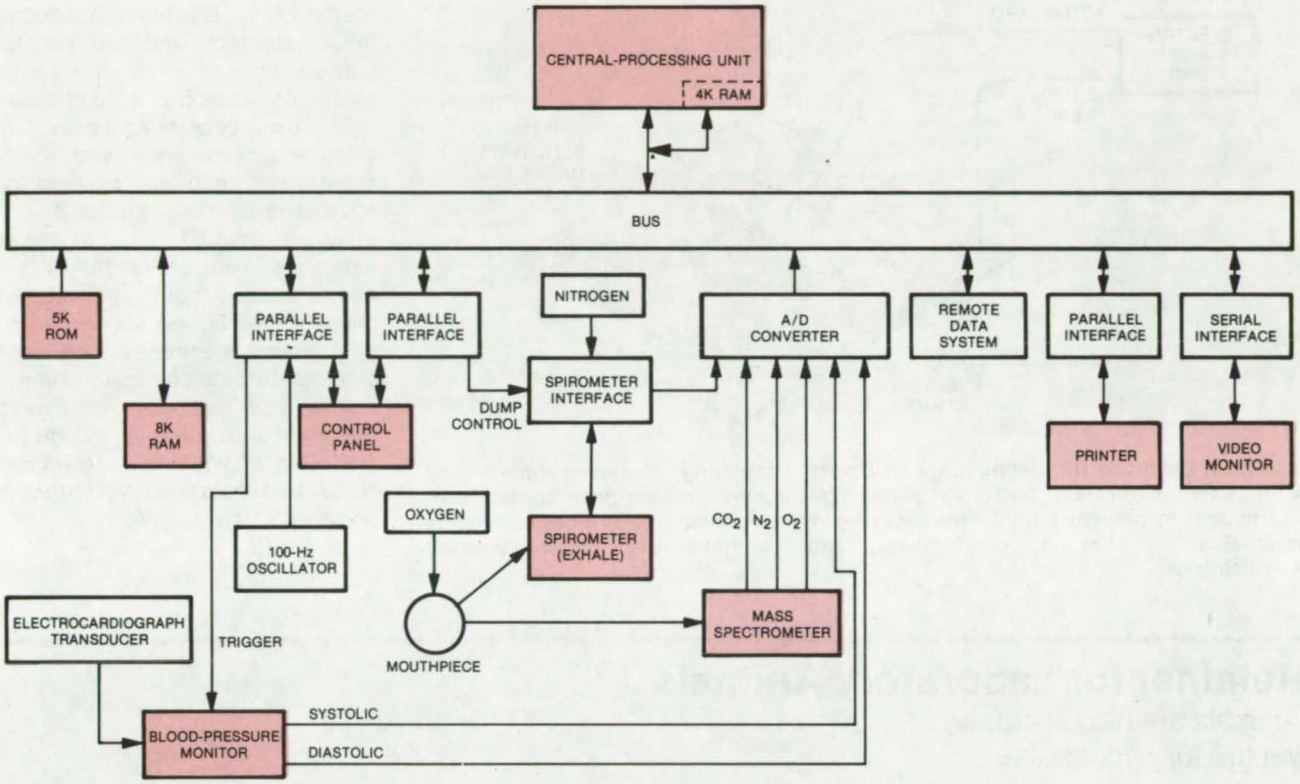

Cardiopulmonary-Monitoring Functions are controlled by a 16-bit-microprocessor CPU. Power consumption is 100 watts, down from 1,000 watts in an earlier, minicomputer-based system.

function test module, a physiological time-constant/pulmonary blood-flow module, and an output module. The initialization module is for subject and mass-spectrometer identification and for test selection (PFT or PTC/PBF). The PFT module guides the subject through the nitrogen-washout and forced-vital-capacity maneuvers. The PTC/PBF module controls an exercise protocol that includes cardiac-output maneuvers (cued by panel lights). Controls for selecting the output device are located on the output module.

This work was done by John A. Rummel and Charles F. Sawin of **Johnson Space Center** *and Melvin C. Buderer, Donald G. Mauldin, and Katherine M. Tamer of Technology Inc. Further information may be found in NASA CR-151688 [N78-21752], "Microprocessor-Based Cardiopulmonary Monitoring System" [$11]. A copy may be purchased [prepayment required] from the National Technical Information Service, Springfield, Virginia 22151.*
MSC-18235

Resterilizable Electrode for Electrosurgery

Conductive elastomers offer good electrical contact and are reusable.

NASA Headquarters, Washington, D.C.

A major problem in early electrosurgical techniques was the occurrence of patient burns due to poor contact with the return electrodes. Electrosurgery uses a radio-frequency current to cut or coagulate living tissue at a point where the electrical circuit is completed. Unwanted electrical heating can occur, however, at the skin-to-ground electrode interface. The key to minimizing this effect is to establish a low-resistance electrical contact between the metal and the skin; the quality of the contact depends on the surface area of the electrode and on the resistance of the skin. A further requirement is that the ground as well as the surgical electrode itself must be sterile.

In the past, large plates have been used for the ground electrodes; these often lost contact as the patient was moved. Coating the metal plates with a conductive substance to fill in the contours proved unsuccessful. The use of a flexible lead electrode coated with a cloth soaked in an electrolyte was a moderate improvement.

Recent experiments have now shown that by using a flexible-polymer/conductive-particle composite, the required electrode properties

(continued on next page)

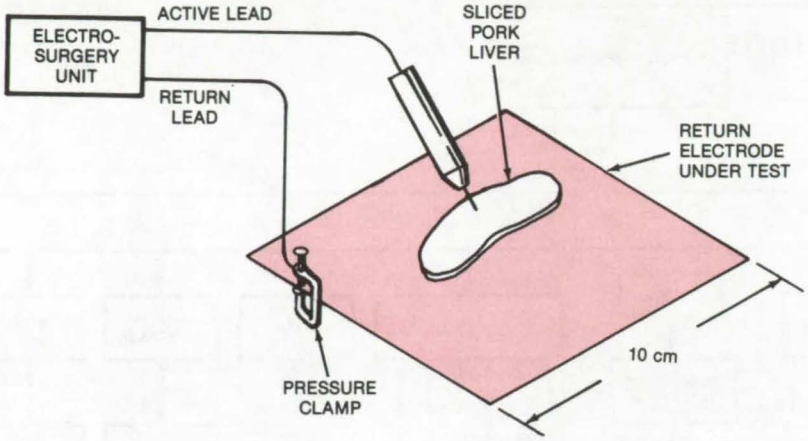

A **Return Electrode for Electrosurgery Circuits,** consisting of silicone rubber filled with carbon, silver flake, and silver-plated glass spheres, makes good contact with the patient to prevent burns. The flexible-polymer/conductive-particle composite maintains its strength, conductivity, and flexibility even after repeated sterilizations.

of flexibility, electrical conductivity, tensile strength, and tear resistance can be retained even after repeated steam sterilization in an autoclave.

The electrodes are fashioned from silicone rubber filled with carbon, silver flake, and silver-plated glass microspheres. The electrode sheets measure about 10 by 10 cm and are 2 mm thick. Test operations on organ and muscle tissue of laboratory animals (see figure) showed that the new ground electrodes allow repeatable, clean cuts and coagulation.

This work was done by Everis R. Engstrom and James C. Houge of the University of Wisconsin—Madison for **NASA Headquarters.** *No further documentation is available.*
HQN-10915

Retainer for Laboratory Animals

Animals are held securely,
yet are fully accessible.

Langley Research Center, Hampton, Virginia

A "bio-retainer" holds laboratory animals in a fixed position for research and clinical experiments. The bio-retainer allows full access to the animals and can be rapidly opened and closed to admit and release the specimens.

The device was originally developed to hold mice while they are exposed to microwave radiation in experiments to determine the relation between microwaves and tumors. It holds the mice in a fixed position during the experiments. The retainer can be easily adapted to hold smaller or larger animals.

The restraining device (see figure) consists of a baseplate, cantilever arms supported by pins, and parallel guides. A test animal is placed between the pair of guides, and the cantilever arm is lowered into position over the animal. (The weight of the arm binds it in a fixed position on the pin; alternatively, a locking screw can hold the arm on the pin.)

The experimental instrumentation is installed in a recess in the arm. The arm can be swung out of the way or removed completely when it is not needed. Additional restraints can be mounted on the guides if necessary.

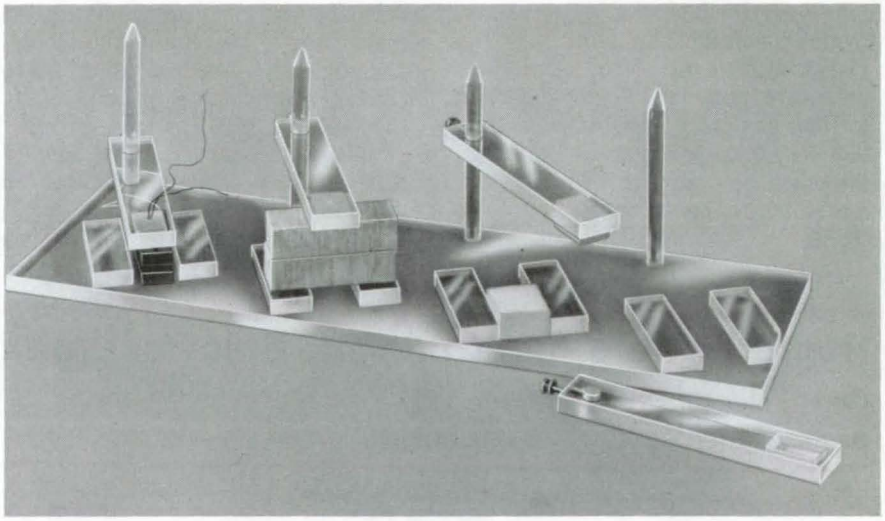

The **Bio-retainer** cantilever arm at the right is removed from its pin to access the work area between the two guides. The second arm from the right is swung aside to expose soft foam material that conforms to the shape of the specimen. The third arm from the right rests on hard-foam blocks that can be used as a base for taping the specimens. At the far left, electrical leads feed through a hole in the cantilever arm. Instrumentation is housed in a recess in the arm.

This work was done by Roland W. Lee of **Langley Research Center.** *For further information, Circle 45 on the TSP Request Card.*

Inquiries concerning rights for the commercial use of this invention should be addressed to the Patent Counsel, Langley Research Center [see page A8]. Refer to LAR-12353.

Improved Myocardium Transducer

An improved pin, held in place by the heart-muscle fibers instead of sutures or barbs, minimizes trauma to the myocardium.

NASA's Jet Propulsion Laboratory, Pasadena, California

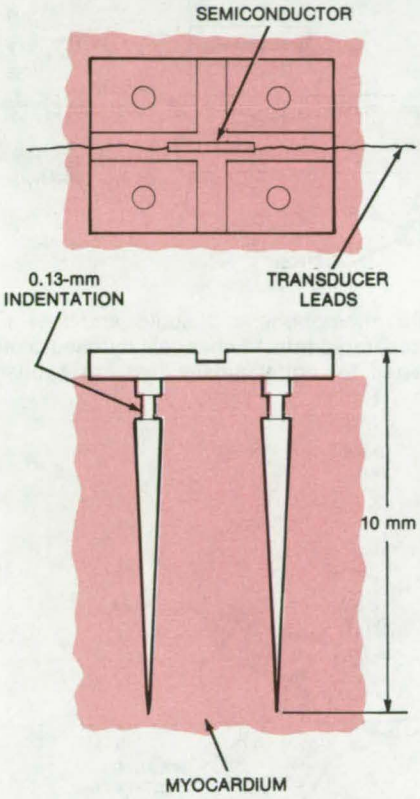

New Transducer Pins have small indentations at their bases. (This drawing exaggerates the dimensions to illustrate the concept.) Epicardial fibers close around the indentations, holding the transducer securely in the heart muscle.

Many different transducers are used in heart research. One type designed to measure forces within the myocardium consists of two or more pins attached to a small beam. A semiconductor device attached to this beam converts the forces acting on the beam into electrical impulses.

This transducer is inserted into a desired location in the myocardium and is held in place by one of two methods:

1. The transducer is sutured in place. This method is time-consuming and traumatic to the myocardium. Sutured transducers are difficult to remove and can sample the force only to the depth of suture, which is hard to reproduce.
2. There are barbs on the pins of the transducer that hold it in place when it is inserted in the myocardium. (See "Myocardial Wall-Thickness Transducer," (NPO-13644), *NASA Tech Briefs* (Spring 1976), Vol. 1, No. 1, p. 83.) These barbs can cause tearing and cutting of the heart muscle when the transducer is removed.

An alternative method of implanting the transducer is to use the newly designed pins shown in the figure. Each pin has a small indentation at the base; epicardial fibers that close around it hold the transducer securely in place. The pins are thin enough to cause a minimum of trauma to the myocardium during implantation and removal.

This work was done by Virgil H. Culler, Cyril Feldstein, and Gilbert W. Lewis of Caltech for **NASA's Jet Propulsion Laboratory.** *For further information, Circle 46 on the TSP Request Card.*
NPO-14107

Implantable Digital Hearing Aid

Sound waves are converted to digital pulses and applied directly to the auditory nerve.

John F. Kennedy Space Center, Florida

A hearing aid that merely amplifies sound entering the ear is ineffective if the inner ear is disabled. It has been proposed that in such cases the electrical output of a hearing aid could be directly connected to the auditory nerve, bypassing the inner ear.

Due to the complex electrical nature of the organ of Corti (the inner portion of the cochlea), however, there had been doubts that an analog voltage applied to the nerve with a single electrode could produce the sensation of sound without considerable distortion and poor fidelity. Therefore a proposed new hearing aid would convert the analog output of a microphone into digital pulses in about 10 channels of audiofrequencies. Each pulse band could be directly connected to the portion of the auditory nerve most sensitive to that frequency range.

(continued on next page)

To encompass the audio range from 0 to 5,000 Hz, the 10-channel system illustrated in Figure 1 has been proposed. A conventional miniature hearing-aid microphone and amplifier are used to obtain the analog voltage. The analog output is divided by 10 band-pass filters to form 10 adjacent channels of 500-Hz widths. A simple transistor switch, biased at a given threshold, converts the analog signal to digital pulses. The digital pulses have either a highly electrically-polarized "on" state or baseline "off" state, which closely resembles the natural mechanism of nerve conduction of the auditory nerve.

As seen in Figure 2, these signals could be conveniently carried to the ear canal with an insulated multiconductor wire that could be made detachable by using a connector at the remote end. From this point the connection to the auditory nerve must be made by surgical implantation, after experimentally determining the point along the basilar membrane normally accustomed to transmitting like signals in the normal hearing process for interpretation as sound.

The complete system, once the techniques for implantation and testing are developed, will effectively bypass the entire mechanical portion of the hearing mechanism from the external ear through the inner ear.

This work was done by Adam M. Kissiah, Jr., of **Kennedy Space Center.** *For further information, Circle 47 on the TSP Request Card.*

This is the invention of a NASA employee, and U.S. Patent No. 4,063,048 has been issued to him. Inquiries concerning license for its commercial development may be addressed to the inventor: Mr. Adam M. Kissiah, Jr., 155 Brandy Lane, Merritt Island, FL 32952.
KSC-11009

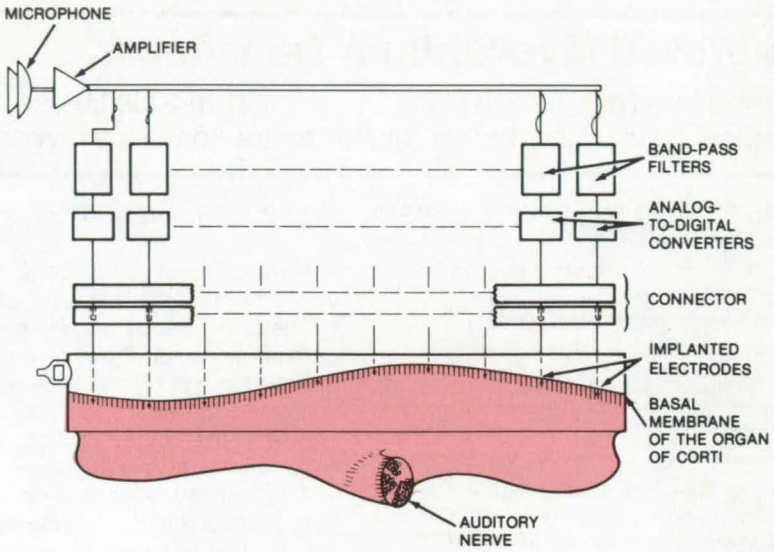

Figure 1. This **Digital Hearing Aid** uses a microphone and audio amplifier to produce an analog electrical signal that is separated into 10 channels by band-pass filters. The analog signals are then converted to digital pulses that are applied directly to the auditory nerve.

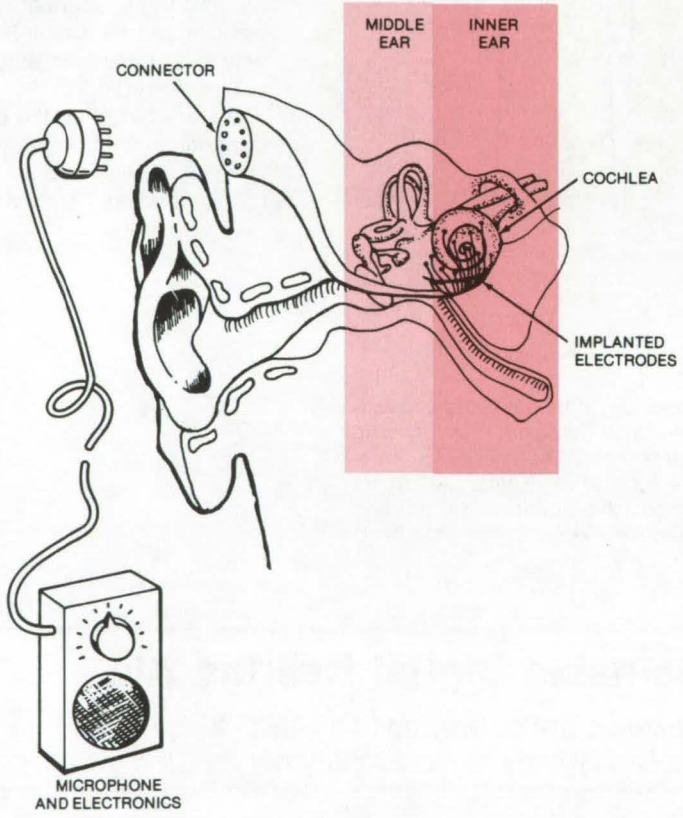

Figure 2. A **Connector Implanted in the Mastoid Area** is one way to join the hearing aid to the surgically implanted electrodes. The wires carrying the digital channels to the electrodes implanted in the basal membrane must be well insulated from each other and from body fluids to prevent signal degradation. (The connector/plug method of stimuli transmission to the inner ear is not the best possible method of transdermal coupling. More cosmetically acceptable methods will be proposed after experimentation.)

Automated Syringe Sampler

Device for remote sampling of air or water in pollution studies

Langley Research Center, Hampton, Virginia

The automated syringe sampler shown in Figure 1 is designed primarily for remotely collecting field samples of air or water from pollution sources and from tracer gases used to track such sources over long distances. It consists of an evacuated glass tube with a rubber septum, or seal, at one end, a double-ended needle, and a small servomechanism. A mounting board is also required, along with two small brackets to hold the needle and adapt the glass tube to the servomechanism. A small signal-conditioning unit was specifically designed to supply a digital signal to the servomechanism and to allow it to be controlled by a simple switch closure. The signal conditioner, shown in Figure 2, uses only a single timer integrated circuit and some outboard components.

To collect a sample, the servomechanism is activated remotely, either by a switch closure or a radio signal. The servomechanism drives the evacuated glass sampling tube forward into the stationary syringe-needle unit, which causes one end of the double-ended needle to puncture the rubber septum. The glass sampling tube then begins to draw a sample of the surrounding fluid (air or water) through the double-ended needle. This continues until the sampling-tube pressure reaches ambient pressure, typically in 5 seconds.

The servomechanism switch is then opened, driving the glass tube in reverse and extracting the syringe needle from the rubber septum. The septum expands and seals the fine hole made by the needle penetration. The fluid sample is removed from the glass sampling tube with a conventional syringe and is injected into the appropriate apparatus, such as a gas chromatograph or mass spectrometer, for analysis.

Because of its small size and weight, the unit can be flown, floated, or carried to essentially any location. It can be used in aircraft, onboard ship, on weather balloons, or placed inside of commercial or residential ventilation ducts or other air-carrying devices.

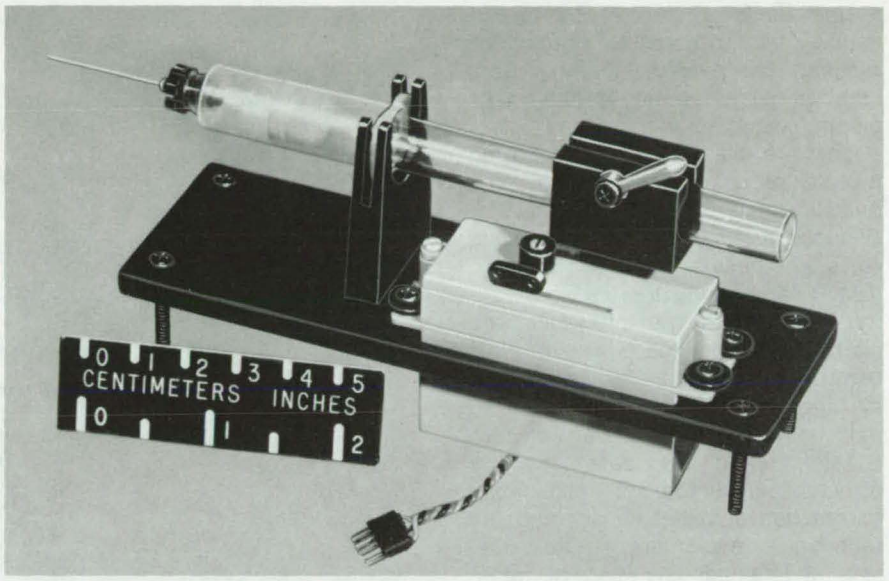

Figure 1. **Automated Syringe Sampler** is small, rugged, and weighs only 5.5 ounces (156 grams). The syringe-needle unit, glass sampling tube, and servomechanism are all available commercially. Only the mounting apparatus and signal-conditioning unit are custom-designed. The unit is self-sealing and essentially leakproof; the glass tube is disposable. It is inexpensive to assemble, easy to transport and store, and is entirely self-contained. A variation of the device substitutes a timing device for the remotely triggered signal to provide timed switch closure for unattended sequential sampling.

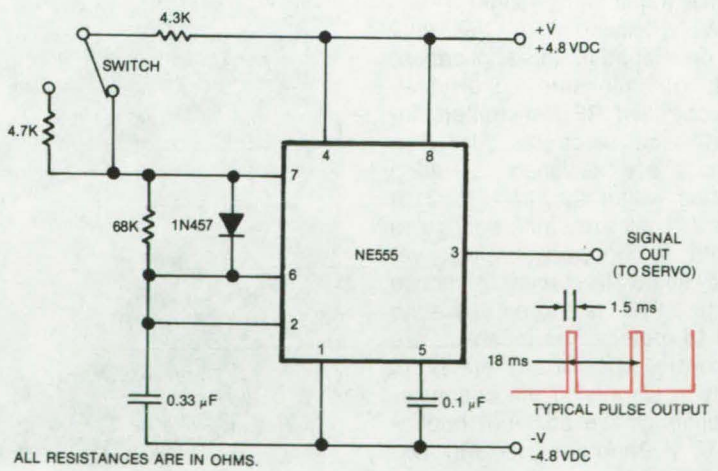

Figure 2. This **Signal Conditioner** produces a stream of pulses that operate the sampler servo. The length of travel of the servo is controlled by the pulse width. By changing the switch position, the width is changed, and the syringe needle is either driven into or extracted from the rubber septum.

This work was done by Gerald C. Purgold of **Langley Research Center.** *No further documentation is available.*

Inquiries concerning rights for the commercial use of this invention should be addressed to the Patent Counsel, Langley Research Center [see page A8]. Refer to LAR-12308.

Wideband EMG Telemetry System

Compact transmitter simplifies multichannel EMG telemetry.

Ames Research Center, Moffett Field, California

One useful technique for determining the orthopedic corrections required by people suffering from cerebral palsy is to monitor their gaits electronically. In this method, electrodes are placed on six opposing muscle groups on each leg, and pressure-triggered step-indicator switches are mounted on both shoe soles. These electromyographic (EMG) and pressure sensors are monitored as the person walks; the information obtained, in an EMG bandwidth of 20 to 2,000 Hz, is used to correlate the activity of the leg muscles with each phase of walking.

Telemetering the data has the obvious advantage of eliminating cables between the subject and the recording equipment. Ordinarily, several data channels would be transmitted by using a multiplexed data transmitter and a single RF link. However, because of the EMG bandwidth requirement of 2,000 Hz and the need for 12 channels, a multiplexed system would be difficult to implement in a low-powered device having a reasonable transmitting range.

A new, wideband EMG telemetry system, developed for this application, consists of miniature, individual, crystal-controlled RF transmitters located at each electrode site. The transmitters are assigned operating frequencies within the 174- to 216-MHz band. They are small enough to be placed at the sensor sites, yet having a linear frequency response from 20 to 2,000 Hz and an operating range of 15 meters. The receivers are crystal-controlled so that there is no ambiguity in identifying the channels. The amplifiers have an input impedance of 10 M Ω and are used with two sensing electrodes per channel.

The use of individual transmitters for each data channel has advantages. By eliminating the need for cables between the electrode sites and a master transmitter, maximum mobility is allowed, preparation time is reduced, and subject comfort is improved. Data channels can be easily added or subtracted.

Figure 1. This **Compact Transmitter** (largest of the three packages) sends data collected by EMG pressure sensors (smaller packages) to a nearby receiver. The data are used to analyze muscle movements in the gaits of patients suffering from cerebral palsy.

The circuit for the EMG transmitter (including batteries) is small enough to be attached at the electrode site (see Figure 1). The circuit was designed to minimize the number of components and the current drain. Figure 2 shows the circuit diagram of the complete unit with preamplifier, subcarrier oscillator, RF transmitter, and battery supply.

The preamplifier gain is set at 56 so that a full-scale input signal of ±3 mV will provide ±168 mV at the modulator input, with a band pass of 20 to 2,000 Hz. The subcarrier oscillator uses a single operational amplifier as a differential pulse-width modulator. Pulse widths are varied ±30 percent with a fixed frequency of 10 kHz. The three operational amplifiers (in the preamplifier and the subcarrier oscillator) are on one integrated-circuit chip. The transmitter is packaged as a disk 3.75 cm in diameter and 0.9 cm thick. Two small silver oxide cells are used as a battery supply. Current drain of the complete RF section is less than 3 mA.

The FM receiver passes the signal to a subcarrier demodulator that retrieves the EMG signal for display on a recorder and a monitoring scope. A circuit diagram of the subcarrier demodulator is shown in Figure 3. The demodulator has a low-pass filter at its input that allows sufficient rise time for threshold detection of the 10-kHz subcarrier, yet reduces any spurious high-frequency responses that might occur during modulation and transmission.

The threshold detector automatically measures the peak-to-peak amplitude of the subcarrier and generates a voltage that is centered at the midpoint of the rectangular waveform. Using this information, the comparator reshapes the subcarrier to a rectangular waveform with fast rise-and-fall times and a constant amplitude. Low-pass filtering of the modulated rectangular waveform reproduces the original EMG.

This work was done by S. A. Rosatino and R. M. Westbrook of **Ames Research Center.** *For further information, Circle 48 on the TSP Request Card.*
ARC-11209

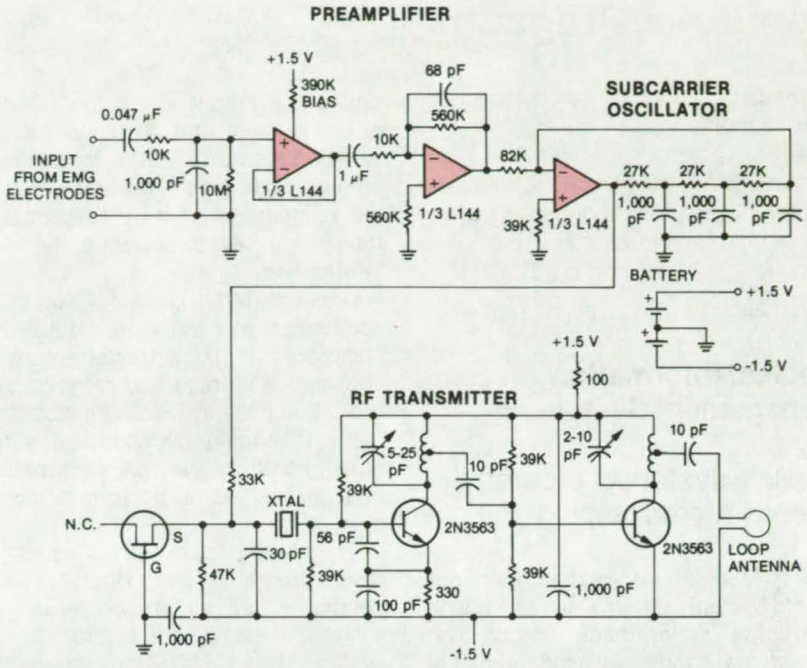

Figure 2. The **Wideband FM Transmitter** of the EMG telemetry system can be packaged in a disk having a diameter of 3.75 cm and a thickness of only 0.9 cm.

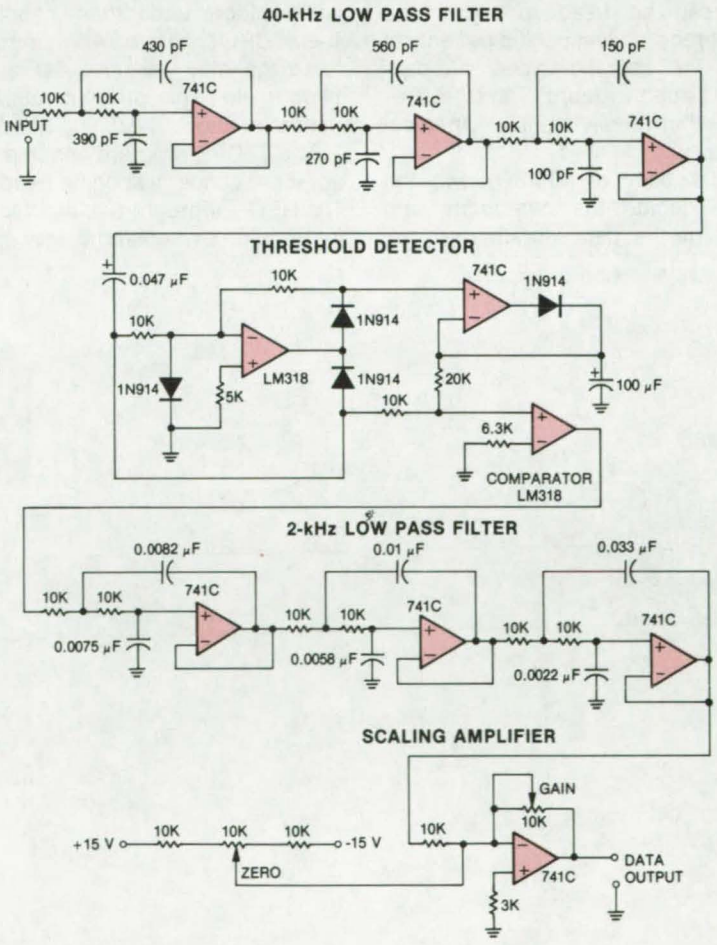

Figure 3. The **Subcarrier Demodulator** in the receiver circuit retrieves the original EMG. The scaling amplifier adjusts the output for uniform gain among several transmitted channels.

Computer Programs

These programs may be obtained at very reasonable cost from COSMIC, a facility sponsored by NASA to make new programs available to the public. For information on program price, size, and availability, circle the reference letter on the COSMIC Request Card in this issue.

Medical Information Management System

Flexible system of programs speeds recordkeeping

The Medical Information Management System (MIMS) is an online interactive information processing system that handles all aspects of data management related to patient care. Characterized by quick and easy access to important information, MIMS can be used to recall the medical record of a specific patient, to search for specific types of data among patient records, and to research other readily-available medical data bases.

The flexibility of MIMS allows the user to decide the categories and formats of the data, to change any data entry without regard to the length of the original data field, to retrieve selected items of data, to generate tabular information assembled from the comparison of all the records in the system, and to generate statistical information.

Although MIMS was developed for application to medical recordkeeping situations, it is a general-purpose information storage and retrieval system. Potential applications could include managing occupational safety data, handling judicial information, and serving as a personnel inquiry system.

The MIMS package consists of seven programs. Each operates independently, but all are connected by references to common files in the system. The HEADER program creates a file of headings (or labels), consisting of from 1 to 20 alphabetic or numeric characters, for data that will be placed under these headings by the STORE program. As many as 160 headings may be used for a single header file. This program allows the user to change an existing header file.

The STORE program enables one to enter data under a specific header file. The RETREV program is used to recall information by defining a very specific or very generalized search. The UPDATE program alters data files by changing an entry in a data record, adding to a data record, or deleting a heading and its corresponding data (or deleting an entire record or records). The SORTER program arranges records according to user-set priorities in either ascending or descending order. The MERGE program merges two sorted data files. The SUPPLEMENT program adds new categories and data to an existing file.

The MIMS programs are written in extended FORTRAN for interactive execution and have been implemented on a CDC 6000-series computer. For use under the CDC FTN compiler, the user will have to supply certain input, output, and file-handling capabilities that are available on the UCS FORTRAN (PFUR) compiler. The largest MIMS program has a central memory requirement of approximately 16K (octal).

This program was written by Sidney Alterescu and Kathleen R. Hipkins of **Goddard Space Flight Center** *and Carl A. Friedman of Federal City College. For further information, Circle D on the COSMIC Request Card.*

GSC-12078

Mechanics

Hardware, Techniques, and Processes

Books and Reports

Computer Programs

Noncontact Optical Communication Between Moving Stations

Concentric light beams and large lenses allow uninterrupted signals between stations with limited relative motion.

Langley Research Center, Hampton, Virginia

An optical coupler allows noncontact data transfer between two parts having several degrees of relative motion. Rotation about one axis and limited axial and radial motions will not interrupt communications.

The data coupler was designed for a very stable platform used in high-resolution pointing experiments conducted onboard the Space Shuttle; it is the link between the spacecraft and the platform, carrying data to be transmitted into space from the platform and data received from space at the platform. If all of the position adjustments of the platform were made with gimbals, the data could be carried by commutators. However, the fine adjustments are made through a noncontacting magnetic suspension, so data must be transferred to and from the platform without disturbing the suspension and without creating electromagnetic interference. Therefore the optical communication link was devised.

The optical coupler consists of three concentric light channels that are coaxial with the rotational axis of the platform (see figure). Channels 1 and 3 are directed from the platform to the base, and channel 2 goes from the base to the platform. (The amount of data received in the experiments is greater than the amount sent out.)

Each channel employs one or more gallium arsenide infrared light-emitting diodes (LED's) as transmitters. The rays from each LED are projected across the gap into lenses that focus the light on photodiode receiving devices.

In channel 1, the innermost channel, the optical path is direct. In channels 2 and 3 (the intermediate and outer channels), mirrors are used to save space. For structural reasons, components of the two inner channels (1 and 2) are supported by spokes; therefore three LED's are used to ensure that at least two light paths to the detectors will always be unobstructed by the spokes.

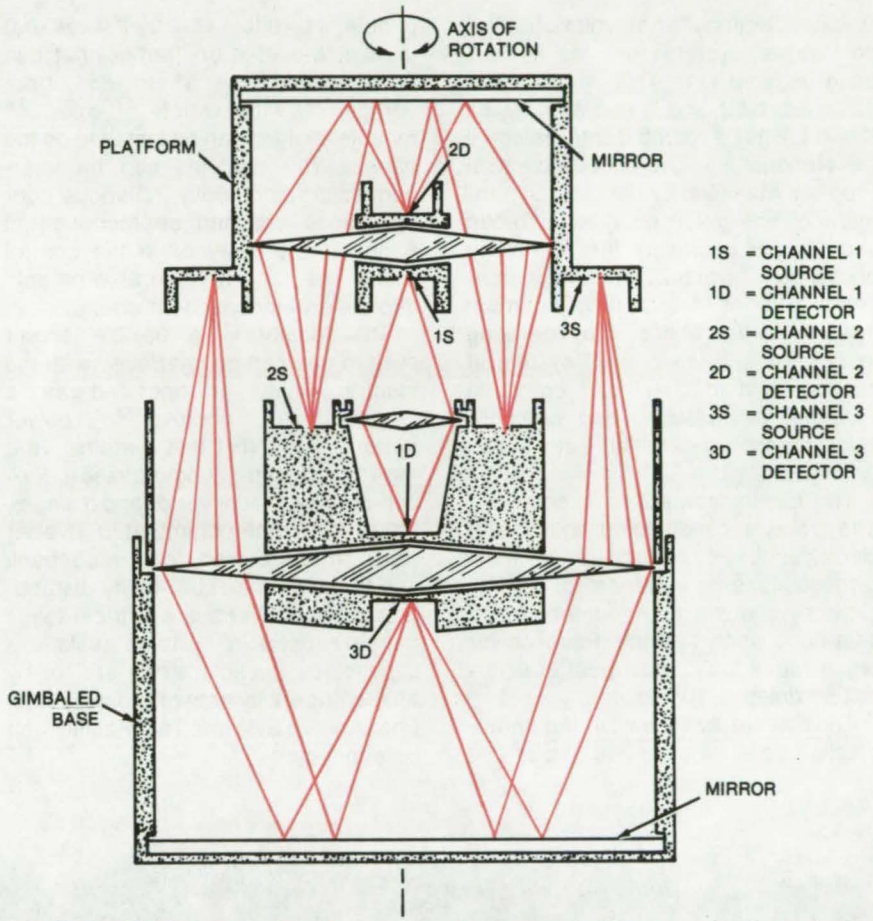

This **Optical Data Coupler** has three channels concentric with the axis of rotation to maintain communication through 360° rotation. Lateral movement and separation along the axis of rotation are accommodated to an extent depending on the sizes of the lenses.

Since the channels are concentric, any amount of axial rotation between platform and base can be accommodated. Up, down, and sideways motion between platform and base is accommodated — within the limits of the worst-case pointing situations — by proper positioning of the LED's and photodiodes and by choosing the focal lengths of the lenses so that the light spots remain within the active areas of the detectors.

Digital data are transmitted by pulse-modulating the light beams in each channel with the data selected for that channel and by detecting the data at the photodiodes as current pulses. Capacitance coupling removes dc dark current from the photodiode output, and an automatic gain-control circuit improves operation over varying signal-to-noise ratios.

This work was done by David C. Cunningham and Brian J. Hamilton of Sperry Rand Corp. for **Langley Research Center.** *For further information, Circle 49 on the TSP Request Card.*

Inquiries concerning rights for the commercial use of this invention should be addressed to the Patent Counsel, Langley Research Center [see page A8]. Refer to LAR-12283.

Photovoltaic Systems Test Facility

Equipment for "breadboarding" and analyzing fairly-large-scale solar-cell power systems

Lewis Research Center, Cleveland, Ohio

A new national photovoltaic (solar-cell) power-system test facility has been established. This facility was designed, built, and is operated by the NASA Lewis Research Center to serve the National Photovoltaic Conversion Program managed by the U.S. Department of Energy. It provides a broad and flexible capability for evaluating photovoltaic systems and design concepts and for determining optimum system configurations and operating modes. As a "breadboard" system, it can be used to check out complete systems, subsystems, and components before installation in actual service.

The facility comprises a solar-cell array, power conditioning equipment, electrical loads, electric-utility interface equipment, batteries for energy storage, and an instrumentation and data-acquisition system. Peak power rating with a full complement of solar-cell modules is 10 kilowatts.

The solar array (shown in the photograph) consists of 240 solar-cell panels, 4 by 8 feet (1.2 by 2.4 meters) in size, mounted on frames that can be inclined from 5° to 85° from vertical. A wide variety of solar-cell module designs can be installed on the panels. The modules can be interconnected electrically in various configurations and can be reconfigured either at the array or in the control room. The full array can also be split into several independent arrays.

The facility is a flexible power system and can be interfaced with the electric utility or operated as a "stand-alone" photovoltaic power system. The initial test systems were assembled with a single-phase 5-kVA self-commutated inverter and a single-phase 8-kW line-commutated inverter transformer-coupled to a load bank and to the load electric-utility distribution network. Various electrical loads that are used in systems tests are supplied by the solar array and/or by an electric-utility network to which the Photovoltaic Systems Test Facility can be connected.

Interface with an electric-utility distribution network is achieved through proper matching transformers and circuit breakers. When the solar array supplies more power than is called for by the load, the excess power is fed into the utility grid. When there is insufficient power from the array, the difference is automatically supplied from the utility network. Energy storage consists of 48 kWh of lead-acid storage batteries of a deep-discharge-cycle-duty type.

The facility includes an extensive instrumentation and data-acquisition system. Transducers measure electrical parameters (voltage, current, power, reactive power), module temperature, weather parameters (wind-speed and wind direction, air temperature, humidity), and insolation. A combined microprocessor/minicomputer with data-acquisition and display systems provides online results during test operations.

The Photovoltaic Systems Test Facility is an installation in which

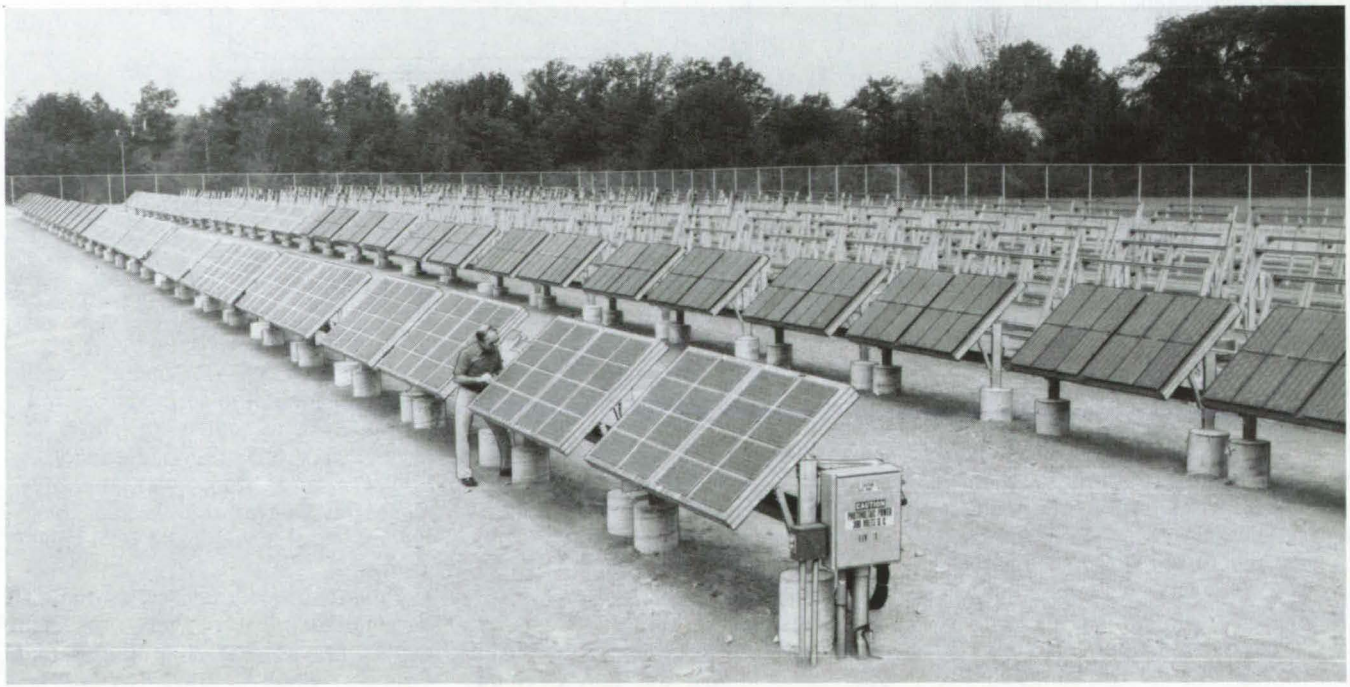

Array of Solar Cells on 240-panels is used at the Photovoltaic Systems Test Facility for analyzing solar-cell power designs. The panels can accommodate various types of cells in electrical configurations that can be set at the array or in a control room.

photovoltaic power systems can be assembled and electrically configured to evaluate system performance and characteristics. The effects of environmental factors (wind, temperature, rain, snow, and dirt) on solar-array performance are observed for study. Also, effects on the environment, such as radiated electromagnetic interference, can be studied.

This work was done by **Lewis Research Center.** *Further information may be found in:*

NASA TM-73787 . [N78-15059], "The ERDA/LeRC Photovoltaic Systems Test Facility," and NASA TM-X-73641 [N77-22609], "ERDA/Lewis Research Center Photovoltaic System Test Facility."

Copies of these reports may be obtained at cost from the Technology Application Center, University of New Mexico *[see page A7].*

LEW-13073

Ruby C-Axis Alinement System

A new room-temperature system locates the C-axis of a ruby slab to within ±3 minutes of arc.

NASA's Jet Propulsion Laboratory, Pasadena, California

Rubies fabricated for maser applications must be alined precisely for cutting their faces at the proper angle to the C-axis. Operation of a maser in the K-band requires that the 1 to 3 and 2 to 4 pump transitions in the ruby be congruent. This occurs at the push/pull angle of 54.7°. Therefore the surface must be ground to within a few minutes of arc of this angle and accurately placed in the maser so that the magnet will generate a field at 54.7° with respect to the ruby C-axis.

A standard procedure for alining a ruby boule is to cool the ruby to 4.2 K (the maser operating temperature) and measure the paramagnetic resonance to determine the C-axis. This procedure can be very time consuming since it requires a lengthy cooldown cycle each time a slab is checked.

A new, room-temperature, C-axis alinement system, shown in the illustration, is simpler and faster. The ruby is tuned (at room temperature) to act as a dielectric resonator in a waveguide. The C-axis can then be located to within ±3 minutes of arc from recordings of paramagnetic absorption of X-band microwave signals, as a function of crystal orientation.

The new system includes a function generator that sweeps a magnet power supply with a sawtooth waveform so that the magnetic field strength varies between 2.4 and 2.6 kilogauss. A ruby slab, for which the C-axis angle has been roughly determined (to within 1°) by optical methods, is placed in a waveguide fixture.

An X-band RF signal is applied to the ruby through a filter, a circulator, and a tuner. Two dips, due to two idler transitions, are recorded on an oscilloscope and are automatically plotted graphically for various field angles. If the dips coincide when the fixture is at an angle other than zero degrees relative to the magnet pole faces, the angle is noted on the vernier, and the ruby slab is removed for regrinding to correct the error.

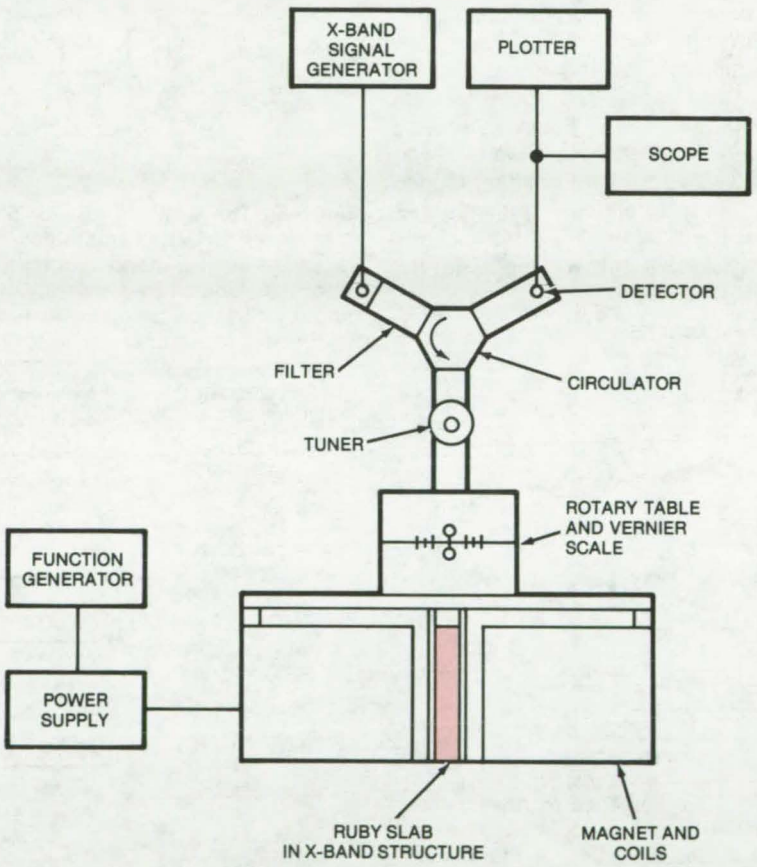

This **Ruby C-Axis Alinement System** tunes the ruby slab for dielectric resonance at room temperature. The C-axis orientation is determined from recorded plots of the paramagnetic absorption, in the X-band, of two idler transitions.

This work was done by Robert C. Clauss and Frank E. McCrea of Caltech for **NASA's Jet Propulsion Laboratory.** *For further information, Circle 50 on the TSP Request Card.*

NPO-14252

Modulation Improves Electro-optic Object Detector

Pulsed source lets sensor monitor parts on production line despite interfering light sources.

Marshall Space Flight Center, Alabama

A new optical detector is used to detect the presence or absence of a silicon wafer at a point along an air track. The detector is a part of an integrated-circuit production line; it is designed to replace a standard non-modulated optical sensor that was sensitive to interference from ambient light and electrical noise and therefore could operate only in the dark. The new detector is not affected by ambient light.

The physical arrangement of the wafer, air track, and detector is depicted in Figure 1. Figure 2 shows the circuitry: A 350-Hz square-wave oscillator keys the light-emitting diode (LED) in an optical transmitter/sensor. The modulated light is picked up by the sensor only when a wafer is directly above it.

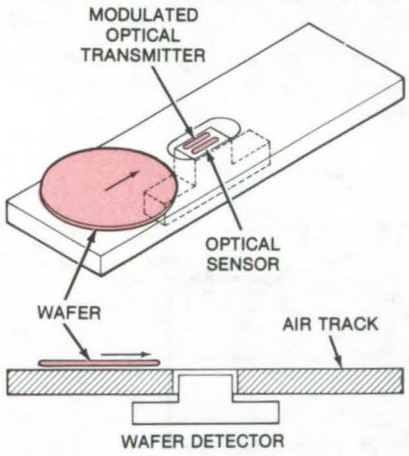

Figure 1. The **Presence or Absence of a Wafer** on the production line is sensed by the reflection of modulated light from the wafer. The transmitter is pulsed so that ambient light does not affect the operation of this device.

The output voltage from the sensor is a square wave that is approximately 185° out of phase with the Q output of the oscillator. When this signal is fed into the Exclusive-OR gate along with the oscillator $\overline{Q}$ output and a wafer is present, the resulting signal will be low 97 percent of the time, as shown in Figure 3.

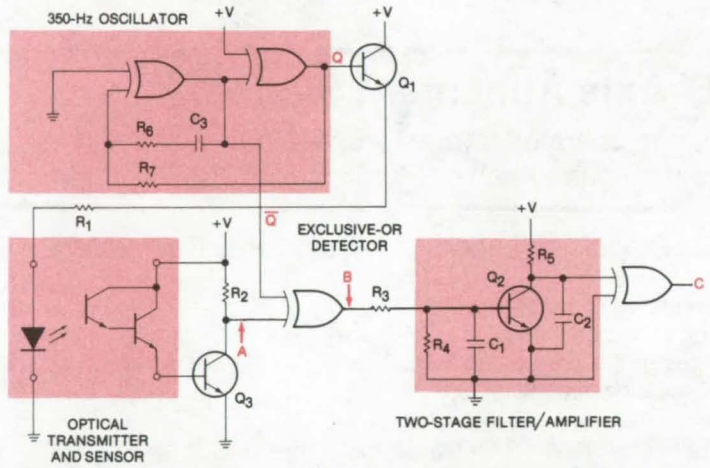

Figure 2. **The Optical Detector** includes an oscillator, an optical transmitter and sensor, and an output amplifier. When the wafer is not present, the detector will not sense the 350-Hz-modulated light emitted by the LED and will not respond to any other light source in the area. With the wafer present, the Exclusive-OR detector output pulses are too short to turn on Q_2; this drives output C high.

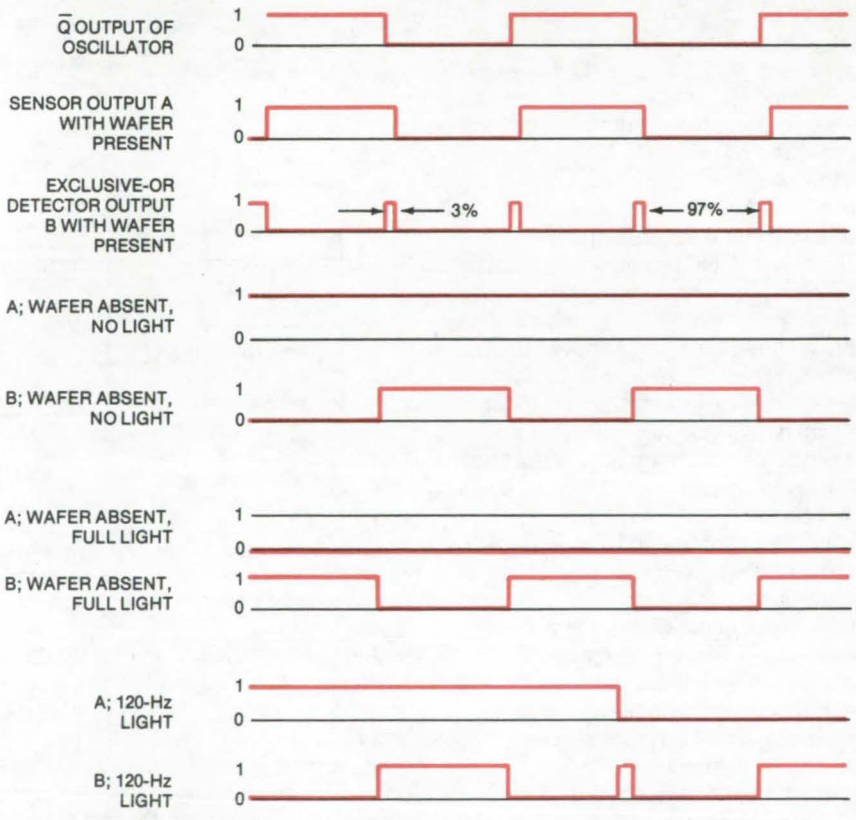

Figure 3. These **Waveforms** show the Exclusive-OR detector output response to different conditions.

When the wafer is not present, the optical detector does not "see" the 350-Hz-modulated light generated by the LED. Instead, the detector senses ambient light, which may be on full time, off full time, or modulated. A continuous light, such as the Sun, saturates the detector and causes output B to oscillate at 50 percent duty cycle, 180° out of phase from oscillator output. When no light is present, the detector is off, and the output B oscillates in phase with the oscillator $\overline{Q}$ output at 50 percent duty cycle. A modulated light (typically 120 Hz flicker from lamps) causes the output B to oscillate out of phase from the $\overline{Q}$ output when the optical sensor is high and in phase when the output of the optical sensor is low. This generates a shifting wave made up of mostly 50-percent duty-cycle pulses.

The output B is fed into a two-stage filter. The first filter (see Figure 2) consists of resistor R_3 in series with the parallel combination of resistor R_4 and capacitor C_1. The values of R_3, R_4, and C_1 are selected so that the turn-on voltage at the base of transistor Q_2 will not be reached unless the output B is high for longer than 5 percent of the oscillator duty cycle. This choice prevents Q_2 from switching when the wafer is present. The second filter, consisting of R_5 and C_2, is designed so that Q_2 must be off for two cycles of the oscillator before capacitor C_2 can charge up to 50 percent of the supply voltage. When C_2 charges to greater than 50 percent of supply voltage, the amplifier output switches from zero to high voltage, indicating the wafer presence. Modulated light will not cause false triggering of this system.

This circuitry allows the detector to operate in normal lighting conditions or in the dark without adjustment of the sensor or electronics. The system is inexpensive to build, does not require special component selection or adjustments, is relatively compact, and operates from a single power supply.

This work was done by James R. Currie and Raymond R. Schansman of **Marshall Space Flight Center.** *No further documentation is available.*

Inquiries concerning rights for the commercial use of this invention should be addressed to the Patent Counsel, Marshall Space Flight Center [see page A8]. Refer to MFS-23776.

Improved Heat-Pipe Wick

A new fabrication process for annular heat-pipe wicks creates smaller pores and higher density.

NASA's Jet Propulsion Laboratory, Pasadena, California

A new fabrication technique, when combined with conventional heat-pipe-wick technology, produces annular wicks with smaller pores, higher density, and greater rigidity than can be obtained using conventional fabrication methods alone.

The operation of an annular-wick alkali-metal-charged heat pipe depends on the dimension of the annular gap and the wick pore size and density. The wick pore size should be as small as possible to maximize capillary pumping pressure. A wick of maximum density with interconnecting open pores is desirable to minimize the amount of working fluid in the wick.

The improved process involves cleaning and double-folding the fine stainless-steel screen (400- to 500-mesh), used as a starting material. The double-folded screen is spot-welded in several places, saturated with water, and is then reduced to one-half its original thickness by a series of rolling passes.

This treatment reduces the pore size of the screen by 50 percent or more. The screen is then processed in the usual way. It is wrapped around a metal mandrel, inserted into an outer tubular metal mandrel, and passed through a drawing die to form a porous rigid tubular structure. The mandrels are removed by preferential chemical etching, and the wicks are sintered to increase further their density and rigidity.

Heat-pipe wicks fabricated by this method have been used to cool thermionic diode modules in the core of a 300-kW nuclear powerplant. The wick parameters obtained by using the new process are shown in the table.

Material	Type 304 Stainless Steel
Length	28.937 in.
Mesh Size (Starting Material)	500 Mesh
Outside Diameter of Annular Wick	0.427 in.
Inside Diameter	0.409 in.
Thickness	0.009 in.
Porosity (Pore Volume/Wick Volume)	31 Percent
Pore Size (Radius)	0.00040 in. (Determined by Bubble Test)
Spacer Wires (Outside Diameter)	0.0045 in.

Parameters of an Improved Annular Heat-Pipe Wick used for heat transfer in a nuclear reactor

This work was done by Frank G. Arcella and Ernest C. Phillips, Jr., of Westinghouse Electric Corp. for **NASA's Jet Propulsion Laboratory.** *For further information, Circle 52 on the TSP Request Card.*

This invention has been patented by NASA [U.S. Patent No. 3964902]. Inquiries concerning nonexclusive or exclusive license for its commercial development should be addressed to the Patent Counsel, NASA Resident Legal Office-JPL [see page A8]. Refer to NPO-13391.

Calculation of Planar-Truss Modal Frequencies

Calculation of planar-truss normal modes
is simplified by using an equivalent circular plate.

Langley Research Center, Hampton, Virginia

A simplified method for calculating the modal frequencies of four types of large-area planar trusses (tetrahedral, pentahedral, hexahedral, and radial-rib) treats the trusses as equivalent circular plates, thus allowing classical plate theory to be used. In the method, the truss is first treated as a sandwich plate; then, the dimensions and essential parameters of an equivalent circular plate are determined; and finally, these parameters (flexural rigidity, area, and density per unit area) are used in classical plate theory to determine the normal modes.

In the approximation of the planar truss by a sandwich plate, the equivalent faceplate thickness is determined by the amount of material in the upper and lower structural members that is effective in resisting bending. This is given by a simple formula for each truss configuration. The faceplate thickness is used to calculate the flexural rigidity of the sandwich plate and then to determine the flexural rigidity of the equivalent circular plate. The circular-plate area and density per unit area are also calculated from known parameters of the original truss.

The process is suitable for programming (on a minicomputer, for example) in an interactive mode. The user would supply the dimensions of the truss and of its members and could rapidly change the input parameters through the keyboard.

The calculations in this approximation technique are simpler than finite-element computations and would require less time. The results are most accurate for the two lowest modes of vibration. In calculations on a seven-ring tetrahedral truss, the frequencies of the two lowest modes were determined to within 3 percent of a finite element simulation.

This work was done by Richard M. Gates of The Boeing Aerospace Co. for **Langley Research Center.** *For further information, Circle 53 on the TSP Request Card.*
LAR-12137

Improved Nutation Controller

An improved nutation controller stabilizes spinning
bodies without precise positioning or calibration.

Goddard Space Flight Center, Greenbelt, Maryland

An improved nutation controller equipped with an angular accelerometer has been flown on the laser geodynamic satellite (LAGEOS) and used in laboratory tests to control nutation of a spinning body. It is superior to conventional devices that use linear accelerometers or rate gyroscopes, since it can be installed without precise positioning relative to the spin axis of the body.

The controller, shown in Figure 1, is rigidly mounted on the spinning body. The spin axis of the body, the axis of an angular accelerometer, and the axis of a flywheel are arranged mutually orthogonal. The accelerometer senses nutation, and its output is processed by a circuit that controls the motor driving the flywheel. By synchronizing clockwise and counterclockwise changes in the flywheel rotation rate with the nutation period, angular momentum can be exchanged between axes in a way that cancels out nutation. Besides damping nutation, the controller could also be used to impart nutation during energy dissipation tests.

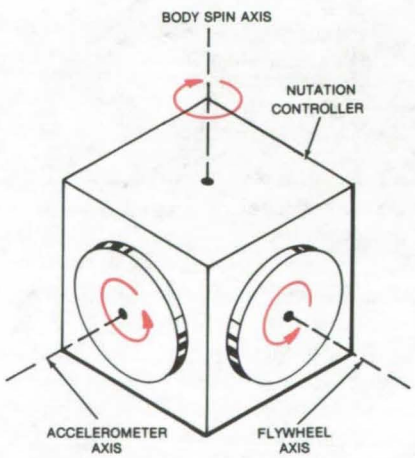

Figure 1. An Active Nutation Controller includes an angular accelerometer and a flywheel. The input axis of the accelerometer, the axis of rotation of the flywheel, and the spin axis of the body are mutually orthogonal.

The output of the angular accelerometer is independent of its distance from the controlled-body spin axis. Thus, its exact location is not critical, and its calibration is not position dependent.

The nutation control circuit is illustrated in Figure 2. When the accelerometer output signal exceeds a preset threshold, a gate is opened to pass pulses from a zero-crossing detector. Two successive zero-crossing pulses define the nutation period. The first pulse enables the up counter, allowing it to be clocked by an oscillator. The second pulse disables the counter at a count representing the period of the nutation cycle. The count is divided by 8 and transferred to a holding register. A down counter is then counted down to zero from the initial count in the holding register.

The down-counter output divides the nutation cycle into eight equal parts and triggers the multivibrator pulses to the decoder circuit. The decoder output, in turn, controls the flywheel drive motor according to a programed strategy to attenuate or to build nutation. The strategy, which was developed by considering the dynamics of the spinning system, requires the motor drive signals to be positive from 45° to 135°, zero from 135° to 225°, negative from 225° to 315°, and zero from 315° to 45° in the nutation cycle. This is the reason for dividing the total nutation period into eight 45° increments. The beat counter controls the decoder for a preset number of periods after the nutation drops below a fixed threshold where, because of noise, the nutation measurements may be inaccurate.

This work was done by James Donohue and Henry C. Hoffman of **Goddard Space Flight Center.** *For further information, Circle 54 on the TSP Request Card.*

This invention is owned by NASA, and a patent application has been filed. Inquiries concerning nonexclusive or exclusive license for its commercial development should be addressed to the Patent Counsel, Goddard Space Flight Center [see page A8]. Refer to GSC-12273.

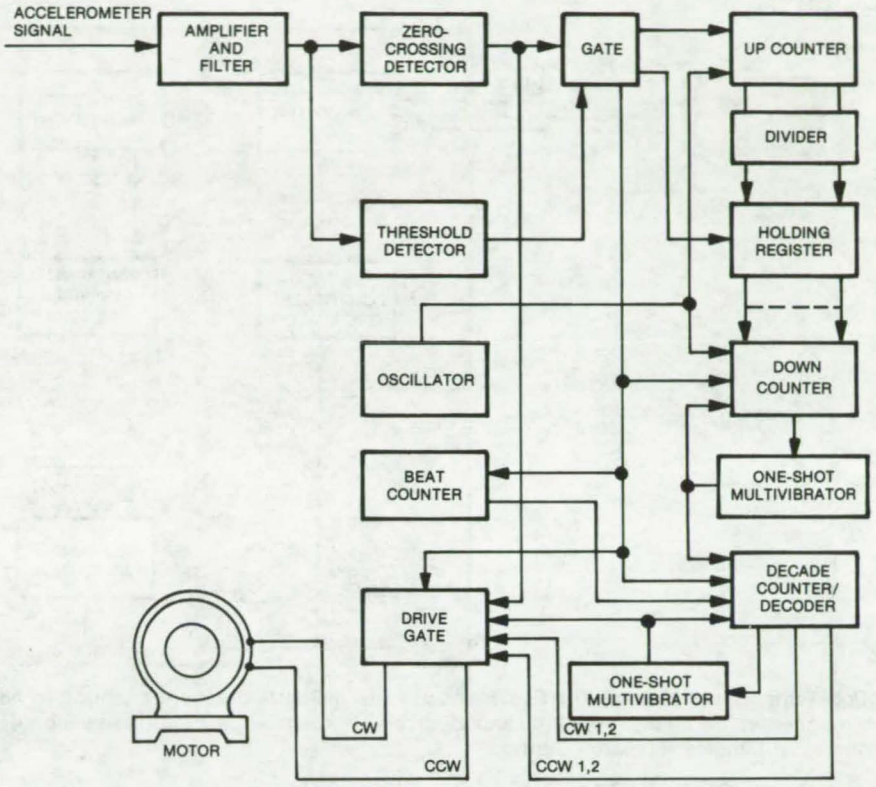

Figure 2. The **Nutation Control Circuit** commands a dc torque motor that drives the flywheel (see Figure 1). The flywheel is driven either clockwise or counterclockwise at programed points in the nutation cycle, to impart or damp nutation.

High-Temperature Microphone System

Pressure changes in gases are measured at elevated temperatures by stable, easily fabricated system.

Langley Research Center, Hampton, Virginia

A microphone system that measures pressure fluctuations in air or other gases is not unduly affected by temperature or rate-of-change of temperature. The system has proved operable at temperatures up to 800° F (430° C).

Prior systems employed a semiconductor pressure transducer, which had a maximum rating of only 260° C, an eddy-current transducer designed for much higher temperatures but involving costly and specialized materials and processing. A probe microphone containing materials subject to deterioration under a hostile environment, and water-cooled conventional transducers, which are impractical in many cases.

The new system (see figure) employs a condenser microphone as the pressure transducer. Its advantages include a low-noise floor, wide dynamic range, wide frequency bandwidth, high mechanical and electrical stability, and low vibration sensitivity. All components of the microphone system are made of inexpensive and readily available materials. All mating parts within the condenser microphone cartridge are either screwed in place or press-fitted; there are no chemical or metallurgical bonds that are subject to deterioration at elevated temperatures. External cooling is not required, and the system can be readily calibrated by means of an electrical insertion voltage.

The three major components of the system are the condenser microphone, the high-temperature cable assembly, and the carrier electronics. Sound pressure fluctuations produce capacitance changes in the condenser microphone, thereby amplitude-modulating a carrier wave transmitted over the cable assembly. The cable assembly, typically 6 meters in length, operates as a half-wavelength transmission line that effectively reflects the condenser microphone to the input terminals of the converter and permits removal of the carrier electronics from the severe operational environment of the condenser microphone.

(continued on next page)

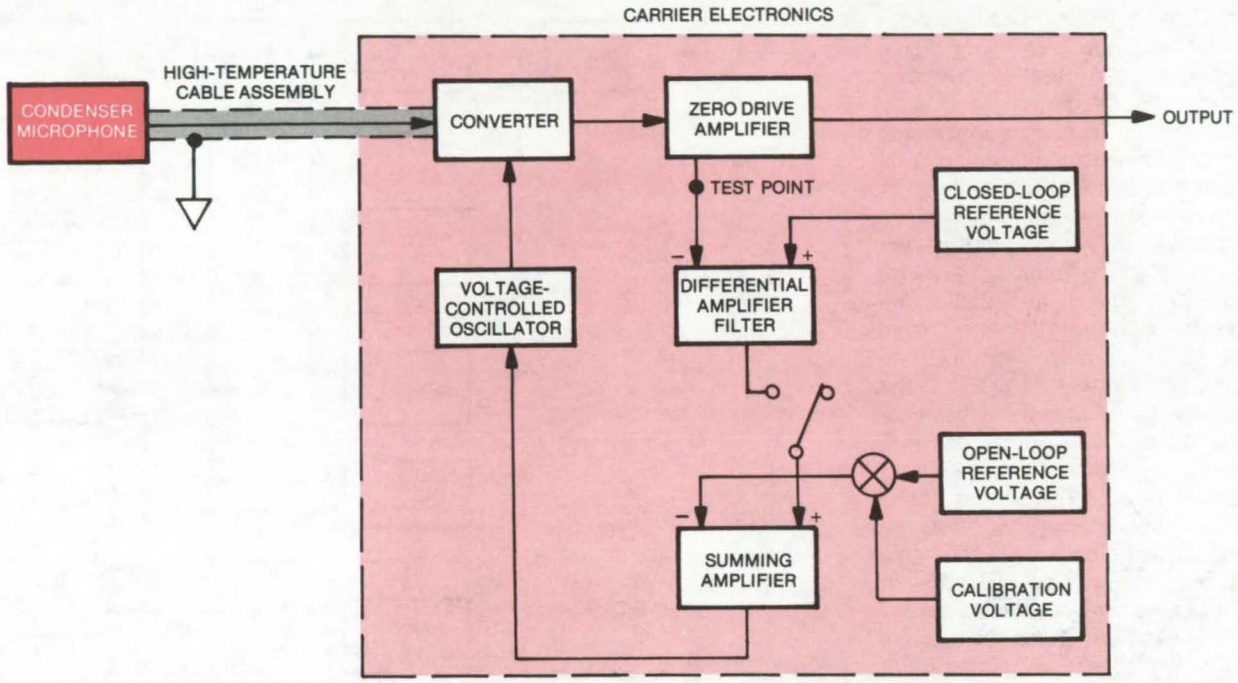

High-Temperature Microphone System is used to measure pressure changes in hot gases. Made primarily from conventional components, it is easily fabricated and relatively inexpensive. A modified version of the one outlined above is used for scramjet studies at Langley Research Center.

The converter detects the acoustical signal and produces an electric current proportional to the sound pressure at the condenser microphone. The electric current is amplified by a zero drive amplifier. Its output signal is applied to a measuring, data-processing, or recording device. An automatic tuning-control feedback loop, consisting of the differential amplifier filter, closed-loop reference voltage, open-loop reference voltage, and summing amplifier, maintains optimum tuning of the carrier voltage, which is provided by the VCO to one of the resonant frequencies of the cable/microphone network. The system allows for electrical calibration by means of a calibration voltage applied to an input of the summing amplifier.

This work was done by Allan J. Zuckerwar of the Old Dominion University Research Foundation for **Langley Research Center.** *For further information, Circle 55 on the TSP Request Card.*

This invention is owned by NASA, and a patent application has been filed. Inquiries concerning nonexclusive or exclusive license for its commercial development should be addressed to the Patent Counsel, Langley Research Center [see page A8]. *Refer to LAR-12375.*

A Solid-State Phase-Insensitive Ultrasonic Transducer

Device requires no additional noise components such as light source.

Langley Research Center, Hampton, Virginia

A photoconductive acoustoelectric transducer (AET) developed at Langley Research Center functions as a phase-insensitive ultrasonic transducer. This solid-state broadband phase-insensitive receiver is easy to use and requires no additional noisy components such as a light or thermal source.

Conventionally piezoelectric, magnetostrictive, capacitive, and electromagnetic transducers are phase-sensitive and convert acoustic pressure into a proportional electrical signal. Their phase sensitivity can lead to erroneous data when the transducer is larger than the acoustic wavelength, because their output is then modulated by phase as well as by amplitude.

An earlier phase-insensitive AET based on the acoustoelectric effect in CdS depended on photon-generated charge carriers to couple to the acoustic wave. This device required a light source that generated electrical noise in the system. A second category of phase-insensitive devices employed thermal converters or radiation pressure detectors. At present, these are complex, bulky devices that require awkward configurations and are not appropriate for transient

nondestructive evaluation (NDE) ultrasonics.

Advantages of the new AET shown in the figure result from its not requiring photon or other excitation and from its phase insensitivity. It is especially useful for measurements in inhomogeneous materials and/or irregular geometries. The device is solid-state, simple, light, and hard to abuse. It has the potential of significantly increasing ultrasonic resolution of material properties for both NDE and medical diagnostics imaging.

This work was done by Joseph S. Heyman of **Langley Research Center.** *For further information, Circle 56 on the TSP Request Card.*

This invention is owned by NASA, and a patent application has been filed. Inquiries concerning nonexclusive or exclusive license for its commercial development should be addressed to the Patent Counsel, Langley Research Center [see page A8]. Refer to LAR-12304.

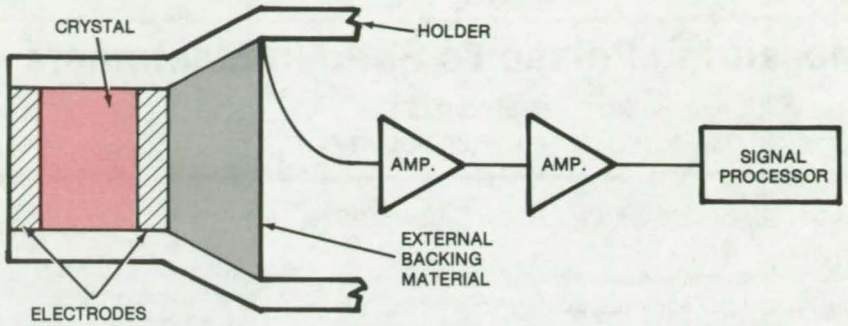

New Photoconductive AET uses a crystal fabricated by thermal annealing of high-conductivity CdS in an argon atmosphere. Once annealed, electrodes and, if necessary, external backing material are applied to the crystal, which is mounted in a holder with an electrical connection to amplifiers and signal-processing systems. An amplifier is usually mounted in the holder to minimize the capacitance that the AET must drive.

NO_2 Measurement by Chemiluminescence

Compact device can detect trace quantities of NO_2 gas and measure its concentration.

Langley Research Center, Hampton, Virginia

Techniques for measuring nitrogen dioxide gas concentration are frequently complex or are insufficiently specific for NO_2. Chemiluminescent methods that have been used usually rely on the light output from a reaction of nitric oxide (NO) with ozone, requiring prior catalytic conversion of NO_2 to NO. No specific chemiluminescent method exists for NO_2.

A more specific chemiluminescent reaction registers the light emitted from a solid material that is heated after being exposed to a gas containing NO_2. The percentage of NO_2 in the gas sample can be determined from the amount of light emitted. Small quantities of NO_2 can be measured, and other gases found in the atmosphere (including other nitrogen oxides) do not interfere with the accuracy of the measurement.

The figure shows the device for detecting NO_2 in a gas sample. The gas is passed over a dry solid material (either 3,5 diaminobenzoic acid or polyvinyl alcohol) for 10 minutes. Then the gas flow is stopped, and the solid is heated to 150° C. If the gas contained NO_2, the heated solid emits light that can be detected by a photomultiplier. During the heating period the light intensity rises to a maximum and decays in 1 or 2 minutes; the heater is then switched off. The signal from the light detector during the heating process is amplified and displayed on the recorder and is integrated to measure the NO_2 concentration in the gas sample.

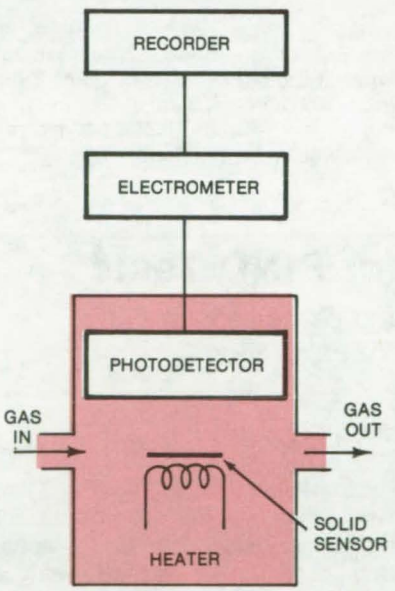

This **NO_2 Measurement Device** uses the chemiluminescent reaction in an NO_2-sensitive solid material. The solid is exposed to a gas sample and then heated; if the sample contained NO_2, the heated solid emits light. The integrated output from the photodetector is a measure of NO_2 concentration.

The quantity of NO_2 retained by the solid builds up over the exposure time but the light is released in a very short time during the heating process. Therefore the sensitivity of the device to NO_2 can be increased by increasing the exposure time, with no increase in heating time. Thus minute quantities of NO_2 can be measured.

Tests of this method in the presence of possible interfering gaseous constituents indicate that it is specific for NO_2. Gases such as SO_2, CO, NO, H_2S, O_2, CO_2, and N_2 produce no light and do not degrade the sensitivity of the chemiluminescent solid.

This work was done by Edmund J. Conway and Robert S. Rogowski of **Langley Research Center** *and R. Ronald Richards of Greenville College. No further documentation is available. LAR-11378*

Measuring Poisson's Ratio in Elastomers

The volume change of a sample under stress is measured by water displacement.

Marshall Space Flight Center, Alabama

A simple water-displacement device rapidly and accurately determines Poisson's ratio for elastomeric materials. The device (see figure) consists of a liquid chamber, a sight glass, and rods for holding the elastomeric specimen; the specimen is a molded disk that is adhesively bonded between the two rods.

The assembly is mounted vertically in a tensile tester, and the liquid chamber is filled with water to a predetermined level. The tensile tester puts a measured stress on the specimen, and the new water level in the sight glass is noted. From the volume of water displaced by the stressed specimen (equal to the change in volume ΔV of the specimen itself) and the change in specimen strain ΔE observed with the tensile tester, Poisson's ratio (μ) can be calculated according to the formula

$$\mu = \frac{1}{2}\left(1 - \frac{1}{V}\frac{\Delta V}{\Delta E}\right)$$

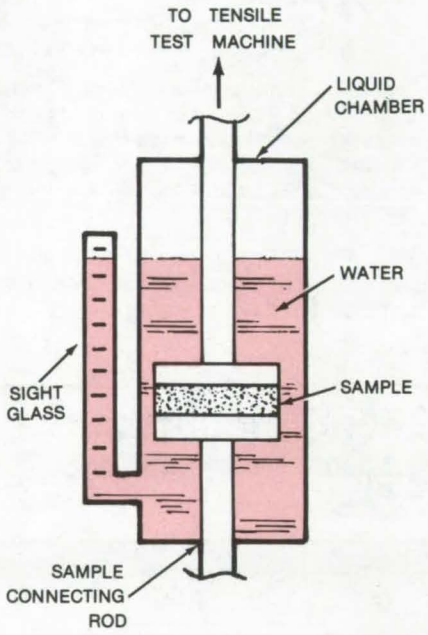

This **Poisson's Ratio Measurement Apparatus** includes a sight glass from which an observer can determine the volume of water displaced by an elastomer under tension.

where V is the original volume of the sample.

Previous methods of measuring Poisson's ratio include gas dilatometers, extensometers, or hand tools for estimating dimensional changes. In the gas dilatometer method, the change in volume is determined by observing the pressure change in a closed system containing the sample. The pressure change is converted to a volume change; however, the results can be inaccurate because they require thermodynamic assumptions and variables that are not always accurately known. The other two methods are approximate.

This work was done by Johnny M. Clemons of **Marshall Space Flight Center.** *No further documentation is available.*
MFS-23878

Calibration Standards for PIND Tests

Standard circuit packages containing particles with known masses aid in test-instrument calibration.

Lyndon B. Johnson Space Center, Houston, Texas

A calibrated set of microcircuit packages containing tiny particles with known masses can be used as reference standards for particle-impact noise detection (PIND) tests. The tests screen packages containing particles that can cause short circuits or other failures. [See "Particle-Impact Noise Detector (PIND)" (MSC-16626) on page 504 of *NASA Tech Briefs*, Vol. 2, No. 4.]

In a PIND test, a microcircuit is shaken while sensitive acoustic instruments "listen" for the sound of particles rattling against the internal walls. The set of reference packages is used when calibrating the PIND test instrumentation. The set consists of common package sizes and shapes. Each package is seeded with a different particle so that the set covers a range of particle masses extending above and below the sensitivity of the PIND test equipment.

The particles are tiny metal spheres. Their diameters are measured with a scanning electron microscope. From these measurements, the mass of each particle is calculated according to the known density of the metal. Several metals are selected to cover the range of masses required for the set.

A sphere is introduced into a circuit package by touching the particle with a toothpick moistened in alcohol and carefully transferring it to the open package. (The sphere clings to the drop of liquid at the tip of the toothpick.) The operation is performed under a microscope. The lid is placed on the package, and it is sealed in the usual way.

This work was done by Saverio Gaudiano of **Johnson Space Center.** *For further information, Circle 57 on the TSP Request Card.*
MSC-18169

Shock During PIND Test Frees Particles

Coshock tool applies impact during vibration to loosen additional stray particles trapped inside hybrid microcircuits.

Marshall Space Flight Center, Alabama

Particle-impact noise-detection (PIND) testing finds loose particles that can cause failure in hybrid microcircuits. In this test the package is vibrated; the noise of the particles is detected with a transducer, is amplified, and is analyzed on an oscilloscope. [This technique is described in "Particle-Impact Noise Detector (PIND)" (MSC-16626), *NASA Tech Briefs*, Vol. 2, No. 4 (Winter 1977), p. 504; "Reclaiming Hybrid Integrated Circuits" (MSC-16463), *NASA Tech Briefs*, Vol. 3, No. 1 (Spring 1978), p. 135; and "Microcircuit-Cleaning Machine" (MSC-16060), *NASA Tech Briefs*, Vol. 3, No. 2 (Summer 1978), p. 299.]

A recent study on PIND has shown that the process not only serves as a test but can be a curative procedure as well; particles can be knocked out of the package by the shock normally used to loosen them for detection. These particles can then be removed from sealed packages through a hole in the cover that is subsequently resealed. Normally a package is impacted first before testing; it has been found that a shock of from 1,500 to 4,000 G (depending on package type) is about 80 percent effective in freeing trapped particles.

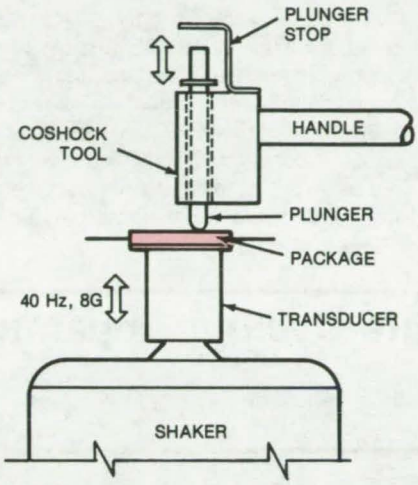

Coshock Tool is used to tap a hybrid package on the PIND tester.

Even better results are obtained when the package is tapped during vibration. A tool for this purpose, shown in the figure, imparts a shock of from 300 to 2,500 G. When this tool, called a coshock tool, is used in conjunction with preshock, 90 to 95 percent of trapped particles are removed. The procedure is not harmful to wire bonds, die bonds, active or passive chips, or hermetic seals.

The report on a study of PIND testing gives a clear, concise description of the procedure and contains much practical information on the design and calibration of the shock tools and procedures for their use.

This work was done by S. V. Caruso of **Marshall Space Flight Center** *and F. Z. Keister of Hughes Aircraft Co. For further information, Circle 58 on the TSP Request Card.*

Inquiries concerning rights for the commercial use of this invention should be addressed to the Patent Counsel, Marshall Space Flight Center [see page A8]. Refer to MFS-23829.

Temperature-Gradient Oven

The temperature of a tubular chamber varies linearly along its length.

Marshall Space Flight Center, Alabama

An oven that creates a linearly-varying temperature gradient can be used for controlled heating (or cooling) of test specimens. It operates on the principle that in the absence of radiative and convective losses a homogeneous conductive rod, with one end hotter than the other, has a linear temperature gradient along its length.

The oven consists of a tube of conductive material with a heat source at one end and a heat sink at the other (see figure). The temperature of the oven cavity through the axis of the tube thus varies linearly along its

(continued on next page)

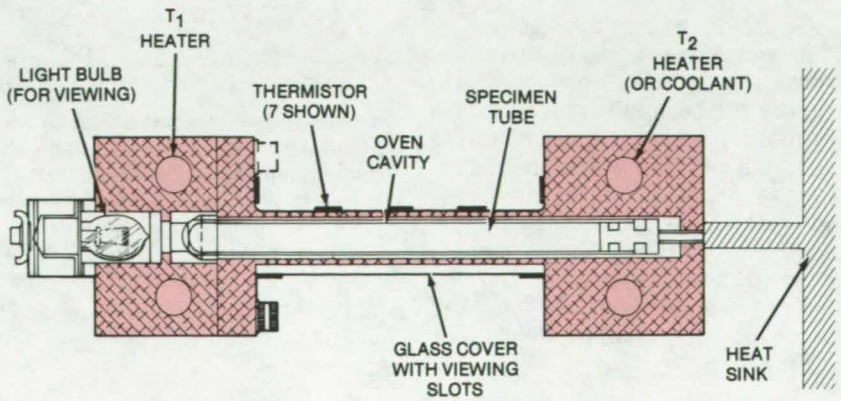

Heat Flows through this tubular oven from high temperature T_1 to lower temperature T_2, creating a linear temperature gradient across specimens in the oven cavity. T_2 can be maintained by a heating element or by the flow of coolant.

length. The slope of the gradient is determined by the temperature difference between the source and the sink. (Heat must be continuously removed at the low-temperature end; otherwise the temperature there will gradually rise until it equals the higher temperature.)

The thin tube wall presents a small cross-sectional area to the heat source and large impedance to heat flow, so that the heat supplied by the source and removed by the sink is kept to a minimum. Heat flow can also be controlled by adjusting the coupling between the low-temperature end of the oven and the heat sink.

The temperature profile in the new oven is more accurately linear than previous tubular ovens that were heated by resistance wire wrapped in a helix around the tube. In such ovens, the temperature profile has a series of steps because the heat is added at regular intervals along the length by the resistance wire.

The new oven was originally developed for use in spacecraft at zero gravity. In such applications, there are no gravitational forces to set up convection currents, and insulation against convective heat loss is not necessary. For most terrestrial uses, the tube would be insulated against convection losses. Also, if the temperature range is high enough that radiative losses are a problem, radiation reflectors may be required to maintain a linear temperature profile.

This work was done by Suey Jue of Grumman Aerospace Corp. for **Marshall Space Flight Center.** *For further information, Circle 59 on the TSP Request Card.*

Inquiries concerning rights for the commercial use of this invention should be addressed to the Patent Counsel, Marshall Space Flight Center [see page A8]. Refer to MFS-23919.

Automated Temperature-Cycling Apparatus

A test apparatus cycles specimens between temperature extremes.

Langley Research Center, Hampton, Virginia

An automated temperature-cycling apparatus, originally developed to test materials for wind tunnels, incorporates two chambers, one at a high temperature and the second at a low temperature. Specimens tested for durability to thermal shock are moved between the two chambers for a specified number of cycles.

The apparatus as shown in the figure has the "hot" chamber at the top and a bottom "cold" chamber filled with liquid nitrogen. The top chamber is essentially an oven heated to the desired temperature level. The test specimen is mounted on a frame driven by a motor. The motor is turned on and off by a thermocouple connected to the specimen.

A test is begun by raising the specimen into the upper chamber and heating it. Once the specimen reaches the desired temperature, the thermocouple signals the motor to lower the specimen into the liquid-nitrogen chamber. When the lower temperature limit is reached, the process is repeated. After a number of cycles, as required by the test, the samples are removed and checked for the effects of thermal shock.

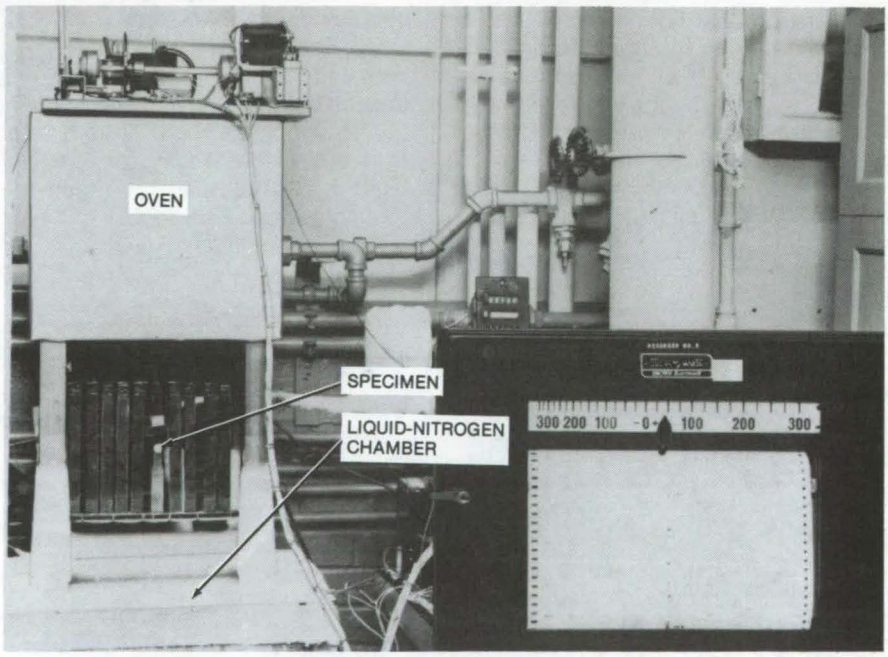

An **Automatic Thermal-Shock Cycling Apparatus** moves the test specimen between high-temperature and low-temperature chambers. The specimen is mounted on a frame driven by an electric motor. The motor is turned on by a thermocouple that monitors the temperature of the specimen.

The entire procedure (other than mounting the sample on the frame) is automatic. It saves time and cost when compared with manual testing.

This work was done by Miles L. Lockard of **Langley Research Center.** *No further documentation is available.*
LAR-12310

Standardized Gas-Temperature Probes

Standardization reduces calibration requirements and associated costs.

Lewis Research Center, Cleveland, Ohio

One of the major costs associated with using thermocouple probes is the expense of calibration. By standardizing on the two designs shown in the figure and by determining the various correction factors for a range of sizes of each design, the requirements for individual calibration are greatly reduced.

Performance characteristics have been determined for 10 sizes of the unshielded design and 5 sizes of the shielded design. Both probe designs are of swaged construction using type K wire with stainless-steel sheath and magnesium oxide insulation. The tests covered a mach number range from 0.2 to 0.9, over a temperature range from ambient to 2,097° F (1,420 K), and through a pressure range from 0.3 to 2.2 atmospheres (30×10^3 to 223×10^3 N/m^2).

The performance characteristics consisted of recovery and radiation correction and time-constant determinations. The recovery correction factors at 0.9 mach number ranged from 0.002 to 0.028. The radiation corrections ranged from 20° to 248° F (11 to 138 K), and the time constants ranged from 0.03 to 1.7 seconds.

Tables and graphs presented in the referenced report compare the characteristics of the various sizes to aid in the selection of a type and size needed for a particular application or for scaling an existing thermocouple design to another size.

The ready availability of the two kinds of standardized thermocouple probes in a range of sizes, with tabulations of their characteristics, permits the easy selection of a probe for a variety of applications with minimal specific calibration. The two general probe designs can be used as individual elements or stacked to form multielement rakes.

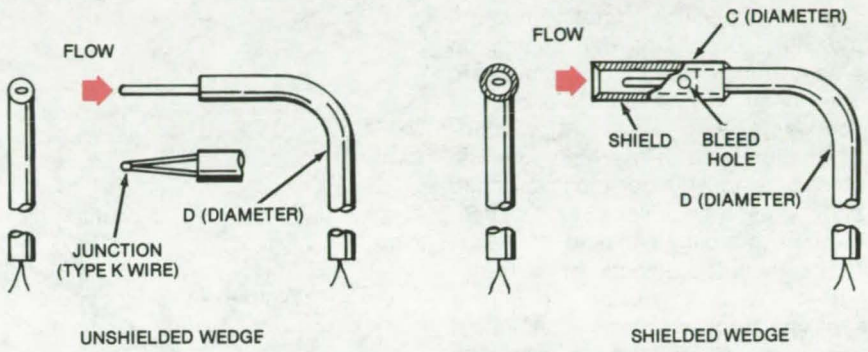

PROBE NUMBER	SWAGED ASSY. DIAM., D		WIRE DIAM.		SHIELD DIAM., C	
	in.	mm	in.	mm	in.	mm
1	0.010	0.25	0.001	0.032	-------	------
2	0.020	0.50	0.004	0.101	-------	------
3	0.032	0.81	0.005	0.13	-------	------
4	0.040	1.02	0.006	0.16	0.064	1.63
5	0.050	1.27	0.010	0.25	-------	------
6	0.062	1.57	0.013	0.32	0.093	2.28
7	0.090	2.29	0.016	0.41	0.125	3.18
8	0.125	3.18	0.020	0.51	0.156	3.96
9	0.188	4.78	0.032	0.81	0.250	6.35
10	0.250	6.35	0.040	1.02	-------	------

Standard Thermocouple Sizes for which performance characteristics have been determined are shown. Shielded and unshielded probes are of swaged construction and use type K wire with stainless sheath and magnesium oxide insulation.

This work was done by George E. Glawe, Raymond Holanda, and Lloyd N. Krause of **Lewis Research Center.** *Further information may be found in NASA TP-1099 [N78-15463], "Recovery and Radiation Corrections and Time Constants of Several Sizes of Shielded and Unshielded Thermocouple Probes for Measuring Gas Temperature," a copy of which may be obtained at cost from the New England Research Application Center* *[see page A7].*

LEW-13059

Orifice Calibration Module

Compact device saves time and improves the accuracy and reliability of pressure measurements.

Langley Research Center, Hampton, Virginia

Small openings (static-pressure orifices), connected by tubing to pressure-measuring equipment, are often used in wind tunnels and other flow systems to measure flow characteristics such as mach number and pressure. A new module allows these static-pressure orifices to be calibrated and rapidly checked for leaks.

The module consists of a transparent plastic cylinder containing separate suction and calibration chambers (see Figure 1). The two chambers are isolated from each other by an O-ring, and the outer (suction) chamber is isolated from the outside environment by another O-ring. Thus, the pressures in the two chambers can be controlled independently. The suction chamber holds the module over the orifice while a controlled pressure is applied via the calibration chamber.

In a previous method of calibrating orifices in wind tunnels, the line between the orifice and its pressure-receiving instrumentation was removed. A calibrated pressure was then applied to the line, and the response of the instrumentation was observed and adjusted if necessary. Finally the line was reconnected to the orifice, and the response of the orifice itself was determined by applying a calibrated pressure, through a plastic tube.

This procedure, which was time consuming and required two technicians to carry out, introduced several opportunities for error. For example, the line could leak when it was reconnected to the orifice, or it could be connected to the wrong orifice. Also, the adequacy of the calibration tube seal varied with the technician's skill.

With the new module, no lines have to be disconnected. Its suction chamber holds it over the orifice, forming a reliable seal and requiring only one technician for calibration. Valves, gages, and tubing are color coded to aid the operator.

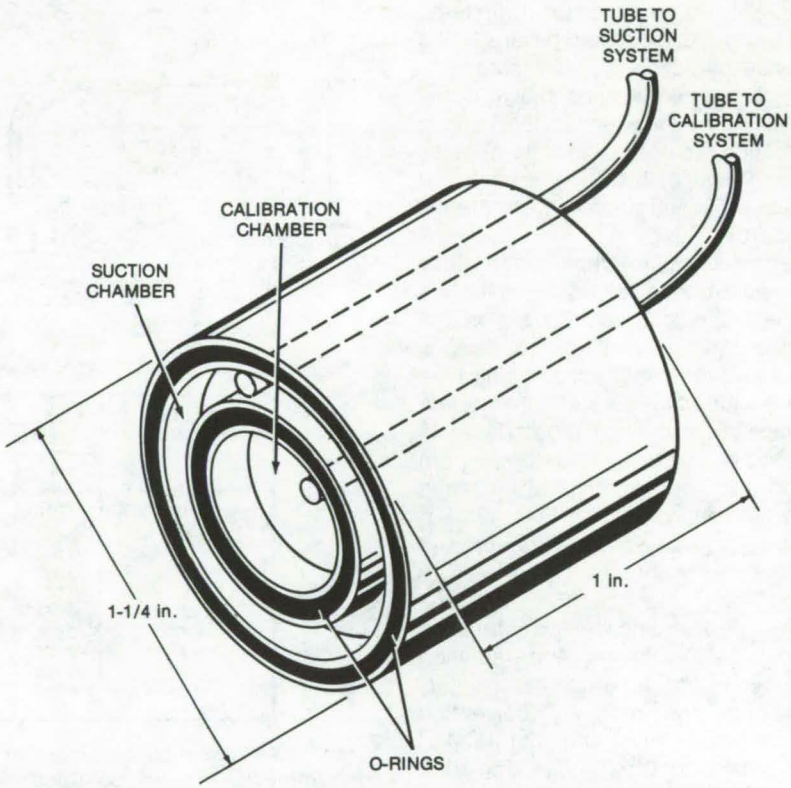

Figure 1. This **Clear Plastic Calibration Module** fits snugly over an orifice, held by suction. Calibrated pressures can be applied to the orifice via the central chamber.

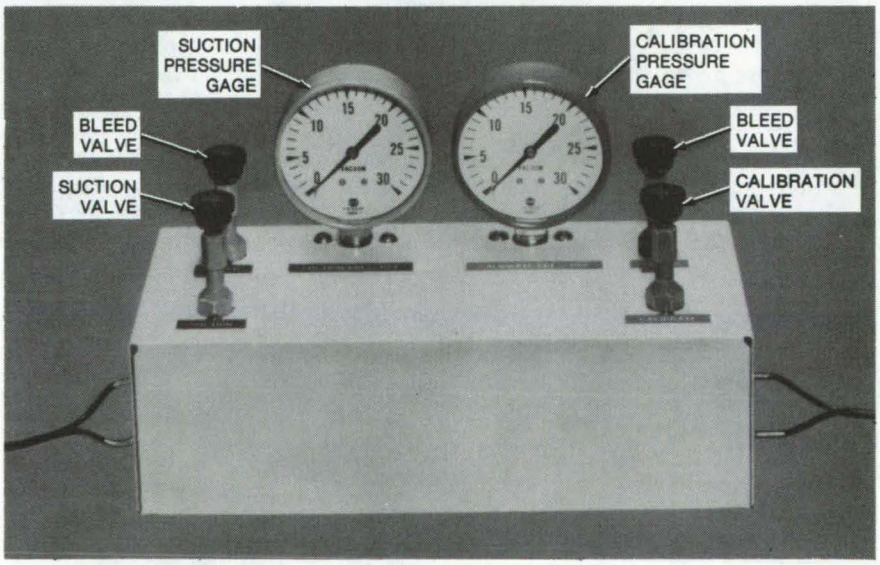

Figure 2. The **Control Box** for the orifice calibration module includes all valving and gages required to apply and vent the suction and calibration pressures.

To use the module, the user positions the calibration chamber over the orifice. (This is easy to do, since the module is transparent.) The suction valve is opened (see Figure 2), and then it is closed when the suction pressure gage indicates that the pressure has stabilized. The module then stays in place by itself.

Next, the user opens the calibration valve to apply a predetermined pressure to the orifice and closes the valve when that pressure has been reached. The user then proceeds with calibration of the orifice and instrumentation. When calibration is complete, bleed valves are opened to release the module.

The module has a flat bottom, but the rubber O-rings can conform to moderately curved surfaces. For surfaces of more pronounced curvature, a module can be specially built to match the contour.

This work was done by Randolph Culotta and Donald L. Posey of **Langley Research Center.** *For further information, Circle 60 on the TSP Request Card.*

Inquiries concerning rights for the commercial use of this invention should be addressed to the Patent Counsel, NASA Resident Legal Office-JPL [see page A8]. Refer to LAR-12269.

Electronically-Scanned Pressure Measurement System

High scan rate and in situ calibration are featured.

Langley Research Center, Hampton, Virginia

Miniature electronically-scanned pressure (ESP) sensors and an associated microcomputer-based data-acquisition unit will provide pressure data at high scan rates for wind-tunnel testing. The ESP system can measure up to 1,024 unknown pressures at data rates as high as 10 kHz with maximum system inaccuracies of ±0.25 percent of full scale. This system is well suited for wind-tunnel testing with short run times or high operational costs. The sensors can be calibrated in place, making it easy to calibrate fully between runs.

The ESP sensors are miniature silicon pressure transducers bonded to a common substrate (see Figure 1).

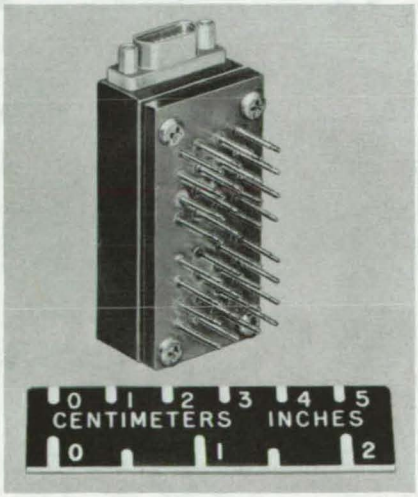

Figure 1. The **32-Channel Electronically-Scanned Pressure Sensor** unit above measures 1 by 2 by 1-3/16 in. (2.5 by 5.1 by 3 cm) and is small enough to be mounted within most wind-tunnel models.

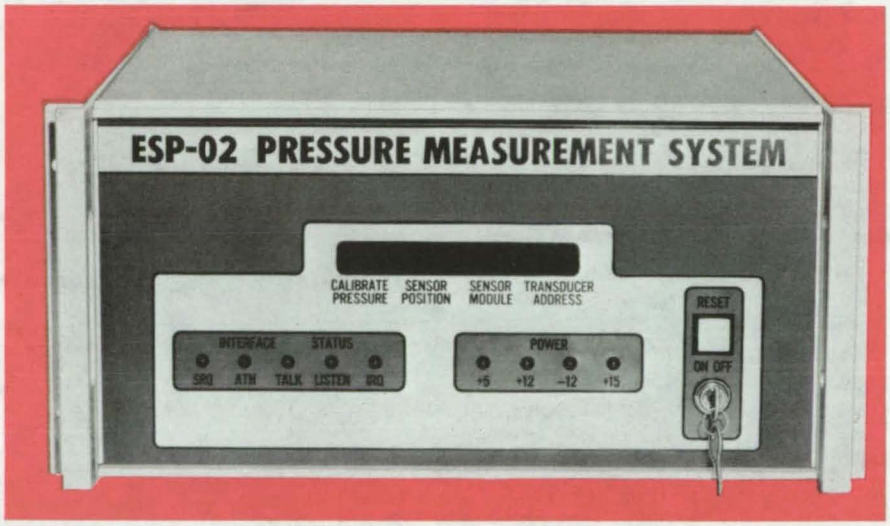

Figure 2. **Data Acquisition and Control Unit** scans raw sensor data, computes pressures, and calibrates sensors.

The differential outputs from each transducer are fed into analog multiplexer chips that are addressed digitally to obtain the output of each transducer at scan rates up to 10 kHz. An internal instrumentation amplifier raises the transducer outputs (±100 mV) to levels (±5 V) compatible with data-acquisition hardware. Thermal zero and sensitivity shifts of the transducers are corrected by use of a calibrate head mounted to the sensor substrate. The head may be pneumatically switched to present calibration pressures to each transducer within the sensor.

Data is acquired by a "Data Acquisition and Control Unit" (DACU). The DACU (see Figure 2) is a microcomputer-based "smart instrument" that can be operated as an independent measurement system or as a peripheral to the wind-tunnel host computer. Several software options permit the DACU to be configured for a wide variety of test requirements. In situ calibration is handled through a three-point calibration in which three pressures (0, 1/2 full-scale, and full-scale) are applied to each transducer while its output is measured.

After calibration, the DACU performs a second-order linear regression on the raw calibration data to produce a characteristic equation for each transducer. The characteristic equations are then used to calculate unknown pressures. The technique produces inaccuracies of no more

(continued on next page)

than ±0.25 percent for full-scale pressures of 15, 50, and 100 psia (10, 35, and 70×10^4 N/m^2). A maximum of 24,000 single-point or averaged data points may be acquired and stored in the system semiconductor memory.

Several data-output routines allow the system to yield the output data in raw counts or in engineering units. In addition, the DACU can be interfaced with computers or terminals through the use of readily-available interfacing hardware.

This work was done by Thaddeus Basta, Jr., Chris Gross, and Douglas B. Juanarena of **Langley Research Center.** *For further information, Circle 61 on the TSP Request Card.*
LAR-12386

Static-Pressure Probe for Small Geometries

A new probe is contoured so that the static orifices can be located closer to the tip.

Langley Research Center, Hampton, Virginia

Static-pressure measurements in large wind tunnels are often made by using a probe similar to the one shown in the upper part of the figure. The static-pressure holes in these probes are located at least 1 centimeter (about 10 tube diameters) downstream of the cone/tube shoulder, where the pressure is very nearly equal to stream static. However, for smaller, high-Reynolds-number geometries, such as nozzles and flow inlets, this probe is not accurate because the flow properties in smaller systems can change significantly over distances that are less than 1 centimeter.

For the smaller geometries, a new static-pressure probe with holes located closer to the tip is much more effective. The new probe is less sensitive to pressure gradients and off-axis variations in the flow direction, which occur over short distances in the smaller systems.

The new design evolved from that of the conventional probe by changing the contour of the shoulder that joins the probe tip to the cylindrical body. At the shoulder of the conventional probe, the static pressure falls abruptly through the free-stream value. However, it does so much too rapidly to be accurately measured. In developing the new design (see figure, center), the shoulder was replaced by smooth fairing between the cone and the tube. The static pressure changes gradually over the faired section and becomes equal to the stream static pressure at a slope of 3° to the probe axis (for a 20° half angle at the cone tip). In the final design (see figure, bottom), the fairing is terminated at the point where its slope is 3° and is joined to another conical section with

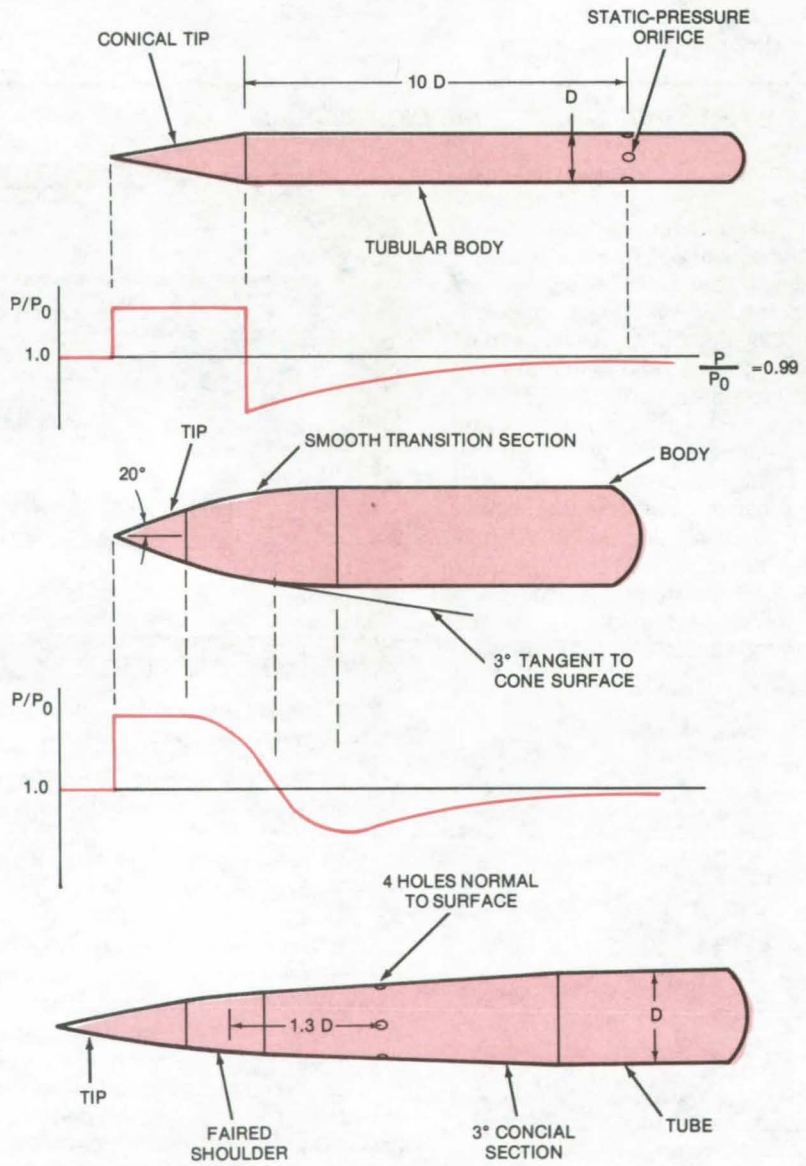

A **New Static-Pressure Probe** is contoured so that the pressure orifices can be located near the probe tip. In the conventional design (top) stream pressure changes abruptly near the cone/tube shoulder. When a smooth transition region is added between the cone and the tube (center) the pressure profile changes gradually. The final design is shown at the bottom.

a half angle of 3°, so that a pressure close to stream static is maintained along the 3° cone section. The static holes are located on the 3° cone.

The new probe was tested at three free-stream mach numbers over an angle-of-attack range of 12°. The measured static pressure was relatively insensitive to the flow speed or the angle of attack, in contrast to a conventional probe that gave scattered measurements over the same range. For best results, the new probe would be tailored to the mach number at which it is used or perhaps calibrated at several mach numbers.

Another advantage of the new probe is that since it is relatively insensitive to changes in the flow direction, other similar probes can be placed close to it without disturbing the measurements.

This work was done by S. Z. Pinckney of **Langley Research Center.** *Further information may be found in NASA TN D-7978 [N75-27305], "A Short Static-Pressure Probe Design for Supersonic Flow," a copy of which may be obtained at cost from the North Carolina Science & Technology Research Center [see page A7].*

This invention has been patented by NASA [U.S. Patent No. 3914997]. Inquiries concerning nonexclusive or exclusive license for its commercial development should be addressed to the Patent Counsel, NASA Resident Legal Office-JPL [see page A8]. Refer to LAR-11552.

Detecting Servo Failures With Software

The servo position is compared with the predictions of a model in software.

Dryden Flight Research Center, Edwards, California

An improved way of detecting hardware failures in servosystems uses a computer model instead of electronic and mechanical failure-detection devices. The new method saves weight and space. It also can be faster and more reliable.

In one application of the system (see figure), a common command signal drives the servo hardware, a software model of the servoamplifier, and the electrohydraulic actuator valve. A microcomputer compares the actual servo-valve position, as measured by a linear variable-displacement transformer (LVDT) and the position predicted by the software model. A discrepancy between the two displacements indicates a failure.

In addition to detecting failures in the servoamplifier and servo valve, the system will also pick up most computer input/output failures. Since a failure of the servo ram LVDT would go undetected (its feedback drives both the model and the hardware), a self-checking version is employed with discrete output activating special failure logic within the computer.

This failure-detection concept was originally developed for the elevon and rudder actuators in high-performance aircraft, but it is adaptable to any system in which low weight, small volume, and rapid response are important.

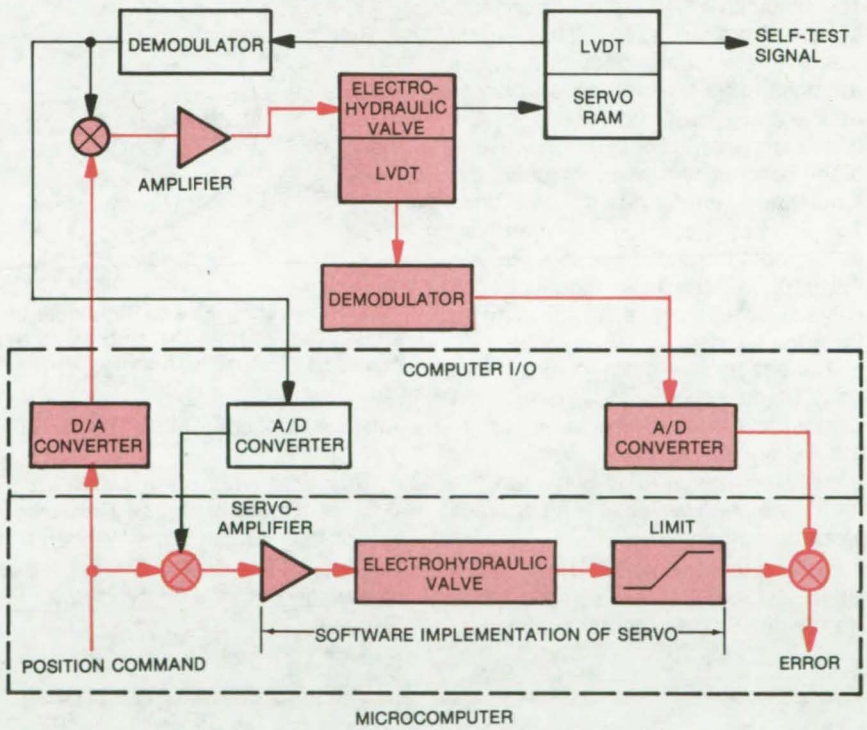

A **Microcomputer Program Models the Servo Position** in this actuator loop. A linear variable-displacement transformer sends data on the servo position to the microcomputer for comparison. The addition of an LVDT to the servo ram allows that component to be checked as well.

This work was done by Dan Lew and Ralph Quam of Rockwell International Corp. for **Dryden Flight Research Center.** *For further information, Circle 62 on the TSP Request Card.*
FRC-11003

Penetrating Fire Extinguisher

Pointed tip driven by an integral ram penetrates barriers to inject a fire-extinguishing chemical.

John F. Kennedy Space Center, Florida

A fire extinguisher with a hard pointed tip can penetrate walls to dispense fire-extinguishing chemicals in hard-to-reach areas. One person can insert and use the extinguisher, which was originally developed for use on the Space Shuttle Orbiter. It can also be used to penetrate metal skins on aircraft, ships, trains, and other vehicles and to pierce wood, plasterboard, metal, or plastic panels in buildings.

The extinguisher has a conical, hardened-steel tip, a long tubular stainless-steel body and nozzle section, and a sliding ram (see figure). To extinguish a fire, the user connects a hose from an extinguishing-agent supply to the tubular body and places the pointed tip against the surface to be pierced. Then, while one of the handles is grasped with one hand, the other hand slides the ram along the tubular body until it hits the stop disk. The impact forces the penetrating head and the nozzle section through the surface. The user then opens a valve to admit the extinguishing agent from the supply.

The nozzle has holes drilled in the body at an angle o 45° so that the discharge streams overlap to spray the extinguishing agent over a wide area. The penetrating tip can be unscrewed and replaced if it becomes worn or blunted.

[See related article, NASA Tech Brief B75-10111, "Powered Fire Nozzle for Fast Penetration of Structures: A Concept" (MSC-19528), June 1975.]

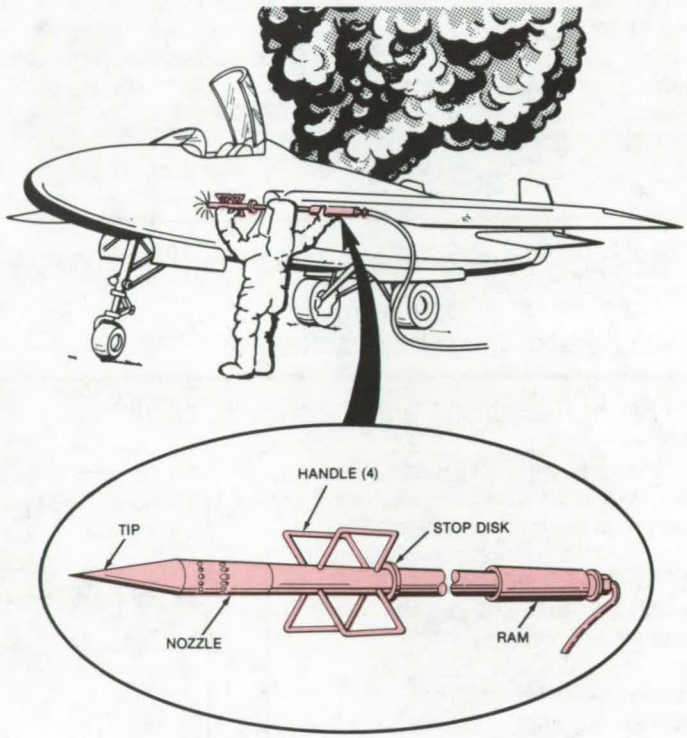

This **Penetrating Fire Extinguisher** can be used by one person. The impact of the sliding ram against the stop disk drives the pointed tip through metal skins, wall panels, and other barriers to inject a fire-extinguishing chemical.

This work was done by Norris C. Gray of **Kennedy Space Center** *and Philip N. Bolton and Robert M. Senseny of The Boeing Co. For further information, Circle 63 on the TSP Request Card.*

This invention is owned by NASA, and a patent application has been filed. Inquiries concerning nonexclusive or exclusive license for its commercial development should be addressed to the Patent Counsel, Kennedy Space Center [see page A8]. Refer to KSC-11064.

High-Temperature Capacitive Pressure Transducer

± 10-psi transducer operates at 1,200° F.

Lewis Research Center, Cleveland, Ohio

A capacitive pressure transducer capable of continuous operation at 1,200° F (920 K) has been developed and evaluated over a full-scale differential pressure range of ±10 psi (69×10^3 N/m^2). The design of the pressure transducer was based on the use of a diaphragm to respond to pressure, on variable capacitive elements arranged to operate as a differential capacitor to measure diaphragm response, and on the use of fused silica for the diaphragm and its supporting assembly.

High-temperature static pressures can be easily measured by using a duct to transfer the pressure to a pressure transducer located in a

moderate temperature environment. However, for accurate measurement of dynamic pressures, it is necessary that the pressure transducer be located at or in the medium being measured.

Several developments were needed to successfully build the high-temperature capacitive pressure transducer, including:

- Bonding together fused-silica components to form the sensing assembly;
- Depositing thin conductive films on the fused-silica components that would reliably withstand the bonding temperature and repeated cycles to 1,200° F;
- Attaching transition lead wires to the conductive films;
- Optimizing signal-conditioning electronics; and
- Using ground shields to reduce the effects of unwanted electrical-property changes.

The bonding problems were solved by using an experimental low-expansion devitrifying frit obtained from a commercial supplier. Acceptable conductive films were obtained by experimenting with various processes, combinations of materials, and application techniques. The lead-wire attachment problems were solved by applying a borosilicate glass over the lead-wire-to-film connection to provide strength or by using a thick-film conductor composition to make the attachment. The zero shift and sensitivity change with temperature problems encountered with the transducer were reduced by modifying the signal-conditioning equipment and by adding conductive-film ground planes to the sensor.

This work was done by Richard L. Egger, Reid A. Mickelsen, Donald W. Nelson, and Everett J. Nelson of The Boeing Aerospace Co. for **Lewis Research Center.** *Further information may be found in NASA CR-135282 [N77-33483], "Development of a High Temperature Capacitive Pressure Transducer," a copy of which may be obtained at cost from the New England Research Application Center* *[see page A7]*.

LEW-13078

Books and Reports

These reports, studies, and handbooks are available from NASA as Technical Support Packages (TSP's) when a Request Card number is cited; otherwise they are available from one of NASA's Industrial Application Centers or the National Technical Information Service.

Directory of Fire Research Specialists

Researchers listed by organization and speciality

A directory has been compiled of 1,475 specialists in the United States and Canada who have made recent contributions to the fire literature, or to the teaching of fire science or related subjects, or who have participated in or supported fire research programs. Specialists are identified in 42 subject areas, e.g., arson, blasts and explosions, buildings, combustion research, combustion toxicology, fire ignition, medical research, and nuclear fire problems. The directory comprises three indexes. The first index lists the specialists alphabetically by name, with organizational affiliations, addresses, telephone numbers, and areas of specialization. The second index lists the 42 subject areas and the specialists in each area. The third index lists 412 organizations and the specialists affiliated with each. Organizational affiliations include corporations, governmental agencies, research institutes, universities, and consultants.

This work was done by Thomas L. Junod and George Mandel of **Lewis Research Center** *and Nora H. Jason of the National Bureau of Standards. Further information may be found in NASA CR-13508 [N77-30271], "Fire Research Specialists: A Directory," a copy of which may be obtained at cost from the New England Research Application Center* *[see page A7]*.

LEW-13123

Computer Programs

These programs may be obtained at very reasonable cost from COSMIC, a facility sponsored by NASA to make new programs available to the public. For information on program price, size, and availability, circle the reference letter on the COSMIC Request Card in this issue.

Nacelle Incremental Drag

Design data for advanced supersonic transports

This program was developed to determine nacelle incremental drag for the NASA arrow-wing configuration of an advanced supersonic transport. It has been recognized that one of the more sensitive problems in the design of a successful supersonic cruising aircraft is that of airframe/engine integration. Recent studies have shown that drag, weight, and wing-camber plane warping are very sensitive to nacelle size and shape. It is important that the engine designer be aware of this sensitivity to engine geometry.

Some engine geometry control can be achieved by the designer with no penalty in engine performance, although on a total system basis, some engine performance degradation may be accepted in trade for reduced drag. This program should prove useful by providing a rapid approximate methodology for comparing alternative propulsion system designs for supersonic transports.

This program uses a table-lookup and interpolation procedure to determine the nacelle incremental drag. Wave drag is represented as a function of free-stream mach number and six independent variables, each a function of nacelle shape and size. Friction drag is defined by four independent variables, each a function of

(continued on next page)

engine geometry. These independent variables are used to determine drag values, using a table of existing drag data points. For drag values not directly available, the program interpolates, or extrapolates, among the available table values.

The program determines a set of data points for use when calculating the drag associated with a given set of values of the independent variables. Once these data points are found, a cubic equation is fitted, and the drag increments are determined.

This program is written in FORTRAN IV for batch execution and has been implemented on an IBM 370-series computer with a central memory requirement of approximately 40K of 8-bit bytes.

This program was written by Arnold W. Knudsen and Ronald Y. Mairs of Rockwell International Corp. for **Lewis Research Center.** *For further information, Circle E on the COSMIC Request Card.*
LEW-12786

Wing Aerodynamics Under Blowing Jets

Characteristics of upper-surface blowing and over-wing blowing.

A theoretical method determines the aerodynamic characteristics of arbitrary wings under the influence of a single centered jet or a pair of jets blowing on or above the plane of the wing. The program is applicable to both upper-surface-blowing and over-wing-blowing configurations. Its most important characteristic is the inclusion of both jet-entrainment and inviscid wing-jet interaction in calculating aerodynamic characteristics of the wing. The entrainment theory is applicable to compressible heated jets, and the interaction theory can be applied to jets with mach number nonuniformity.

The program is restricted to configurations that employ a single centered jet or a pair of symmetrically located jets. The jet is always assumed to blow parallel to the root chord of the wing, but it may have any mach number or temperature. The free-stream velocity must be subsonic. Wing-jet geometry limitations require that the root and tip chords of the wing and flaps be parallel to the free stream.

The main assumptions used in developing the theory are: (1) the flow perturbations, both inside and outside the jet, satisfy the Prandtl-Glauert equation, and all boundary conditions have been linearized; (2) the jet is either rectangular or circular with constant cross section and constant properties in the unperturbed flow for the purpose of interaction calculations; and (3) no fuselage, nacelles, or wing thickness are accounted for.

The aerodynamic characteristics that the program will calculate include: (1) the spanwise and chordwise pressure distributions across the wing for both jet-on and wing-alone cases; (2) the spanwise distribution of sectional lift, induced drag, and pitching moment coefficients due to circulation for both jet-on and wing-alone cases; (3) the total lift-induced drag and the moment coefficients due to circulation when both entrainment and interaction are accounted for; (4) the total lift, drag, and moment coefficients due to circulation are calculated for over-wing-blowing configurations, recognizing only entrainment effects and thus, establishing the relative importance of entrainment and interaction for a particular configuration; (5) the force and moment coefficients due to Coanda turning of the jet are calculated for upper-surface-blowing configurations; and (6) the total force and moment coefficients are calculated for the wing-alone case.

This program is written in FORTRAN and has been implemented on a CDC 6000-series computer with a central memory requirement of approximately 72K (octal) of 60-bit words.

This program was written by Charles H. Fox, Jr., of **Langley Research Center** *and Greg L. Fillman and C. Edward Lan of the University of Kansas. For further information, Circle F on the COSMIC Request Card.*
LAR-12256

Analysis of Beam Columns

Displacement method used to find moments and loads

A new FORTRAN IV program determines displacements, bending moments, and critical column loads for straight elastic beams or column beams. The analytical approach is based on the displacement method utilizing finite-difference approximations. Single bay and multibay problems with any transverse loading condition and any boundary condition may be solved. A Newton-Raphson iteration is used to find the lowest critical column load. The program should prove very useful in a large number of routine structural-analysis applications.

The displacement method used assumes that deflections are the primary unknowns. Displacements are determined directly and are then used to establish boundary conditions. Relationships between internal forces and deflections are first expressed in the form of differential equations. The differential equations are then transformed into simultaneous linear equations, using finite-difference approximations. Generalized boundary conditions have been derived to fit the finite-difference equations uniquely.

Boundary conditions may be free, fixed, simply supported, or elastically restrained against translation and rotation and may have a small initial displacement. Multispans are optional, with the allowance for the intermediate supports being elastic. The loads on the beam may be concentrated at a single point or allowed to vary uniformly across the beam.

Inputs include beam description, concentrated loads, distributed loads, applied moments, translational reaction, rotational reaction, initial deflection, and the number of grid points to be used in solution computation. Outputs include input-data echo, translational and rotational reactions, moment and deflections for the selected grid point, and iterations leading to the critical column load.

This program is written in double-precision FORTRAN IV for batch execution and has been implemented on an IBM 360 computer with a central memory requirement of approximately 82K of 8-bit bytes.

This program was written by Lawrence I. Guidry of Rockwell International Corp. for **Johnson Space Center.** *For further information, Circle G on the COSMIC Request Card.*
MSC-18009

Solar-Electric Geocentric Transfer

Trajectories for solar-electric satellites with attitude constraints

A time-optimal or nearly-time-optimal trajectory computer program has been developed for solar-electric geocentric transfer with or without attitude constraints and with an optional initial high-thrust stage.

The program is designed for analysis of solar-electric propulsion vehicles that involve attitude constraints; however, it has been generalized to consider any of the following configurations: (1) yaw motion only, (2) yaw and roll only, and (3) unconstrained motion.

The program is used to calculate the time-optimal or nearly-time-optimal geocentric trajectories. It uses the method of averaging to reduce computer time by orders of magnitude compared to a precision integrated trajectory. The averaged rates of change of the mean values of the state and costate are found by numerical quadrature.

The differential equations for the mean state and costate may then be integrated in large time steps (typically days). A set of nonsingular orbital elements is used to avoid numerical difficulties for eccentricities and inclinations at or near zero. The radiation model is analytic to reduce run time. Included in the code are options for consideration of oblateness, solar motion, shadowing with or without a delay in thruster startup, an analytic-radiation and power-degradation model, and an initial high-thrust stage of one or two impulses or specified ΔV.

A costate formulation of the problem yields a two-point boundary value problem that is solved by a Newton iteration on the initial costate and value of transfer time. Initial values of the unspecified states and costates and a guess for the transfer time are chosen. An optimal trajectory is then generated by integrating the averaged state and costate using a Runge-Kutta method. A Gaussian quadrature averages the state and costate derivative over an orbit. This will generate an optimal trajectory to the wrong terminal state. A sensitivity matrix is then generated by varying the initial conditions and running a set of neighboring trajectories. A Newton iteration on the initial conditions is then used to drive the terminal errors to within specified bounds. The final converged trajectory is a minimum time trajectory (nearly minimum time for attitude constraints) for the specified velocity increment in the high-thrust phase (if included).

The attitude constraint causes power to become a function of thrust direction and Sun direction, and the time-optimal thrust direction becomes a complex function of primer vector direction. The analysis for the attitude constrained case is considerably more complicated than for the unconstrained case.

For the zero roll and pitch case, a suboptimal control is developed that is nearly time optimal, uses less fuel than the time optimal, and is obtained from the solution of a cubic equation. The solution may yield discontinuous changes in the thrust direction. The time delay in thruster startup is modeled as a quadratic function of time in shadow. The proton and electron radiation field is modeled as equivalent 1-MeV particle flux as a function of spacecraft altitude and latitude as well as the solar-cell shield thickness. The power loss function is modeled as an analytic function of fluence, cell thickness, and base resistivity. Spacecraft parameters such as yaw angle and Sun incidence angles may be displayed.

Further refinements of the program could include extending the valid region of the radiation model to those low altitudes between latitudes of 50° and 75°, and effects to make the program more efficient in terms of individual trajectory calculations and convergence characteristics in order to reduce run time further.

The program is written in double precision and FORTRAN. It has been compiled in FORTRAN IV and used on an IBM/360 computer, and with minor modifications, in FORTRAN V on a UNIVAC 1110 computer.

This program was written by Harvey L. Malchow and Lester L. Sackett of The Charles Stark Draper Laboratory, Inc., for **Lewis Research Center.** *For further information, Circle H on the COSMIC Request Card.*

LEW-12939

Convectively Cooled Structures

A finite-element program for steady-state thermal analysis

In the past, thermal analysis of convectively cooled or heated structures with unknown fluid temperatures was performed by the lumped-parameter finite-difference method, and the structural analysis was performed by the finite-element method. A new program, TAP 1, was developed as an aid in the thermal analysis of structures heated or cooled by internal fluid flow.

TAP 1 uses the finite-element method for forced-convection thermal analysis, thus simplifying data preparation and providing a more efficient interface between independent thermal and structural analyses. Although TAP 1 was developed in support of research on the development of convectively cooled structures for scramjet engines and hypersonic aircraft, the program may be utilized to analyze thermally a variety of general heat-transfer problems, such as those encountered in nuclear-reactor and solar-collector systems.

TAP 1 uses the finite-element approach to the steady-state thermal analysis of structures that employ conductive and convective heat transfer. Two conduction/convection elements, a rod and a quadrilateral, are available for representing the solid region of the convectively cooled (or heated) structure. A mass-transport-convection element and a surface-convection element with unknown fluid temperatures are available for modeling the convective heat transfer in the fluid passages of the structure. Two special integrated conduction/convection elements, a tube-and-fluid element and a plate-fin-and-fluid element, are also available. The finite-element formuation produces a set of nonlinear algebraic equations expressed in matrix form in terms of the temperature-dependent system-conductance matrix, the unknown nodal-temperature vector, and the system nodal-head load vector. For nonlinear thermal analysis due to temperature-dependent thermal parameters, TAP 1 uses the Newton-Raphson iteration algorithm. Program output includes

(continued on next page)

nodal temperatures and element heat fluxes. Pressure drops in fluids may be computed as an option. A companion plotting program for displaying the finite-element model and predicted temperature distributions is included.

TAP 1 is written in FORTRAN IV and has been implemented in batch mode on a CDC 6000-series computer with a central memory requirement of approximately 48K (decimal) of 60-bit words.

This program was written by Allan R. Wieting of **Langley Research Center** *and Earl A. Thornton of Old Dominion University. For further information, Circle J on the COSMIC Request Card.*
LAR-12347

Analyses of Cracked Orthotropic Sheets

Finite-element analysis of plane anisotropic sheets

This computer program was developed to perform a two-dimensional elastostatic analysis of plane anisotropic homogeneous sheets with through-the-thickness cracks and temperature gradients. The finite-element method is one of the most effective approaches available for plane elasticity problems having irregular boundaries or discontinuous boundary conditions. In the past, the use of conventional finite elements proved expensive and inefficient because they required the use of a large number of elements near the crack tip to represent the extreme stress gradient. To circumvent this economic problem, elements that contain the crack-tip stress singularity, called cracked finite elements, have been developed.

This program includes cracked finite elements that incorporate many terms in the expansion of the crack-tip stress field, not just the dominant singular term. These two high-order cracked elements, one for symmetric applications and one for unsymmetric applications, have a balance between actual degrees of freedom and the number of nodal displacement components, allowing the analyst to add a cracked element to an assembly in the same manner as a conventional element. Accurate results obtained with both elements indicate that a high degree of displacement compatibility exists at the interface of the high-order cracked elements and conventional elements.

The finite-element approach used is based on the direct stiffness method. Conventional finite elements available include an axial element, a linear spring element, and isotropic and anisotropic triangular elements. High-order finite elements available include 8-node symmetric (isotropic and anisotropic) and 10-node unsymmetric (isotropic and anisotropic) cracked elements. The shape of the cracked elements was chosen to fit conveniently into models using the commonly-used constant-strain triangle. The input segment of the program incorporates a data generator to simplify input requirements. During the input sequence, a node-resequencing bandwidth reduction algorithm is used to minimize execution time. A bonded Cholesky decomposition procedure is used to solve the system of equations. A thermal stress capability is included. Output includes modal displacements, stresses in conventional elements, stress-intensity factors, and strain-energy release rates in the cracked elements.

The program is written in FORTRAN IV for execution in batch mode and has been implemented on a CDC 6000-series computer with a central memory requirement of approximately 250K (octal) of 60-bit words without segmentation. The program can be overlayed to reduce greatly the core requirement.

This program was written by J.A. Aberson and J.M. Anderson of the Georgia Institute of Technology and W. J. Batdorf and Chorng-Shin Chu of Lockheed-Georgia Co. for **Langley Research Center.** *For further information, Circle K on the COSMIC Request Card.*
LAR-12288

Predicting Rotor Rotation Noise

Program calculates the noise spectrum of a stationary helicopter rotor in an inviscid fluid.

Multiple sets of measured or hypothetical high-frequency blade-loading coefficients have been used to calculate the rotational noise of stationary helicopter rotors. Empirical or hypothetical blade surface-pressure spectra may be used by the program to calculate blade station-loading spectra, chordwise and spanwise integrated blade-loading spectra, and far-field rotational noise spectra. Any of five standard in-line functions describing the chordwise distribution of the blade loading can be chosen to study parametrically the acoustic predictions.

Rotational noise (the noise a rotor would generate in an inviscid fluid) originates in the periodic forces on the rotating blade. Such noise has a characteristic frequency spectrum consisting of discrete components that are multiples of a fundamental frequency. The governing unconvected wave equation for a nondissipating medium is expressed in terms of the sound pressure, the fluctuating force, and the sound speed, using the Einstein tensor convention. In solving the wave equation, it is assumed that the rotor system as a whole is stationary and that the inflow conditions are nonuniform. Approximations are made on the assumptions that the observer remains in the far field and that the load is concentrated over a small area at some effective radius. Once the fluctuating pressures on the rotor disk are determined, the far-field radiated discrete noise can be calculated.

This program is written in FORTRAN IV for the CDC FTN compiler using the Overlay capability and has been implemented on a CDC 6000-series computer with a central memory requirement of approximately 66K octal of 60-bit words. A Calcomp plotter system is required for plotted output.

This program was written by Robert N. Hosier of the U.S. Army Air Mobility R & D Laboratory, Ramani Ramakrishnan of George Washington University, and Donald Randall of Computer Sciences Corp. for **Langley Research Center.** *For further information, Circle L on the COSMIC Request Card.*
LAR-12098

Machinery

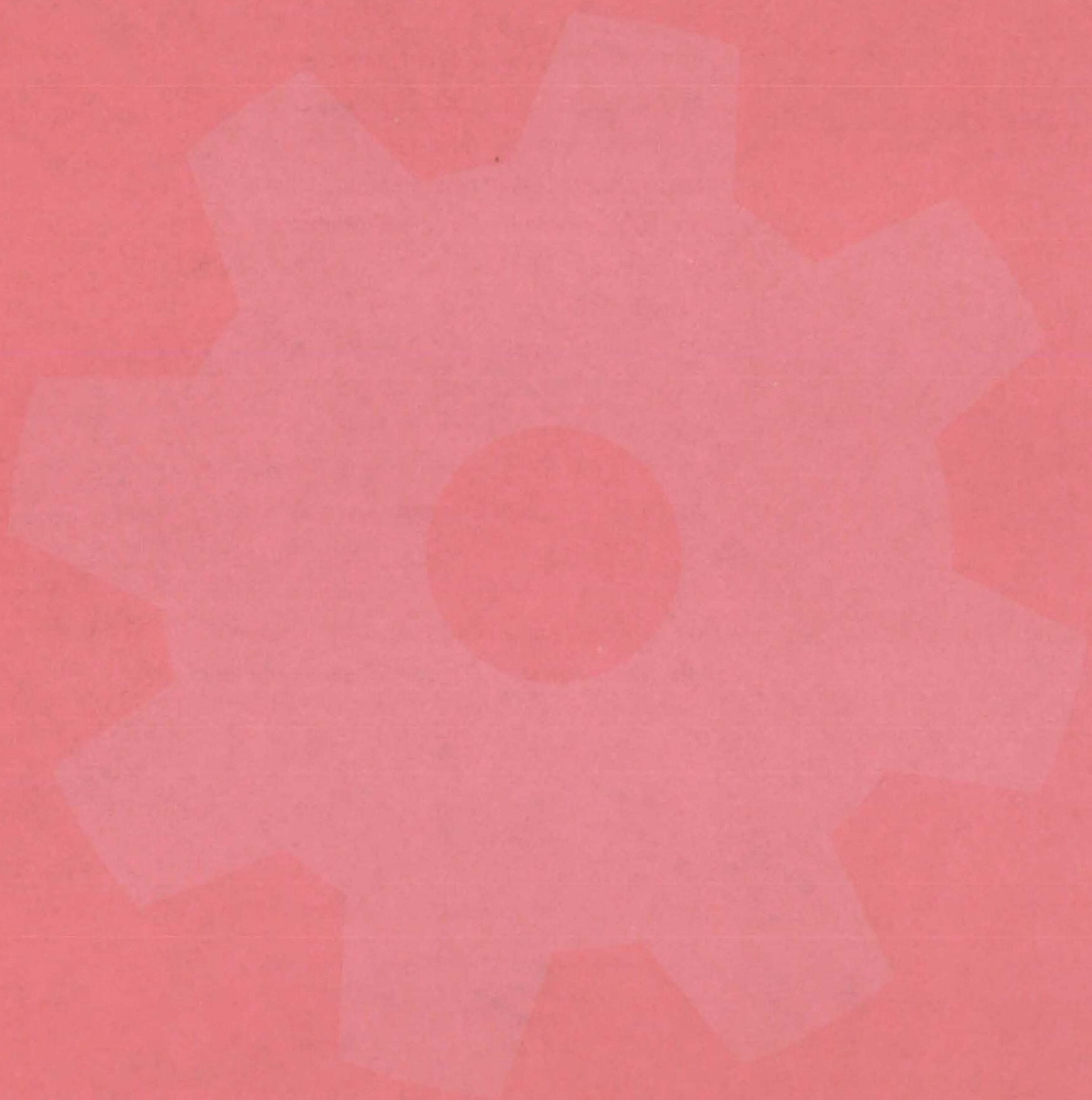

Hardware, Techniques, and Processes

Books and Reports

Coupler for Moving Vehicles

Compact, lightweight mechanism gently couples and decouples moving objects.

Goddard Space Flight Center, Greenbelt, Maryland

A coupling mechanism for two moving objects gradually orients and restrains the captured object, avoiding any abrupt contact with the parent vehicle. Developed to allow the Space Shuttle to link up with satellites, the mechanism could also be used on oceangoing vessels to retrieve or deploy submerged objects or as a coupling device between aircraft. When releasing an object, the mechanism is so gentle that the object is ejected with essentially the same speed and direction as the parent vehicle.

In its simplest form, the mechanism is an iris mounted in a ring at the end of a manipulating arm. An operator positions the arm so that the ring encircles the object to be captured, then slowly closes the iris until it holds the object securely.

For most applications, a double iris (see Figure 1) would be used to orient the object as well as to capture it. The operator controls the capture in a series of steps (Figure 2). First, the ring, with the irises fully open, is positioned around the object (in the illustrated case, a projection on a spacecraft). Then iris 1 is closed to about half its fully open diameter, moving the object slightly so that it is closer to its final, fully alined position.

At this point, the object deploys an end restraint, an antennalike structure that keeps it from slipping out of the ring. Next, iris 2 is partially closed, further realining the object.

Then, telescoping tracks between irises 1 and 2 separate them, making it easier to aline the object along the

(continued on next page)

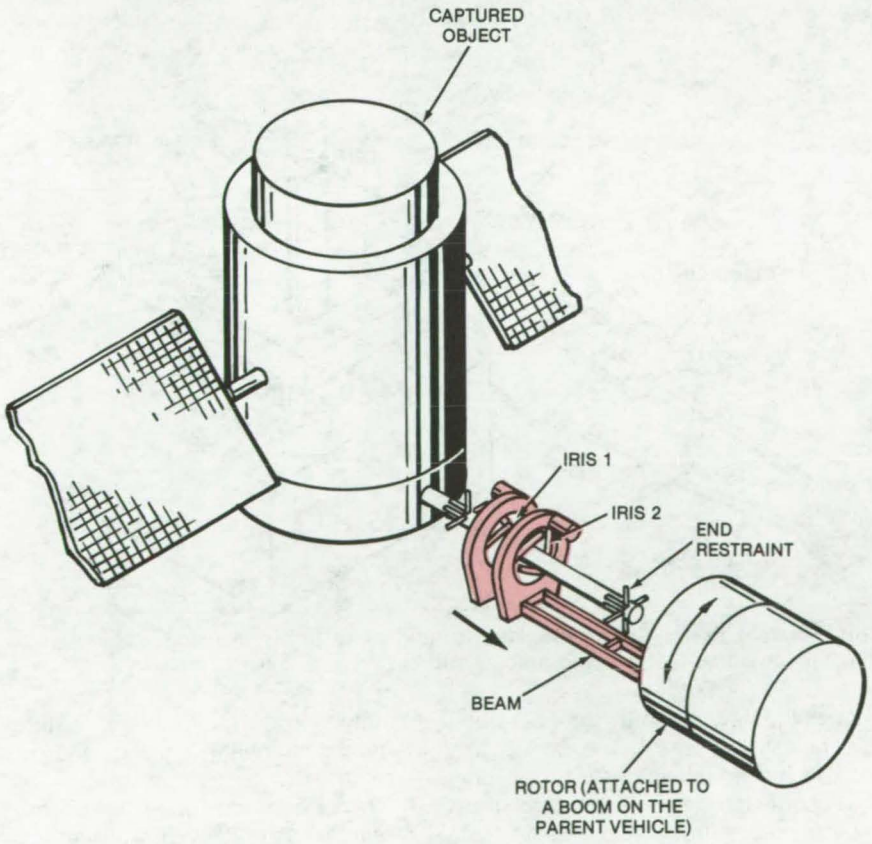

Figure 1. **Gentle Coupling Mechanism** includes two, three-blade irises supported by a beam attached to a rotatable assembly. Iris 1 is fixed at the end of the beam; iris 2 is moved toward the rotor to capture the object.

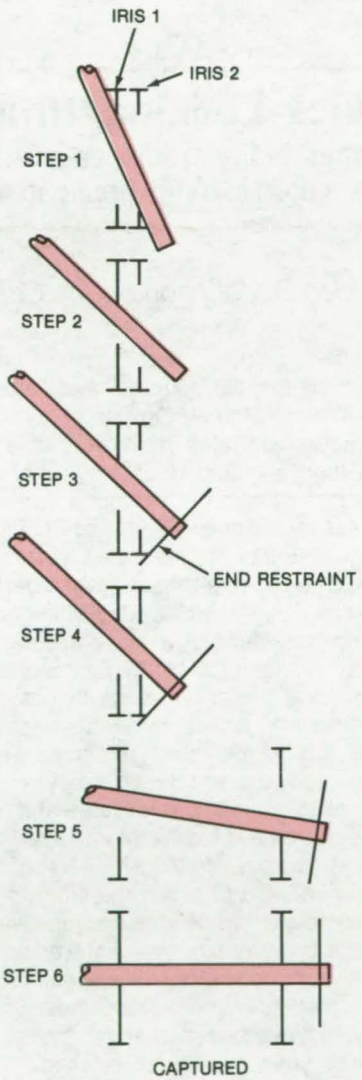

Figure 2. This **Sequence of Steps** is used in capturing an object: (1) two irises are positioned around the object; (2) iris 1 is closed to about half its fully open diameter; (3) an end restraint is deployed; (4) iris 2 is partially closed; (5) the irises are separated; and (6) the irises are closed.

axis of the mechanism; and finally, the irises are gently closed to complete the capture. To release the object, the end restraint is retracted and the irises are opened.

A single-iris version of the coupler uses a 4-element iris in which the elements are much broader than in the double-iris configuration. In this design, the elements reorient the object as it is being captured. The benefits of the single- and double-iris configurations depend upon the stability and mass of the craft to be maneuvered.

The mechanism can accommodate gross misalinements between object and vehicle and can handle a wide range of sizes. It also can be designed to capture spinning bodies, if the irises are mounted so that they too can spin.

The mechanism is much lighter and more compact than the massive mechanical linkages that have been used to aline manned spacecraft for capture. It also allows the operation to be controlled at a greater (and safer) distance.

The "object" can be an end receptor on the craft or vehicle to be captured. The receptor may be positioned so that any forces exerted through its length will pass through the center of gravity of both craft in order to prevent attitude asymmetries from being set up. The end receptor can be extended to protect the two spacecraft from collisions and to provide the operator with a better view.

This work was done by Arthur A. Rudmann of **Goddard Space Flight Center.** *For further information, Circle 64 on the TSP Request Card.*

This invention is owned by NASA, and a patent application has been filed. Inquiries concerning nonexclusive or exclusive license for its commercial development should be addressed to the Patent Counsel, Goddard Space Flight Center [see page A8]. *Refer to GSC-12322.*

Quick-Locking/Unlocking Retainer

Spring retainer replaces a wingnut and a stud in many applications.

Lyndon B. Johnson Space Center, Houston, Texas

When holding two small parts together in test fixtures and other applications, the spring clip shown in the figure will often be more convenient than a clamp or a wingnut-and-stud combination. Developed for an impact-resistance tester at liquid-oxygen temperature, the retainer should be especially useful when parts must be frequently moved or changed.

The retainer is a stainless-steel spring similar to a safety pin. Slotted tongues at the spring ends fit onto a grooved pin. In the materials-impact test for which the retainer was developed, the specimen is held in a cup filled with liquid oxygen and is impacted by a measured force applied to a striker pin. Previously, a wingnut had been used to retain the pin and a guide plate while a weight was dropped on the pin. At least 20 trials are necessary to evaluate a specimen, and the specimen cup must be removed after each trial so that the liquid oxygen can be replenished.

With the previous setup, the test operator repeatedly had to unscrew and rescrew the wingnut, and remove and replace the spacers and washers, while wearing gloves for protection against a temperature of -195° C. This was a time-consuming and sometimes difficult procedure because the wingnut tended to freeze to the stud.

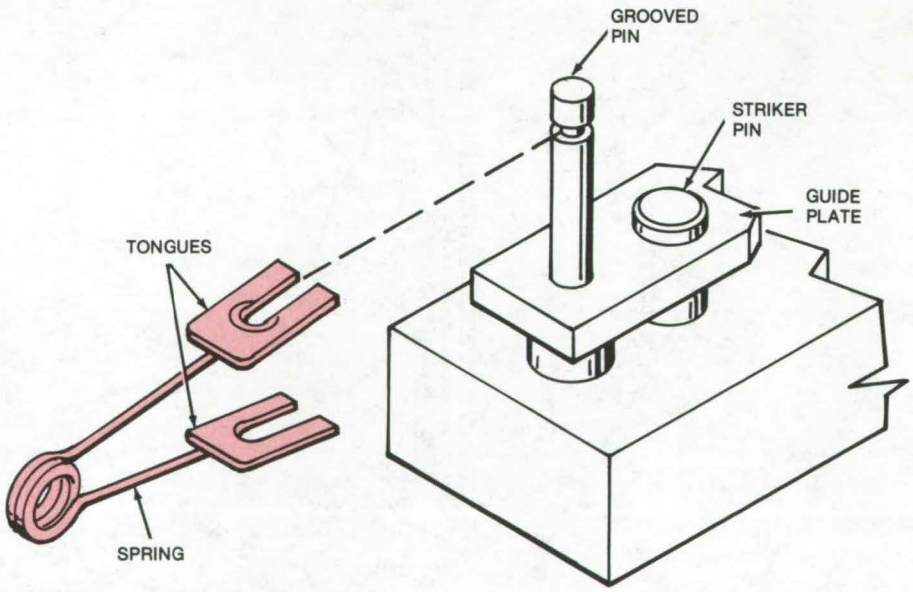

This **Retainer Exerts Spring Pressure** to hold parts firmly in place, yet it can be disconnected and reconnected quickly and easily.

With the new retainer, the operator has only to compress the spring to remove it or to replace it. A recess on the upper tongue ensures that the retainer seats firmly in a slot on the guide pin. There is no danger of freezing, and most importantly, the time to replace a specimen cup is reduced by about 90 percent.

The fast and smooth action of the retainer should make it useful in a variety of tools, jigs, and fixtures requiring frequent locking and unlocking.

This work was done by George Okamoto and Billy B. Williams of Rockwell International Corp. for **Johnson Space Center.** *For further information, Circle 65 on the TSP Request Card.*

MSC-18048

Antibackoff Lock for Nuts and Bolts

Locking device can be installed without removing bolts.

Lyndon B. Johnson Space Center, Houston, Texas

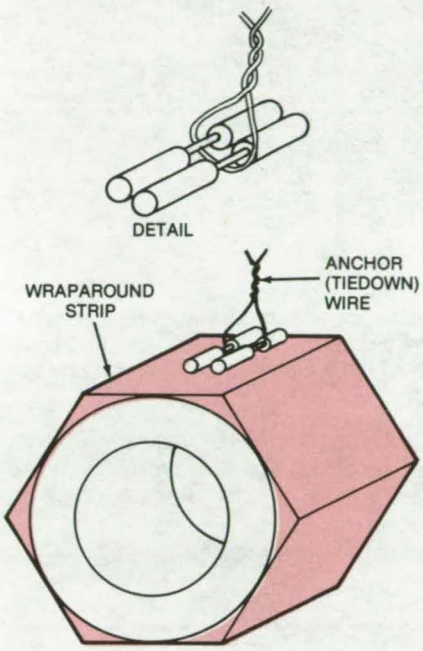

Figure 1. The **Antibackoff Fastener** is shown attached to a hexagonal nut. A pin holds the wraparound strip (in color) on the nut and serves as the attachment point for a securing wire. The wire can be tied or spot welded to a stationary point to keep the nut from rotating.

A simple antibackoff lock, designed for a hydraulic system, could be used to keep any nut or bolt in place under vibration. Unlike lockwashers, glue, and other techniques used to lock in nuts and bolts, this lock strip, as shown in Figure 1, can be attached to already-installed boltheads.

In essence, the lock is a strip that fits around the bolthead and is then tightly "tied" to a fixed point to keep the bolt (or nut) from rotating and coming loose. The strip (Figure 2) can be cut for various-sized bolts and nuts. When wrapped around the bolthead, it is held tight by a pin that is also used to attach the "tiedown" wire that keeps it from loosening.

This work was done by James M. Fealy of **Johnson Space Center.** *No further documentation is available.*
MSC-16472

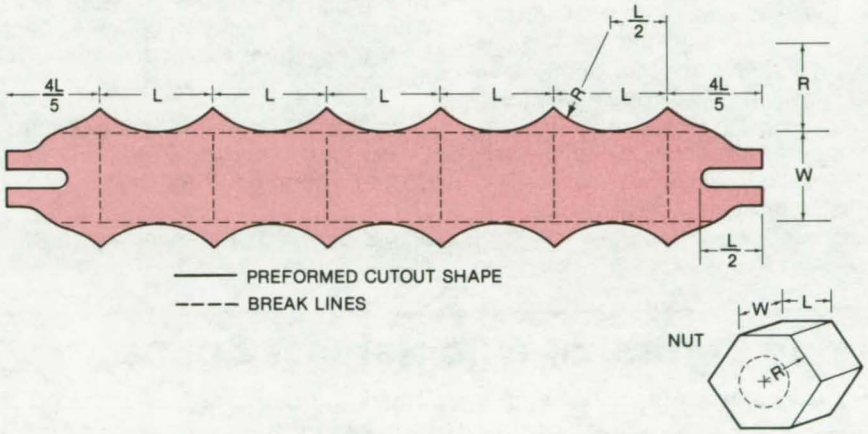

Figure 2. **Preformed Wraparound Strips** can be cut for various sizes and shapes of bolts. The slotted ends are rolled and welded to act as channels for the lockpin that holds the strip on the nut.

Device for Pinching Off Metal Tubes

Gas samples are trapped inside thin metal tubes by a toggle clamp.

Goddard Space Flight Center, Greenbelt, Maryland

Conventional devices for trapping gas samples inside small-diameter metal tubes have not been entirely effective. When explosively actuated devices were tested for use on interplanetary space probes, the tubes would often fracture, allowing samples trapped for analysis by spectrometers to leak out. Conical or ball valves were also tested but were rejected because they required hard, high-temperature materials that were difficult to machine to the necessary tolerances.

A new solution uses a toggle mechanism to compress the tube. This device is easily actuated and seals off the tube without fracture. It is spring loaded and is triggered by a control arm and a pin. A small roller is driven against the tube, pinching it with sufficient force to form an effective gas seal.

The mechanism, as shown in the illustration, includes two links driven by a plunger. The plunger is biased by a compression spring held by a pin. The link shown on the left pivots about a fixed axis, while the link on the right is free to translate horizontally on a fixed plate. This link includes a pushrod that carries a roller that is driven against the tube.

(continued on next page)

The tube is attached to a stopblock. A second stopblock is located below the plunger. The height of this block and the horizontal screw adjustment on the stopblock supporting the tube determine the amount of travel of the moving parts.

The mechanism is actuated by an arm connected to the pin. When the pin is removed, the spring pushes the plunger driving the pushrod against the tube. The roller strikes the tube with a force that can be about 800 times greater than the downward force exerted by the spring. This design is intended to trap gas samples that may be at temperatures and pressures of 900° F (485° C) and 100 atmospheres (10.14×10^6 N/m^2), respectively in the atmosphere of Venus.

In the space-probe application, the mechanism is triggered by remote control and is not reset. For other applications it may be reset manually by removing the threaded spring cap and moving the plunger and the pin back to their initial positions. The spring is tensioned by tightening the spring cap.

This work was done by Edwin O. Stengard of **Goddard Space Flight Center.** *For further information, Circle 66 on the TSP Request Card.*

This invention is owned by NASA, and a patent application has been filed. Inquiries concerning nonexclusive or exclusive license for its commercial development should be addressed to the Patent Counsel, Goddard Space Flight Center [see page A8]. Refer to GSC-12274.

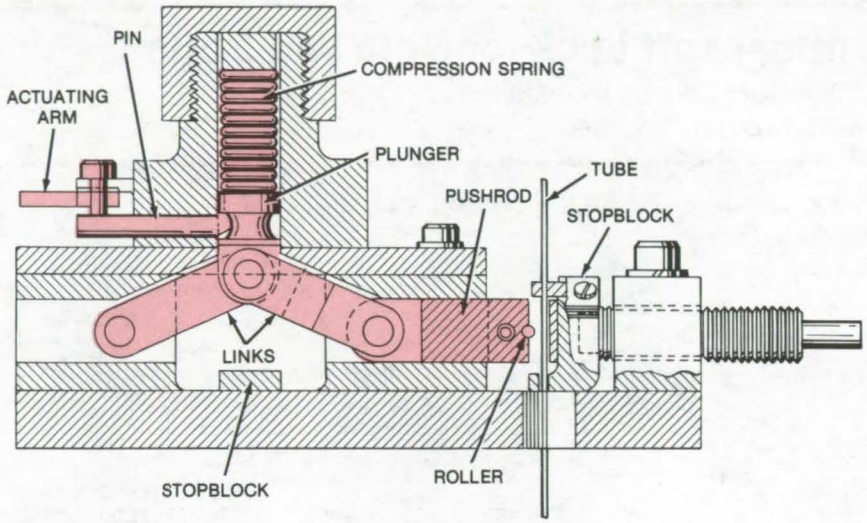

This **Toggle Mechanism** is shown in its initial position before striking the tube. When the pin is removed, the spring forces the plunger down against the stopblock, while the push link moves to the right. The tube is pinched without fracturing by the roller.

Spring Control of Wire Harness Loops

Negator spring control guides wire harness between a movable and a fixed structure.

Lyndon B. Johnson Space Center, Houston, Texas

In aircraft and spacecraft rudder assemblies, electrical wiring passes through a critical area between the moving rudder and a fixed support on the tail section. The wire is usually looped in this area to accommodate the relative motion; however, since the movement of the loop is not easily predicted, the wires can be severed or jammed by adjacent components.

This problem is prevented by a new spring device mounted on the fixed tail section that controls the movement of the wire loop throughout the motion of the rudder. The device, as shown in the illustration, includes a cable slide connected to a negator spring assembly. The electrical wire passes through the cable slide. The slide is a piece of aluminum tubing bent into a 60° arc, with flared ends. The inside of the slide is coated with a smooth material such as Teflon, to reduce friction.

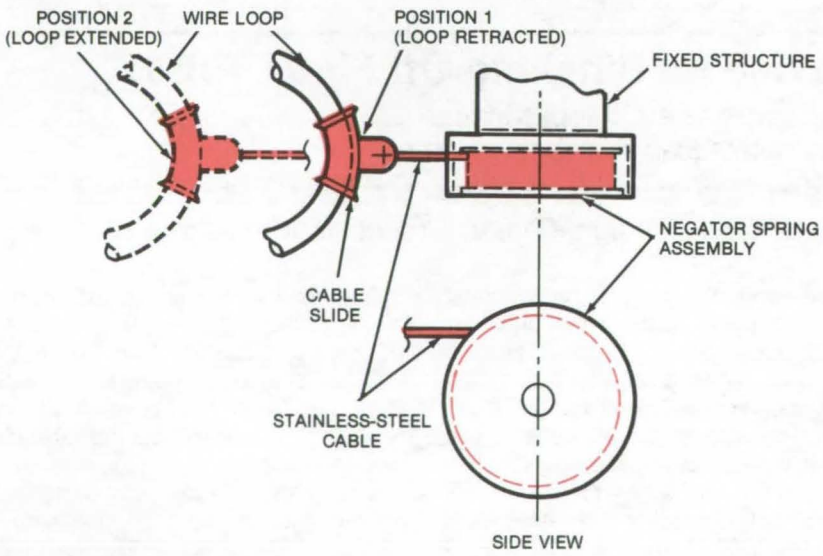

This **Negator Spring Control** prevents the electrical wire harness loop from jamming or being severed as the wire moves in response to changes in the position of an aircraft rudder. The spring-loaded coiled cable controls the wire loop, regardless of the rudder movement.

A stainless-steel cable is connected to an eyelet on the cable slide. The other end of this cable is joined to the negator spring assembly. Sufficient cable length is left on the negator spring reel to allow for the maximum rudder movement. The negator spring assembly thus serves as a spring-loaded coiled cable to restrict the movement of the wire harness loop.

As the rudder moves left or right, the negator spring releases just enough of the coiled cable to maintain constant tension. This reduces the diameter of the loop because the distance between a wire clamp on the rudder and the fixed vertical tail becomes larger. When the rudder returns to its trailing position, the cable is coiled back into the negator assembly, which brings the wire loop back to its original diameter. The cable slide remains at the apex of the loop (adjacent to the negator spring) during the entire motion.

This work was done by Pasquale J. Curcio of Fairchild Republic Co. for **Johnson Space Center.** *No further documentation is available.*
MSC-18246

Noncontacting Valve-Position Indicator

The position of a sealed valve or other movable part is indicated without penetrating the housing.

Lyndon B. Johnson Space Center, Houston, Texas

A magnetic position-sensing technique allows the on/off condition of a valve to be determined without using an electromechanical switch or other device that requires penetration of the pressure wall of the valve. The sensor, employing two samarium-cobalt magnets and a Hall-effect transducer, gives an accurate indication of whether the valve is open or closed and increases the overall reliability of the valve itself. The technique can be used in any application that requires knowledge of the position of a component that is inside a sealed housing. Specific valve-control applications include fluid-flow systems, engine control, railroad vehicles, and chemical processing.

As shown in the illustration, the sensor is not physically connected to the valve body. This eliminates a potential failure point. The samarium-cobalt magnets are attached to the stem of the valve and are alined facing north pole to north pole. The very sharp and intense magnetic field from between the magnets penetrates the metallic pressure wall enclosing the valve. Outside the wall a Hall-effect transducer senses the magnetic field intensity. When the valve closes, the stem and magnets move away from the Hall chip. The resulting change in output Hall voltage is detected and converted into a position signal.

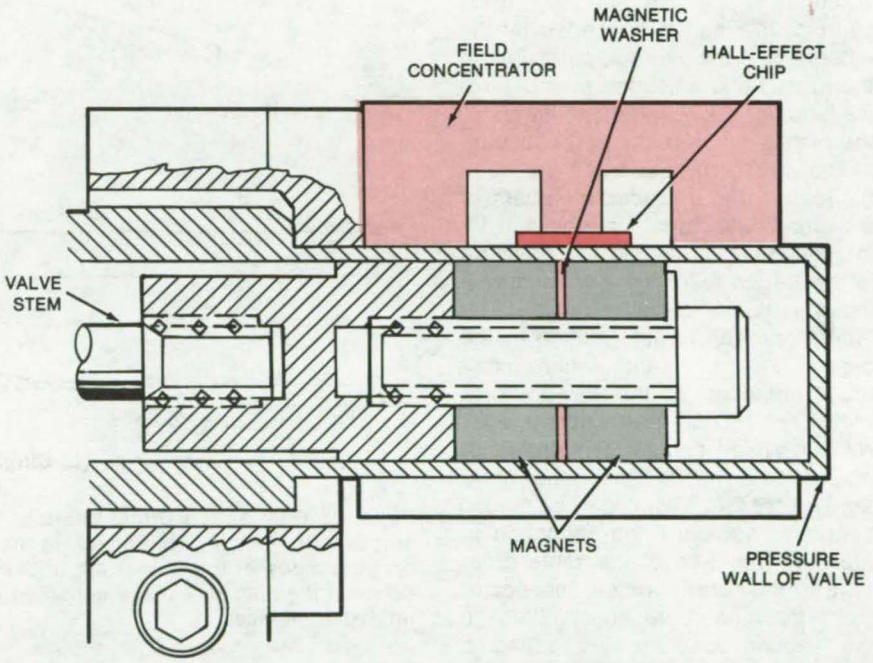

Flux From Magnets connected to the stem of a hydraulic valve penetrates the pressure wall and is sensed by a Hall-effect transducer outside the wall. When the valve closes, moving the stem and magnets, the voltage from the transducer decreases; thus the stem position is indicated without any physical contact. The north-pole-to-north-pole orientation of the magnets plus the magnetic washer and flux concentrator localize the flux to a very narrow [0.050- to 0.100-inch (1.3- to 2.5-mm)] region in the Hall chip.

This work was done by Edward A. Crovella and Richard D. Cummins of Carleton Controls Corp. and James M. Wada of Rockwell International Corp. for **Johnson Space Center.** *For further information, including a circuit schematic, Circle 67 on the TSP Request Card.*
MSC-16048

Improved Gas Thrust Bearings

Dual-action and multipad gas thrust bearings can carry larger loads.

Lewis Research Center, Cleveland, Ohio

Two variations of gas-lubricated thrust bearings extend substantially the load-carrying range over existing gas bearings. These are the "dual-action" and "cantilever-mounted" gas bearings.

Dual-Action Bearing

The load-carrying capacity in hydrodynamic bearings results from pressure generated within a lubricant film in a gap that is convergent in the direction of motion of the bearing surfaces. In a bidirectional thrust bearing, the load is supported by the difference in the average pressures in the loaded and unloaded members of the bearing; the higher that difference, the higher the load-carrying capacity.

The pressure difference between the loaded and unloaded members of a bidirectional thrust bearing can be increased by increasing the pressure in the loaded member or by decreasing it in the unloaded member. The latter approach is not justified in the case of liquid lubricants, where maximum reduction in the low-pressure region can be only 1 atmosphere (10^5 N/m^2), which can be two orders of magnitude lower than the usual pressure increase. With gas-lubricated bearings, however, the reduction in pressure might be of the same order as the pressure increase and could, therefore, contribute substantially to the bearing load-carrying capacity. The principle of the dual-action bearing, shown schematically in Figure 1(a), is that it utilizes hydrodynamic effects on both sides of the runner.

In Figure 1(b) the single-action thrust bearing runner rotates next to a stationary member (sector pad or grooved disk), so that the rotation is in the direction of film convergence, and above-ambient pressures are generated in the lubricant film. In Figure 1(a), the dual-action bearing with an identical stationary member next to the other surface of the runner, rotation in the direction of film divergence of that member is obtained, and pressures below ambient are generated on that surface.

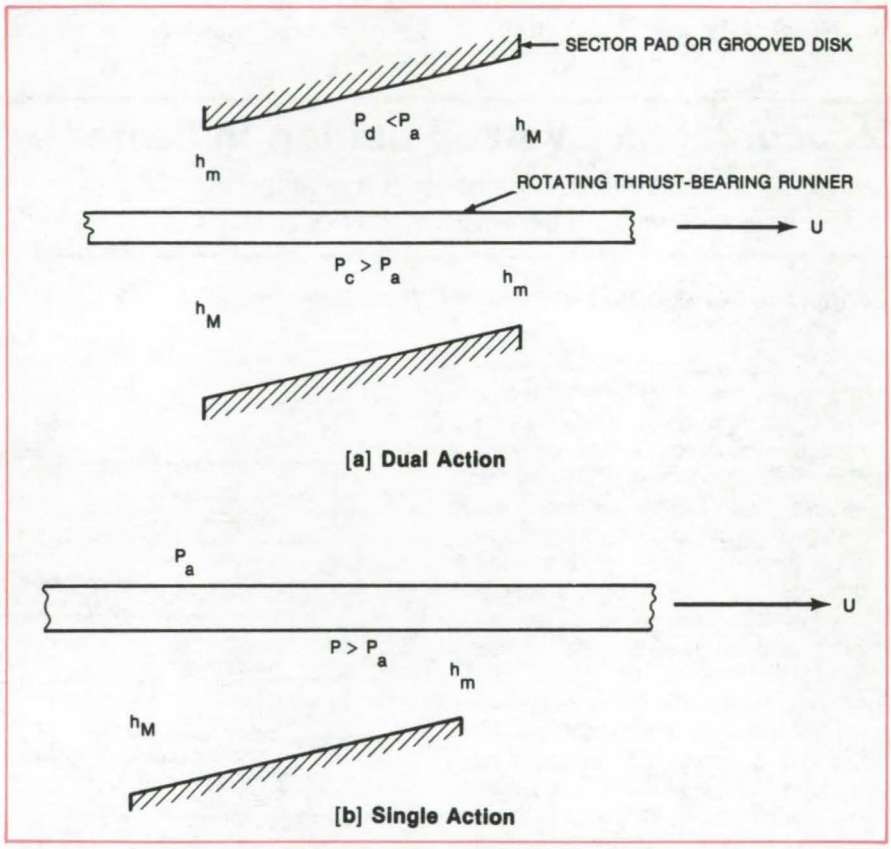

Figure 1. **Dual-Action Thrust Bearings** (a. above) can support a higher load than a single-action bearing (b. above). In the dual-action bearing, hydrodynamic effects on both sides of the runner are utilized to achieve a greater pressure differential between the loaded and the unloaded member by decreasing the pressure on the unloaded member.

The load-carrying capacity of the dual-action gas thrust bearing is more than 90 percent greater than that of the single-action bearing over the whole range of compressibility numbers. Design is not limited to flat sector pads; other configurations such as stepped pads and grooved disks can be used as stationary members.

Cantilever-Mounted Thrust Bearing

The resilient-pad gas thrust bearing does not contain any elastomers in the bearing assembly. The bearing consists of sector-shaped pads mounted on flexible beams (see Figure 2). This new bearing can be started and stopped without external pressurization, is tolerant to contaminant particle ingestion, and is not limited in operating temperature by the presence of organic materials such as elastomers.

The load-carrying and stiffness characteristics of the pad are related to the elasticity of the beam. The single, cantilever-mounted pad serves as a basic unit in various multiple-pad bearings.

Analysis has shown that the load capacity of a flat, sector-shaped pad is maximized whenever the pad tilt results in a uniformly-minimum film thickness along its trailing edge. The optimum design is more easily achieved by using straight cantilever beams.

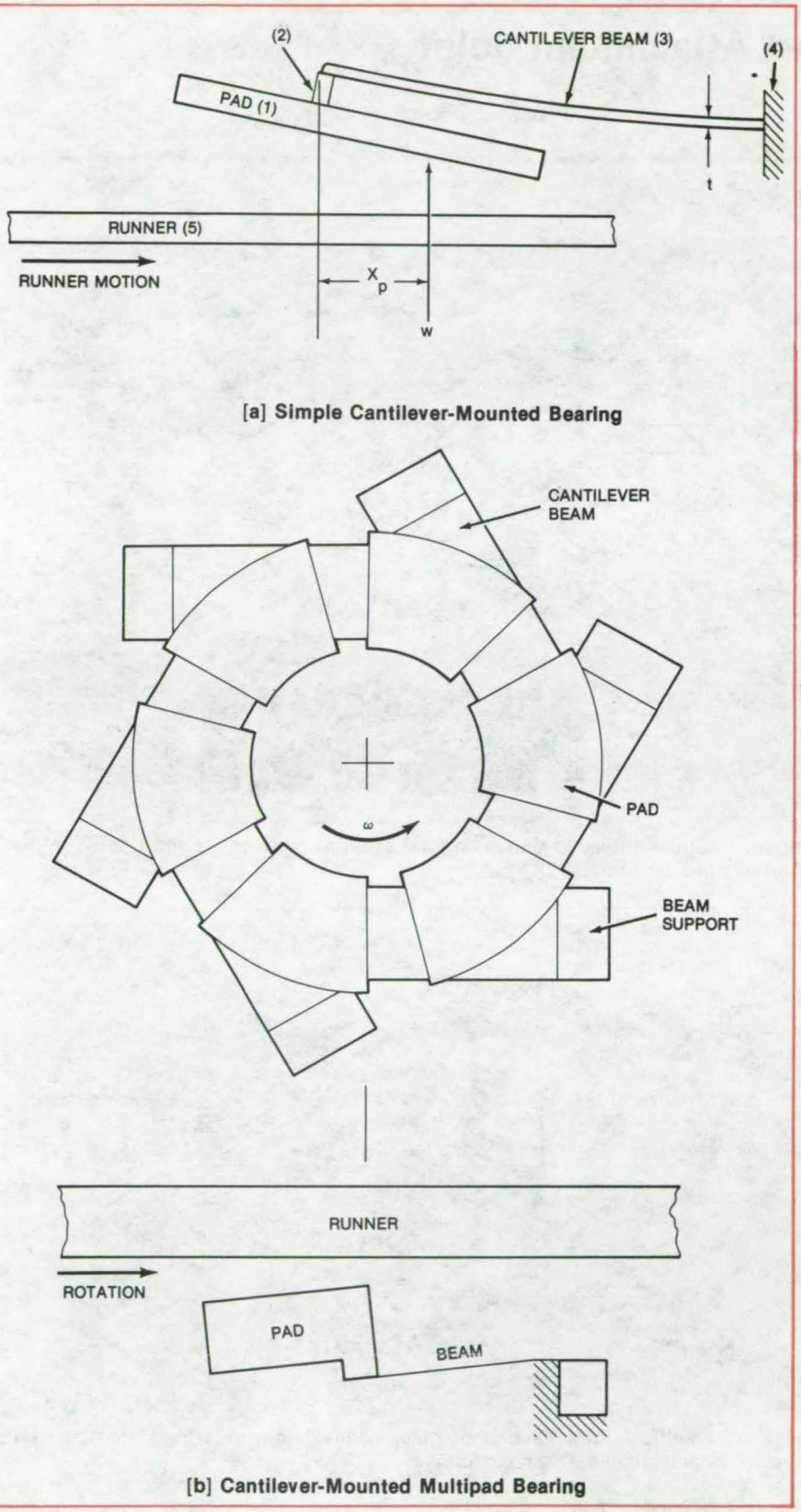

Figure 2. **Cantilever-Mounted Thrust Bearing** has load-carrying and stiffness characteristics dependent on the elasticity of the cantilever beam. The simplest one-pad configuration is shown in (a) above; this basic unit can be used in multiple-pad bearings as shown in (b).

Figure 2(a) illustrates the simplest configuration — a pad (1) is rigidly mounted along a line (2) on a resilient cantilever beam (3). The beam is rigidly mounted along its other edge (4). A load W acts on the pad, deflects the beam and assures a converging film in the direction of runner (5) motion. (The deflection should be such that the runner touches the pad only at its trailing edge.) The converging clearance maintains the hydrodynamic lubricating film to support the load.

The bearing characteristics depend on the amount of pad tilt at its mounting (2) and on the deflection of the cantilever beam. The deflection is a function of beam dimensions (thickness, width, and length), of beam material, and of the distance X_p between the point where load is applied and the pivot line.

Procedures exist for optimizing the design of the gas bearing at a given set of design conditions. The operating characteristics of an optimized bearing design were determined for a range of operating speeds.

The advantages of this bearing are: greater tolerance to dirt ingestion, good initial lift-off characteristics, and operational capability over a wide temperature range.

This work was done by William J. Anderson and Izhak Etsion of **Lewis Research Center.** *Further information may be found in:*

NASA TN D-8279 [N76-29598], "Dual-Action Gas Thrust Bearing for Improved Load Capacity," and NASA TN D-8221 [N76-24588], "Analysis & Design of a Cantilever-Mounted Resilient-Pad Gas-Lubricated Thrust Bearing."

Copies of these reports may be obtained at cost from the New England Research Application Center *[see page A7]*.

This invention is owned by NASA, and a patent application has been filed. Inquiries concerning nonexclusive or exclusive license for its commercial development should be addressed to the Patent Counsel, Lewis Research Center *[see page A8]*.

LEW-12569

Quick-Connect Threaded Attachment Joint

Plastic or metal parts aline and engage with little rotation.

Langley Research Center, Hampton, Virginia

A threaded tapered joint is self-alining and tightens with only 65° of rotation for quick connects and disconnects. Made of injection-molded plastics or cast or machined aluminum, the joint can carry wires, tubes, liquids, or gases.

The joint (Figure 1) consists of male and female sections, each containing multiple thread starts (four are shown in the photo) on a steep (35°) conical surface. The equivalent pitch is 20 threads per inch (8 threads per cm), and the maximum diameter of 2.0 inches (5.1 cm) tapers down to 1.15 inches (2.9 cm). The thickness of the conical portion of the male and female parts varies to maintain a constant cross section, thereby maximizing load-carrying ability and minimizing weight.

When the two parts of the joint are brought together (a cone within a cone), their shapes aline them. Small projections on the male section and slots on the female section further aid alinement; slight rotation of the male form clockwise or counterclockwise engages the projections in the slots. At this point, the threads begin to engage, and the male section is rotated clockwise until the joint is fully engaged and torqued.

The joint is disengaged by rotating the male form counterclockwise until its projections aline with the slots in the female form. The sections are then separated by pulling them apart longitudinally.

Once the threads begin to engage, only 65° of additional rotation are required to make up the joint. Longitudinal motion during this rotation is only 0.036 inch (0.9 mm). Other combinations of cone angle, threads, and pitches are possible, allowing makeup rotations from 190° to 35°.

Depending on the particular needs, for the plastic parts, molding material can be compounded with graphite fibers, carbon black, or other additives to impart electrical conductivity, ultraviolet protection, or proper surface emissivity. The surfaces of the parts can be coated by painting or vapor deposition. The mold tooling can readily accommodate various part thicknesses and thread and alinement configurations. The cast aluminum parts are manufactured using the lost wax process and matched molds for injection molding the wax forms.

The sections of the joint can be permanently bonded. An encapsulated adhesive can be applied to one section and activated by motion of one thread

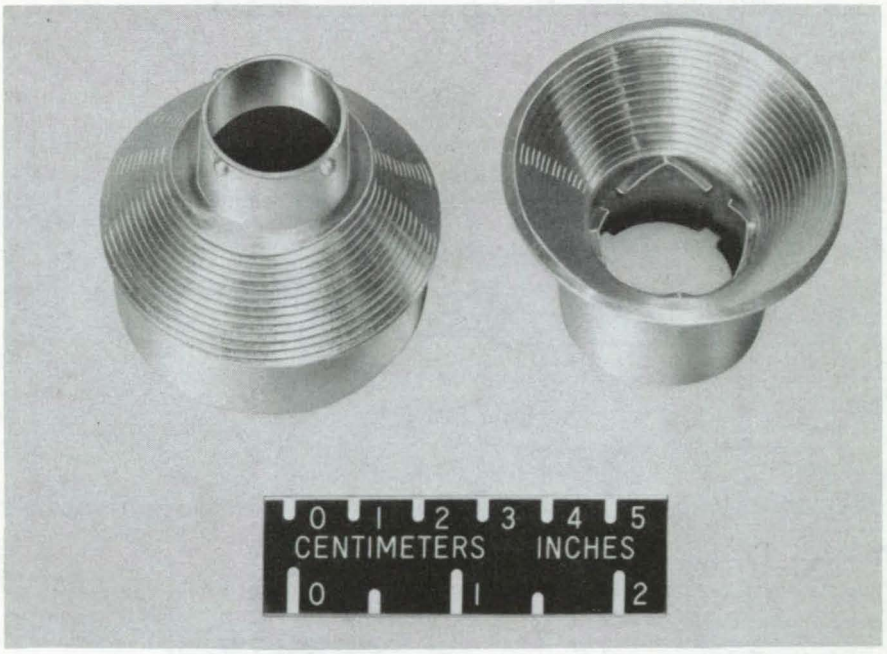

Figure 1. Steep **Threaded Cones** on joint sections aline easily and tighten in less than one-quarter turn.

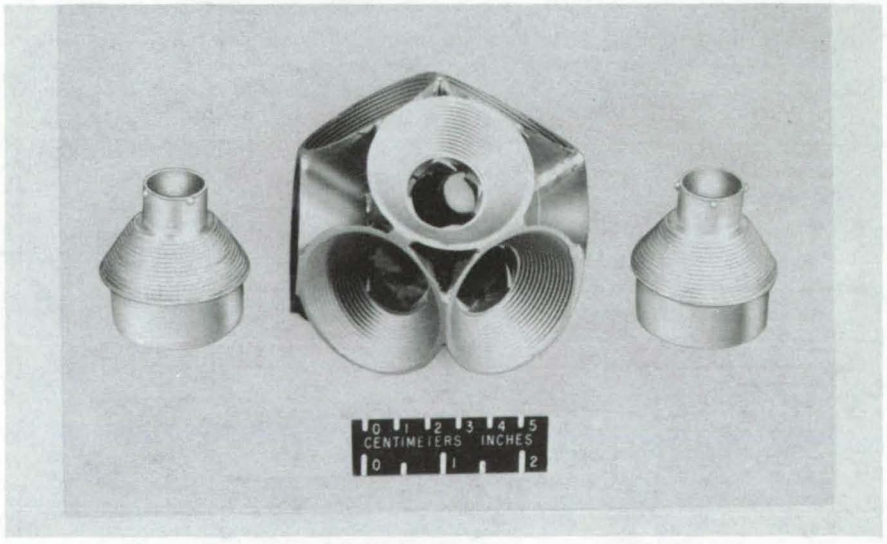

Figure 2. **Multiple-Joint Version** of quick-connect joint has high strength. Part shown accommodates nine connections.

against the other; or a two-component adhesive can be applied, one component to the male form and one to the female form, and again activated by relative motion of the threads.

Another variation is a multiple-joint assembly (Figure 2) that makes maximum use of the intersection of female cones to stiffen the assembly. The multiple joint illustrated consists of six identical female connectors in one plane, 60° apart, and three other female connectors 120° apart with centerlines inclined 57° from the six-connector plane. All centerlines intersect at a common point. This assembly, made from a 65-percent glass-loaded polyimide, can withstand a 1,700-pound (7,500-N) tensile load. For even higher load-carrying ability, the joint can be cast or machined from metal.

This work was done by Melvin H. Lucy, William R. Messick, and Peter Vasquez of **Langley Research Center.** *For further information, Circle 68 on the TSP Request Card.*

Inquiries concerning rights for the commercial use of this invention should be addressed to the Patent Counsel, Langley Research Center [see page A8]. Refer to LAR-12232.

Simulator for Training Remote-Manipulator Operators

Six-degree-of-freedom simulator uses economical components.

Lyndon B. Johnson Space Center, Houston, Texas

A training simulator for remote-manipulator operators employs optical effects to reduce the required mechanical motion. This reduction in complexity makes this or a similar system cost-effective for training manipulator operators, such as those in industries handling nuclear wastes and hazardous chemicals.

The system as shown simulates six degrees of freedom; i.e., roll, pitch, yaw, lateral displacement, longitudinal displacement, and distance changes. Roll, pitch, and yaw are simulated by controlling the attitude of the payload pan/tilt unit with respect to the TV camera, which remains fixed at this point. For example, roll is simulated by panning the payload pan/tilt unit in the required direction and rate around the camera line-of-sight axis. Pitch and yaw are similarly accomplished around the other axes.

Lateral and longitudinal displacements are simulated by operating both the camera and the payload pan/tilt units simultaneously. In lateral displacement, the payload is rolled in the desired direction while the camera is panned in the opposite direction at the same rate. Both units must have equal angles from their original positions. Longitudinal displacement is simulated by pitching the payload and tilting the camera at equal rates to maintain the camera line-of-sight perpendicular to the payload longitudinal axis. Payload distance errors in both of these maneuvers are corrected by adjusting the camera zoom lens.

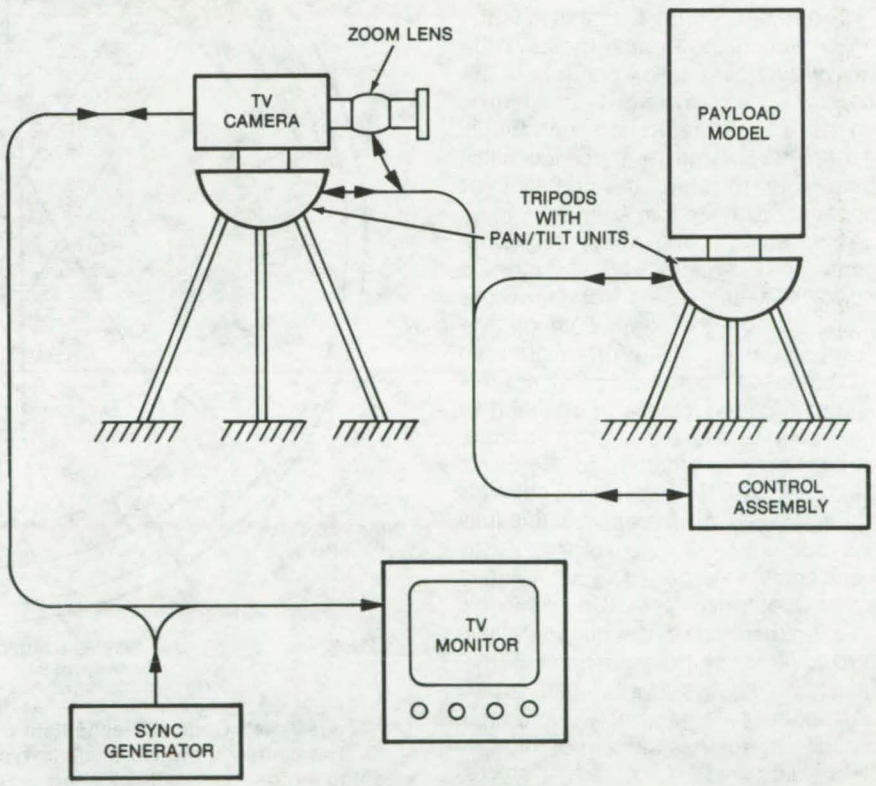

Displacement Simulator, for Space Shuttle payload handling, uses a TV camera focused onto a payload model. The operator manipulates the control assembly, which is connected to both pan/tilt units and the zoom lens. Payload movement is observed on a TV monitor.

Distance changes are simulated simply by operating the zoom lens. The payload moves closer by zooming the lens in (teleposition) and moves away by zooming the lens out (wide-angle position).

This work was done by David H. Orr and Loran C. Ward of McDonnell Douglas Corp. for **Johnson Space Center.** *For further information, Circle 69 on the TSP Request Card.*
MSC-14921

Shaft Speed Control

A simple mechanism equalizes the speed of rotation of two concentric shafts.

NASA's Jet Propulsion Laboratory, Pasadena, California

A proposed mechanism controls rotation of a heavy-duty shaft by mechanical comparison with the rotation of a small, precise, stepper motor. Developed for unfurling solar sails on spacecraft, the mechanism can be used to limit winding and unwinding speeds of large spools and reels and in many other mechanical applications requiring shaft speed control. The new mechanism is lighter and simpler than conventional speed controllers.

The speed controller is shown in the figure without the stepper motor or the heavy-duty shaft it controls. The controller employs two concentric shafts: a center reference shaft that is geared down from a precision stepping motor to rotate at a constant set speed and a feedback shaft that is geared up from the heavy-duty work shaft. The gearing is such that the two concentric shafts will rotate at the same speed if the heavy-duty shaft is operating at the desired rotation rate.

The speed-control components are a spring-loaded roller arm attached to the center reference shaft and a brakeshoe arm attached to the outer feedback shaft. The rollers of the spring-loaded arm press against the curved arms of the brakes with considerable force. If the "control angle" between the two arms is smaller than some design angle the brakes are not pressed against the housing. The two shafts then rotate independently and freely, and the stepper motor has no effect on the heavy-duty shaft.

Should, however, the heavy-duty shaft rotate faster than desired, the feedback shaft will rotate faster than the reference shaft, and the control angle will increase. An increase in the control angle means that the rollers move along the curved brake arms toward the brakes. The spring force of the roller arm presses the brakes against the surrounding stationary cylinder, slowing down the feedback shaft.

Since the feedback shaft is connected to the working heavy-duty shaft, that too is slowed down. The braking continues until the feedback shaft and reference shaft are again rotating at the same speed (i.e., the work-shaft speed has been brought into tolerance). Then the control angle will have reduced to the point at which the roller arms do not press the brakes against the cylinder.

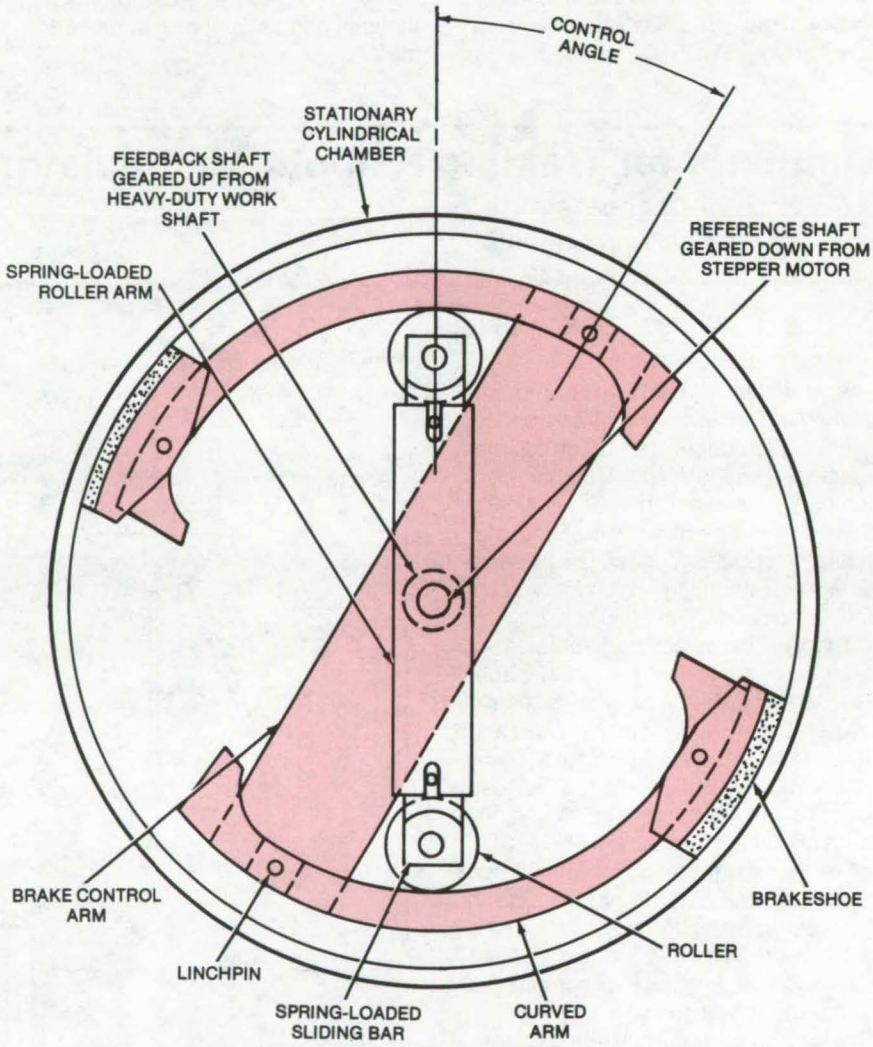

The Shaft-Speed Control Mechanism uses mechanical feedback to control a work shaft. The center reference shaft is typically gear-driven at 50 rpm by a precision stepping motor. The feedback shaft is typically gear-driven by a 1-rpm work shaft at 50 rpm. Should the work shaft speed up, the control angle increases, and the brakes are applied to reduce the feedback-shaft (and thus work-shaft) speed.

This work was done by Allen G. Ford of Caltech for **NASA's Jet Propulsion Laboratory.** *For further information, Circle 70 on the TSP Request Card.*

This invention is owned by NASA, and a patent application has been filed. Inquiries concerning nonexclusive or exclusive license for its commercial development should be addressed to the Patent Counsel, NASA Resident Legal Office-JPL [see page A8]. Refer to NPO-14170

Stable Hydraulic Pressure Regulator

Neither sensing line restrictors nor frictional dampers are required for stability.

Lewis Research Center, Cleveland, Ohio

A hydraulic pressure regulator that is stable without the use of sensing line restrictors or frictional dampers has been analytically derived and experimentally verified. The analysis presents a method by which stability margin, response, and droop magnitude can be incorporated during the design of direct-acting hydraulic pressure regulators.

One of the most frequently occurring problems in hydraulic circuits is the elimination of pressure regulator instability. The regulator is usually the only active element among the dynamically-coupled hydraulic elements. The stability is determined by the interaction of the regulator and the coupled passive elements of the circuit. Stability is necessary for an acceptable regulator performance, but any stabilizing method that causes an increase in response time or droop magnitude is not always acceptable.

The sensing line orifice frequently used for stabilization degrades response by very rapidly imposing a limit on the velocity of the variable orifice element of the regulator. Heavy mechanical damping of the variable orifice element can produce steady-state error or cause limit cycle oscillation. When instability is the result of a high gain over the stability limit, the small line orifice or large mechanical damping that is required to obtain stable operation may so severely restrict valve action that control effectiveness is lost.

The new regulator design methods that are derived provide two methods through which stability can be obtained in the complete absence of a line orifice or of mechanical damping.

The analysis is based on a generalized block diagram that represents three elements: the pressure regulator, the flow or pressure generator, and the coupled load. The coupled load is represented by its impedance. The diagram yields the open-loop transfer function of the system for any load with a circuit impedance that can be expressed. The analysis is applied to the pump-supplied relief valve circuit, the load-supplied counterbalance valve circuit, and the pressure-supplied reducing valve circuit. Relationships are provided for use in design to incorporate a specific gain margin for stability and for Bode diagram verification. Closed-loop transfer functions are given from which the dynamic response of flow and pressure can be calculated from regulator design constants and circuit parameters.

A system was designed to verify experimentally two of the major concepts derived mathematically: (1) the stability limit under parallel capacitive plus resistive load and (2) the stability effect of the tuned stabilizer. The system consisted of (1) a positive displacement pump coupled to a variable-speed drive, (2) a relief valve pressure regulator, (3) an air-charged piston accumulator (tuned stabilizer), and (4) a manually-adjustable load valve (orifice). Both concepts showed close agreement with the mathematical analysis.

This work was done by Harold Gold of **Lewis Research Center.** *Further information may be found in NASA TM-X-73687 [N78-10415], "The Design of Hydraulic Pressure Regulators That Are Stable Without the Use of Sensing Line Restrictors or Frictional Dampers," a copy of which may be obtained at cost from the New England Research Application Center* *[see page A7].*

LEW-13058

Automated Syringe Sampler

A device for remote sampling of air or water in pollution studies is operated by a servomechanism. The servo, which is activated remotely by a switch closure or a radio signal, drives an evacuated glass tube against a stationary double-ended needle. The sample is collected through the needle, which punctures the rubber septum of the glass tube. After a predetermined time, typically 5 seconds, the servo is activated again, driving the glass tube in reverse and extracting the syringe from the septum.

(See page 393.)

Ruby C-Axis Alinement System

A precision C-axis alinement system for rubies operates at room temperature. The C-axis is located to within ±3 minutes of arc from the recordings of paramagnetic absorption of X-band microwave signals. A ruby slab, for which the C-axis angle has been roughly determined to within 1° by optical methods, is placed in a waveguide fixture, and an X-band RF signal is applied to the ruby. Two dips, due to idler transitions, are recorded for various field angles. The ruby slab is ground so that the dips coincide when the fixture is at zero degrees relative to the magnet pole faces.

(See page 401.)

Precision Cleaver for "Soft" Crystals

A new machine cuts soft crystals to uniform 5-mil slices. The machine incorporates a cutter blade secured in a vertically adjustable holder. The holder is adjusted to obtain the desired cutting depth, and the blade is moved horizontally at that level by a drive motor. The motor pushes the blade through the crystal at a speed controlled by a velocity feedback mechanism. The cut crystal pieces are separated by two platens holding the pieces via vacuum. Cutting accuracy is within 1 mil.

(See page 366.)

Latching Solenoid for Cryogenic Valves

Special alloy retains its current-limiting resistance at low temperatures.

Lyndon B. Johnson Space Center, Houston, Texas

Conventional, magnetically latching solenoids with copper windings are not suitable for use at cryogenic temperatures (near 20.5 K or lower) because the resistance of copper drops sharply as the temperature is decreased. For a constant supply voltage, the coil would draw excessive current if operated in this temperature range. However, by replacing part of the copper windings with a low-resistance, low-temperature-coefficient alloy, a latching solenoid with built-in current limiting can be constructed for use at cryogenic temperatures. Such a solenoid has been tested and is being used successfully to control the flow of liquid oxygen and liquid hydrogen in the Space Shuttle. In this solenoid, which operates at a supply voltage of 32 volts, the modified windings limit the current to a maximum of 5 amperes when the temperature is 20.5 K.

Both the pull-in coil and the delatching coil in the new solenoid consist of a winding of copper and a winding of the alloy (see figure). The resistance of the alloy varies little with temperature and is larger than that of copper at very low temperatures. It is, however, lower than that of high-resistance alloys, such as those used in resistance-heating elements, and will therefore operate at lower voltages (and lower power consumption) for the same current and number of windings. It also makes a smaller and lighter solenoid than is possible with high-resistance alloys.

When a voltage is temporarily applied across the pull-in coil of the new solenoid, the magnetic force overcomes the tension of the spring and pulls the armature into the field of a permanent magnet, which holds the armature in the pulled-in position. When a voltage is applied across the delatching coil, the field of the coil temporarily nullifies that of the permanent magnet and allows the spring to move the armature, returning it to its original delatched position.

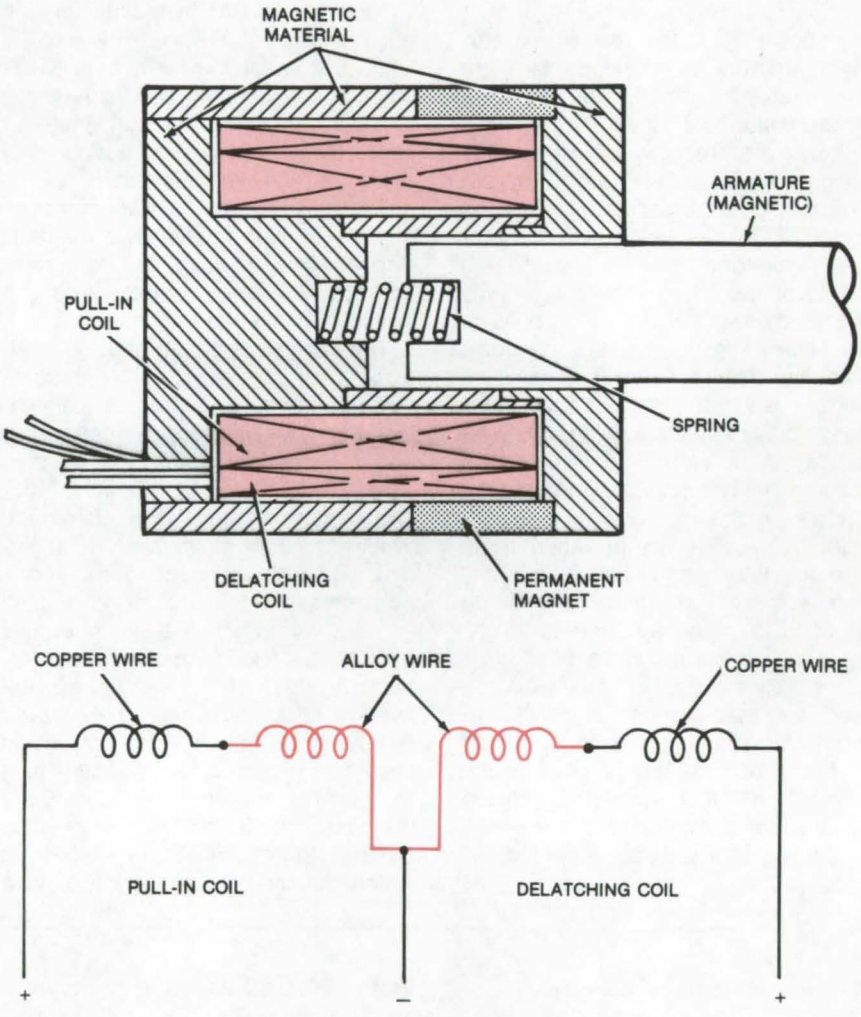

DETAILS OF SOLENOID

The **Pull-In and Delatching Coils** of a cryogenic solenoid contain copper and a low-resistance, low-temperature-coefficient alloy to limit the current at low temperatures.

This work was done by William S. Wang of Consolidated Controls Corp. for **Johnson Space Center.** *No further documentation is available.*

Inquiries concerning rights for the commercial use of this invention should be addressed to the Patent Counsel, Johnson Space Center [see page A8]. Refer to MSC-18106.

Insulator for Cryogenic Joints

Semirigid polyurethane foam is firm enough not to collapse yet soft enough not to crack in extreme cold.

Marshall Space Flight Center, Alabama

An insulator for joints in cryogenic piping prevents liquid air from condensing on the joint as cold liquid gases flow through it. The insulating material is semirigid polyurethane foam. Unlike soft foam insulators, the new insulator does not deteriorate and collapse from the effects of water and air and can be removed and reused. Also, unlike rigid foams, it does not tend to crack at low temperatures.

This insulator is suitable for pipes carrying liquid hydrogen, liquid air, liquefied natural gas, and other low-temperature fluids. The insulating material, which is a molded polyurethane-foam shell, is placed over the joint (see figure), and a silicone-elastomer cover, reinforced with glass fabric is placed over it. The silicone cover is sealed and clamped to the adjoining pipes.

The silicone cover retards flames, and the glass-fabric reinforcement protects the foam against accidential damage from tools during installation and maintenance.

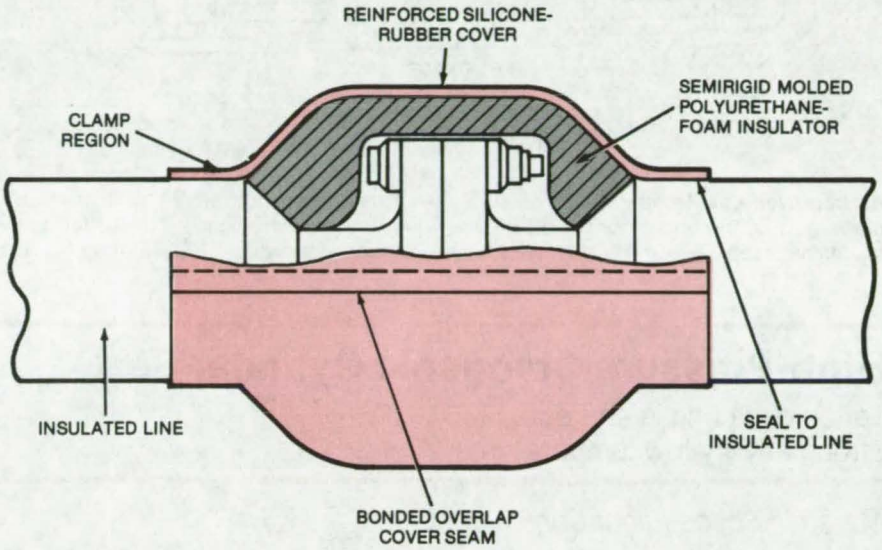

Cold-Joint Insulator made of semirigid polyurethane is covered by reinforced silicone that is sealed to itself by an overlap joint.

This work was done by Elden L. Hawkinson of Rockwell International Corp. for **Marshall Space Flight Center.** *No further documentation is available.*
MFS-19361

Low-Leakage Low-Temperature Valve

Resilient closure mechanism protects against leakage at temperatures as low as −95.5° C.

Lyndon B. Johnson Space Center, Houston, Texas

A new valve seals tightly against cold fluids, even after thousands of opening-and-closing cycles. Because the valve is made of corrosion-resistant steel (CRES), it is also compatible with corrosive fluids. It has been successfully tested for minimum seat leakage at pressures up to 350 psig (2.41×10^6 N/m^2) and temperatures down to −140° F (−95.5° C).

In the new valve, the poppet (see figure on next page) consists of a precision-machined Teflon seal held in place by a CRES retainer that is electron-beam-welded to the CRES poppet body. A CRES garter spring pushes on the Teflon seal so that it protrudes about 0.01 in. (0.025 cm) beyond the poppet face when the valve is open. A thin metal washer prevents the garter spring from digging into the Teflon seal.

When the valve is closed, the garter spring presses the seal against the valve seat, forming a tight closure. A bleed hole in the poppet body admits fluid to the inlet side of the seal, providing additional sealing pressure.

The sealing properties of the Teflon flange last through thousands of closures because the impact of closing is absorbed partly by the garter spring and partly by the poppet outer face, so that the Teflon seal is protected against cold flow and permanent deformation.

The valve was originally designed to handle liquid nitrogen tetroxide and monomethyl hydrazine. It successfully survived pressure tests at 525 psig (3.62×10^6 N/m^2) for 3 minutes and 4,000 open-and-close cycles at temperatures between −65° and +150° F (−54° and +66° C) including 1,000 cycles at −65° F. Helium leakage was

(continued on next page)

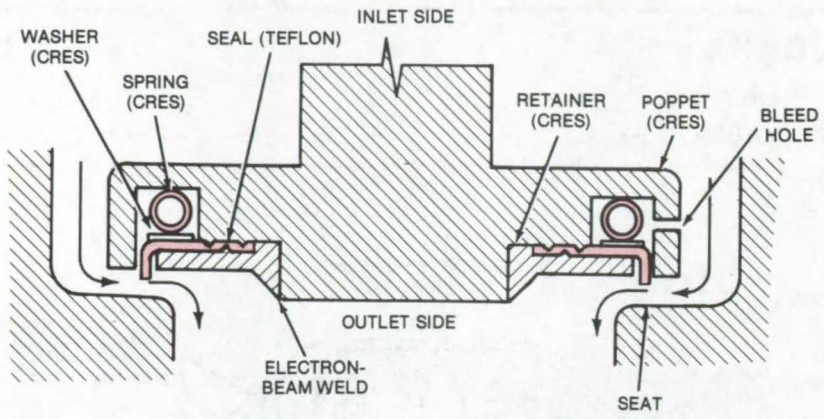

An **Improved Low-Temperature Valve** has a corrosion-resistant steel spring that absorbs part of the impact on a Teflon seal when the valve is closed. The Teflon protrudes between 0.008 and 0.010 in. (0.015 and 0.025 cm) below the CRES retainer.

less than 1.0 standard cubic centimeter per hour (scm^3/h) at 350 psig and −65° F. Leakage was less than 2.0 scm^3/h at −140° F at the same pressure.

This work was done by William S. Wang of Consolidated Controls Corp. for **Johnson Space Center.** *No further documentation is available.*
MSC-18087

High-Pressure Cryogenic Cylinder Seal

Teflon delta ring is soft but strong at very low temperatures.

Marshall Space Flight Center, Alabama

A triangular-cross-section Teflon ring seals against cryogenic fluid, at temperature where standard wedge or U-rings fail. The new "delta" ring can be mounted in a groove in either a piston or bore (see figure).

Both wedge and U-rings tend to split into two rings at cryogenic temperatures and thus destroy seal integrity. These types of rings shrink and pull away from the sealing surfaces when they are cooled; this shrinkage and the pressure from the cryogenic fluid induce stresses that split the ring.

The delta ring, on the other hand, covers the gap between piston and cylinder and is held in place by a split metal ring and a wave spring. The small cross section of the Teflon seal allows it to stretch as it is cooled with relatively low loading from the wave spring. The Teflon stays soft even at very low temperatures and thus keeps the gap covered. It retains its strength, however, and does not extrude in the gap under pressure from the cryogenic fluid.

The delta ring has been successfully tested at 11,000 psi (76×10^6 N/m^2), which is twice the pressure that a U-seal can withstand in the same application.

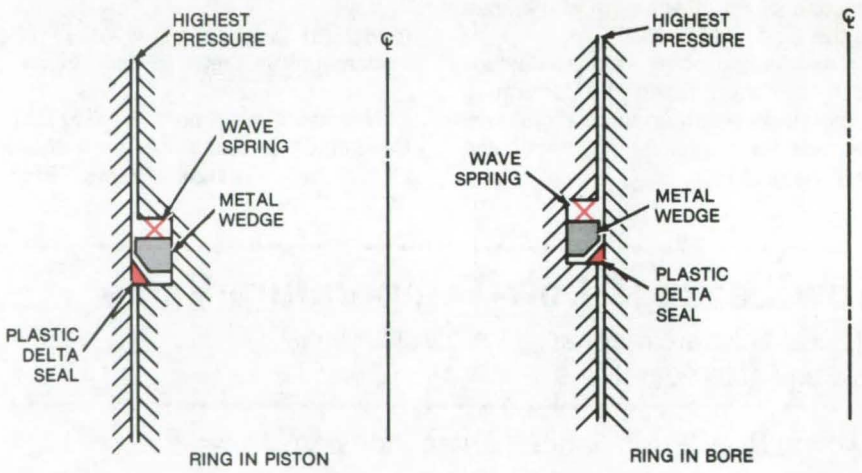

This triangular-cross-section **Delta Ring,** with the aid of a wave spring and a metal wedge, seals a cylinder in either piston or bore mounting.

This work was done by Mel E. Burr of Rockwell International Corp. for **Marshall Space Flight Center.** *For further information, Circle 72 on the TSP Request Card.*
MFS-19335

Inquiries concerning rights for the commercial use of this invention should be addressed to the Patent Counsel, Marshall Space Flight Center [see page A8]. Refer to MFS-19335.

Vacuum Leadthrough for Hydrogen Maser

Nonmagnetic leadthrough withstands severe thermal shocks.

NASA's Jet Propulsion Laboratory, Pasadena, California

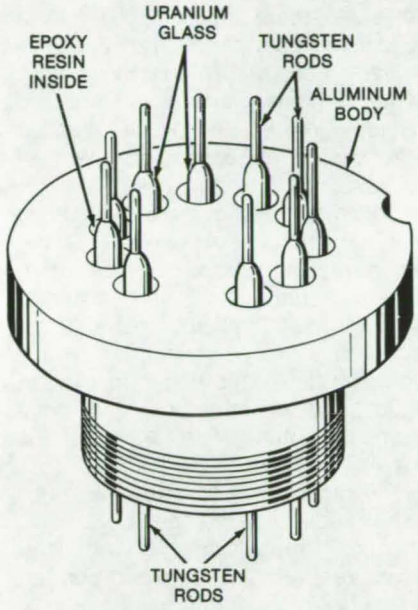

A Multipin Nonmagnetic Vacuum Leadthrough shows tungsten rods sealed with uranium glass.

Considerable work has been done with epoxy resins to obtain vacuum-tight seals with tungsten rod leadthroughs. These nonmagnetic leadthroughs are used in a hydrogen maser for electrical interconnection into the vacuum chamber. Earlier efforts to produce vacuum-tight seals had not been very successful because the seals failed during tests when the temperature was varied from -20° to 120° C.

An improved seal uses uranium glass to form a vacuum seal to the tungsten rod. An epoxy resin seals this glass-coated rod to the aluminum body. A typical multipin arrangement is shown in the illustration. The vacuum chamber is typically at 10^{-6} torr (1.3×10^{-4} N/m^2) at 46° C and is subjected to temperatures of 20° to 100° C during bakeout.

The new connector was tested successfully, using a rapid drop in temperature from 100° C to the temperature of liquid nitrogen (-196° C) in a few seconds. A vacuum test showed that the connector retained a vacuum lower than 10^{-8} torr (1.3×10^{-6} N/m^2) with no degradation in performance.

Each connector was subjected to temperature cycling between -65° to 150° C, six to seven times over a 16-hour period. To date, none of the connectors has failed this test.

This work was done by Dean A. Norris of Caltech for **NASA's Jet Propulsion Laboratory.** *For further information, Circle 73 on the TSP Request Card.*
NPO-14148

Books and Reports

These reports, studies, and handbooks are available from NASA as Technical Support Packages (TSP's) when a Request Card number is cited; otherwise they are available from one of NASA's Industrial Application Centers or the National Technical Information Service.

Electric and Hybrid Vehicles

Report assesses state-of-the-art in vehicle development.

A 598-page report has been published that presents data that characterize the state-of-the-art electric and hybrid (combined electric and heat engine) vehicles. Performance data for a representative number of electric and hybrid vehicles were obtained from track and dynamometer tests. User experience information was obtained from fleet operators and individual owners of electric vehicles. Data on performance and physical characteristics of a large number of vehicles were obtained from manufacturers and the available literature.

This report is the result of the Electric and Hybrid Research, Development , and Demonstration Act of 1976 (Public Law 94-413), which required that data be developed characterizing the state-of-the-art of electric and hybrid vehicles. The Energy Research and Development Administration (ERDA) (now the U.S. Department of Energy) was given the responsibility for implementing the Act. The National Aeronautics and Space Administration (NASA) was requested by the ERDA to develop data in support of the state-of-the-art characterization. The NASA Lewis Research Center was responsible for this project.

The purpose of this study was to characterize the general state-of-the-art of electric and hybrid vehicles, rather than to present the specific performance of particular vehicles. Vehicles selected for test and evaluation were those believed to represent collectively the state-of-the-art. User experience information was collected on over one-third of an estimated 2,000 American-built electric vehicles of all types currently operating in the United States and Canada. Detailed information also was obtained on the operation of 44 electric and hybrid buses. Additional data were collected from the literature on other vehicles in operation abroad. The report emphasizes vehicle performance,

(continued on next page)

reliability, maintenance, and driveability, but comfort, serviceability, and other characteristics of electric vehicles are also discussed.

This work was done by the Electric and Hybrid Vehicle Project Office of **Lewis Research Center.** *Further information may be found in NASA TM-73756 [N78-18988], "State-of-the-Art Assessment of Electric and Hybrid Vehicles," a copy of which may be obtained at cost from the Technology Application Center, University of New Mexico* *[see page A7].*

LEW-13077

Lines, Bellows, Flexible Hoses, and Filters

Design criteria monograph developed from NASA experience

This monograph was written to organize and present significant experience and knowledge accumulated by NASA in development and operational programs. The purpose is to assist system designers. It reviews and assesses current design practices and from them establishes guidance for achieving greater consistency in design, increased reliability in the end product, and greater efficiency in the design effort.

A liquid-propellant rocket engine and the vehicle using it represent an assembly of fluid-flow components that must be interconnected. These interconnections are provided by the lines, bellows, and flexible hoses. The fluids in a given system are maintained at a required level of cleanliness by filters that remove contaminant material.

The successful design of line or duct assemblies and their components for rocket propulsion systems is based on many considerations and factors. Some considerations are quite basic and are well grounded in theory, while others are more subtle and have been learned through many failure analyses and experiments.

The major problems in line assemblies have involved the details of the flexible-joint elements utilized. Less frequent problems have involved the entire assembly and include mechanical vibration, corrosion, contamination, thermal-cycling fatigue, static-seal leakage, handling damage, and mismade parts. The major problems with the flexible elements, in addition to those just listed, have been fatigue failures (from flexure and mechanical or flow-induced vibration), buckling-instability failure, and failure of the duct-to-bellows attachment joint. The major problems in filter design have been determining the amount of built-in, system-generated, and environmental contaminants to be filtered; contaminant capacity; flow versus pressure drop for filter elements; and the physical size of filter required to satisfy the system requirements.

The monograph begins with a discussion of the line assembly that treats the key design elements in the assembly in the logical, chronological order in which a designer would proceed. Bellows (including linkages, liners, and associated components), flexible hoses, and filters then are treated in order. Some of the design considerations in these areas overlap. For example, similar considerations apply to the design of line assemblies with flexible joints and to the design of a flexible-hose assembly; also, considerations for design of a bellows in a flexible joint are similar to those for a bellows in a flexible-hose innercore.

The monograph comprises two major sections: State of the Art, and Design Criteria and Recommended Practices. References complement the text.

Both major sections are divided into four subjects: Line Assembly (routing, sizing, pressure drop, vibration, components, materials, and testing); Bellows Joint (bellows, restraint, attachment, and flow liners); Flexible Hose (routing, sizing, innercore, braid, end construction, and bend moment); Filters (filter element and case).

The monograph is one of a series being published on space vehicle chemical propulsion, environment, structures, and guidance and control. A list of all monographs issued prior to this one is presented on the final pages of the report cited below.

This work was done by the Space Propulsion & Power Division of **Lewis Research Center.** *Further information may be found in NASA SP-8123 [N78-16089], "Liquid Rocket Lines, Bellows, Flexible Hoses, and Filters," a copy of which may be obtained at cost from the New England Research Application Center* *[see page A7].*

LEW-13075

Fabrication Technology

Hardware, Techniques, and Processes

Books and Reports

High-Gradient Continuous-Casting Furnace

High gradient allows rapid growth rates in directionally-solidified eutectic alloys.

Lewis Research Center, Cleveland, Ohio

The continuing demand for longer life, higher strength, or higher use temperature from high-temperature superalloys has created interest in the directionally-solidified eutectic (DSE) alloy systems because of their unique and attractive properties.

With currently available equipment, DSE alloys must be solidified at very slow rates (less than 1 cm/h) in order to produce the fully alined structure that gives them their unique properties. The critical growth rate above which alinement cannot be obtained is governed by the equation $G/R = C$, where G is the thermal gradient at the solidification front, R is the critical growth rate, and C is a constant. Slow production processes are generally not economical; therefore, it is desirable to make R as large as possible. Thus G must be increased. The conventional way of increasing G is to increase the degree of liquid melt superheat. This procedure in turn creates severe melt/mold reaction problems.

The high-gradient continuous-casting furnace, a significant improvement over conventional furnaces, achieves much higher values of G without requiring high degrees of superheat. Potential melt/mold reactions are minimized, and greater growth rates are permitted than are possible using conventional DSE casting methods.

A schematic of the basic furnace design is shown in the figure. The high value of G is obtained by a combination of high power across the liquid zone and close spacing between the hot graphite and the flowing coolant. High superheat in the liquid is avoided because the molten liquid layer is thin.

Two prototype furnaces have been built, each for a different alloy melting-point range: tin-lead at 392° F (473 K) and aluminum-copper at 1,022° F (823 K). Both have demonstrated values of G in excess of 1,123 K/cm. This thermal gradient is at least 573 K/cm better than the highest values found in the literature for similar specimens of these alloys 0.24 in. (6 mm) in diameter. The design is currently being modified to construct a third prototype for a nickel-base eutectic alloy to demonstrate the applicability of this innovation in the range of temperatures of commercial interest for turbine engine materials.

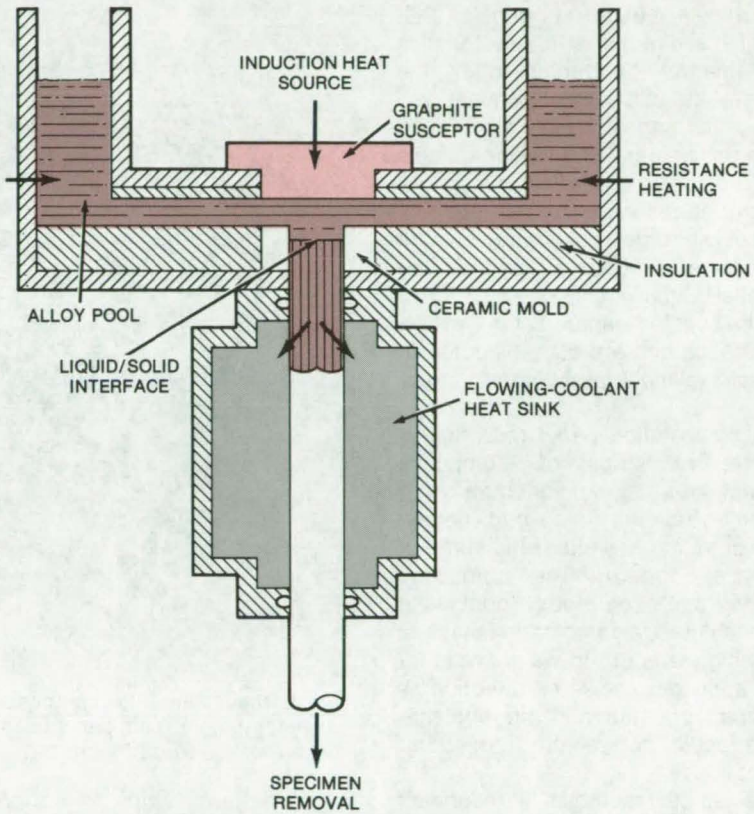

Continuous-Casting Furnace achieves a high thermal gradient by combining extensive power across the liquid zone with little space between the hot graphite and the flowing coolant.

This furnace design should permit cost reductions in the directional solidification process through its increased solidification rates, which reduces melt/mold interaction. It could be used to produce structural engineering materials for any application requiring the properties of directionally-solidified eutectic materials.

This work was done by Coulson M. Scheuermann of **Lewis Research Center** *and Merton C. Flemings, Michael A. Neff, Bernard A. Rickinson, and Kenneth P. Young of the Massachusetts Institute of Technology. No further documentation is available.*

Title to this invention has been waived under the provisions of the National Aeronautics and Space Act [42 U.S.C. 2457(f)] to the Massachusetts Institute of Technology, Cambridge, Massachusetts 02139.

LEW-12934

Lattice Panels With High Structural Efficiency

By orienting strips for maximum strength a composite lattice panel can be made nearly as strong as "conventional" composite panels.

Langley Research Center, Hampton, Virginia

"Lattice" structural panels that exploit the directional characteristics of filamentary materials offer the strength and stiffness of conventional composite panels, but are much lighter in weight. The lattice panels were originally conceived for large-area structures in spacecraft (such as for solar-energy collectors) where stiffness rather than strength is the essential requirement; however, they can be custom-tailored for various applications and are also expected to be useful in moderately loaded structures.

A typical lattice panel (see figure) consists of strips of composite material in a regular geometric arrangement on an open-grid honeycomb core that has either the same or a similar pattern. The composite material could be epoxy containing graphite fibers, a combination that has a very high strength-to-weight ratio for loads applied in the same direction as the fiber orientation. Different materials could be selected for other applications.

The lattice resembles a redundant truss and, like such a truss, has high structural efficiency (strength-to-weight). The panel is considerably more efficient at light loading than conventional sandwich panels, since in the latter, glue weight, skin thickness, and core density cannot be reduced below certain minimum levels, even if the loading is expected to be very light.

The spacing, the width, and the angle of the strips in the lattice panels can be changed as necessary. Multiple layers can be laminated together in any orientation on selected strips; and one or more strips can be omitted in an otherwise isotropic pattern. When the panel must support a low-pressure lateral load, a film or a multi-ply laminate can be bonded over the entire surface.

The panels are made in an aluminum mold into which slots have been machined according to the desired lattice pattern. Strips of epoxy tape preimpregnated with graphite are laid in the slots.

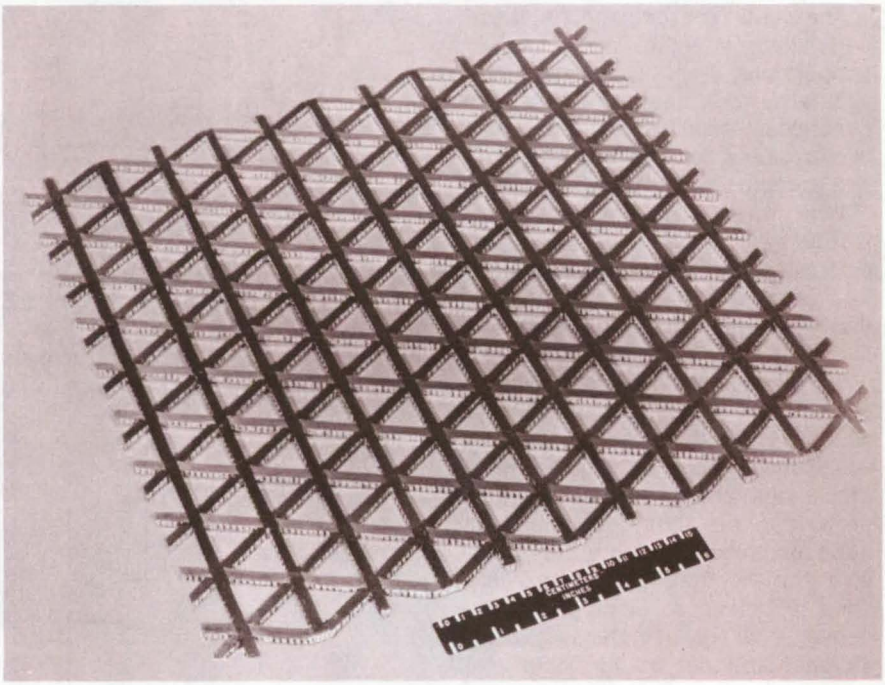

This **Lattice Panel** is composed of epoxy/graphite-fiber strips bonded to a honeycomb core. This panel uses strips 0.25 in. (0.63 cm) in width having a lattice spacing of 1.5 in. (3.75 cm).

A honeycomb core is cut out in the lattice pattern. A special cutting tool has been developed for this operation. The tool uses a single-edge razor blade as the cutting edge. A spring-loaded plunger removes the cut section from the tool after the section has been cut. The template is cut from thin aluminum sheet on a numerically-controlled milling machine.

The core is coated with an epoxy resin for bonding and is placed on the strips in the mold. The mold is covered and loaded with weights, and the mold is heated gently to cure the bonding resin. The low heat also allows the resin to flow, improving the bonds between strips.

Next, the panel is removed from the mold, is vacuum-bagged, and is placed in an oven to cure the resin in the graphite. For this step, the panel must be removed from the mold because the relative expansions of the panel and the aluminum mold would cause bending or cracking. However, if the mold were machined from a low-expansion material such as graphite or ceramic, the lattice could be completely bonded and cured in the mold.

This work was done by Martin M. Mikulas, Jr., and Marvin D. Rhodes of **Langley Research Center.** *Further information may be found in NASA TMX-72771 [N75-32160], "Composite Lattice Structure," a copy of which may be obtained at cost from the North Carolina Science & Technology Research Center* *[see page A7]*.

This invention has been patented by NASA [U.S. Patent No. 4052523 and 4063981]. Inquiries concerning non-exclusive or exclusive license for its commercial development should be addressed to the Patent Counsel, Langley Research Center *[see page A8]*. *Refer to LAR-11898.*

Low-Cost Graphite/Epoxy Structural Panels

Improved manufacturing process precures components of composite panels prior to assembly.

Marshall Space Flight Center, Alabama

To reduce the weight of spacecraft body structures, wide varieties of shell panel designs and manufacturing methods have been investigated by the aerospace industry. A promising structural design makes use of graphite/epoxy materials fashioned into a thin laminate skin and a grid structure for stiffening. At present these panels are made by an expensive manual process that costs $40 to $200 per pound. (Aluminum and titanium alloy panels, by comparison, cost $2 to $15 per pound.) However, a new fabrication technique can make graphite/epoxy panels less expensive.

The improved process separately cures the graphite/epoxy skin, stiffener ribs, and stiffener grid. After curing, the panels are assembled using a special adhesive (see Figure 1). The stiffening grid, which is the most complex and time-consuming component to make individually for each panel, is cured as a whole billet and later sliced into many grids (see Figure 2). These improvements make the process adaptable to mass production techniques.

The skin laminates are placed on an aluminum tool and cured in an autoclave. In mass production, up to 20 laminates can be cured in one run. A similar process can be used to produce quantities of stiffener ribs; they are cut from a precured large flat graphite/epoxy laminate. The ribs stiffen the foam/fiberglass web grid, as can be seen in Figure 1. Web grid details are grooved to different depths in different directions so that stiffener ribs may be interlocked, providing improved structural strength. Film adhesive bonds the components into a single, integral panel.

The fibers of the graphite/epoxy laminate can be placed in preferred directions, such as axially on stiffener flanges or cross-plied on stiffener shear webs. Other laminate orientations can be used for special applications. With the implementation of cost-effective manufacturing techniques,

(continued on next page)

Figure 1. This **Lightweight Graphite/Epoxy Panel Assembly,** consisting of a thin skin reinforced with stiffeners, can resist design loads without buckling or breaking.

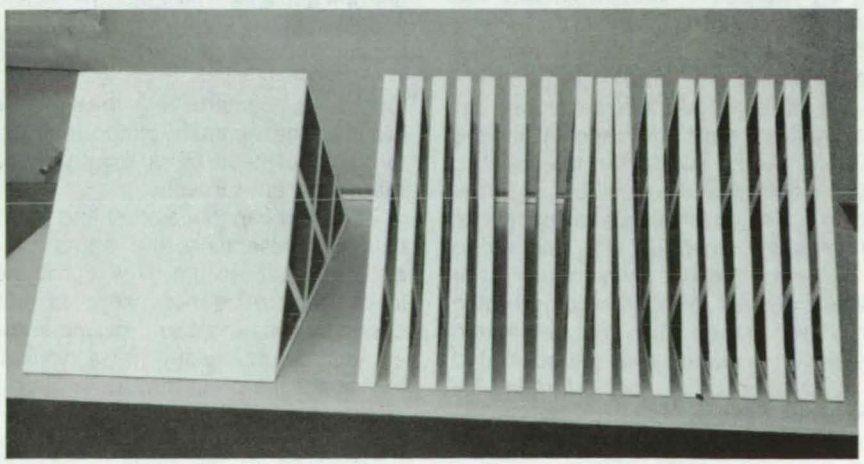

Figure 2. **Economical Mass Production** of stiffener grids is achieved by curing a billet and then slicing it into sections.

uses of the graphite/epoxy laminate panels may be found in other areas such as the auto industry.

This work was done by John R. Lager, Dan Padilla, Walter F. Thiemet, and Donald A. Thomas of Martin Marietta Corp. for **Marshall Space Flight Center.** *For further information, Circle 74 on the TSP Request Card.*

Inquiries concerning rights for the commercial use of this invention should be addressed to the Patent Counsel, Marshall Space Flight Center [see page A8]. Refer to MFS-23871.

Welding Fixture for Thin Metal Parts

A simple fixture applies constant uniform pressure to thin parts.

Goddard Space Flight Center, Greenbelt, Maryland

Thin metal parts present special problems in welding because they tend to warp when exposed to high heat, making it difficult to maintain uniform contact between the mating surfaces over the entire weld joint. In some cases, airgaps can develop, degrading the integrity of the weld. Although this can be troublesome with tack or spot welding, it is totally unacceptable when welding pressure vessels and other hermetically sealed containers.

Many of these difficulties can be eliminated by using a welding fixture similar to the one shown in the figure. Originally conceived for welding end caps to ultrathin cylindrical housings for implantable medical electronics, the basic approach, that of supporting the entire part contour and applying uniform pressure to the joint, should be useful in fabricating other lightweight metal structures.

The welding fixture has three essential components: a spring-finger collet that applies pressure to the joint, a compressing device for tightening the collet, and a mandrel that supports the parts. Besides preserving the contour of the parts, the mandrel also functions as a heat sink.

In the configuration developed for cylindrical housings, shown in the figure, two screws fasten the collet to the mandrel and adjust the mandrel height. The collet is installed so that its fingers are lined up with the entire circumference over which the parts are in contact. Next, the compressing device, shaped like an open-ended cylinder, is placed over the collet and is tightened by a screw through its bottom surface. As the screw is turned, it compresses the fingers around the entire circumference, forcing the metal parts together and readying them for welding.

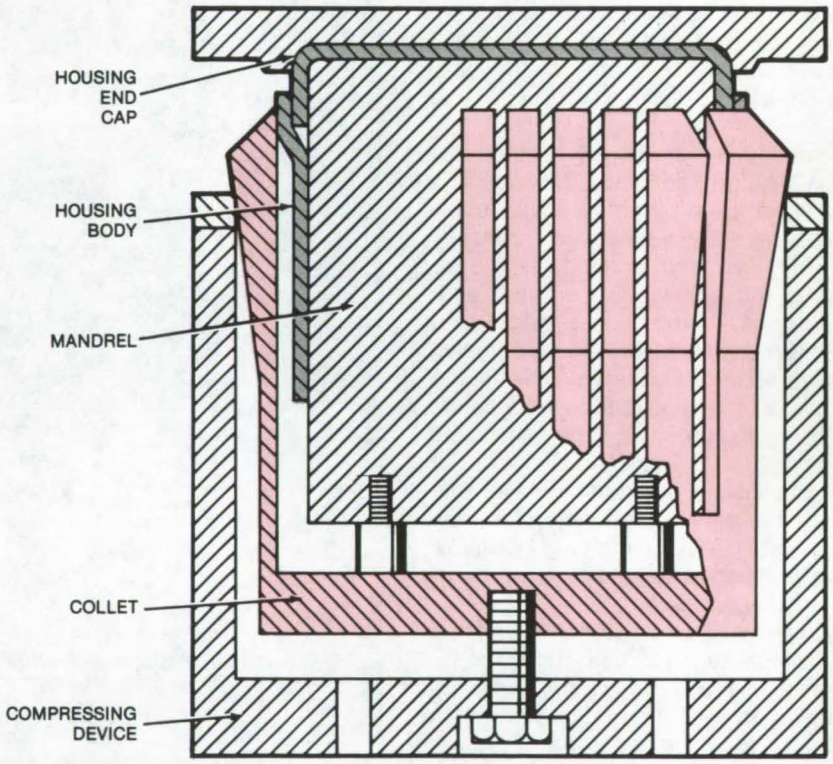

This Welding Fixture holds two thin metal cylindrical parts (in gray) together with uniform pressure. The spring-finger collet maintains a tight grip over the metal parts to eliminate any airgaps. This method can be used to prepare miniature housings for implantable medical electronics and to fabricate other thin metal structures.

To weld a cap to the other end of the housing, essentially the same procedure is carried out except that the inner mandrel is not used. In this case, the first end cap provides some of the structural rigidity that is required to prevent the parts from deforming.

This work was done by Sidney R. McClure of **Goddard Space Flight Center.** *For further information, Circle 75 on the TSP Request Card.*

This invention is owned by NASA, and, a patent application has been filed. Inquiries concerning nonexclusive or exclusive license for its commercial development should be addressed to the Patent Counsel, Goddard Space Flight Center [see page A8]. Refer to GSC-12318.

Holding Fixture for Variable-Contour Parts

Array of vacuum cups on spindles holds parts for safe machining and other processing.

Lyndon B. Johnson Space Center, Houston, Texas

An array of vacuum-cup spindles mounted on a specially designed housing (see Figure 1) acts as a chuck to hold irregularly shaped objects. Each spindle is a hollow cylinder with openings on both ends; suction applied through each spindle holds the cup flush against the variable-contour part. A coiled spring is located on the bottom of each spindle for vertical support (see Figure 2).

When the part is laid on the cups, each spindle moves up or down to adjust to its shape. Next, a vacuum is pulled through each spindle, securing the cups flush against the contoured part. Then air pressure is applied through a separate compartment in the housing to actuate a rubber diaphragm that pushes V-shaped locking plugs against the sides of spindles, locking them in a fixed position.

The variable-contour part resting on this fixture is held firmly enough for machining, coating, or other mechanical treatment.

This work was done by Cyrus C. Haynie, Poley N. Packer, and Paul P. Zebus of Rockwell International Corp. for **Johnson Space Center.** *For further information, Circle 76 on the TSP Request Card.*

This invention is owned by NASA, and a patent application has been filed. Inquiries concerning nonexclusive or exclusive license for its commercial development should be addressed to the Patent Counsel, Johnson Space Center [see page A8]. Refer to MSC-16270.

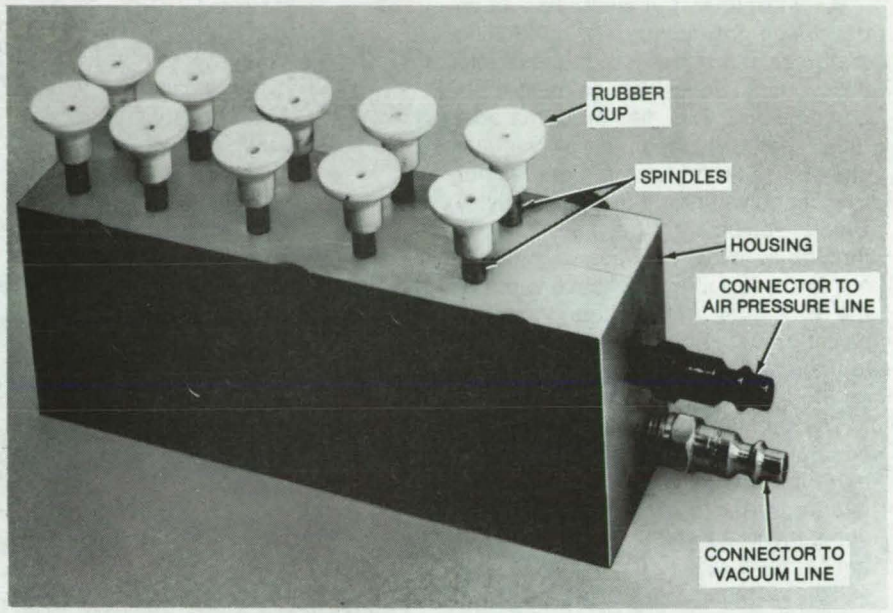

Figure 1. **Vacuum-Chuck Fixture** for securing variable-contour parts uses spindles with rubber cups.

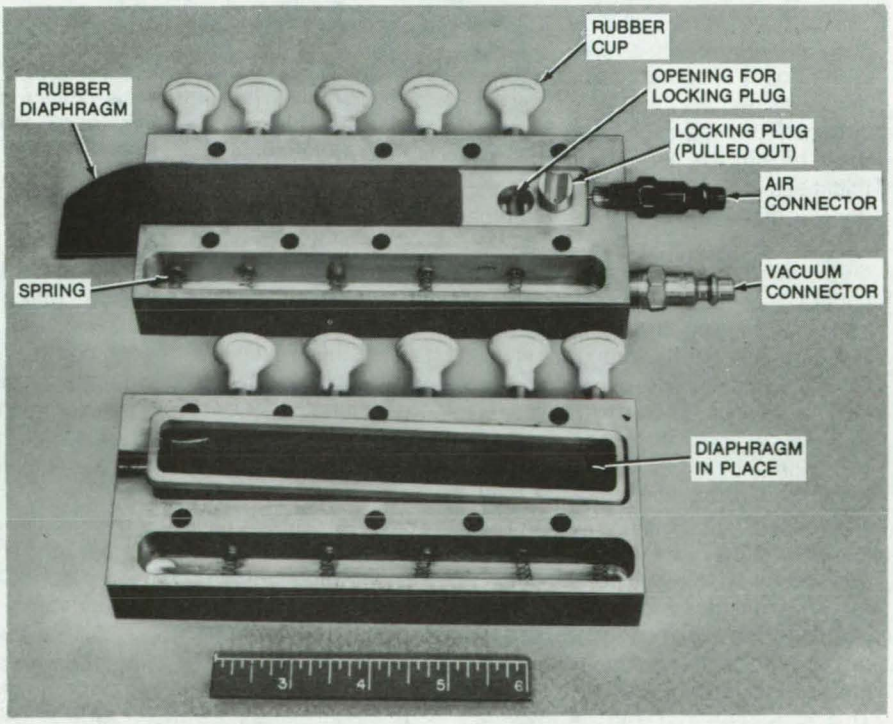

Figure 2. **Partially Disassembled** view of the fixture shows the springs that allow the spindles to adapt to parts contours and shows the diaphragm and locking plug of the air-pressure-operated arrangement for locking the spindles in place.

Control of Dielectric Film Deposition

Airgap capacitor in deposition chamber is used to monitor deposition.

Lewis Research Center, Cleveland, Ohio

An inexpensive method has been developed for accurately controlling and measuring dielectric film thickness during deposition on electronic components. The dielectric material must be deposited in a vacuum chamber. Starting with a dimer rather than a polymer and using relatively simple equipment, the dimer moves through a two-step heating process and is converted to a reactive vapor of the monomer. When this vapor is passed over components at room temperature, the vapor polymerizes on the surface rapidly and uniformly.

The problem has been to regulate accurately the coating process to meet the target film thickness on the interior surfaces of hybrid electronic components as well as to maintain the critical feed rate in the range of film thickness from 0.4 to 4 mils (0.0 to 0.1 mm). [Oscillating quartz crystals are commonly used to measure thin-film thickness below 0.1 mil (0.003 mm).]

This new method uses an inexpensive, variable-airgap capacitor shown in the figure. The important feature in the capacitor is that the distance between the opposite-polarity plates must be no less than twice the film thickness to be measured. The capacitor is located in the vacuum chamber during the deposition process. The dielectric film being deposited continuously coats the capacitor plates, as well as the electronic components being processed; the vacuum between the plates (dielectric constant, E_r = 1.0) is displaced with the coating material, which has a greater dielectric constant.

As the film thickness on the plates increases, there is a measurable rise in capacitance. Various sizes of capacitor can be used depending on the film thickness desired. As an example, the dielectric material used for Space Shuttle components had a dielectric constant of 2.95 at 10^3 Hz. This is 5.7 pF per mil of thickness (0.23 pF per micrometer), using a capacitor with a 4-mil (0.1-mm) gap. The capacitor signal is conditioned by an autoranging capacitance bridge and fed into a data-acquisition system. The critical feed rate (deposition rate) is maintained by plotting capacitance as a function of time and adjusting the dielectric (vaporizer) temperature over the predetermined deposition time.

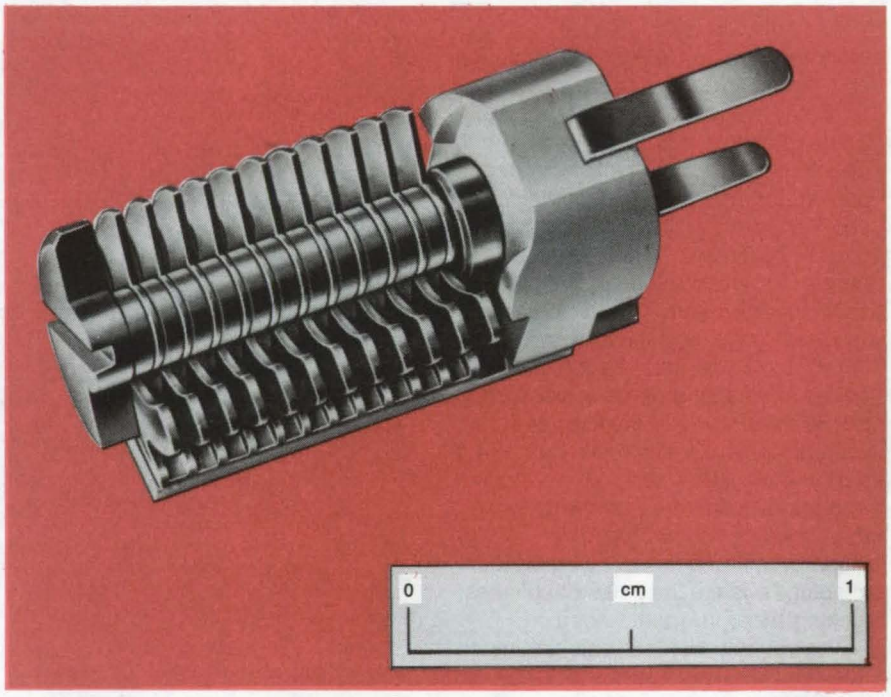

Variable-Airgap Capacitor is placed in the vacuum chamber during deposition of dielectric films. Dielectric film on the capacitor plates changes the capacitance, which is monitored for control of the process. As indicated in the text example, accuracy will depend on the dielectric constant of the film. Many materials have dielectric constants with values greater than 3 (viz Al_2O_3 = 10). Since capacitance is a direct function of the dielectric constant, the higher that value, the more accurate the control.

Through the use of the desired film-thickness capacitance signal and a programed limit-set point, the deposition process will automatically stop at the desired film thickness. The capacitor can be reused until the aggregate thickness of the deposited film equals one-half the plate-to-plate gap. Since the capacitors cost less than $2 each, they are usually discarded rather than cleaned for reuse.

The coating process is completely uniform over edges, points, and internal areas. Areas not requiring coating can be masked. Since the deposition process is accomplished at or near room temperature, there is no risk of thermal damage to the coated components. With this new control method, deposition material is fully utilized, and no excess coating is necessary to insure protection of the coated parts.

This work was done by Edwin C. Graebner and Thomas J. Riley of **Lewis Research Center.** *No further documentation is available.*
LEW-13092

Repairing Pin-Fin Cold Plates

Inexpensive technique avoids high temperatures that deform thin stainless steel plates.

Lyndon B. Johnson Space Center, Houston, Texas

Stainless-steel pin-fin cold plates are frequently used as walls in heat exchangers and pressurized containers. Since the face surfaces of these plates can be relatively thin (on the order of 0.3 mm) they may be easily perforated during handling. Repairs are difficult because the high temperatures of conventional brazing or welding can deform the plate.

A new approach for making a flush repair of a perforation in the face of the cold plate involves installing a repair disk in a prepared area surrounding the perforation. The disk is first tack-welded into place and is then torch-brazed at the edges, using a silver braze-alloy ring and flux paste.

The procedure is shown in the illustration. First, the depressed area surrounding the perforation is machined (spot-faced) to accept the disk. In a typical application developed for the Space Shuttle, the repair disks were 0.005 in. (0.127 mm) thick and 0.250 in. (6.35 mm) in diameter. The disk is tack-welded in place, using a capacitance discharge. In the next step, a ring of silver braze alloy and flux paste is applied around the disk edge, which is then torch-brazed. The repaired surface is finished by trimming the excess alloy.

Cold plates repaired by this method have been tested successfully at pressures of 135 psi (932×10^3 N/m2). Because the repair disks have small diameters, the repaired area can sustain greater loads than the larger unsupported areas of the faceplate.

This work was done by Emil P. Ruppe of Rockwell International Corp. for **Johnson Space Center.** *No further documentation is available.*
MSC-16424

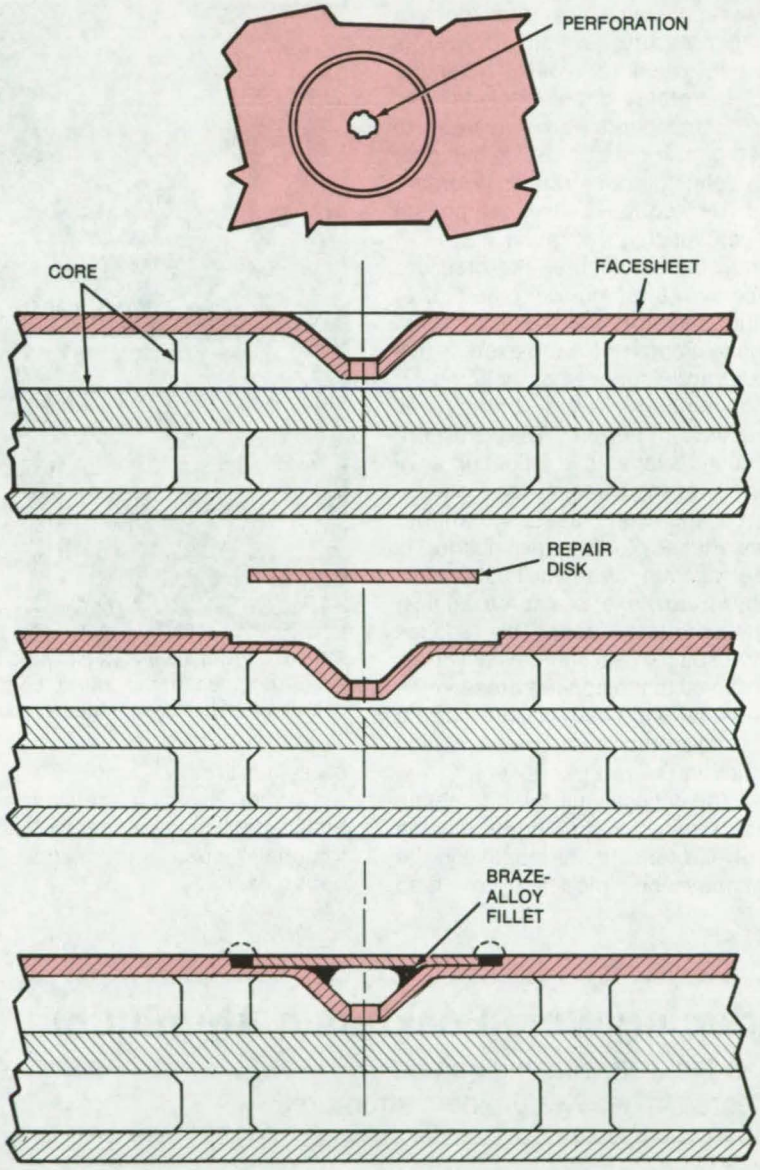

In an **Effective Cold-Plate Repair Technique,** the perforated area is spot-faced (top) to accept a repair disk (center). The disk is tack-welded into place, and then it is brazed, using a silver braze-alloy ring with flux paste around the disk edges. The repaired area is dressed down flush with the plate surface (bottom).

Riveting-Force Gage

A gage monitors riveting forces applied when components are mounted on printed-circuit boards.

NASA's Jet Propulsion Laboratory, Pasadena, California

The application of the correct riveting pressure (swaging force) is important when terminals, mounting studs, integrated-circuit sockets, and other components are riveted to printed-circuit substrates. If the rivet is too tight, the substrate may break; and if it is too loose, the component may not withstand vibration.

A new gage measures the pressure applied by a swaging tool (see figure) and thus monitors the riveting forces. The gage incorporates a piezoresistive pressure transducer, a potentiometer, a milliammeter, and a battery, all connected in series. The pressure transducer is located in a floating anvil assembly of the swaging tool.

When the swaging tool hammer strikes the anvil, the anvil fixture is forced against the anvil shoulder, which, in turn, exerts a force against the pressure transducer. This reduces the transducer resistance, which is proportional to the applied pressure. A proportional increase in the current flow is registered on the meter, which indicates in the range between 0 and 50 μA. The gage is calibrated to obtain a predetermined microampere reading for a given pressure. Alternatively, the gage may be modified to read pressure directly.

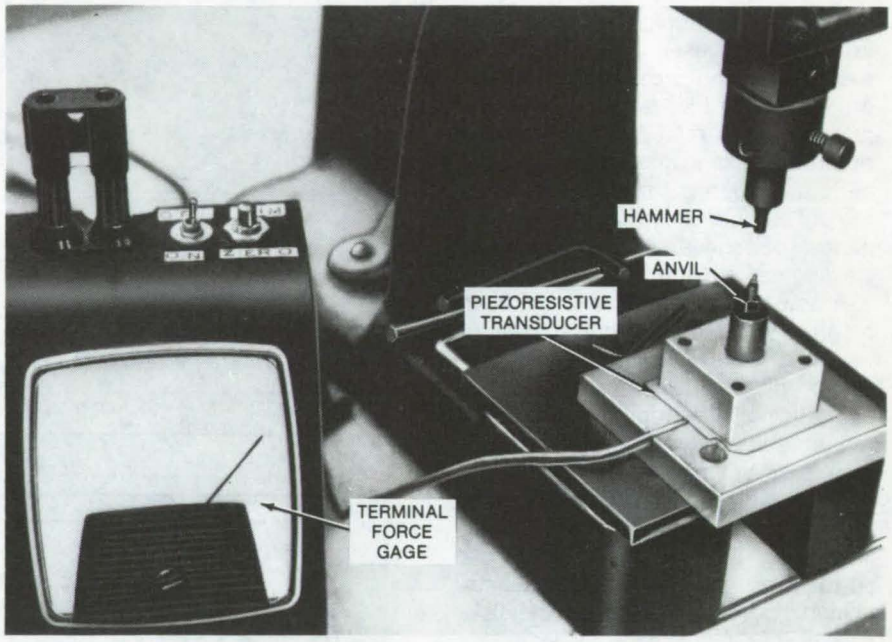

This **Swaging Tool Has Been Fitted With a Force Gage** to determine riveting forces accurately when mounting components on printed-circuit boards. A pressure-sensitive transducer is placed between the anvil and the baseplate.

Correct swaging pressures have been established for specific substrate materials such as phenolics and ceramics.

This work was done by James W. Rotta, Jr., of Caltech for **NASA's Jet Propulsion Laboratory.** *For further information, Circle 77 on the TSP Request Card.*
NPO-13477

Reducing Weld Peaking in Aluminum

Excessive weld peaking can be corrected in heavy aluminum structures.

Marshall Space Flight Center, Alabama

Weld peaking can weaken welded joints and make it difficult to aline mating parts. It can also degrade the appearance of welded assemblies. Peaking due to weld shrinkage can be predicted in simple structures; however, in complex assemblies, peaking is not predictable because of unknown stress induced by fixturing, stresses propagated from other welds in the assembly, and stresses that arise during machining and forming.

A new study finds that excessive peaking can be corrected by taking advantage of the shrinkage forces that develop during welding. The corrective procedure was developed by studying welded joints on the Space Shuttle rocket booster. Typical weld joint thicknesses were 1.375 in. (3.493 cm), welded from both sides.

Data collected during the experiments show variations in peaking along a single joint and from one joint to the next. Since no obvious patterns were observed, it was concluded that the variations were due to nonwelding stresses such as those from fixturing. This conclusion is supported by other tests that show consistent peaking on unstressed welds.

It was found that approximately 1° of peaking per pass resulted when welding either grooved joints or flush weld joints; the amount of peaking is unrelated to the amount of filler wire added. In addition, welding on a crown results in less peaking than welding on a flush surface or in a groove.

The following steps can be taken to correct excessive peaking:

1. Identify and measure the extent of the peaking.
2. Shave off the weld head flush on the opposite side of the peaked joint.
3. Mount the assembly on a support to reduce all external forces on the joint to a minimum.
4. Make a weld pass on the weld head centerline, using the same weld parameters as those for the fill passes, without adding a filler wire.
5. Measure the peaking, and repeat the operation as necessary.

Approximately 1° change is expected per pass on a 1.375-in. weld joint, provided that there are no external stresses on the joint area. When the peaking varies along the weld joint, the weld energy must be varied to compensate for the nonuniformity.

This work was done by E. Bayless, R. Poorman, and J. Sexton of **Marshall Space Flight Center.** *Further information may be found in NASA TM-78176 [N78-25427], "Weld Peaking on Heavy Aluminum Structures," a copy of which may be obtained at cost from the New England Research Application Center [see page A7].*

MFS-23973

Process for Growing Thin Polished Silicon Sheets

Single-crystal sheets pulled from molten silicon floating on a refractory melt would require no slicing or polishing.

NASA's Jet Propulsion Laboratory, Pasadena, California

In conventional methods of producing silicon substrates for solar cells and other solid-state devices, bulk ingots of silicon are sliced into wafers and then lapped or polished. These mechanical finishing operations, which can add considerably to the cost of the solid-state device, are not necessary in a proposed new process that would grow polished silicon sheets directly from the liquid melt.

In the proposed new method, the single-crystal sheet is drawn from a thin layer of molten silicon floating on a pool of molten refractory material. As the temperature is lowered through the melting point of the silicon, the smooth upper and lower surfaces of the liquid are "frozen," yielding a flat highly-polished solid sheet.

Two variations have been suggested: a vertical process based on the commonly-used Czochralski method for growing silicon ingots and a horizontal process that could be adapted for continuous production.

In the vertical-growth method (Figure 1), a small seed of silicon is introduced from the top, and the melt temperature is reduced gradually to allow crystallization. When the temperature drops to 800° C, the seed is slowly pulled upward, carrying with it a polished silicon-crystal sheet. When the silicon melt is used up, the furnace is opened and recharged with

(continued on next page)

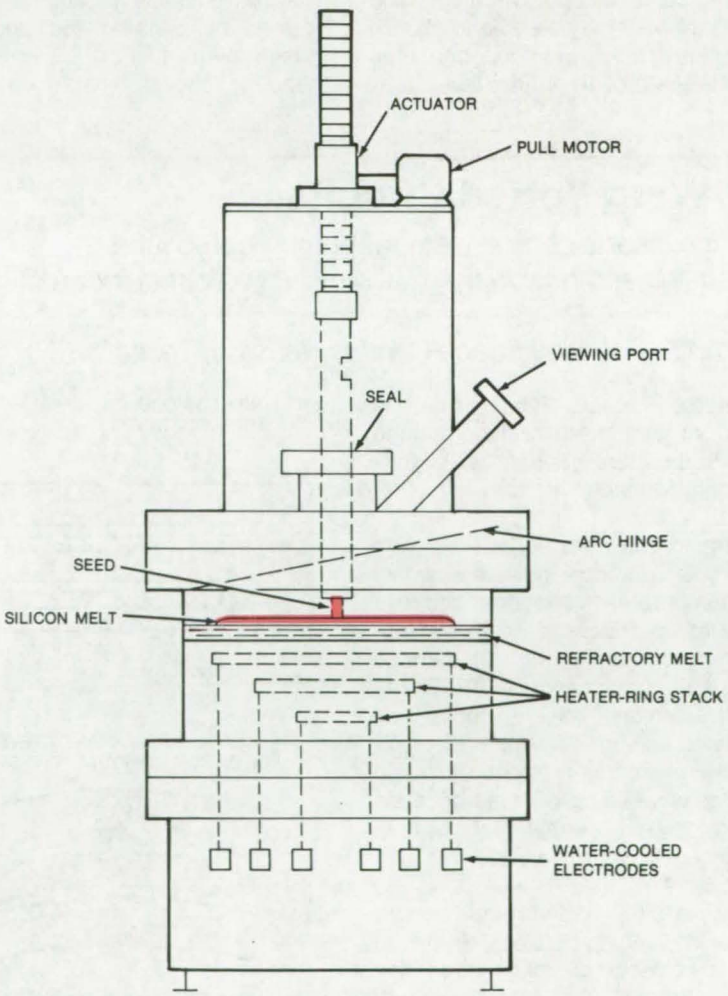

Figure 1. In a **Vertical Process** for growing polished single-crystal sheets of silicon, molten silicon is solidified and lifted in one piece off a molten substrate of refractory material. The stainless-steel melt chamber is water cooled.

fresh silicon. The temperature is raised, and the cycle is repeated.

In the horizontal-growth version (Figure 2), the silicon melt is elevated to the level of a slot in the side of the chamber, through which the seed is inserted; the solidified sheet is then pulled out. A heater creates a temperature gradient that controls the growth interface and the growth rate and helps to avoid thermal shock. The silicon melt can be replenished from a separate container, making continuous automated production possible.

Both processes would yield a smoothly finished surface. The silicon sheet can be used as a substrate for chemical vapor deposition without further mechanical preparation.

The refractory melt that supports the silicon should be nonreactive with silicon and should have a lower melting point. It should also have a low vapor pressure. Possible materials are chlorides and fluorides of barium, calcium, and strontium. The refractory melt may be able to absorb impurities from the silicon and thus obviate postgrowth purification.

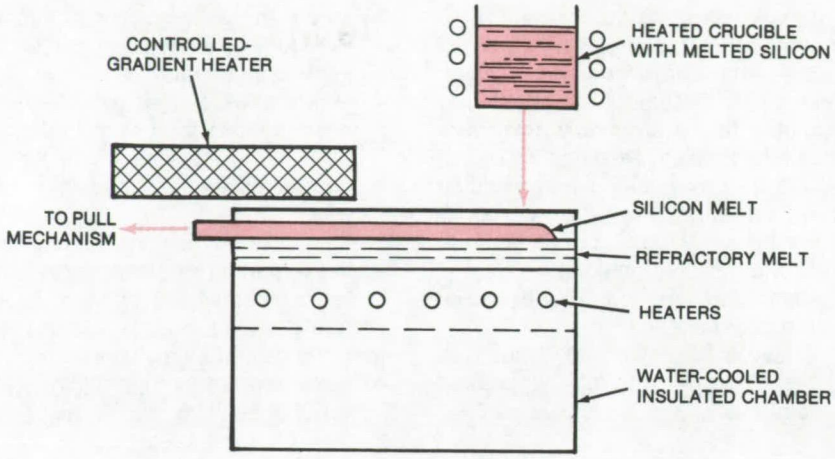

Figure 2. A Horizontal Process removes a continuous sheet of silicon through a slot in the side of the melt container. The process would proceed in a chamber containing an inert gas such as argon.

Because of the small amount of material in the melts, energy for heating is greatly reduced. Also, because the silicon is in thin sheets, it may be possible to dope it as it is formed by passing the appropriate gases over it. For convenience in handling, the sheet can be cut into pieces as it emerges from the pulling machine.

This work was done by Charles C. Radics of Caltech for **NASA's Jet Propulsion Laboratory.** *For further information, Circle 27 on the TSP Request Card.*
NPO-14172

No-Warp Potted Circuits

Sponge inserts compensate for potting-compound expansion and relieve thermal stresses on circuit boards.

Lyndon B. Johnson Space Center, Houston, Texas

Potted printed-circuit boards can be kept from warping by placing sponge pads on the circuit boards when they are encapsulated in potting compound.

Warping can be a serious problem when potted boards are subjected to wide temperature variations, because temperature-induced stresses can distort the assembly enough to damage wiring and components. In the Space Shuttle Orbiter, for example, an excessive number of potted 10-channel thermocouple-reference-junction modules were being rejected because of warping after thermal-cycle tests in the range of -160° to +280° F (-107° to +138° C).

The warping was brought under control by adding 1/8-in. (3.2-mm) pads of closed-cell silicone sponge rubber before the modules were potted in silicone compound (see figure).

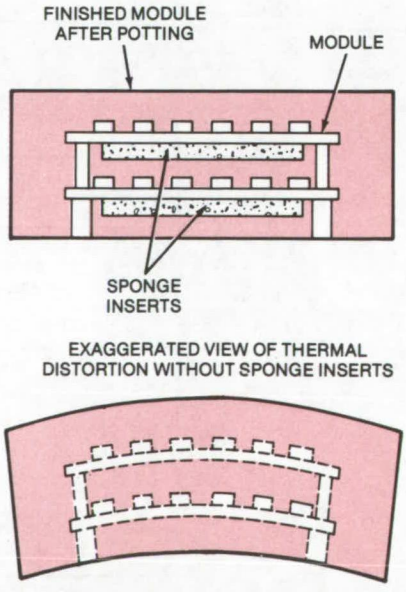

Isocellular Silicone Sponge Pads keep electronic circuit boards flat even when temperature varies over a wide range.

The sponge pads not only reduce warpage as the temperature of the environment changes but also relieve stresses on the circuit board as the potting compound shrinks during curing. Thus the technique might be expected to improve the quality of production runs of PC boards intended for applications in environments less severe than those for aerospace equipment. Moreover, the pads reduce the weight of the modules because they weigh far less than the potting compound they displace.

This work was done by Wayne W. Robinson of Rockwell International Corp. for **Johnson Space Center.** *No further documentation is available.*
MSC-19729

Fastener for Thin Fragile Materials

Two-part fastener secures
delicate parts without damaging them.

Lyndon B. Johnson Space Center, Houston, Texas

A new two-piece fastener is ideal for securing thin delicate parts that might be damaged by conventional fasteners, such as rivets or upset collars. Nevertheless, the strength of the new fastener approaches that of a riveted connection. It is easily fabricated, is tamperproof, and will not unlock under stress or vibration. Moreover, assemblies can be taken apart if necessary by drilling through the fastener — an option not available if an adhesive bond is used.

The fastener consists of a plastic button and a spring-steel collar (see figure). These parts have a large contact area, to distribute loads on delicate assemblies, and a low profile so that they can fit into narrow spaces.

The button contains two detents spaced 90° apart. The collar has a retention slot and a lip. To engage the fastener, the upper detent on the button is inserted into a matching slot on the bottom of the collar. The button is then rotated and pushed to guide the lower detent through the same slot. This procedure bends open the spring-steel tabs at the top of the collar. The button is then rotated again so that the upper detent alines with the slot between the tabs. At this point the tabs snap back into their original positions, locking the upper detent firmly in place. The tabs also apply spring pressure against the lower detent, capturing the button in the collar and exerting a compressive force that retains the assembly.

Both the button and the collar contain holes for spanner-type tools. One tool would hold the collar while the other would turn the button. If there is enough clearance around the assembly, both the button and the collar can be provided with tabs that would allow the fastener to be tightened with the fingers.

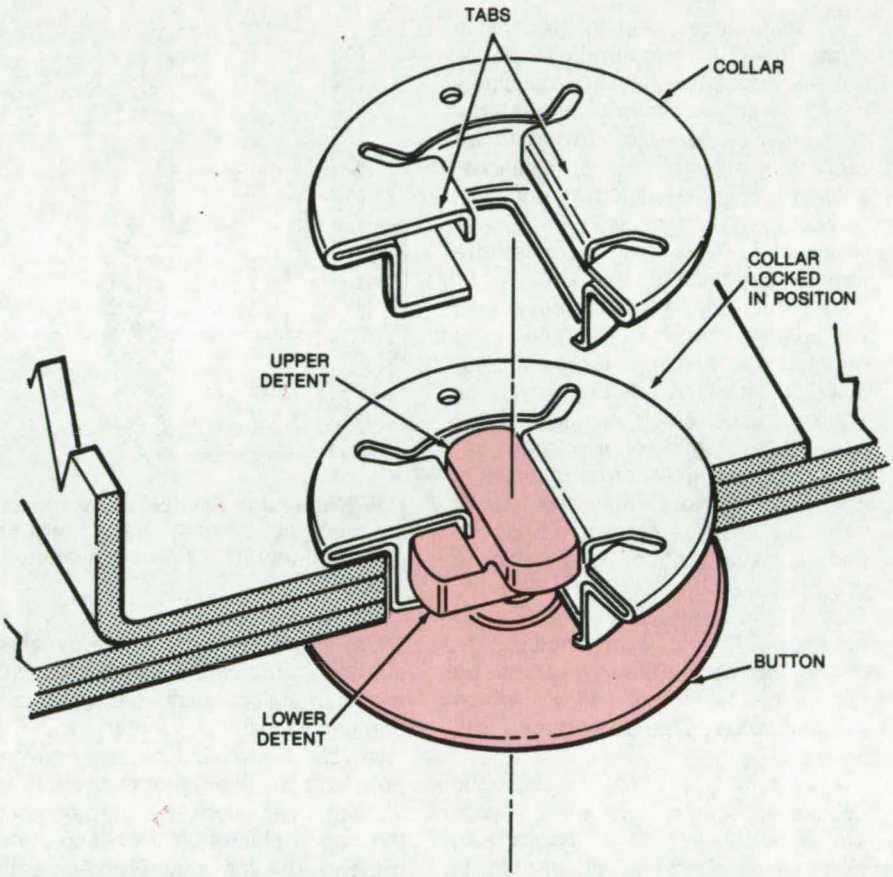

Tabs on a Collar press against the lower detent of a button so that collar and button exert a compressive force on thin-section parts, holding them firmly together.

The two parts could be made by conventional mass-production methods: the button by injection molding and the collar by forming seamless tubing. Each element is one piece, so no bench labor or assembly procedures would be needed.

The fastener is suitable for materials ranging in density from sheet metal to fabric sandwiches. Parts as thin as 0.050 inch (0.127 cm) can be readily accommodated.

This work was done by Stanley Sokol of Rockwell International Corp. for **Johnson Space Center.** *No further documentation is available.*
MSC-18097

Ceramic-to-Metal Vacuum Seal

A knife-edge joint between metal and ceramic absorbs stress from unequal expansion and contraction.

NASA's Jet Propulsion Laboratory, Pasadena, California

A knife-edge sealing technique forms reliable, vacuum-tight bonds between materials having very different thermal-expansion characteristics, such as ceramic and Monel (or equivalent alloys). With conventional sealing techniques, such as butt-joint or compression seals, the bonds would tend to crack under severe temperature cycling.

The knife-edge seal was developed for bonding ceramic to metal in a nonmagnetic package for an image-dissector tube. A material such as Kovar is usually selected for metal/ceramic packages for electronic devices because the thermal expansion coefficient of Kovar matches that of ceramics such as beryllia. For these materials, conventional seals can be used because the metal and ceramic expand and contract together (up to about 700° C). However, because the image dissector tube had to be nonmagnetic, Monel alloy, which expands twice as fast as ceramic, was selected.

The knife-edge seal is thin and flexible and can absorb shear, hoop, and bonding stresses at the joint so that the seal remains vacuum-tight. In addition, the metal cap alines itself with the ceramic base in the proper position for bonding (see figure).

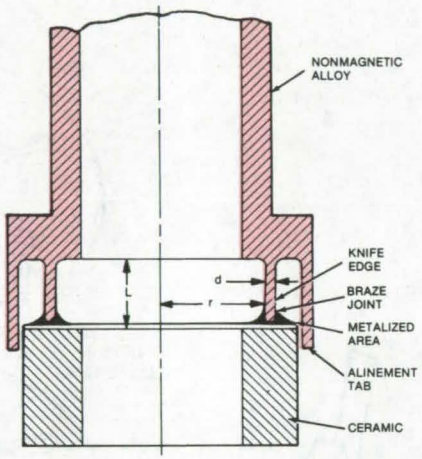

This **Knife-Edge Seal** between a metal cap and a ceramic base remains vacuum-tight under severe temperature cycling.

To form the seal, the sealing surface on the ceramic is coated with a thin metallic layer that is braze-compatible with the metal cap. The layer can be applied by any conventional metalization process, such as vacuum deposition. The knife edge on the cap is placed on a brazing-metal preform on the metalized ceramic base. Three tabs on the cap aline it with the base. The assembly is heated to 800° C in a wet hydrogen atmosphere, and the brazing metal joins the knife edge to the metalized layer of the ceramic.

The height of the knife edge (L) is a critical dimension, since it must be large enough to yield with thermal stress as the package cools down after brazing. The minimum height depends on the thickness (d) of the knife edge and radius (r) of the cap and on the elastic moduli of the materials. For the Monel/ceramic combination, the minimum height is $5\sqrt{dr}$. For other materials, the proportionality constant might have a value other than 5.

In tests, sealed packages with the correct knife-edge height [0.20 in. (0.51 cm), for a thickness of 0.011 in. (0.028 cm) and a radius of 0.45 in. (1.1 cm)] were temperature-cycled four times from room temperature to 400° C at a rate of 10° C per minute. No stress cracks were found. For lower knife-edge heights, however, cracks appeared in the braze material or the ceramic.

This work was done by Otmar H. Sackerlotzky of Weston Instruments, Inc., for **NASA's Jet Propulsion Laboratory.** *For further information, Circle 31 on the TSP Request Card.*
NPO-13803

Improved Method of Solar-Cell Assembly

Transparent silicone adhesive and plastic covers reduce assembly costs.

Lewis Research Center, Cleveland, Ohio

A simple method has been developed to bond solar-cell modules between a rigid or flexible base and a plastic protective cover. The method relies on using one of several commercially-available, transparent, silicone adhesives as the bonding agent.

Prototype solar-cell modules assembled using the adhesive bonding process have performed well under long-term exposure testing. Consequently, the method offers potential for facilitating the assembly of large modules of solar cells for either space or terrestrial photovoltaic converter applications.

The process involves spreading a thin layer (less than 2 to 3 mils) of silicone adhesive on one side of both the base and plastic cover to be used or directly on the cells. Next, a "solar-cell sandwich" is made by placing the module on the adhesive-covered base and covering the module with the adhesive-coated plastic cover or by placing the coated cells between the cover and the base. The unit is then placed between silicone-rubber sheets and held in a press under moderate pressure to insure complete contact between the various layers.

Various materials have been used for bases and covers in prototype

module assemblies. Base materials have included anodized aluminum, fiberglass, polyimide film, and Formica; while plastic covers have been made from 2- and 5-mil fluorinated ethylene propylenes and perfluoroalkoxy, polyethersulfone, and polycarbonate resin.

Previous methods of solar-cell assembly required using individual quartz or glass covers for cell protection. Glass covers have also been applied using a transparent adhesive. However, quartz or glass covers are expensive, and labor costs are high when cells must be covered individually.

With the adhesive bonding method, solar-cell modules can be assembled easily and rapidly. Since the plastic covers are not applied under conditions of high temperature and pressure, no stresses are introduced in the final package. Should it ever be necessary to repair or replace some part of the assembly, it may be possible to remove the cover without destroying the package since the adhesive remains flexible.

This work was done by Jacob D. Broder, Americo F. Forestieri, and Joseph Mandelkorn of **Lewis Research Center.** *Further information may be found in:*

NASA TM-X-52875 [N70-41903], "Improvements in Silicon Solar Cell Cover glass Assembly and Packaging Using FEP Teflon,"

NASA TM-X-73674 [N77-26615], "Preliminary Results of Accelerated Exposure Testing of Solar Cell System Components," and

NASA TM-X-73655 [N77-22610], "Real Time Outdoor Exposure Testing of Solar Cell Modules and component Materials."

Copies of these reports may be obtained at cost from the Technology Application Center, University of New Mexico [see page A7].

Inquiries concerning rights for the commercial use of this invention should be addressed to the Patent Counsel, Lewis Research Center [see page A8]. Refer to LEW-12729.

Circuit-Lead Trimming Template

Accurate low-cost device eliminates short leads on circuit cards.

Lyndon B. Johnson Space Center, Houston, Texas

A template for use in trimming leads on production wiring boards is a low-cost means for eliminating rejections for short leads and improving lead-length uniformity. The use of conventional spacer strips to guide an operator's cutting tool often resulted in component leads being cut outside of the allowable tolerance limits. The spacer strip protected the lead that was to be trimmed from only one side so the cutter angle could easily vary to produce a slanted cut and a long or short lead.

Such failures can be avoided by using cutting templates rather than spacer strips. The template, as seen in the figure, is simply an unclad piece of printed-circuit board material that is drilled, using the same drill control tape used in making the original production board. Any revisions in the component layout of the board can therefore be made simultaneously in the template. The diameter of the drill holes is 0.081 in. (2 mm), which is large enough to clear the solder fillet as well as the lead. The lead length is simply the thickness of the template used.

This work was done by Kierman O'Farrell and Edward Winn of Sperry Rand Corp. for **Johnson Space Center.** *No further documentation is available.*

MSC-16589

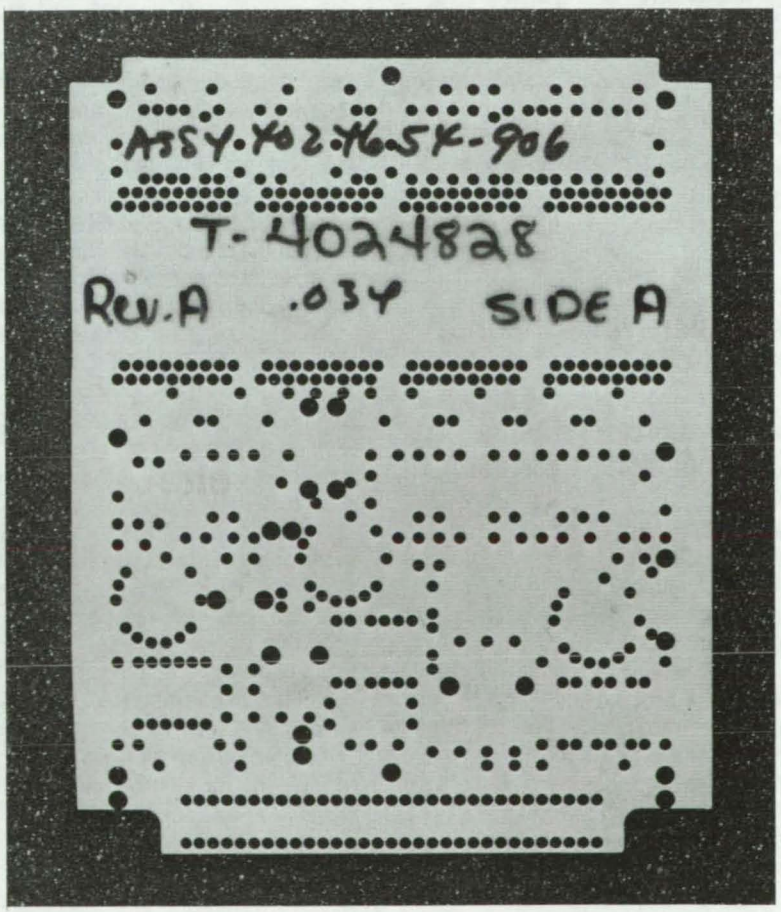

The **Lead-Trim Template** is an exact copy of a production board, except that the holes are oversized. The template is placed over the foil side of the production board, and all the protruding leads are cut close to the template surface.

Breather Cloth for Vacuum Curing

Fine-weave textile does not mar smooth finishes.

Lyndon B. Johnson Space Center, Houston, Texas

A finely-woven nylon cloth that has been treated with Teflon improves vacuum adhesive bonding of coatings to substrates. The cloth is placed over a coating; and the entire assembly, including the substrate, the coating, and the cloth, is placed in a plastic vacuum bag for curing. The cloth allows the coating to "breathe" when the bag is evacuated. Without the cloth, air becomes trapped between the coating and the bag, hampering the curing process.

The cloth was developed for the thermal-control radiators on the Orbiter spacecraft, in which a silver-Teflon coating is applied to the radiator panels. In this application, the coating must have a smooth mirrorlike surface and must follow the contours of the radiator substrate. The breather cloth had a thread count in the wrap direction of 165 threads/in. (65 threads/cm) and 110 threads/in. (43 threads/cm) in the weave direction. Thread thickness was 0.005 in. (0.012 cm); the cloth area density was 2 oz/yd^2 (0.0068 g/cm^2). This breather-cloth weave is so fine that it leaves no discernible pattern on the surface after the bagging operation.

Even if a mirror finish is not required, the fine weave is advantageous because it is semitransparent. Parts can thus be inspected visually before curing to ensure that no defects have been introduced in the bagging operation. Other possible applications for the cloth include bonding film coatings to solar concentrators and collectors.

This work was done by Madison W. Reed of Vought Corp. for **Johnson Space Center.** *No further documentation is available.*
MSC-18063

Books and Reports

These reports, studies, and handbooks are available from NASA as Technical Support Packages (TSP's) when a Request Card number is cited; otherwise they are available from one of NASA's Industrial Application Centers or the National Technical Information Service.

Processing High-Strength Steel Alloys

Specifications for fabricating parts from high-strength steel

A four-part report describes processing procedures for high-strength alloy steel, suitable for use in pistons, piston rods, cylinder barrels, and other critical applications. One alloy, HP9-4-30 steel, is considered; however, the procedures should be relevant to the processing of other high-strength alloys.

Part I of the report describes procedures for electroless nickel-plating, including surface preparation methods. Before plating, scale and oxide are removed by grit or wet blasting, grinding, machining, polishing, or anode pickling. For grinding, the parts must also be stress-relieved. Following these steps, the surface is cleaned, using a degreaser or alkaline cleaner, and then it is shot-peened and cleaned by glass-bead blasting prior to electroplating. This is followed by embrittlement relief (within 4 hours after plating), inspection, and storage.

The rules for heat treatment of the alloy, described in part II of the report, require that all rough machining and drilling be done before heat treatment, leaving a minimum of 0.050 in. (1.270 mm) of stock on all surfaces. Specific heat treatments are given for process annealing, normalizing and tempering, austenitizing, and preparation for swaging. These treatments include one or more high-temperature cycles followed by air cooling. The correct temperatures, heating times, and oven atmospheres are discussed in detail.

Machining procedures are covered in part III. Parts are machined using carbide tools, although cobalt or premium-grade high-speed tool steel is also suitable. The report outlines a number of sequences to be followed when machining and heat-treatment steps are combined. In addition, specific machining operations such as cutting, turning, milling, and drilling are discussed. The types of tools, tool sharpness, speed, and tolerance considerations are all included. Certain operations require the use of coolants.

The shot-peening processes, covered in part IV, use cast-steel shot size between 70 and 170. The final heat treatment is completed prior to peening. A smooth surface finish is prepared with all sharp corners and edges rounded to 0.010 to 0.015 in. (0.254 to 0.381 mm). The shot must be free from rust, dirt, oil, and grease and must be preused (conditioned) to remove any sharp edges. All designated areas are shot-peened 100 percent to saturation at a specific intensity. The residue from shot-peening is removed by glass-bead blasting at an intensity below that of the peening operation. To improve the finish, the peened surfaces may be honed or lapped to a specified depth.

This work was done by Larry E. McKnight of Bertea Corp. for **Johnson Space Center.** *To obtain a copy of the report, Circle 51 on the TSP Request Card.*
MSC-16172

Mathematics and Information Sciences

Processing Multispectral Signals From a Discrete-Sensor Array

Four-color multispectral camera is simpler because of a new technique for handling the electrical signals.

NASA's Jet Propulsion Laboratory, Pasadena, California

A new technique for encoding and decoding color-image signals from an array of discrete sensors simplifies fabrication of a remote-sensing imaging system. Using "matrix encoding," it is not necessary to precisely aline spectral filters with the charge-coupled devices (CCD) that are the discrete elements in the array. The matrix encoding technique treats the elements in groups of four (2×2) to produce an output corresponding to the multispectral image exposed to the elements.

Each element in the group is exposed to more than one spectral bandpass; the only alinement criterion is that each group of elements be exposed to all four of the spectral bands (red, blue, green, and infrared). The calibration matrix is determined by exposing each group to one spectral band at a time. This matrix then is used to decode the information.

The proposed method uses a composite spectral filter (see Figure 1) consisting of a periodic array of four spectral bandpasses. The filter is placed in the image plane of an imaging system so that each sensor element samples a combination of the four colors. Because of physical system constraints, a relay lens is used to project the filtered image onto a sensor located in the second image plane.

In mathematical terms, each sensor element measures an independent linear combination of the four-color brightness when considered in groups of four. If the brightnesses of the four colors are described as red (R), green (G), blue (B), and infrared (IR), then the response (I) of a typical group of detectors is given by

$$\begin{bmatrix} I_1 \\ I_2 \\ I_3 \\ I_4 \end{bmatrix} = \mathbf{M} \times \begin{bmatrix} R \\ G \\ B \\ IR \end{bmatrix}$$

where **M** is a 4 by 4 transformation matrix that is determined by the particular pattern of the filter over the four sensor elements and the responsivities of those elements. The sensor responses may then be converted into digital numbers in the same way that a typical CCD monochromatic image is encoded. From this step through decommutation of the imaging data in the ground processing, the video signal behaves exactly as does a standard monochromatic video signal.

(continued on next page)

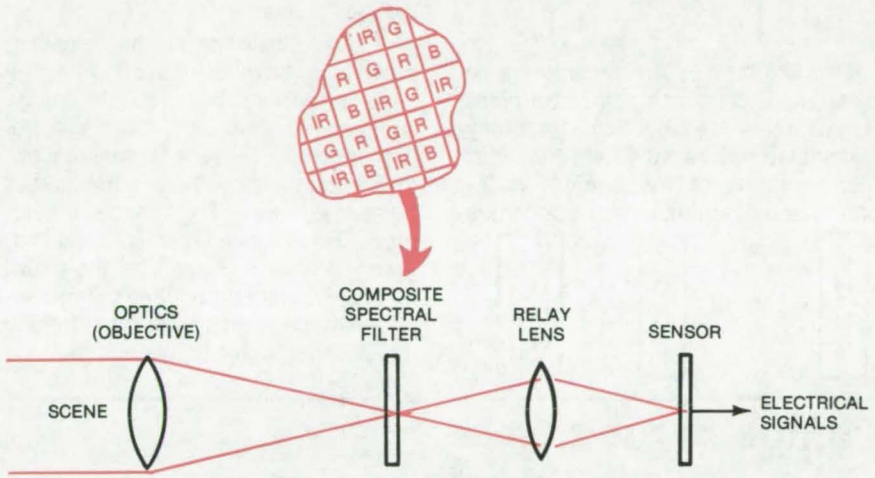

Figure 1. The proposed **Image Processing System** includes a composite spectral filter that projects image information on a CCD array sensor for image processing. This arrangement simplifies the fabrication of CCD sensor array cameras by relaxing the precision of alinement required between the filter and the sensor. The color pattern of the filter is shown in the insert.

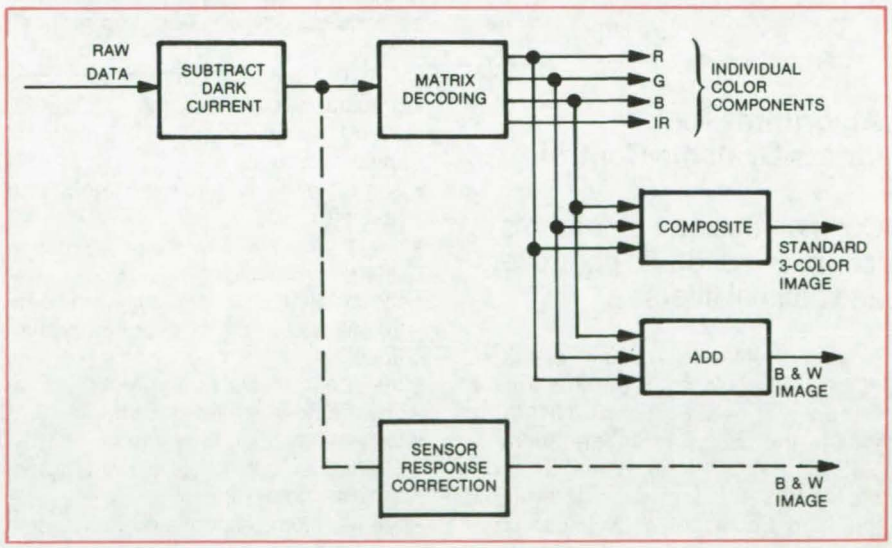

Figure 2. A **Matrix Decoding Scheme** shows what can be done with the electrical signals that represent image information. For comparison, the dotted portion shows a processing flow for a monochromatic image obtained without the matrix encoding/decoding technique.

Decoding of the four color signals requires knowledge of the **M** matrix at the decoding station. In general the colors are decoded using the matrix inverse of **M**:

$$\begin{bmatrix} R \\ G \\ B \\ IR \end{bmatrix} = \mathbf{M}^{-1} \times \begin{bmatrix} I_1 \\ I_2 \\ I_3 \\ I_4 \end{bmatrix}$$

The **M** matrices are determined by calibration, using one color at a time. If the camera is exposed to a uniformly illuminated source with a spectral filter matching one of the camera passbands (e.g., red), equation 1 becomes

$$\begin{bmatrix} I_1 \\ I_2 \\ I_3 \\ I_4 \end{bmatrix} = \mathbf{M} \times \begin{bmatrix} R \\ O \\ O \\ O \end{bmatrix} = R \begin{bmatrix} M_{11} \\ M_{21} \\ M31 \\ M_{41} \end{bmatrix}$$

Thus, if the brightness of red is known, four matrix elements are determined. This process, which applies to each quadruple of picture elements, is then repeated with the light source filtered to match each of the three remaining spectral filters, thereby determining the remaining matrix elements. The **M** matrices are then inverted to $\mathbf{M}^{-1}$ for decoding.

A block diagram of the decoding process is shown in Figure 2. After the dark current is subtracted, the image is decoded into its four spectral components. These components are then used individually or combined in numerous ways. The standard color product is achieved by displaying red, green, and blue signals in their own colors. A single broadband black-and-white image is achieved by summing the decoded color components.

The amount of computer processing in the matrix decoding process is not large in comparison to standard processing used on existing digital, remote-sensing systems. The matrices have 16 elements each, and there are 800x800 matrices for a total of about 10 million words. An existing system using four cameras employ 9.6 million words per camera.

This work was done by John B. Wellman of Caltech for **NASA's Jet Propulsion Laboratory.** *For further information, Circle 71 on the TSP Request Card.*

Inquiries concerning rights for the commercial use of this invention should be addressed to the Patent Counsel, NASA Resident Legal Office-JPL [see page A8]. Refer to NPO-14211.

Computer Programs

These programs may be obtained at very reasonable cost from COSMIC, a facility sponsored by NASA to make new programs available to the public. For information on program price, size, and availability, circle the reference letter on the COSMIC Request Card in this issue.

Algorithms for Linear-Systems Control

Optimal regulator algorithms for linear-quadratic controllers and optimal filters.

A control-theory design package, "Optimal Regulator Algorithms for the Control of Linear Systems" (ORACLS), aids in the design of linear-quadratic-Gaussian (LQG) controllers and optimal filters. It is applicable to systems that can be modeled by linear time-invariant differential or difference equations. ORACLS is a rigorous tool for dealing with multi-input multi-output dynamic systems in continuous and discrete forms.

A collection of subroutines can be used to formulate, manipulate, and solve various LQG design problems. There is considerable flexibility at each operational state through the use of primary subroutines at four levels: input-output, basic vector-matrix operations, analyses of linear time-invariant systems, and control synthesis based on LQG methodology.

The input-output routines read and write numerical matrices, print heading information, and accumulate output information. The basic vector-matrix operations include addition, subtraction, multiplication, equation, norm construction, tracing, transposition, scaling, juxtaposition, and construction of null and identity matrices. The analysis routines compute:

- The eigenvalues and eigenvectors of real matrices,
- the relative stability of a given matrix (matrix factorization),
- the solution of linear constant-coefficient vector-matrix algebraic equations,
- the controllability properties of a linear time-invariant system,
- the steady-state covariance matrix of an open-loop stable system forced by white noise, and
- the transient response of continuous linear time-invariant systems.

The control-law design routines of ORACLS implement some of the more common techniques of time-invariant LQG methodology. For the finite-duration optimal linear regulator problem with noise-free measurements, continuous dynamics, and integral performance index, a routine implements the negative exponential method for finding both the transient and steady-state solutions to the matrix Riccati equation. For the discrete version of this problem, the method of backward differencing is applied to find the solutions to the discrete Riccati equation.

Another routine solves the steady-state Riccati equation by the Newton algorithms described by Kleinman, for continuous problems, and by Hewer, for discrete problems. Still another calculates the prefilter gain to eliminate control-state cross-product terms in the quadratic performance index and the weighting matrices for the sampled-data optimal linear regulator problem.

For cases with measurement noise, duality theory and optimal regulator algorithms are used to calculate solutions to the continuous and discrete Kalman-Bucy filter problems. Finally, routines are included to implement the continuous and discrete forms of the explicit (model-in-the-system) and implicit (model-in-the-performance-index) model-following theory. These latter routines generate linear control laws that cause the output of a time-invariant dynamical system to track the output of a prescribed model.

In order to apply ORACLS, the user must write an executive (driver) program that inputs the problem coefficients, formulates and selects the routines to be used to solve the problem, and specifies the desired output. The ORACLS routines are written in FORTRAN IV for batch execution and have been implemented on a CDC 6000-series computer with a central

memory requirement of approximately 13K octal of 60-bit words.

This program was written by Ernest S. Armstrong of **Langley Research Center.** *For further information, Circle M on the COSMIC Request Card.*
LAR-12313

Multipurpose System Simulator

Program compares and evaluates computer systems.

The Multipurpose System Simulator (MPSS) was developed to evaluate the relative performance of competitive computer systems and to isolate areas for enhancement in existing or proposed systems. The model can simulate multiple central-processing-unit (CPU) interactive systems. Each system to be studied must be described by a hardware configuration, a data load, and the set of associated software to be processed by each computer CPU.

The model simulates the operation of the specified computer system and provides performance measures for the given data load. The resulting measures from various proposed systems can then be compared to determine which system best satisfies a given set of requirements. After a particular system is selected, the model can be used to monitor the projected performance of the evolving hardware and software structure.

The model is propagated on a time-step basis. Data blocks arriving from outside the system are scheduled in bursts for entry into the simulated system. Data blocks transferred between CPU's are dynamically entered into the appropriate queue at the simulated time they are sent plus an I/O handling time. When software is executed in an interruptible mode, explicit task queues are modeled to treat data-block and software-module tasks. Software modules of the appropriate priority are handled in a first-in/first-out manner within each queue.

The model input consists of CPU, memory peripheral device (PER), and communications-line and bus-hardware characteristics and linkages. It also includes simulated data-block types and system arrival rates (constant, periodic, or Poisson probabilistic options) and associated executable sequences of software modules for each data-block type. For each type of simulated software module, specifications of its number of effective instructions, priority, and detailed PER utilization are declared. The performance parameters measured by the model include CPU processing and idle times, data-block backlogs, data-block response times, individual software-module response times, communications-line usage, and statistics on PER utilization and contention.

The program is written in FORTRAN IV for the IBM FORTRAN H compiler and IBM OS Assembler for execution in the batch mode. This program has been implemented on an IBM 360-series computer with a central memory requirement of approximately 350K of 8-bit bytes.

This program was written by C.A. Packard of **Goddard Space Flight Center.** *For further information, Circle N on the COSMIC Request Card.*
GSC-12333

Plotting Shear-Flow Forces

Force on quadrilateral panels presented on CRT

Structural analysts can use a new computer program to study the shear-flow and in-plane forces characteristic of quadrilateral panels subjected to different loading conditions. The digital outputs are presented for engineers and management, with various options to allow the bulk of the data to be analyzed quickly. Shear-flow and normal forces for the quadrilateral elements in a finite-element model are provided as CRT plots.

The program acts as a post-processor of finite-element structural analysis programs. The required inputs include shear flows, normal forces, group-element selection, load-case selection, topology, coordinates, and projected-view option. The panels to be plotted may be quadrilateral elements or panels made up of two or three triangular membrane elements. There may even be two sets of overlapping triangular elements to take out the stiffness-bias characteristics.

The program reads in the control cards and any other option cards as dictated by the control cards. To insure that the correct types of data are processed and that there are headers for printout purposes, an error-checking procedure is included. Data are expected to be in the COMBINE format. After the data have been recovered and checked, the desired CRT plots are produced. The program can plot up to nine panels per frame.

This program is written in FORTRAN IV for interactive execution and has been implemented on an IBM 370 with a central memory requirement of approximately 90K of 8-bit bytes. The program requires a load library that is supplied as an IBM IEHMOVE unloaded partitioned data set. An interactive graphics CRT is required.

This program was written by Tetsuo Furuike and Jack C. Long of Rockwell International Corp. for **Johnson Space Center.** *For further information, Circle P on the COSMIC Request Card.*
MSC-18013

Spares-Optimized Model

Forecasts of required quantities and costs

A computerized spares optimization for the Space Shuttle Project comprises an analytical process for developing spares quantification and budget forecasts. The model, which assesses the risk associated with the recommended spares quantities, is an economical way to determine the best mix of a large number of spare types.

Marginal analysis techniques are used to compute an optimum mix of spare units that will maximize the probability of spares sufficiency per unit cost within a subsystem budget constraint or a subsystem probability of spares sufficiency constraint. Additional support-function measurements related to the identified spares are also provided.

The "sparing concept" on which the model is based is that when a line-replaceable unit fails, it is necessary to remove that unit, replace it with a

(continued on next page)

spare from inventory, and send the "failed" unit to a repair facility. For each line-replaceable unit installed on a vehicle, a number of spares will be in the process of being routed to a repair facility, being repaired at the facility, enroute to inventory, or available in inventory.

If a spare is available in inventory when a demand is made, the demand is filled immediately; if not, a back-order is generated, and a waiting time ensues until a spare is available. A limitation of the model is that spares are single-indentured only; that is, spares are optimized individually but not jointly. The model uses Poisson's exponential binomial limit theorem to compute the probability of spares sufficiency.

The punched-card input to this program includes:

- program data, such as title and run identification, and operating parameters,
- subsystem data, such as subsystem title, budget constraint in dollars, and probability of sufficiency constraint, and
- spares data, such as part number, nomenclature, expected issue rate, maintenance correction factor, condemnation rate, unit cost, pipeline time, minimum quantity, and quantity per vehicle.

The outputs of the model are 11 reports, including cost, quantity, and waiting time for spares; a summary of subsystem requirements; and graphic output of points used to plot the curve of cost versus probability of sufficiency. Plotting capabilities are required in order to produce the graphical outputs directly.

The program is written in FORTRAN IV for execution in the batch mode on an IBM 360/370-series computer under OS with a central memory requirement of approximately 400K of 8-bit bytes. The program requires a load library that is included in IBM IEHMOVE format.

This program was written by Alan W. Cain and Robert E. Paulin of Rockwell International Corp. for **Johnson Space Center.** *For further information, Circle R on the COSMIC Request Card.*
MSC-18015

A Parameter-Estimation Subroutine Package

Streamlined subroutines for parameter estimation and filtering

This estimation subroutine package comprises fast, efficient, and simple least-squares data-processing algorithms for use in orbit determination and related analyses. Very reliable and general algorithms have been documented in such works as "Solving Least Squares Problems" by Lawson and Hanson. It has been found that, except for pathological cases, one can streamline the least-square algorithm codes with a significant reduction of core requirements and computation time. This package contains a collection of streamlined subroutines that can be used to solve a large variety of parameter-estimation and filtering problems. Special routines are included for problems with colored process noise and covariance (factor) mapping.

The subroutines are based on algorithms that, for the most part, involve triangular and/or symmetric matrices. To reduce storage requirements, matrices are stored in vector form. The user has little direct contact with the vector-subscripting algorithms and may input and output all matrices in full matrix format.

Subroutine matrix calculations available include: computation of updated U-D factors corresponding to a rank one modification; permutation of the rows and columns of a matrix; replacement of a positive semidefinite matrix by its upper (or lower) Cholesky factor; computation of the inverse of an upper triangular vector stored matrix; combination of an upper triangular vector stored matrix with a rectangular doubly-subscripted matrix by means of Householder orthogonal transformations; computation of updated U-D covariance factors and estimates from an a priori estimate and measurement; and weighted Gram-Schmidt matrix triangularization.

There are 31 subroutines, written in FORTRAN IV, which have been thoroughly documented and tested. The system has been implemented on a UNIVAC 1100-series computer under control of EXEC 8. The subroutines are generally portable, with the exception of several FORMAT-statement-related and @-"comment"-symbol UNIVAC-dependent anomalies.

This program was written by Gerald J. Bierman and Melba W. Nead of Caltech for **NASA's Jet Propulsion Laboratory.** *For further information, Circle S on the COSMIC Request Card.*
NPO-14263

SUBJECT INDEX

Page intentionally left blank

National Aeronautics and
Space Administration

Washington, D.C.
20546

SPECIAL FOURTH-CLASS RATE
BOOK

FOURTH-CLASS MAIL
POSTAGE & FEES PAID
NASA
WASHINGTON, D.C.
PERMIT No. G 27

NASA

The exits of Boston's Exeter Street Theater are lighted by multimode electronic lights, commercial spinoffs from a lighting system developed for the Apollo and Skylab manned spacecraft. These compact, lightweight, multimode lights are very reliable.